Quantum metrology with nonclassical states of atomic ensembles

Luca Pezzè and Augusto Smerzi

QSTAR, INO-CNR and LENS, Largo Enrico Fermi 2, 50125 Firenze, Italy

Markus K. Oberthaler

Kirchhoff-Institut für Physik, Universität Heidelberg, Im Neuenheimer Feld 227, 69120 Heidelberg, Germany

Roman Schmied and Philipp Treutlein

Department of Physics, University of Basel, Klingelbergstrasse 82, 4056 Basel, Switzerland

(published 5 September 2018)

Quantum technologies exploit entanglement to revolutionize computing, measurements, and communications. This has stimulated the research in different areas of physics to engineer and manipulate fragile many-particle entangled states. Progress has been particularly rapid for atoms. Thanks to the large and tunable nonlinearities and the well-developed techniques for trapping, controlling, and counting, many groundbreaking experiments have demonstrated the generation of entangled states of trapped ions, cold, and ultracold gases of neutral atoms. Moreover, atoms can strongly couple to external forces and fields, which makes them ideal for ultraprecise sensing and time keeping. All these factors call for generating nonclassical atomic states designed for phase estimation in atomic clocks and atom interferometers, exploiting many-body entanglement to increase the sensitivity of precision measurements. The goal of this article is to review and illustrate the theory and the experiments with atomic ensembles that have demonstrated many-particle entanglement and quantum-enhanced metrology.

DOI: 10.1103/RevModPhys.90.035005

CONTENTS

I. Introduction 2
A. Entanglement and interferometric sensitivity enhancement: Exemplary cases 3
B. Entanglement useful for quantum-enhanced metrology 3
C. Generation of metrologically useful entanglement in atomic ensembles 4
D. Outline 5
II. Fundamentals 5
A. Collective spin systems 5
1. Single spin 5
2. Many spins 5
3. Many spins in a symmetrized state 6
4. Collective rotations 6
B. Phase estimation 6
1. Cramér-Rao bound and Fisher information 6
2. Lower bound to the Fisher information 7
3. Upper bound to the Fisher information: The quantum Fisher information 7
a. Convexity and additivity 8
b. Optimal measurements 8
c. Optimal rotation direction 8
4. Phase sensitivity and statistical distance 8
5. The maximum likelihood estimator 9
6. Method of moments 9
7. Bayesian estimation 10
C. Entanglement and phase sensitivity 10
1. Multiparticle entanglement 10
2. Sensitivity bound for separable states: The standard quantum limit 11
3. Coherent spin states 11
4. Useful entanglement for quantum metrology 11
5. Metrological spin squeezing 13
a. Optimal spin-squeezed states 13
b. Spin squeezing and bosonic quadrature squeezing 13
c. Spin squeezing, entanglement, and Fisher information 14
6. Dicke states 14
7. NOON states 15
8. Further notions of spin squeezing and their relation to entanglement 15
a. Squeezing parameter of Kitagawa and Ueda 15
b. Entanglement witnessed by mean values and variances of spin operators 16
c. Spin squeezing and entanglement of symmetric states 16
d. Planar spin-squeezed states 17
9. Einstein-Podolsky-Rosen entanglement and Bell correlations 17
a. Continuous variable and Einstein-Podolsky-Rosen entanglement 17
b. Bell correlations 17
D. Tomography of spin states 18
1. Spin-noise tomography 18

 © 2018 American Physical Society

2. Visualizing spin states 18
a. Wigner distribution 18
b. Husimi-Kano representation 19
c. Glauber-Sudarshan representation 19
E. Detection of atomic states 19
1. Atom counting 19
a. Resonant absorption imaging 19
b. Resonant fluorescence imaging 19
2. Quantum nondemolition measurements of atom number 20
a. Faraday effect 20
b. Dispersion 20
c. Cavity-enhanced detection 20
3. Inhomogeneous spin coupling and effective spin 20
III. Entanglement via Atomic Collisions: The Bosonic Josephson Junction 20
A. Metrologically useful entanglement in the ground state of the bosonic Josephson junction 22
1. Ground state for positive nonlinearities 23
a. Rabi regime, $0 < \Lambda \ll 1$ 23
b. Josephson regime, $1 \ll \Lambda \ll N^2$ 23
c. Fock regime, $\Lambda \gg N^2$ 24
2. Ground state for negative nonlinearities 24
a. Disordered phase, $-1 < \Lambda < 0$ 24
b. Ordered phase, $\Lambda < -1$ 24
3. Adiabatic splitting 24
4. Experimental spin squeezing in the ground state of the BJJ 25
B. One-axis twisting dynamics 26
1. Spin squeezing and particle entanglement 27
2. Quantum interferometry 27
3. Bell correlations 28
C. Twist-and-turn dynamics 28
1. Entanglement beyond spin squeezing 29
D. Entanglement of two spatially separated Bose-Einstein condensates 30
IV. Entanglement via Atomic Collisions: Spin-mixing Dynamics 30
A. Spinor Bose-Einstein condensates 30
1. Spin-changing collisions 30
2. Metrologically useful entanglement in the ground state of the spin-mixing Hamiltonian 32
3. Quantum spin-mixing dynamics in the low-depletion limit 32
B. Population correlations and twin-Fock state 33
1. Number squeezing 33
2. Quantum interferometry with twin-Fock states 33
3. Particle entanglement 34
4. Adiabatic state preparation 34
C. Quadrature squeezing and squeezed-vacuum state 35
1. Quadrature squeezing 35
2. Continuous variable and EPR entanglement 35
3. Interferometry with squeezed vacuum 35
4. Nonlinear SU(1,1) interferometry 36
D. Other protocols to create correlated atomic pairs 36
V. Entanglement Creation via Atom-light Interaction 37
A. Quantum state preparation using nondestructive measurements 37
1. Quantum nondemolition measurements in free space 37
2. Cavity-based quantum nondemolition measurements in the dispersive regime 39
3. Heralded atomic entanglement created by single-photon detection 40
4. Cavity-based quantum nondemolition measurements in the normal mode splitting regime 41
5. Quantum state preparation via quantum Zeno dynamics 42
B. Light-mediated coherent interaction between distant atoms 42
C. Quantum state transfer from nonclassical light to atoms 43
VI. Entangled States of Trapped Ions 44
A. Generation of metrologically useful entangled states of many ions 44
B. Quantum metrology with trapped ions 45
1. Quantum metrology with two ions 45
2. Quantum metrology with GHZ states of several ions 46
3. Spin squeezing and useful entanglement of many ions 47
VII. Working Entanglement-enhanced Interferometers and Prospects for Applications 47
A. The influence of noise and decoherence 48
1. General results 48
2. Uncorrelated decoherence 48
3. Correlated phase noise, differential interferometry, and decoherence-free subspaces 49
4. Error correction 50
5. Particle losses 51
6. Finite detection efficiency and interaction-based readout 51
B. Atomic clocks 52
1. Entanglement-assisted atomic clocks 53
2. Proposals for entanglement-assisted lattice clocks and atom interferometers 53
C. Optical magnetomenters 54
1. Entanglement-assisted optical magnetometers 54
D. Scanning probe magnetometers using Bose-Einstein condensates 54
E. Nonlocal phase encoding 55
VIII. Outlook 56
Acknowledgments 56
References 56

I. INTRODUCTION

The precise measurement of physical quantities such as the strength of a field, a force, or time plays a crucial role in the advancement of physics. Precision measurements are very often obtained by mapping the physical quantity to a phase shift that can be determined using interferometric techniques. Phase estimation follows the general scheme outlined in Fig. 1: a probe state $\hat{\rho}_0$ of N particles is prepared, acquires a phase shift θ, and is finally detected. An estimate $\Theta(\mu)$ of the phase shift is obtained from the measurement outcome μ. This conceptually simple scheme is common to all interferometric sensors: from gravitational wave detectors to atomic clocks, gyroscopes, and gravimeters, just to name a few. The goal is to estimate θ with the smallest possible uncertainty $\Delta\theta$ given finite resources such as time and number of particles. The noise that determines $\Delta\theta$ can be of a technical (classical) or fundamental (quantum) nature

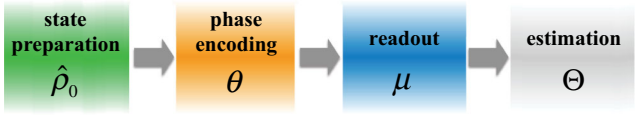

FIG. 1. Building blocks of phase estimation: (i) preparation of the probe state $\hat{\rho}_0$, (ii) encoding of a phase shift θ that depends on the physical quantity of interest, (iii) readout, where μ indicates a generic measurement result, and (iv) estimation, where the estimator $\Theta(\mu)$ is a function of the measurement result(s). The uncertainty $\Delta\theta$ of the estimation depends crucially on all of these operations.

(Helstrom, 1976; Holevo, 1982; Braunstein and Caves, 1994). Current two-mode atomic sensors are limited by the so-called standard quantum limit $\Delta\theta_{\mathrm{SQL}} = 1/\sqrt{N}$ inherent in probes using a finite number of uncorrelated (Giovannetti, Lloyd, and Maccone, 2006) or classically correlated (Pezzè and Smerzi, 2009) particles. Yet the standard quantum limit is not fundamental (Caves, 1981; Bondurant and Shapiro, 1984; Yurke, McCall, and Klauder, 1986). Quantum-enhanced metrology studies how to exploit quantum resources, such as squeezing and entanglement, to overcome this classical bound (Giovannetti, Lloyd, and Maccone, 2004, 2011; Pezzè and Smerzi, 2014; Tóth and Apellaniz, 2014). Research on quantum metrology with atomic ensembles also sheds new light on fundamental questions about many-particle entanglement (Amico *et al.*, 2008; Gühne and Tóth, 2009; Horodecki *et al.*, 2009) and related concepts, such as Einstein-Podolsky-Rosen correlations (Reid *et al.*, 2009) and Bell nonlocality (Brunner *et al.*, 2014).

Since the systems of interest for quantum metrology often contain thousands or even millions of particles, it is generally not possible to address, detect, and manipulate all particles individually. Moreover, the finite number of measurements limits the possibility to fully reconstruct the generated quantum states. These limitations call for conceptually new approaches to the characterization of entanglement that rely on a finite number of coarse-grained measurements. In fact, many schemes for quantum metrology require only collective manipulations and measurements on the entire atomic ensemble. Still, the results of such measurements allow one to draw many interesting conclusions about the underlying quantum correlations between the particles.

A. Entanglement and interferometric sensitivity enhancement: Exemplary cases

We illustrate here how the standard quantum limit arises in interferometry and how it can be overcome using entanglement. Consider a Ramsey interferometer sequence (Ramsey, 1963) between two quantum states $|a\rangle$ and $|b\rangle$; see Sec. II. Let us discuss first the case of a single atom initially prepared in the probe state $|a\rangle$. The atom is transformed to $(|a\rangle + |b\rangle)/\sqrt{2}$ by a resonant $\pi/2$ pulse corresponding to the first beam splitter of the interferometer. During the subsequent interrogation time, $|a\rangle$ and $|b\rangle$ acquire a relative phase θ, such that the state evolves to $(e^{-i\theta/2}|a\rangle + e^{i\theta/2}|b\rangle)/\sqrt{2}$. The phase θ encodes the quantity to be measured. Finally, a second resonant $\pi/2$ pulse (the second beam splitter) is applied so that the output state is $\cos(\theta/2)|a\rangle + \sin(\theta/2)|b\rangle$. The phase θ can now be estimated, for instance, by measuring the population difference $\hat{M} = |a\rangle\langle a| - |b\rangle\langle b|$ between the two states. In this simple example the interferometer signal is the expectation value $\langle\hat{M}\rangle = \cos\theta$ while the noise at the output is quantified by the variance $\Delta^2\hat{M} = \sin^2\theta$.

If we now repeat the same interferometric procedure with N uncorrelated atoms, the signal $\langle\hat{M}\rangle$, where $\hat{M} = \sum_{i=1}^{N} |a\rangle_i\langle a| - |b\rangle_i\langle b|$ is now the population difference of N atoms, will be simply given by N times that of a single atom. Because the atoms are uncorrelated, the variance $\Delta^2\hat{M}$ will also be multiplied by a factor N and correspondingly the standard deviation $\Delta\hat{M}$ will increase by $\sqrt{N}$. Overall, this results in a phase uncertainty of $\Delta\theta = \Delta\hat{M}/|d\langle\hat{M}\rangle/d\theta| = 1/\sqrt{N}$. This is precisely the standard quantum limit $\Delta\theta_{\mathrm{SQL}}$, which arises from the binomial statistics of the N uncorrelated particles.

Overcoming this sensitivity limit requires entanglement between the particles. One possibility, suggested by the above formula, is to engineer quantum correlations that lead to subbinomial statistics $\Delta^2 M < N$ at the point of maximum slope of the signal, while keeping that slope (i.e., the interferometer contrast) of the order of N. In this way, a phase uncertainty of $\Delta\theta < 1/\sqrt{N}$ can be achieved. States that satisfy these conditions are called spin squeezed[1] (Wineland *et al.*, 1992, 1994) and are an important class of useful states in quantum metrology (Ma *et al.*, 2011). Spin-squeezed states can be created by making the atoms interact with each other for a relatively short time (Kitagawa and Ueda, 1993) generating entanglement between them (Sørensen *et al.*, 2001; Sørensen and Mølmer, 2001).

Spin-squeezed states are only a small subset of the full class of entangled states that are useful for quantum-enhanced metrology. A prominent example is the Greenberger-Horne-Zeilinger (GHZ) state $(|a\rangle^{\otimes N} + |b\rangle^{\otimes N})/\sqrt{2}$ (also indicated as NOON state when considering bosonic particles), which is not spin squeezed but can nevertheless provide phase sensitivities beyond the standard quantum limit (Bollinger *et al.*, 1996; Lee, Kok, and Dowling, 2002).

B. Entanglement useful for quantum-enhanced metrology

In the context of phase estimation, the idea that quantum correlations are necessary to overcome the standard quantum limit emerged already in pioneering works (Yurke, McCall, and Klauder, 1986; Wineland *et al.*, 1992; Kitagawa and Ueda, 1993). In recent years, it has been clarified that only a special class of quantum correlations can be exploited to estimate an interferometric phase with sensitivity overcoming $\Delta\theta_{\mathrm{SQL}}$. This class of entangled states is fully identified by the quantum

[1]Indeed we will later see that $d\langle\hat{M}\rangle/d\theta$ and $\Delta^2\hat{M}$ can be written in terms of mean and variance of collective spin operators; see Sec. II.A.

Fisher information F_Q. The quantum Fisher information is inversely proportional to the maximum phase sensitivity achievable for a given probe state and interferometric transformation: the so-called quantum Cramér-Rao bound $\Delta\theta_{QCR} = 1/\sqrt{F_Q}$ (Helstrom, 1967; Braunstein and Caves, 1994). It thus represents the figure of merit for the sensitivity of a generic parameter-estimation problem involving quantum states and will be largely discussed in this review. The condition $F_Q > N$ (Pezzè and Smerzi, 2009) is sufficient for entanglement and necessary and sufficient for the entanglement useful for quantum metrology: it identifies the class of states characterized by $\Delta\theta_{QCR} < \Delta\theta_{SQL}$, i.e., those that can be used to overcome the standard quantum limit in any two-mode interferometer where the phase shift is generated by a local Hamiltonian. Spin-squeezed, GHZ and NOON states fulfill the condition $F_Q > N$. Phase uncertainties down to $\Delta\theta = 1/\sqrt{kN}$ can be obtained with metrologically useful k-particle entangled states (Hyllus, Laskowski *et al.*, 2012; Tóth, 2012). In the absence of noise, the ultimate limit is $\Delta\theta_{HL} = 1/N$, the so-called Heisenberg limit (Yurke, McCall, and Klauder, 1986; Holland and Burnett, 1993; Giovannetti, Lloyd, and Maccone, 2006), which can be reached with metrologically useful genuine N-particle entangled states ($k = N$).

C. Generation of metrologically useful entanglement in atomic ensembles

A variety of techniques have been used to generate entangled states useful for quantum metrology with atomic ensembles. The crucial ingredient is interaction between the particles, for instance atom-atom collisions in Bose-Einstein condensates, atom-light interactions in cold thermal ensembles (including experiments performed with warm vapors in glass cells), or combined electrostatic and ion-light interaction in ion chains. Figure 2 summarizes the experimental achievements (the gain of phase sensitivity relative to the standard quantum limit) as a function of the number of particles. Stars in Fig. 2 show the measured phase sensitivity gain obtained after a full interferometer sequence using entangled states as input to the atom interferometer. Filled circles report witnesses of metrologically useful entanglement (i.e., spin squeezing and Fisher information) measured on experimentally generated states, representing potential improvement in sensitivity.

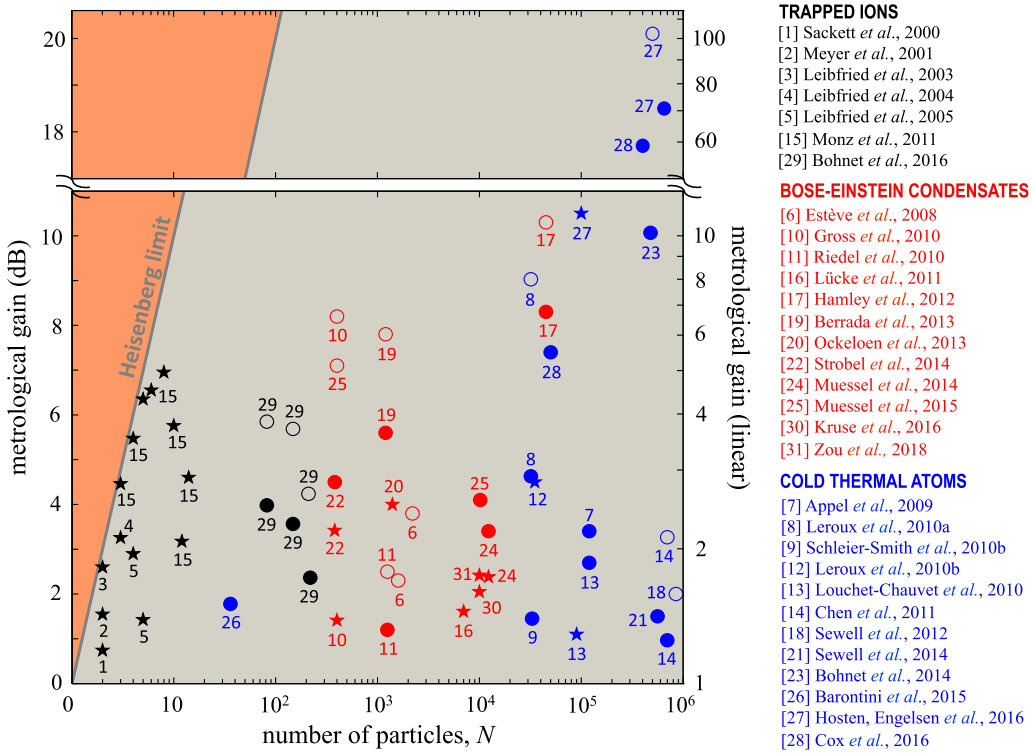

FIG. 2. Gain of phase sensitivity over the standard quantum limit $\Delta\theta_{SQL} = 1/\sqrt{N}$ achieved experimentally with trapped ions (black symbols), Bose-Einstein condensates (red), and cold thermal ensembles (blue). The gain is shown on logarithmic [left, dB, $10\log_{10}(\Delta\theta_{SQL}/\Delta\theta)^2$] and linear [right, $(\Delta\theta_{SQL}/\Delta\theta)^2$] scales. The solid thick line is the Heisenberg limit $\Delta\theta_{HL} = 1/N$. Stars refer to directly measured phase sensitivity gains, performing a full phase estimation experiment. Circles are expected gains based on a characterization of the quantum state, e.g., calculated as $\Delta\theta = \xi_R/\sqrt{N}$, where ξ_R is the spin-squeezing parameter or as $\Delta\theta = 1/\sqrt{F_Q}$, where F is the Fisher information. Filled (open) circles indicate results obtained (inferred) without (with) subtraction of technical and/or imaging noise. Every symbol is accompanied by a number (in chronological order) corresponding to the reference reported in the side table. Here N is the total number of particles or, in the presence of fluctuations, the mean total.

Open circles are inferred values, being obtained after subtraction of detection noise. The Heisenberg limit has been reached with up to $N \sim 10$ trapped ions. Attaining this ultimate bound with a much larger number of particles is beyond current technology as it requires the creation and protection of large amounts of entanglement. Nevertheless, metrological gains up to $(\Delta\theta_{\mathrm{SQL}}/\Delta\theta)^2 \sim 100$ have been reported with large atomic ensembles (Cox *et al.*, 2016; Hosten, Engelsen *et al.*, 2016). A glance at Fig. 2 reveals how quantum metrology with atomic ensembles is a very active area of research in physics. Moreover, the reported results prove that the field is now mature enough to take the step from proofs of principle to technological applications.

D. Outline

This review presents modern developments of phase estimation techniques in atomic systems aided by quantum-mechanical entanglement, as well as fundamental studies of the associated entangled states. In Sec. II, we give a theoretical overview of quantum-enhanced metrology. We first discuss the concepts of spin squeezing and Fisher information considering spin-1/2 particles. We then illustrate different atomic systems where quantum-enhanced phase estimation or, at least, the creation of useful entanglement for quantum metrology has been demonstrated. Sections III and IV review the generation of entangled states in Bose-Einstein condensates. Section V describes the generation of entangled states of many atoms through the common coupling to an external light field. Section VI describes metrology with ensembles of trapped ions. Finally, Sec. VII gives an overview of the experimentally realized entanglement-enhanced interferometers and the realistic perspective to increase the sensitivity of state-of-the-art atomic clocks and magnetometers. This section also discusses the impact of noise in the different interferometric protocols.

II. FUNDAMENTALS

In this review we consider systems and operations involving N particles and assume that all of their degrees of freedom are restricted to only two modes (single-particle states) that we identify as $|a\rangle$ and $|b\rangle$. These can be two hyperfine states of an atom, as in a Ramsey interferometer (Ramsey, 1963), two energy levels of a trapping potential, or two spatially separated arms, as in a Mach-Zehnder interferometer (Zehnder, 1891; Mach, 1892); see Fig. 3. The interferometer operations are collective, acting on all particles in an identical way. The idealized formal description of these interferometer models is mathematically equivalent (Wineland *et al.*, 1994; Lee, Kok, and Dowling, 2002): as discussed in Sec. II.A, it corresponds to the rotation of a collective spin (Yurke, McCall, and Klauder, 1986).

A. Collective spin systems

1. Single spin

By identifying mode $|a\rangle$ with spin up and mode $|b\rangle$ with spin down, a (two-mode) atom can be described as an effective spin-1/2 particle: a qubit (Peres, 1995; Nielsen and Chuang, 2000). Any pure state of a single qubit can be written as $|\vartheta,\varphi\rangle = \cos(\vartheta/2)|a\rangle + e^{i\varphi}\sin(\vartheta/2)|b\rangle$, with $0 \le \vartheta \le \pi$ and $0 \le \varphi < 2\pi$ the polar and azimuthal angle, respectively, in the Bloch sphere. Pure states satisfy $\langle\hat{\boldsymbol{\sigma}}\rangle = \boldsymbol{s}$, where $\hat{\boldsymbol{\sigma}} = \{\hat{\sigma}_x, \hat{\sigma}_y, \hat{\sigma}_z\}$ is the Pauli vector and $\boldsymbol{s} = \{\sin\vartheta\cos\varphi, \sin\vartheta\sin\varphi, \cos\vartheta\}$ is the mean spin direction with $|\boldsymbol{s}| = 1$. Mixed qubit states can be expressed as $\hat{\rho} = (\mathbb{1} + \boldsymbol{s}\cdot\hat{\boldsymbol{\sigma}})/2$ and have an additional degree of freedom given by the length of the spin vector $0 \le |\boldsymbol{s}| \le 1$, such that the effective state vector $\boldsymbol{s}$ lies inside the Bloch sphere.

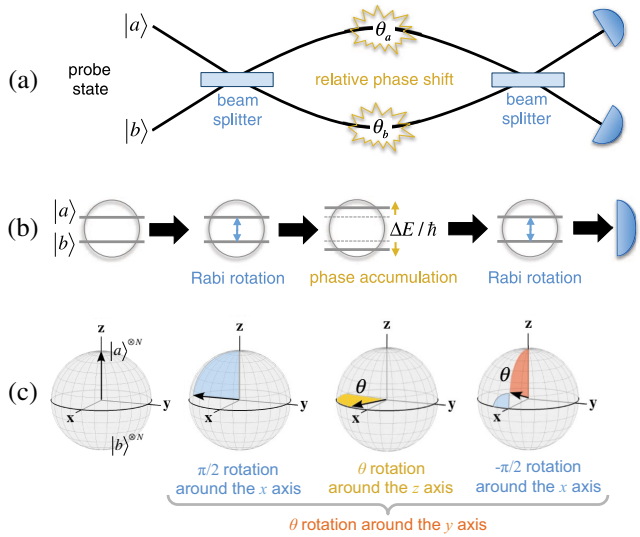

FIG. 3. Two-mode interferometers. In a Mach-Zehnder interferometer (a) two spatial modes $|a\rangle$ and $|b\rangle$ are combined on a balanced beam splitter, followed by a relative phase shift $\theta = \theta_a - \theta_b$ between the two arms, and finally recombined on a second balanced beam splitter. In a Ramsey interferometer (b) a resonant Rabi rotation creates a balanced superposition between two internal states $|a\rangle$ and $|b\rangle$, followed by a relative phase shift $\theta = (\Delta E/\hbar)T_{\mathrm{R}}$ given by the energy difference ΔE between these states multiplied by the interrogation time T_{R}. Finally a second resonant Rabi rotation recombines the two modes. (c) Equivalent representation of Mach-Zehnder and Ramsey interferometer operations as rotations of the collective spin on the generalized Bloch sphere. The initial state here $|a\rangle^{\otimes N}$ is pointing toward the north pole. The full sequence is equivalent to the rotation of an angle θ around the y axis.

2. Many spins

To describe an ensemble of N distinguishable qubits, we can introduce the collective spin vector $\hat{\boldsymbol{J}} = \{\hat{J}_x, \hat{J}_y, \hat{J}_z\}$, where

$$\hat{J}_x = \frac{1}{2}\sum_{l=1}^{N}\hat{\sigma}_x^{(l)}, \quad \hat{J}_y = \frac{1}{2}\sum_{l=1}^{N}\hat{\sigma}_y^{(l)}, \quad \hat{J}_z = \frac{1}{2}\sum_{l=1}^{N}\hat{\sigma}_z^{(l)}, \tag{1}$$

and $\hat{\boldsymbol{\sigma}}^{(l)}$ is the Pauli vector of the lth particle. In particular, $\hat{J}_z$ is half the difference in the populations of the two modes. The operators (1) satisfy the angular momentum commutation relations

$$[\hat{J}_x,\hat{J}_y]=i\hat{J}_z,\qquad [\hat{J}_z,\hat{J}_x]=i\hat{J}_y,\qquad [\hat{J}_y,\hat{J}_z]=i\hat{J}_x, \quad (2)$$

and have a linear degenerate spectrum spanning the 2^N-dimensional Hilbert space. The well-known set of states $|J,M\rangle$ forms a basis, where $\hat{\boldsymbol{J}}^2|J,M\rangle=J(J+1)|J,M\rangle$ and $\hat{J}_z|J,M\rangle=M|J,M\rangle$, with $J\in\{N/2,N/2-1,\ldots\}$ as well as $M\in\{-J,-J+1,\ldots,+J\}$ (Biederharn and Louck, 1981).

3. Many spins in a symmetrized state

The Hilbert space spanned by many-qubit states symmetric under particle exchange is that of total spin $J=N/2$, which is the maximum allowed spin length for N particles. This Hilbert space has dimension $N+1$, linearly increasing with the number of qubits. Symmetric qubit states are naturally obtained for N indistinguishable bosons and are described by the elegant formalism developed by Schwinger in the 1950s (Biederharn and Louck, 1981). Angular momentum operators are expressed in terms of bosonic creation $\hat{a}^\dagger$ and $\hat{b}^\dagger$ and annihilation $\hat{a}$ and $\hat{b}$ operators for the two modes $|a\rangle$ and $|b\rangle$:

$$\hat{J}_x=\frac{\hat{a}^\dagger\hat{b}+\hat{b}^\dagger\hat{a}}{2},\qquad \hat{J}_y=\frac{\hat{a}^\dagger\hat{b}-\hat{b}^\dagger\hat{a}}{2i},\qquad \hat{J}_z=\frac{\hat{a}^\dagger\hat{a}-\hat{b}^\dagger\hat{b}}{2}. \quad (3)$$

They satisfy the commutation relations (2) and commute with the total number of particles $\hat{N}=\hat{a}^\dagger\hat{a}+\hat{b}^\dagger\hat{b}$. The common eigenstates of $\hat{J}_z$ and $\hat{\boldsymbol{J}}^2=(\hat{N}/2)(\hat{N}/2+1)$ are called Dicke states (Dicke, 1954) or two-mode Fock states,

$$|m_z\rangle=|N/2+m\rangle_a|N/2-m\rangle_b=\frac{(\hat{a}^\dagger)^{N/2+m}}{\sqrt{(N/2+m)!}}\frac{(\hat{b}^\dagger)^{N/2-m}}{\sqrt{(N/2-m)!}}|\mathrm{vac}\rangle, \quad (4)$$

where $|\mathrm{vac}\rangle$ is the vacuum. They correspond to the symmetrized combinations of $N/2+m$ particles in mode $|a\rangle$ and $N/2-m$ particles in mode $|b\rangle$, where $m=-N/2,-N/2+1,\ldots,N/2$. The eigenstates $|m_{\boldsymbol{n}}\rangle$ of $\hat{J}_{\boldsymbol{n}}=\boldsymbol{n}\cdot\hat{\boldsymbol{J}}$, where $\boldsymbol{n}$ is an arbitrary spin direction, can be obtained by a proper rotation of $|m_z\rangle$: $|m_x\rangle=e^{-i(\pi/2)\hat{J}_y}|m_z\rangle$ and $|m_y\rangle=e^{i(\pi/2)\hat{J}_x}|m_z\rangle$, for instance. Finally, it is useful to introduce raising and lowering operators $\hat{J}_\pm=\hat{J}_x\pm i\hat{J}_y$ ($\hat{J}_+=\hat{a}^\dagger\hat{b}$ and $\hat{J}_-=\hat{b}^\dagger\hat{a}$), transforming the Dicke states as $\hat{J}_\pm|m_z\rangle=\sqrt{(N/2)(N/2+1)-m(m\pm1)}|(m\pm1)_z\rangle$.

4. Collective rotations

Any unitary transformation of a single qubit is a rotation $e^{-i(\theta/2)\hat{\sigma}_{\boldsymbol{n}}}$ on the Bloch sphere, where $\boldsymbol{n}$ and θ are the rotation axis and rotation angle, respectively. With N qubits, each locally rotated about the same axis $\boldsymbol{n}$ and angle θ, the transformation is $\bigotimes_{l=1}^N e^{-i(\theta/2)\hat{\sigma}_{\boldsymbol{n}}^{(l)}}=e^{-i\theta\hat{J}_{\boldsymbol{n}}}$. This collective rotation is the idealized model of most of the interferometric transformations discussed in this review. In the collective spin language, a balanced beam splitter is described by $e^{-i(\pi/2)\hat{J}_x}$, and a relative phase shift by $e^{-i\theta\hat{J}_z}$. Combining the three transformations $e^{i(\pi/2)\hat{J}_x}e^{-i\theta\hat{J}_z}e^{-i(\pi/2)\hat{J}_x}=e^{-i\theta\hat{J}_y}$, the whole interferometer sequence [Mach-Zehnder, Fig. 3(a), or Ramsey, Fig. 3(b)] is equivalent to a collective rotation around the y axis on the generalized Bloch sphere of maximum radius $N/2$ (Yurke, McCall, and Klauder, 1986); see Fig. 3(c).

B. Phase estimation

An interferometer transforms a probe state $\hat{\rho}_0$ depending on the value of an unknown phase shift θ. Following the general scheme of Fig. 1, the parameter θ cannot be measured directly and its estimation proceeds from the results of measurements performed on identical copies of the output state $\hat{\rho}_\theta$ of the interferometer. There are good and bad choices for a measurement observable. Optimal ones (that we will quantify and discuss in more detail later) are those characterized by a statistical distribution of measurement results that is maximally sensitive to changes of θ. We indicate as $P(\mu|\theta)$ the probability of a result[2] μ given that the parameter has the value θ. The conditional probability of observing the sequence $\boldsymbol{\mu}=\{\mu_1,\ldots,\mu_\nu\}$ of ν independent measurements is $P(\boldsymbol{\mu}|\theta)=\prod_{i=1}^\nu P(\mu_i|\theta)$. An estimator $\Theta(\boldsymbol{\mu})$ is a generic function associating each set of measurement outcomes $\boldsymbol{\mu}$ with an estimate of θ. For instance, a familiar estimator can be obtained from the interference fringes of a Ramsey interferometer (and belong to a more general estimation technique known as the method of moments discussed in Sec. II.B.6). Since the estimator is a function of random outcomes, it is itself a random variable. It is thus characterized by a θ-dependent statistical mean value $\bar{\Theta}=\sum_{\boldsymbol{\mu}}P(\boldsymbol{\mu}|\theta)\Theta(\boldsymbol{\mu})$ and variance

$$(\Delta\theta)^2=\sum_{\boldsymbol{\mu}}P(\boldsymbol{\mu}|\theta)[\Theta(\boldsymbol{\mu})-\bar{\Theta}]^2, \quad (5)$$

the sum extending over all possible sequences of ν measurement results. Different estimators can yield very different values when applied to the same measured data. In the following, we will be interested in locally unbiased estimators, i.e., those satisfying $\bar{\Theta}=\theta$ and $\partial\bar{\Theta}/\partial\theta=1$, so that the statistical average yields the true parameter value.

1. Cramér-Rao bound and Fisher information

How precise can a statistical estimation be? Are there any fundamental limits? The first answer came in the 1940s with the works of Fréchet (1943), Rao (1945), and Cramér (1946), who independently found a lower bound to the variance (5) of any arbitrary estimator. The Cramér-Rao bound is one of the most important results in parameter-estimation theory. For

[2]In a simple scenario, μ is the eigenvalue of an observable. In a more general situation, the measurement is described by a positive-operator-values measure (POVM). A POVM is a set of Hermitian operators $\{\hat{E}(\mu)\}$ parametrized by μ (Nielsen and Chuang, 2000) that are positive, $\hat{E}(\mu)\geq 0$, to guarantee non-negative probabilities $P(\mu|\theta)=\mathrm{Tr}[\hat{\rho}_\theta\hat{E}(\mu)]\geq 0$, and satisfy $\sum_\mu\hat{E}(\mu)=\mathbb{1}$, to ensure normalization $\sum_\mu P(\mu|\theta)=1$.

an unbiased estimator and ν independent measurements, the Cramér-Rao bound reads

$$\Delta\theta \geq \Delta\theta_{\mathrm{CR}} = \frac{1}{\sqrt{\nu F(\theta)}}, \tag{6}$$

where

$$F(\theta) = \sum_{\mu} \frac{1}{P(\mu|\theta)} \left(\frac{\partial P(\mu|\theta)}{\partial\theta}\right)^2 \tag{7}$$

is the Fisher information (Fisher, 1922, 1925), the sum extending over all possible values of μ. The factor $1/\sqrt{\nu}$ in Eq. (6) is the statistical improvement when performing independent measurements on identical copies of the probe state. The Cramér-Rao bound assumes mild differentiability properties of the likelihood function $P(\boldsymbol{\mu}|\theta)$ and thus holds under very general conditions[3]; see, for instance, Kay (1993). No general unbiased estimator is known for small ν. In the central limit $\nu \gg 1$ at least one efficient and unbiased estimator exists in general: the maximum of the likelihood; see Sec. II.B.5.

2. Lower bound to the Fisher information

A lower bound to the Fisher information can be obtained from the rate of change with θ of specific moments of the probability distribution (Pezzè and Smerzi, 2009):

$$F(\theta) \geq \frac{1}{(\Delta\mu)^2} \left(\frac{d\bar{\mu}}{d\theta}\right)^2, \tag{8}$$

where $\bar{\mu} = \sum_{\mu} P(\mu|\theta)\mu$, and $(\Delta\mu)^2 = \sum_{\mu} P(\mu|\theta)(\mu - \bar{\mu})^2$. The Fisher information is larger because it takes into account the change with θ of the full probability distribution, rather than some moments.

Lower bounds to the Fisher information can also be obtained from reduced probability distributions. These are useful, for instance, when estimating the phase shift encoded in a many-body distribution from the reduced one-body density, e.g., from the intensity of a spatial interference pattern (Chwedeńczuk *et al.*, 2012). One finds

$$F(\theta) \geq \frac{N F_1(\theta)}{1 + (N-1)C/F_1(\theta)}, \tag{9}$$

where

$$F_1(\theta) = \int dx \frac{1}{P_1(x|\theta)} \left(\frac{dP_1(x|\theta)}{d\theta}\right)^2$$

is the Fisher information corresponding to the one-body density $P_1(x|\theta)$, and the coefficient

$$C = \int dx_1 \int dx_2 \frac{P_2(x_1, x_2|\theta)}{P_1(x_1|\theta)P_1(x_2|\theta)} \frac{dP_1(x_1|\theta)}{d\theta} \frac{dP_1(x_2|\theta)}{d\theta} \tag{10}$$

further depends on the two-body density $P_2(x_1, x_2|\theta)$. Note that $C = 0$ in the absence of correlations, namely, $P_2(x_1, x_2|\theta) = P_1(x_1|\theta)P_1(x_2|\theta)$, and in this case Eq. (9) reduces to $F(\theta) \geq N F_1(\theta)$.

3. Upper bound to the Fisher information: The quantum Fisher information

An upper bound to the Fisher information is obtained by maximizing Eq. (7) over all possible generalized measurements in quantum mechanics (Braunstein and Caves, 1994), $F_{\mathrm{Q}}[\hat{\rho}_\theta] = \max_{\{\hat{E}\}} F(\theta)$, called the quantum Fisher information (see footnote [2] for the notion of generalized measurements and their connection to conditional probabilities). We have $F(\theta) \leq F_{\mathrm{Q}}[\hat{\rho}_\theta]$, and the corresponding bound on the phase sensitivity for unbiased estimators and ν independent measurements is

$$\Delta\theta_{\mathrm{CR}} \geq \Delta\theta_{\mathrm{QCR}} = \frac{1}{\sqrt{\nu F_{\mathrm{Q}}[\hat{\rho}_\theta]}}, \tag{11}$$

called the quantum Cramér-Rao bound (Helstrom, 1967). The quantum Fisher information and the quantum Cramér-Rao bound allow one to calculate the optimal phase sensitivity of any given probe state and interferometer transformation; for recent reviews, see Paris (2009), Giovannetti, Lloyd, and Maccone (2011), Pezzè and Smerzi (2014), and Tóth and Apellaniz (2014). The quantum Fisher information can be expressed as the variance $F_{\mathrm{Q}}[\hat{\rho}_\theta] = (\Delta\hat{L})^2$ of a θ-dependent Hermitian operator $\hat{L}$ called the symmetric logarithmic derivative and defined by $\partial_\theta\hat{\rho}_\theta = (\hat{\rho}_\theta\hat{L} + \hat{L}\hat{\rho}_\theta)/2$ (Helstrom, 1967, 1976; Holevo, 1982). A general expression of the quantum Fisher information can be found in terms of the spectral decomposition of the output state $\hat{\rho}_\theta = \sum_\kappa q_\kappa |\kappa\rangle\langle\kappa|$ where both the eigenvalues $q_\kappa \geq 0$ and the associated eigenvectors $|\kappa\rangle$ depend on θ (Braunstein and Caves, 1994; Braunstein, Caves, and Milburn, 1996):

$$F_{\mathrm{Q}}[\hat{\rho}_\theta] = \sum_{\substack{\kappa,\kappa' \\ q_\kappa + q_{\kappa'} > 0}} \frac{2}{q_\kappa + q_{\kappa'}} |\langle\kappa'|\partial_\theta\hat{\rho}_\theta|\kappa\rangle|^2, \tag{12}$$

showing that $F_{\mathrm{Q}}[\hat{\rho}_\theta]$ depends solely on $\hat{\rho}_\theta$ and its first derivative $\partial_\theta\hat{\rho}_\theta$. This equation can also be rewritten as

$$F_{\mathrm{Q}}[\hat{\rho}_\theta] = \sum_{\kappa} \frac{(\partial_\theta q_\kappa)^2}{q_\kappa} + 2 \sum_{\substack{\kappa,\kappa' \\ q_\kappa + q_{\kappa'} > 0}} \frac{(q_\kappa - q_{\kappa'})^2}{q_\kappa + q_{\kappa'}} |\langle\kappa'|\partial_\theta\kappa\rangle|^2. \tag{13}$$

The first term quantifies the information about θ encoded in q_κ and corresponds to the Fisher information obtained when projecting over the eigenstates of $\hat{\rho}_\theta$. The second term accounts for the change of eigenstates with θ (we indicate $|\partial_\theta\kappa\rangle \equiv \partial_\theta|\kappa\rangle$). For pure states, $\hat{\rho}_\theta = |\psi_\theta\rangle\langle\psi_\theta|$, the first term in Eq. (13)

[3]The Cramér-Rao theorem follows from $\sum_{\boldsymbol{\mu}} \partial_\theta P(\boldsymbol{\mu}|\theta) = 0$ that implies $\partial_\theta\bar{\Theta} = \sum_{\boldsymbol{\mu}} [\Theta(\boldsymbol{\mu}) - \bar{\Theta}]\partial_\theta P(\boldsymbol{\mu}|\theta)$, and the Cauchy-Schwarz inequality $(\partial_\theta\bar{\Theta})^2 \leq (\Delta\theta)^2 \sum_{\boldsymbol{\mu}} P(\boldsymbol{\mu}|\theta)[\partial_\theta \log P(\boldsymbol{\mu}|\theta)]^2$. The equality is obtained if and only if $\partial_\theta \log P(\boldsymbol{\mu}|\theta) = \lambda[\Theta(\boldsymbol{\mu}) - \bar{\Theta}]$ with λ independent on $\boldsymbol{\mu}$. Equation (6) is recovered when $\partial_\theta\bar{\Theta} = 1$, using the additivity of the Fisher information $\sum_{\boldsymbol{\mu}} P(\boldsymbol{\mu}|\theta)[\partial_\theta \log P(\boldsymbol{\mu}|\theta)]^2 = \nu F(\theta)$.

vanishes, while the second term simplifies to $F_Q[|\psi_\theta\rangle] = 4(\langle\partial_\theta\psi_\theta|\partial_\theta\psi_\theta\rangle - |\langle\partial_\theta\psi_\theta|\psi_\theta\rangle|^2)$.

For unitary transformations generated by some Hermitian operator $\hat{H}$, we have $\partial_\theta\hat{\rho}_\theta = i[\hat{\rho}_\theta, \hat{H}]$, and Eq. (13) becomes[4] (Braunstein and Caves, 1994; Braunstein, Caves, and Milburn, 1996)

$$F_Q[\hat{\rho}_0, \hat{H}] = 2\sum_{\substack{\kappa,\kappa' \\ q_\kappa + q_{\kappa'} > 0}} \frac{(q_\kappa - q_{\kappa'})^2}{q_\kappa + q_{\kappa'}} |\langle\kappa'|\hat{H}|\kappa\rangle|^2. \tag{14}$$

For pure states $|\psi_0\rangle$, Eq. (14) reduces to $F_Q[|\psi_0\rangle, \hat{H}] = 4(\Delta\hat{H})^2$. For mixed states, $F_Q[\hat{\rho}_0, \hat{H}] \leq 4(\Delta\hat{H})^2$. It is worth recalling here that $4(\Delta\hat{H})^2 \leq (h_{\max} - h_{\min})^2$, where $h_{\max}$ and $h_{\min}$ are the maximum and minimum eigenvalues of $\hat{H}$ with eigenvectors $|h_{\max}\rangle$ and $|h_{\min}\rangle$, respectively. This bound is saturated by the states $(|h_{\max}\rangle + e^{i\phi}|h_{\min}\rangle)/\sqrt{2}$, with arbitrary real ϕ, which are optimal input states for noiseless quantum metrology (Giovannetti, Lloyd, and Maccone, 2006). In the presence of noise, the search for optimal quantum states is less straightforward as discussed in Sec. VII.A.

a. Convexity and additivity

The quantum Fisher information is convex in the state:

$$F_Q[p\hat{\rho}_\theta^{(1)} + (1-p)\hat{\rho}_\theta^{(2)}] \leq pF_Q[\hat{\rho}_\theta^{(1)}] + (1-p)F_Q[\hat{\rho}_\theta^{(2)}], \tag{15}$$

with $0 \leq p \leq 1$. This expresses the fact that mixing quantum states cannot increase the achievable estimation sensitivity. The inequality (15) can be proved using the convexity of the Fisher information (Cohen, 1968; Pezzè and Smerzi, 2014).

The quantum Fisher information of independent subsystems is additive:

$$F_Q[\hat{\rho}_\theta^{(1)} \otimes \hat{\rho}_\theta^{(2)}] = F_Q[\hat{\rho}_\theta^{(1)}] + F_Q[\hat{\rho}_\theta^{(2)}]. \tag{16}$$

In particular, for an m-fold tensor product $\hat{\rho}_\theta^{\otimes m}$ we obtain an m-fold increase of the quantum Fisher information, $F_Q[\hat{\rho}_\theta^{\otimes m}] = mF_Q[\hat{\rho}_\theta]$. A demonstration of Eq. (16) can be found for instance in Pezzè and Smerzi (2014).

b. Optimal measurements

The equality $F(\theta) = F_Q[\hat{\rho}_\theta]$ can always be achieved by optimizing over all possible measurements. An optimal choice of measurement for both pure and mixed states is given by the set of projectors onto the eigenstates of $\hat{L}$ (Braunstein and Caves, 1994). This set of observables is necessary and sufficient for the saturation of the quantum Fisher information whenever $\hat{\rho}_\theta$ is invertible and only sufficient otherwise. In particular, for pure states and unitary transformations, the quantum Fisher information can be saturated, in the limit $\theta \to 0$, by a dichotomic measurement given by the projection onto the probe state itself $|\psi_0\rangle\langle\psi_0|$ and onto the orthogonal subspace $\mathbb{1} - |\psi_0\rangle\langle\psi_0|$ (Pezzè and Smerzi, 2014). It should be noted that the symmetric logarithmic derivative, and thus also the optimal measurement, generally depends on θ, even for unitary transformations. Nevertheless, without any prior knowledge of θ, the quantum Cramér-Rao bound can be saturated in the asymptotic limit of large ν using adaptive schemes (Hayashi, 2005; Fujiwara, 2006).

c. Optimal rotation direction

Given a probe state, and considering a unitary transformation generated by $\hat{H} = \hat{J}_{\boldsymbol{n}}$, it is possible to optimize the rotation direction $\boldsymbol{n}$ in order to maximize the quantum Fisher information (Hyllus, Gühne, and Smerzi, 2010). This optimum is given by the maximum eigenvalue of the 3×3 matrix

$$[\boldsymbol{\Gamma}_Q]_{ij} = 2\sum_{\substack{\kappa,\kappa' \\ q_\kappa + q_{\kappa'} > 0}} \frac{(q_\kappa - q_{\kappa'})^2}{q_\kappa + q_{\kappa'}} \langle\kappa'|\hat{J}_i|\kappa\rangle\langle\kappa|\hat{J}_j|\kappa'\rangle, \tag{17}$$

with $i, j = x, y, z$, and the optimal direction by the corresponding eigenvector. For pure states $[\boldsymbol{\Gamma}_Q]_{ij} = 2(\langle\hat{J}_i\hat{J}_j\rangle + \langle\hat{J}_j\hat{J}_i\rangle) - 4\langle\hat{J}_i\rangle\langle\hat{J}_j\rangle$.

4. Phase sensitivity and statistical distance

Parameter estimation is naturally related to the problem of distinguishing neighboring quantum states along a path in the parameter space (Wootters, 1981; Braunstein and Caves, 1994). Heuristically, the phase sensitivity of an interferometer can be understood as the smallest phase shift for which the output state $\hat{\rho}_\theta$ of the interferometer can be distinguished from the input $\hat{\rho}_0$. We introduce a statistical distance between probability distributions,

$$d_H^2(P_0, P_\theta) = 1 - \mathcal{F}_{cl}(P, P_\theta), \tag{18}$$

called the Hellinger distance, where $\mathcal{F}_{cl}(P_0, P_\theta) \equiv \sum_\mu \sqrt{P(\mu|0)P(\mu|\theta)}$ is the statistical fidelity, or overlap, between probability distributions, also known as the Bhattacharyya coefficient (Bhattacharyya, 1943). d_H is nonnegative, $0 \leq d_H \leq 1$, and its Taylor expansion reads

$$d_H^2(P_0, P_\theta) = \frac{F(0)}{8}\theta^2 + \mathcal{O}(\theta^3). \tag{19}$$

This equation reveals that the Fisher information is the square of a statistical speed $v_H = \partial d_H/\partial\theta = \sqrt{F(0)/8}$. It measures the rate at which a probability distribution varies when tuning the phase parameter θ. Equation (19) has been used to extract the Fisher information experimentally (Strobel *et al.*, 2014); see Sec. III.C. As Eq. (18) depends on the specific measurement, it is possible to associate different statistical distances to the same quantum states. This justifies the introduction of a distance between quantum states by maximizing $d_H^2(P_0, P_\theta)$ over all possible generalized measurements (i.e., over all POVM sets, see footnote [2]), $d_B^2(\hat{\rho}_0, \hat{\rho}_\theta) = \max_{\{\hat{E}\}} d_H^2(P_0, P_\theta)$ (Fuchs and Caves, 1995), called the Bures distance (Bures, 1969). Hübner (1992) showed that

[4]We use the notation $F_Q[\hat{\rho}_\theta]$ to indicate the quantum Fisher information for a generic transformation of the probe state, and $F_Q[\hat{\rho}_0, \hat{H}]$ for unitary transformations.

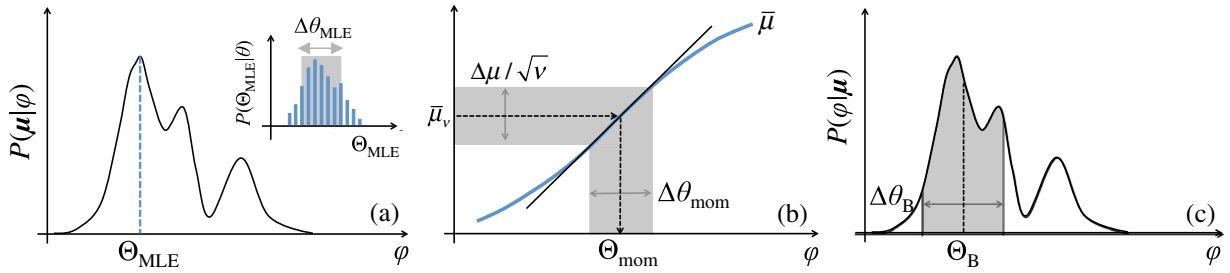

FIG. 4. Schematic representation of different phase estimation protocols. (a) Maximum likelihood estimation. $\Theta_{\rm MLE}(\boldsymbol{\mu})$ is the absolute maximum (dashed line) of the likelihood function $P(\boldsymbol{\mu}|\varphi)$ (solid line) corresponding to the observed sequence of results $\boldsymbol{\mu}$. As schematically shown in the inset, the phase sensitivity $\Delta\theta_{\rm MLE}$ is identified as the root-mean-square fluctuation (shaded region) of the statistical distribution of $\Theta_{\rm MLE}$, obtained by repeating the measurements several times (at a fixed value of θ). (b) Method of moments. The blue line is $\bar{\mu}$ as a function of the parameter φ. Via this functional monotonic behavior, it is possible to associate to the measured mean value $\bar{\mu}_\nu$ the phase estimate $\Theta_{\rm mom}(\boldsymbol{\mu})$. The phase uncertainty $\Delta\theta_{\rm mom}$ follows from the statistical uncertainty $\Delta\mu/\sqrt{\nu}$ of $\bar{\mu}_\nu$ (gray region). For $\nu \gg 1$, $\Delta\theta_{\rm mom}$ has a simple expression, Eq. (23), obtained by error propagation, locally approximating $\bar{\mu}$ by the tangent to the curve (thin black line). (c) Bayesian estimation. Posterior probability distribution $P(\varphi|\boldsymbol{\mu})$ (solid line). The phase estimate $\Theta_{\rm B}(\boldsymbol{\mu})$ can be chosen as the weighted averaged phase. The integral $\int_{\Delta\theta_{\rm B}} d\varphi P(\varphi|\boldsymbol{\mu})$ gives the probability that the true phase value falls into the confidence interval $\Delta\theta_{\rm B}$ (gray region) around $\Theta_{\rm B}$.

$$d_{\rm B}^2(\hat{\rho}_0,\hat{\rho}_\theta) = 1 - \mathcal{F}_{\rm Q}(\hat{\rho}_0,\hat{\rho}_\theta), \tag{20}$$

where $\mathcal{F}_{\rm Q}(\hat{\rho}_0,\hat{\rho}_\theta) = {\rm Tr}[\sqrt{\sqrt{\hat{\rho}_\theta}\hat{\rho}_0\sqrt{\hat{\rho}_\theta}}]$ is the transition probability (Uhlmann, 1976) or the quantum fidelity between states (Jozsa, 1994); see Bengtsson and Zyczkowski (2006) and Spehner (2014) for reviews. Uhlmann's theorem (Uhlmann, 1976) states that $\mathcal{F}_{\rm Q}(\hat{\rho},\hat{\sigma}) = \max_{|\psi\rangle,|\phi\rangle}|\langle\psi|\phi\rangle|$, where the maximization runs over all purifications $|\psi\rangle$ of $\hat{\rho}$ and $|\phi\rangle$ of $\hat{\sigma}$ (Nielsen and Chuang, 2000). In particular, $\mathcal{F}_{\rm Q}(|\psi\rangle,|\phi\rangle) = |\langle\psi|\phi\rangle|$ for pure states. A Taylor expansion of Eq. (20) for small θ gives

$$d_{\rm B}^2(\hat{\rho}_0,\hat{\rho}_\theta) = \frac{F_{\rm Q}[\hat{\rho}_0]}{8}\theta^2 + \mathcal{O}(\theta^3). \tag{21}$$

The quantum Fisher information is thus the square of a quantum statistical speed $v_{\rm Q} = \partial d_{\rm B}/\partial\theta = \sqrt{F_{\rm Q}[\hat{\rho}_0]/8}$, maximized over all possible generalized measurements. The quantum Fisher information has also been related to the dynamical susceptibility (Hauke *et al.*, 2016), while bounds have been derived by Frérot and Roscilde (2016) and Apellaniz *et al.* (2017).

5. The maximum likelihood estimator

The maximum likelihood estimator (MLE) is the phase value that maximizes the likelihood of the observed measurement sequence $\boldsymbol{\mu}$; see Fig. 4(a): $\Theta_{\rm MLE}(\boldsymbol{\mu}) = {\rm argmax}_\varphi P(\boldsymbol{\mu}|\varphi)$. The key role played by $\Theta_{\rm MLE}(\boldsymbol{\mu})$ in parameter estimation is due to its asymptotic properties for independent measurements. For sufficiently large ν, the distribution of the maximum likelihood estimator tends to a Gaussian centered at the true value θ and of variance equal to the inverse Fisher information (Lehmann and Casella, 2003):

$$P(\Theta_{\rm MLE}|\theta) = \sqrt{\frac{\nu F(\theta)}{2\pi}}e^{-[\nu F(\theta)/2](\theta-\Theta_{\rm MLE})^2}. \tag{22}$$

Therefore, the maximum likelihood estimator is asymptotically unbiased and its variance saturates the Cramér-Rao bound $\Delta\theta_{\rm MLE} = 1/\sqrt{\nu F(\theta)}$. In the central limit, any estimator is as good as, or worse than, the maximum likelihood estimate.

6. Method of moments

The method of moments exploits the variation with the phase shift θ of collective properties of the probability distribution, such as the mean value $\bar{\mu}$ and variance $(\Delta\mu)^2$. Let us take the average $\bar{\mu}_\nu = (1/\nu)\sum_{i=1}^{\nu}\mu_i$ of ν measurements results $\mu_1,\ldots,\mu_\nu$. The estimator $\Theta_{\rm mom}$ is the value for which $\bar{\mu}$ is equal to $\bar{\mu}_\nu$; see Fig. 4(b). Applying this method requires $\bar{\mu}$ to be a monotonous function of the parameter θ at least in a local region of parameter values determined from prior knowledge. The sensitivity of this estimator can be calculated by error propagation[5] giving

$$\Delta\theta_{\rm mom} = \frac{\Delta\mu}{\sqrt{\nu}|d\bar{\mu}/d\theta|}. \tag{23}$$

As expected on general grounds and proved by Eq. (8), the method of moments is not optimal in general, $\Delta\theta_{\rm mom} \leq \Delta\theta_{\rm CR}$, with no guarantee of saturation even in the central limit. The equality $\Delta\theta_{\rm mom} = \Delta\theta_{\rm CR}$ is obtained when the probability distribution is Gaussian,

$$P(\mu|\theta) = \frac{e^{-(\mu-\bar{\mu})^2/[2(\Delta\mu)^2]}}{\sqrt{2\pi(\Delta\mu)^2}}, \tag{24}$$

and $d(\Delta\mu)/d\theta \ll d\bar{\mu}/d\theta$, such that the changes of the complete probability distribution are fully captured by the shift of its mean value (Pezzè and Smerzi, 2014).

[5]A Taylor expansion of $\bar{\mu}_\nu$ around the true value θ gives $\bar{\mu}_\nu \approx \bar{\mu} + (d\bar{\mu}/d\theta)(\Theta_{\rm mom} - \theta)$. We obtain Eq. (23) by identifying $\bar{\mu}_\nu - \bar{\mu} \approx \Delta\mu/\sqrt{\nu}$ (valid for $\nu \gg 1$) and $\Theta_{\rm mom} - \theta \approx \Delta\theta_{\rm mom}$.

Nevertheless, due to its simplicity, Eq. (23) is largely used in the literature to calculate the phase sensitivity of an interferometer for various input states and measurement observables (Yurke, McCall, and Klauder, 1986; Wineland *et al.*, 1994; Dowling, 1998). For instance, in the case of unitary rotations generated by $\hat{H}=\hat{J}_y$ (as in Ramsey and Mach-Zehnder interferometers) and taking $\hat{J}_z$ as a measurement observable, Eq. (23) in the limit $\theta\approx 0$ can be rewritten as

$$\Delta\theta_{\rm mom}=\frac{\Delta\hat{J}_z}{\sqrt{\nu}|\langle\hat{J}_x\rangle|}. \tag{25}$$

This equation is useful to introduce the concept of metrological spin squeezing; see Sec. II.C.5. We recall that Eqs. (23) and (25) are valid for a sufficiently large number of measurements.

Finally, there are many examples in the literature where a small $\Delta\theta_{\rm mom}$ is obtained for phase values where $\Delta\mu,\ d\bar{\mu}/d\theta\to 0$, while the ratio $\Delta\mu/|d\bar{\mu}/d\theta|$ remains finite (Yurke, McCall, and Klauder, 1986; Kim *et al.*, 1998). These "sweet spots" are very sensitive to technical noise: an infinitesimal amount of noise may prevent $\Delta\mu$ from vanishing, while leaving unchanged $d\bar{\mu}/d\theta$, such that $\Delta\theta_{\rm mom}$ diverges (Lücke *et al.*, 2011).

7. Bayesian estimation

The cornerstone of Bayesian inference is Bayes's theorem. Let us consider two random variables x and y. Their joint probability density can be expressed as $P(x,y)=P(x|y)P(y)$ in terms of the conditional probability $P(x|y)$ and the marginal probability distribution $P(y)=\int dx P(x,y)$. Bayes's theorem

$$P(x|y)=\frac{P(y|x)P(x)}{P(y)} \tag{26}$$

follows from the symmetry of the joint probability $P(x,y)=P(y|x)P(x)$.

We recall that, in a phase inference problem, the set of measurement results $\boldsymbol{\mu}$ is generated by a fixed and unknown value θ according to the likelihood $P(\boldsymbol{\mu}|\theta)$. In the Bayesian approach to the estimation of θ one introduces a random variable φ and uses the Bayes's theorem to define the posterior probability $P(\varphi|\boldsymbol{\mu})=P(\boldsymbol{\mu}|\varphi)P(\varphi)/P(\boldsymbol{\mu})$. $P(\varphi)$ is the prior probability distribution that quantifies our (*a priori*) ignorance of the true value of the interferometric phase, i.e., before any measurements were done. One often has no prior knowledge of the phase (maximum ignorance), which is expressed by a flat prior distribution $P(\varphi)=1/(2\pi)$. Bayes's theorem allows one to update our knowledge about the interferometric phase θ by including measurement results, since $P(\boldsymbol{\mu}|\varphi)$ can be calculated directly (see the introduction of Sec. II.B) and $P(\boldsymbol{\mu})$ is determined by the normalization $\int_0^{2\pi}P(\varphi|\boldsymbol{\mu})d\varphi=1$. The posterior probability $P(\varphi|\boldsymbol{\mu})$ provides a degree of belief, or plausibility, that $\varphi=\theta$ (i.e., that φ is the true value of the phase), in the light of the measurement data $\boldsymbol{\mu}$. This is radically different from the standard frequentist view where the probability is defined as the infinite-sample limit of the outcome frequency of an observed event. Having the posterior distribution $P(\varphi|\boldsymbol{\mu})$, we can consider any phase φ as the estimate; see Fig. 4(c). In practice, it is convenient to choose the weighted averaged $\int_0^{2\pi}\varphi P(\varphi|\boldsymbol{\mu})d\varphi$, or the phase corresponding to the maximum of the probability $\mathrm{argmax}_\varphi P(\varphi|\boldsymbol{\mu})$, since the corresponding mean square fluctuations saturate the Cramér-Rao bound (see later). We can further calculate the probability that the chosen estimate falls into a certain interval $[\theta_1,\theta_2]$ by integrating $\int_{\theta_1}^{\theta_2}P(\varphi|\boldsymbol{\mu})d\varphi$. To take into account the periodicity of the probability, quantities such as $\int_0^{2\pi}e^{i\varphi}P(\varphi|\boldsymbol{\mu})d\varphi$ can be calculated. Remarkably, Bayesian estimation is asymptotically consistent: as the number of measurements increases, the posterior probability distribution assigns more weight in the vicinity of the true value. The Laplace-Bernstein–von Mises theorem (Lehmann and Casella, 2003; Gill, 2008; Pezzè and Smerzi, 2014) demonstrates that, under quite general conditions,

$$P(\varphi|\theta)=\sqrt{\frac{\nu F(\theta)}{2\pi}}e^{-[\nu F(\theta)/2](\theta-\varphi)^2}, \tag{27}$$

to leading order in ν, for $\nu\gg 1$. In this limit, the posterior probability becomes normally distributed, centered at the true value of the parameter, and with a variance inversely proportional to the Fisher information. See Van Trees and Bell (2007) and Li *et al.* (2018) for an overview of bounds in Bayesian phase estimation.

C. Entanglement and phase sensitivity

In this section we show how entanglement can offer a precision enhancement in quantum metrology. We start with the formal definition of multiparticle entanglement and then clarify, via the Fisher information introduced in the previous section, the notion of useful entanglement for quantum metrology.

1. Multiparticle entanglement

Let us consider a system of N particles (labeled as $l=1,2,\ldots,N$), each particle realizing a qubit. A pure quantum state is separable in the particles if it can be written as a product

$$|\psi_{\rm sep}\rangle=|\psi^{(1)}\rangle\otimes|\psi^{(2)}\rangle\otimes\cdots\otimes|\psi^{(N)}\rangle, \tag{28}$$

where $|\psi^{(l)}\rangle$ is the state of the lth qubit. A mixed state is separable if it can be written as a mixture of product states (Werner, 1989),

$$\hat{\rho}_{\rm sep}=\sum_q p_q|\psi_{{\rm sep},q}\rangle\langle\psi_{{\rm sep},q}|, \tag{29}$$

with $p_q\geq 0$ and $\sum_q p_q=1$. States that are not separable are called entangled (Gühne and Tóth, 2009; Horodecki *et al.*, 2009). In the case of $N=2$ particles, any quantum state is either separable or entangled. For $N>2$, we need further classifications (Dür, Vidal, and Cirac, 2000). Multiparticle

entanglement is quantified by the number of particles in the largest nonseparable subset. In analogy with Eq. (28), a pure state of N particles is k separable (also indicated as k producible in the literature) if it can be written as

$$|\psi_{k\ \mathrm{sep}}\rangle = |\psi_{N_1}\rangle \otimes |\psi_{N_2}\rangle \otimes \cdots \otimes |\psi_{N_M}\rangle, \tag{30}$$

where $|\psi_{N_l}\rangle$ is a state of $N_l \leq k$ particles and $\sum_{l=1}^{M} N_l = N$. A mixed state is k separable if it can be written as a mixture of k-separable pure states (Gühne, Tóth, and Briegel, 2005)

$$\hat{\rho}_{k\ \mathrm{sep}} = \sum_q p_q |\psi_{k\ \mathrm{sep},q}\rangle\langle\psi_{k\ \mathrm{sep},q}|. \tag{31}$$

A state that is k separable but not $(k-1)$ separable is called k-particle entangled: it contains at least one state of k particles that does not factorize. Using another terminology (Sørensen and Mølmer, 2001), it has an entanglement depth larger than $k-1$. In maximally entangled states ($k = N$) each particle is entangled with all the others. Finally, note that k-separable states form a convex set containing the set of k'-separable states with $k' < k$ (Gühne and Tóth, 2009).

2. Sensitivity bound for separable states: The standard quantum limit

The quantum Fisher information of any separable state of N qubits is upper bounded (Pezzè and Smerzi, 2009):

$$F_{\mathrm{Q}}[\hat{\rho}_{\mathrm{sep}}, \hat{J}_{\boldsymbol{n}}] \leq N. \tag{32}$$

This inequality follows from the convexity and additivity of the quantum Fisher information and uses $4(\Delta\hat{\sigma}_{\boldsymbol{n}})^2 \leq 1$ (Pezzè and Smerzi, 2014). As a consequence of Eqs. (11) and (32), the maximum phase sensitivity achievable with separable states is (Giovannetti, Lloyd, and Maccone, 2006)

$$\Delta\theta_{\mathrm{SQL}} = \frac{1}{\sqrt{N\nu}}, \tag{33}$$

generally indicated as the shot noise or standard quantum limit. This bound is independent of the specific measurement and estimator and refers to unitary collective transformations that are local in the particles. In Eq. (33) N and ν play the same role: repeating the phase estimation ν times with one particle has the same sensitivity bound as repeating the phase estimation 1 time with $N = \nu$ particles in a separable state.

3. Coherent spin states

The notion of coherent spin states was introduced by Radcliffe (1971) and Arecchi *et al.* (1972) as a generalization of the field coherent states first discussed by Glauber (1963); see Zhang, Feng, and Gilmore (1990) for a review. Coherent spin states are constructed as the product of N qubits (spins $1/2$) in pure states all pointing along the same mean spin direction $\boldsymbol{s} = \{\sin\vartheta\cos\varphi, \sin\vartheta\sin\varphi, \cos\vartheta\}$:

$$|\vartheta, \varphi, N\rangle = \bigotimes_{l=1}^{N} \left[\cos\frac{\vartheta}{2}|a\rangle_l + e^{i\varphi}\sin\frac{\vartheta}{2}|b\rangle_l\right]. \tag{34}$$

Equation (34) is the eigenstate of $\hat{J}_{\boldsymbol{s}}$ with the maximum eigenvalue of $N/2$. The coherent spin state is a product state and no quantum entanglement is present between the qubits. $|\vartheta, \varphi, N\rangle$ can also be written as a binomial sum of Dicke states with (Arecchi *et al.*, 1972)

$$\langle m_z|\vartheta, \varphi, N\rangle = \sqrt{\binom{N}{N/2+m}}\left(\cos\frac{\vartheta}{2}\right)^{N/2-m}\left(\sin\frac{\vartheta}{2}\right)^{N/2+m} \times e^{-i(m+N/2)\varphi}. \tag{35}$$

When measuring the spin component of $|\vartheta, \varphi, N\rangle$ along any direction $\perp$ orthogonal to $\boldsymbol{s}$, each individual atom is projected with equal probability into the up and down eigenstates along this axis, with eigenvalues $\pm 1/2$, respectively: we thus have $\langle\hat{J}_{\perp}\rangle = 0$, and $(\Delta\hat{J}_{\perp})^2 = N/4$ (Yurke, McCall, and Klauder, 1986; Itano *et al.*, 1993).

Coherent spin states are optimal separable states for metrology. They saturate the equality sign in Eq. (32) and thus reach the standard quantum limit. Let us consider the rotation of $|\vartheta, \varphi, N\rangle$ around a direction $\boldsymbol{n}$ perpendicular to the mean spin direction $\boldsymbol{s}$ (here $\boldsymbol{s}$, $\boldsymbol{n}$, and $\perp$ are mutually orthogonal). This rotation displaces the coherent spin state on the surface of the Bloch sphere; see Fig. 5(a). The initial and final states become distinguishable after rotating by an angle θ_{min} heuristically giving the phase sensitivity of the state. This rotation angle can be obtained from a geometric reasoning (Yurke, McCall, and Klauder, 1986): we have $\Delta\hat{J}_{\perp} \approx \langle\hat{J}_{\boldsymbol{s}}\rangle \sin\theta_{\mathrm{min}}$, giving $\theta_{\mathrm{min}} \approx 1/\sqrt{N}$ for $N \gg 1$. More rigorously, the squared Bures distance, Eq. (20), between $|\vartheta, \varphi, N\rangle$ and the rotated $e^{-i\theta\hat{J}_{\boldsymbol{n}}}|\vartheta, \varphi, N\rangle$ is

$$d_{\mathrm{B}}^2(|\vartheta, \varphi, N\rangle, e^{-i\theta\hat{J}_{\boldsymbol{n}}}|\vartheta, \varphi, N\rangle) = 1 - \cos^N(\theta/2), \tag{36}$$

that is, $d_{\mathrm{B}}^2 = N\theta^2/8 + \mathcal{O}(\theta^4)$ for small values of θ. According to Eq. (21) we obtain a quantum Fisher information $F_{\mathrm{Q}}[|\vartheta, \varphi, N\rangle, \hat{J}_{\boldsymbol{n}}] = 4(\Delta\hat{J}_{\boldsymbol{n}})^2 = N$. With the method of moments, Eq. (25), we find a phase sensitivity $\Delta\theta_{\mathrm{mom}} = \Delta\hat{J}_{\perp}/(\sqrt{\nu}|\langle\hat{J}_{\boldsymbol{s}}\rangle|) = 1/\sqrt{\nu N}$ (Yurke, McCall, and Klauder, 1986; Itano *et al.*, 1993): while $|\langle\hat{J}_{\boldsymbol{s}}\rangle| = N/2$ reaches its maximum value, it is the quantum projection noise of uncorrelated atoms $(\Delta\hat{J}_{\perp})^2 = N/4$ that limits the achievable sensitivity (Wineland *et al.*, 1992, 1994; Itano *et al.*, 1993). For any rotation around an axis orthogonal to the mean spin direction, coherent spin states thus satisfy $\Delta\theta_{\mathrm{QCR}} = \Delta\theta_{\mathrm{SQL}}$.

4. Useful entanglement for quantum metrology

The violation of Eq. (32), i.e.,

$$F_{\mathrm{Q}}[\hat{\rho}, \hat{J}_{\boldsymbol{n}}] > N, \tag{37}$$

is a sufficient condition for particle entanglement in the state $\hat{\rho}$. To be more precise, the inequality (37) is the condition of useful entanglement for quantum metrology: it is a necessary and sufficient condition for a quantum state to be useful in the estimation of a phase shift θ, with an interferometer implementing the transformation $e^{-i\theta\hat{J}_{\boldsymbol{n}}}$, with a

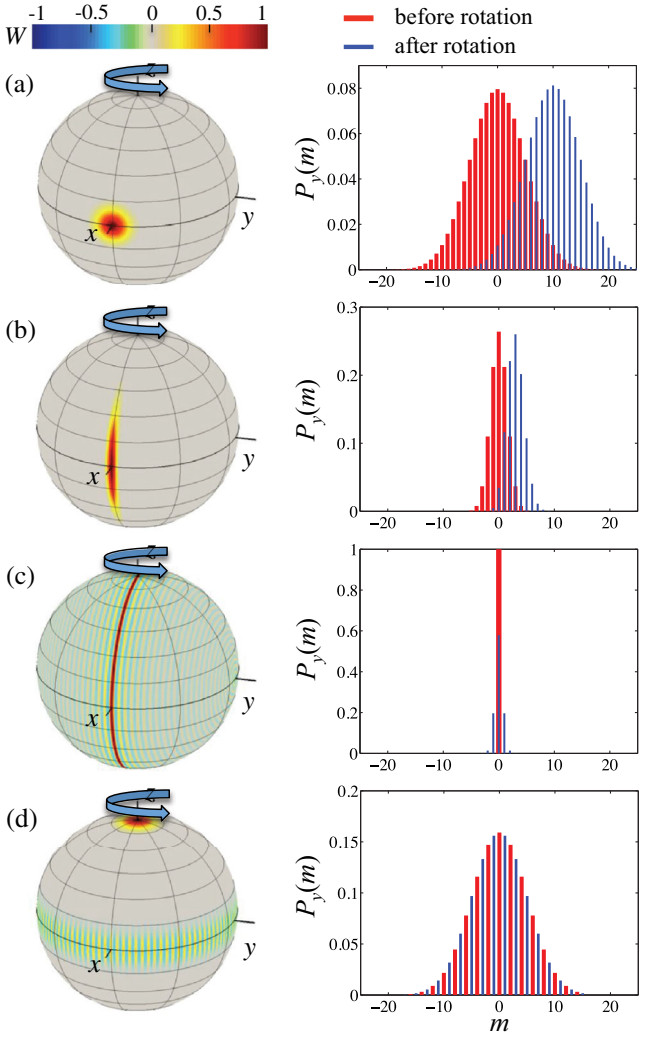

FIG. 5. Rotation of different quantum states. Wigner distribution normalized by its maximum value (left column), see Sec. II.D, and spin probability $P_y(m) = |\langle m_y|\psi\rangle|^2$ along the y direction (thick red histograms, right column) of different quantum states $|\psi\rangle$: (a) a coherent spin state pointing along the positive x axis, $|\pi/2, 0, N\rangle$ (Sec. II.C.3); (b) a spin-squeezed state with $\xi_R^2 = 0.1$ (Sec. II.C.5); (c) a twin-Fock state (Sec. II.C.6); and (d) a NOON state (Sec. II.C.7). The thin blue histogram is $P_y(m) = |\langle m_y|e^{-i\theta\hat{J}_z}|\psi\rangle|^2$ obtained after a rotation of the state by an angle $\theta = 2/\sqrt{N}$ in (a), $\theta = 2\xi_R/\sqrt{N}$ in (b), $\theta = 2/N$ in (c), and $\theta = \pi/N$ in (d). Here $N = 100$.

sensitivity overcoming the standard quantum limit (Pezzè and Smerzi, 2009). Not all entangled states are useful for quantum metrology. Yet, useless entangled states for quantum metrology might be useful for other quantum technologies. It should also be noted that not all useful entangled states for quantum metrology are equally useful: large quantum Fisher information requires large entanglement depth. For states of type (31), we have (Hyllus, Laskowski *et al.*, 2012; Tóth, 2012)

$$F_Q[\hat{\rho}_{k\,\mathrm{sep}}, \hat{J}_{\boldsymbol{n}}] \leq \mathfrak{s}k^2 + \mathfrak{r}^2, \tag{38}$$

where $\mathfrak{s} = \lfloor N/k \rfloor$ is the integer part of N/k, and $\mathfrak{r} = N - \mathfrak{s}k$ (note that $\mathfrak{s}k^2 + \mathfrak{r}^2 = Nk$ when N is divisible by k). If the

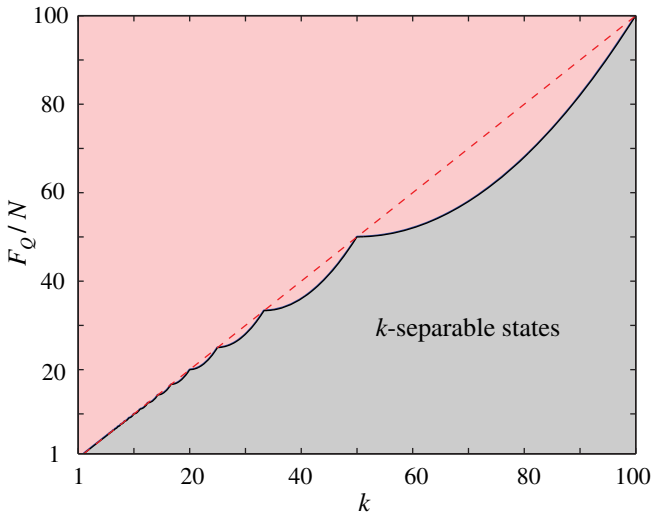

FIG. 6. Useful k-particle entanglement for quantum metrology. k-separable states have a quantum Fisher information bounded by the solid line, Eq. (38). The dashed line is $F_Q/N = k$. Here $N = 100$. Adapted from Hyllus, Laskowski *et al.*, 2012.

bound (38) is surpassed, then the probe state contains metrologically useful $(k+1)$-particle entanglement: when used as an input state of the interferometer defined by the transformation $e^{-i\theta\hat{J}_{\boldsymbol{n}}}$, this state enables a phase sensitivity better than any k-separable state. The bound (38) increases monotonically with k (see Fig. 6), in particular, $F_Q[\hat{\rho}_{k\,\mathrm{sep}}, \hat{J}_{\boldsymbol{n}}] \leq Nk$. The maximum value of the quantum Fisher information is obtained for genuine N-particle entangled states $k = N$ giving (Pezzè and Smerzi, 2009)

$$F_Q[\hat{\rho}, \hat{J}_{\boldsymbol{n}}] \leq N^2. \tag{39}$$

Equation (39) defines the ultimate Heisenberg limit[6] [7] of phase sensitivity (Giovannetti, Lloyd, and Maccone, 2006),

$$\Delta\theta_{\mathrm{HL}} = \frac{1}{N\sqrt{\nu}}. \tag{40}$$

The difference between Eqs. (33) and (40) is a faster scaling of the phase sensitivity with the number of particles, which cannot be obtained by exploiting classical correlations among

[6]The name "Heisenberg limit" was first introduced by Holland and Burnett (1993) referring to the heuristic number-phase Heisenberg uncertainty relation $\Delta\theta\Delta N \geq 1$. We refer to the Heisenberg *scaling* of phase sensitivity when $\Delta\theta = \mathcal{O}(N^{-1})$.

[7]It is possible to maximize the phase sensitivity by optimizing the number of particles N entering into the interferometer multiplied by the times ν that the measurement is performed (Braunstein, Lane, and Caves, 1992; Lane, Braunstein, and Caves, 1993; Pezzè, 2013). This provides a definition of Heisenberg limit $1/N_T$, where $N_T = N\nu_{\mathrm{opt}}$, and ν_{opt} is the optimal number of measurements that maximize the phase sensitivity for a fixed number of particles N. Since ν_{opt} may depend on N, there might be, in principle, states having a Fisher information larger than N but a phase sensitivity above the standard quantum limit $1/\sqrt{N_T}$.

the qubits. Still the standard quantum limit can be surpassed using separable states at the expense of other resources (Giovannetti, Lloyd, and Maccone, 2006) such as, for instance, exploiting a multiround protocol (Higgins *et al.*, 2007).

We note that the quantum Fisher information is bounded by $F_Q[\hat{\rho}, \hat{J}_{\boldsymbol{n}}] \leq 4(\Delta\hat{J}_{\boldsymbol{n}})^2 \leq (2J)^2 \leq N^2$, where $\sqrt{J(J+1)}$ is the spin length. This shows that the most sensitive states lie in a subspace with maximum spin $J = N/2$, namely, those symmetric under particle exchange (see Sec. II.A).

Equations (33) and (40) can be generalized to transformations $e^{-i\theta\sum_{l=1}^{N}\hat{h}^{(l)}}$, where $\hat{h}^{(l)}$ is an arbitrary local Hamiltonian for the lth particles (that can be a generic qudit). Taking $\hat{h}^{(l)} = \hat{h}$ for all N particles, we have $\Delta\theta_{\mathrm{SQL}} = 1/(\delta h\sqrt{N\nu})$, and $\Delta\theta_{\mathrm{HL}} = 1/(\delta h N\sqrt{\nu})$ (Giovannetti, Lloyd, and Maccone, 2006), where $\delta h = |h_{\max} - h_{\min}|$, and $h_{\max}$ and $h_{\min}$ are the maximum and minimum eigenvalues of $\hat{h}$, respectively.

We finally note that not all N-particle entangled states reach the Heisenberg limit, as exemplified by the W state $|W\rangle = |(\pm N/2 \mp 1)_z\rangle$, which corresponds to a Dicke state with one excitation. While the W state is N-particle entangled (Dür, Vidal, and Cirac, 2000), its quantum Fisher information amounts only to $3N - 2$.

5. Metrological spin squeezing

Spin-squeezed states are a class of states having squeezed spin variance along a certain direction, at the cost of antisqueezed variance along an orthogonal direction. Spin squeezing is one of the most successful approaches to witness large-scale quantum entanglement beating the standard quantum limit in interferometry.

Let us consider the unitary rotation of a state on the Bloch sphere around an axis $\boldsymbol{n}$ perpendicular to the mean spin direction $\boldsymbol{s}$, see Fig. 5(b), and calculate the phase sensitivity according to the error propagation formula, Eq. (25). We can write $\Delta\theta_{\mathrm{mom}} = \xi_{\mathrm{R}}/\sqrt{\nu N}$,[8] where

$$\xi_{\mathrm{R}}^2 = \frac{N(\Delta\hat{J}_\perp)^2}{\langle\hat{J}_s\rangle^2}, \tag{41}$$

and $\perp$ is orthogonal to both $\boldsymbol{s}$ and $\boldsymbol{n}$. ξ_{R} is the spin-squeezing parameter introduced by Wineland *et al.* (1992, 1994). If $\xi_{\mathrm{R}}^2 < 1$ holds, the state is said to be (metrologically) spin squeezed along the $\perp$ axis (Wineland *et al.*, 1992, 1994) and it can be used to overcome the standard quantum limit (i.e., reaching $\Delta\theta_{\mathrm{mom}} < 1/\sqrt{\nu N}$). This requires states having spin fluctuations orthogonal to the rotation axis smaller than the projection noise of uncorrelated atoms, i.e., $(\Delta\hat{J}_\perp)^2 < N/4$, and sufficiently large spin length $\langle\hat{J}_s\rangle$.

[8]In the literature, it is possible to find different notations for the metrological spin-squeezing parameter (e.g., ξ and ξ_{S} are also commonly used). Here we follow the notation first introduced by Wineland *et al.* (1994) and used in a previous review (Ma *et al.*, 2011). In particular, in this review we will use ξ_{S} to indicate the Kitagawa and Ueda (1993) spin-squeezing parameter, see Eq. (51).

a. Optimal spin-squeezed states

Optimal spin-squeezed states are searched among the so-called minimum uncertainty states (Aragone *et al.*, 1974; Rashid, 1978; Wòdkiewicz and Eberly, 1985). These states saturate the Heisenberg uncertainty relation

$$(\Delta\hat{J}_{\boldsymbol{n}})^2(\Delta\hat{J}_\perp)^2 \geq |\langle\hat{J}_s\rangle|^2/4, \tag{42}$$

since $[\hat{J}_{\boldsymbol{n}}, \hat{J}_\perp] = i\hat{J}_s$. We thus have $\xi_{\mathrm{R}}^2 = N/[4(\Delta\hat{J}_{\boldsymbol{n}})^2]$ and a lower bound to ξ_{R}^2 is obtained by maximizing $(\Delta\hat{J}_{\boldsymbol{n}})^2$, giving (Hillery and Mlodinow, 1993; Agarwal and Puri, 1994)

$$\xi_{\mathrm{R}}^2 \geq \frac{2}{N+2}. \tag{43}$$

This bound can be saturated by the state $\sqrt{1-\alpha^2}|0_\perp\rangle + \alpha(|1_\perp\rangle + |-1_\perp\rangle)/\sqrt{2}$ in the limit $\alpha \mapsto 0$ (Brif and Mann, 1996), where $|m_\perp\rangle$ are Dicke states defined in Sec. II.A. Note that spin-squeezed states can achieve a Heisenberg scaling of phase sensitivity $\Delta\theta_{\mathrm{mom}} = \mathcal{O}(N^{-1})$, but not the Heisenberg limit (40) for $N > 2$. Optimal spin-squeezed states for even values of N and fixed values of $\langle\hat{J}_s\rangle$ are given by the ground state of the Hamiltonian $\hat{J}_\perp^2 - \lambda\hat{J}_s$, where $\lambda \geq 0$ is a Lagrange multiplier (Sørensen and Mølmer, 2001).

b. Spin squeezing and bosonic quadrature squeezing

In the case of probe states having $N \gg 1$ and a strong population imbalance between the two modes, spin squeezing can be well approximated by single-mode quadrature squeezing. Let $|a\rangle$ be the highly populated mode (continuous-variable limit $\langle\hat{a}^\dagger\hat{a}\rangle \approx N \gg 1$) and perform the Holstein-Primakoff transformation (Duan, Cirac, and Zoller, 2002; Wang and Sanders, 2003a; Madsen and Mølmer, 2004) $\hat{J}_+/\sqrt{N} \mapsto \hat{b}$, $\hat{J}_-/\sqrt{N} \mapsto \hat{b}^\dagger$, and $2\hat{J}_z/N \mapsto 1$, formally equivalent to the mean-field replacement $\hat{a} \mapsto \sqrt{N}$. Within this approximation, the rescaled spin operators $\sqrt{2/N}\hat{J}_x$ and $\sqrt{2/N}\hat{J}_y$ map onto the position $\sqrt{2/N}\hat{J}_x \mapsto (\hat{b} + \hat{b}^\dagger)/\sqrt{2} = \hat{X}$ and momentum $\sqrt{2/N}\hat{J}_y \mapsto (\hat{b} - \hat{b}^\dagger)/(i\sqrt{2}) = \hat{P}$ quadrature operators (Scully and Zubairy, 1997), respectively. We thus find

$$\xi_{\mathrm{R}}^2 = 2(\Delta\hat{Q})^2, \tag{44}$$

where $\hat{Q} = (\hat{b}e^{-i\phi} + \hat{b}^\dagger e^{i\phi})/\sqrt{2} = \hat{X}\cos\phi + \hat{P}\sin\phi$ and $0 \leq \phi < 2\pi$. Equation (44) shows the equivalence between the metrological spin-squeezing parameter and the quadrature variance, within the approximations. In particular, the rotation $e^{-i\theta\hat{J}_y}$ maps onto a displacement of the state along the X direction in the quadrature plane by an amount $\theta\sqrt{N/2}$, generated by $e^{-i\theta\sqrt{N/2}\hat{P}}$; see Fig. 7. When squeezing the quadrature variance below the vacuum noise limit, i.e., $(\Delta\hat{Q})^2 < 1/2$, it is possible to overcome the standard quantum limit of phase sensitivity, i.e., $\xi_{\mathrm{R}}^2 < 1$. The sensitivity of interferometers using a probe state with all atoms in a single mode can be increased by feeding the other mode with a

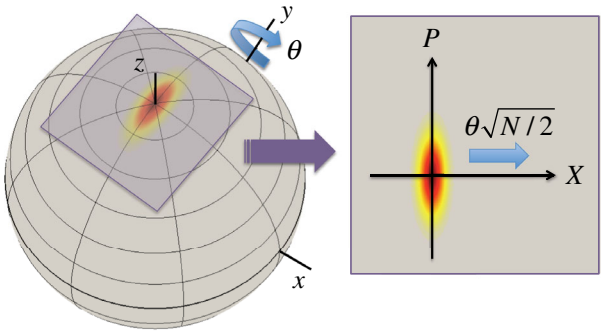

FIG. 7. Relation between spin squeezing and quadrature squeezing. For $\langle \hat{J}_z \rangle \approx N/2 \gg 1$, the Bloch sphere can be approximated locally as a plane orthogonal to the mean spin direction (here the z axis). Spin squeezing along the $\hat{J}_x$ axis is equivalent to squeezing of the $\hat{X}$ quadrature. A rotation around the y axis is equivalent to a displacement in the X direction.

quadrature-squeezed state as first proposed by Caves (1981) for an optical interferometer.

c. Spin squeezing, entanglement, and Fisher information

Spin squeezing $\xi_R < 1$ is a sufficient condition for useful particle entanglement in metrology (Sørensen *et al.*, 2001). Furthermore, Sørensen and Mølmer (2001) showed that the degree of spin squeezing is related to metrologically useful k-particle entanglement: for a given spin length, smaller and smaller values of ξ_R can be obtained only by increasing the entanglement depth; see Fig. 8. The quantum Fisher information detects entanglement in a larger set of states than those recognized by metrological spin squeezing (Pezzè and Smerzi, 2009):

$$\frac{N}{F_Q[\hat{\rho}, \hat{J}_{\boldsymbol{n}}]} \leq \xi_R^2. \tag{45}$$

This inequality, which follows from Eq. (8), shows that if a state is spin squeezed, $\xi_R^2 < 1$, it also satisfies the condition of metrologically useful entanglement, $F_Q[\hat{\rho}, \hat{J}_{\boldsymbol{n}}] > N$. The contrary is not true: there are states that are not spin squeezed and yet entangled and useful for quantum metrology. The Dicke and NOON states, discussed later, are important examples.

6. Dicke states

Dicke states, Eq. (4), have a precise relative number of particles between the two modes and a completely undefined phase. They are not spin squeezed (Wang and Mølmer, 2002). A direct calculation of the quantum Fisher information gives

$$F_Q[|m_z\rangle, \hat{J}_\perp] = \frac{N^2}{2} - 2m^2 + N \tag{46}$$

for any rotation direction $\perp$ orthogonal to the z axis. Dicke states with $m = \pm N/2$ are coherent spin states; those with $m \neq \pm N/2$ are metrologically usefully entangled. From the perspective of quantum metrology, the most interesting Dicke

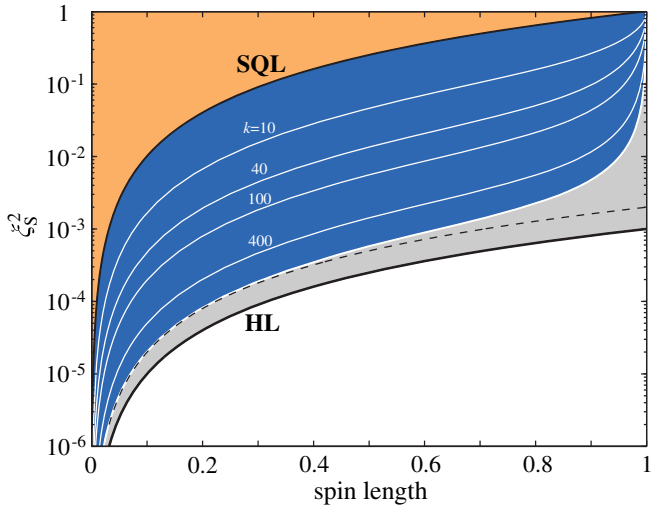

FIG. 8. ξ_S^2 vs ξ_R^2. The metrological spin-squeezing parameter ξ_R^2 is given by the ratio between the Kitagawa-Ueda spin-squeezing parameter ξ_S^2 and the squared spin length (Ramsey contrast) $2|\langle \hat{J}_s \rangle|/N$. $\xi_R^2 < 1$ is found in the blue (dark) region: the upper limit is the standard quantum limit (SQL), while the lower limit is the bound obtained for optimal spin-squeezed states; see Sec. II.C.5.a. The dashed line is Eq. (43), which is tight in the limit $\langle \hat{J}_s \rangle \to 0$. The lower thick black line is the Heisenberg limit (HL). The orange region above the SQL highlights the regime of parameters showing $\xi_S^2 < 1$ but no metrological spin squeezing (i.e., $\xi_R^2 \geq 1$). The white lines are lower bounds to ξ_R^2 obtained for k-particle entangled states (Sørensen and Mølmer, 2001). The gray region is not accessible by metrological spin-squeezed states. Here $N = 1000$.

state is the twin-Fock state (Holland and Burnett, 1993; Sanders and Milburn, 1995), $|N/2\rangle_a |N/2\rangle_b = |0_z\rangle$, corresponding to $N/2$ particles in each mode. It can be visualized as a ring on the equator of the Bloch sphere; see Fig. 5(c) for a plot of the rotated ring, $|0_y\rangle = e^{-i(\pi/2)\hat{J}_x}|0_z\rangle$. The rotation of $|0_z\rangle$ of an angle $\pi/2$ around the x axis converts the well-defined number difference into a well-defined relative phase between the two modes. It should be noted that the twin-Fock state has zero mean spin length, $\langle \hat{J}_x \rangle, \langle \hat{J}_y \rangle, \langle \hat{J}_z \rangle = 0$. Therefore, the metrologically useful entanglement of the twin-Fock state cannot be exploited when measuring the relative number of particles. A possible phase sensitive signal is the variance of the relative population (Kim *et al.*, 1998). The phase sensitivity calculated via the method of moments strongly depends on θ: for $\theta \approx 0$ and $N \gg 1$, we have

$$(\Delta\theta)^2 = \frac{(\Delta \hat{J}_z^2)^2}{\nu (d\langle \hat{J}_z^2 \rangle / d\theta)^2} = \frac{2}{\nu(N^2 + 2N)} + \mathcal{O}(\theta^2), \tag{47}$$

which is a factor of 2 above the Heisenberg limit at $\theta = 0$ and remains below the standard quantum limit for $\theta \lesssim 1/\sqrt{N}$. Similar results can be obtained with error propagation when estimating the phase shift from the measurement of the parity operator (Campos, Gerry, and Benmoussa, 2003; Gerry, Campos, and Benmoussa, 2004). Parity measures the difference in populations between even and odd eigenstates of $\hat{J}_z$

and can be difficult to implement for large spins. A θ-independent phase sensitivity can be reached when measuring the number of particles at the output ports of the interferometer and using a maximum likelihood estimator or a Bayesian method for sufficiently large number ν of repeated measurements (Holland and Burnett, 1993; Pezzè and Smerzi, 2006; Krischek *et al.*, 2011).

Squeezing the number of particles at both inputs of the interferometer is not necessary to overcome the standard quantum limit (Pezzè and Smerzi, 2013). Let us consider a probe state $\hat{\rho} = \hat{\rho}_a \otimes |N/2\rangle_b\langle N/2|$, where $\hat{\rho}_a$ is an arbitrary state in mode $|a\rangle$ with mean particle number N_a and $|N/2\rangle_b$ is a Fock state of $N/2$ particles in mode $|b\rangle$. We find

$$F_{\mathrm{Q}}[\hat{\rho}_a \otimes |N/2\rangle_b\langle N/2|, \hat{J}_y] = NN_a + \frac{N}{2} + N_a. \quad (48)$$

Heisenberg scaling is achieved when $N_a = N/2$, without any assumptions on $\hat{\rho}_a$. In particular, existing interferometers that operate with uncorrelated atoms can be improved by replacing the vacuum state in one of the two input ports by a Fock state.

7. NOON states

The Heisenberg limit can be saturated by the state

$$|\mathrm{NOON}\rangle = \frac{|N\rangle_a|0\rangle_b + e^{i\phi}|0\rangle_a|N\rangle_b}{\sqrt{2}}, \quad (49)$$

given by a coherent superposition of all particles in mode $|a\rangle$ and all particles in mode $|b\rangle$, where ϕ is an arbitrary phase. This state is called the NOON state (Lee, Kok, and Dowling, 2002) when considering indistinguishable bosonic particles. When considering distinguishable particles, as ions in a Paul trap for instance, see Sec. VI, the state (49) is generally called a "Schrödinger cat" (Bollinger *et al.*, 1996; Leibfried *et al.*, 2005) or a Greenberger-Horne-Zeilinger state (Monz *et al.*, 2011), originally introduced by Greenberger *et al.* (1990) for three particles. A look at the Wigner distribution of the NOON state, see Fig. 5(d) (left), reveals substructures of angular size $1/N$ given by spherical harmonic contributions Y_k^q with the maximum allowed value $k = N$ (Schmied and Treutlein, 2011). Rotating the NOON state around the z axis, the initial and final states become distinguishable after a rotation angle $\theta_{\min} \approx 1/N$. The squared Bures distance between the probe and the rotated state is

$$d_{\mathrm{B}}^2(|\mathrm{NOON}\rangle, e^{-i\theta\hat{J}_z}|\mathrm{NOON}\rangle) = 1 - \cos(N\theta/2), \quad (50)$$

which oscillates in phase N time faster than the corresponding overlap for a coherent spin state, Eq. (36), and is $d_{\mathrm{B}}^2 = N^2\theta^2/8 + \mathcal{O}(\theta^4)$ for small θ (Pezzè and Smerzi, 2007). According to Eq. (21), we obtain $F_Q[|\mathrm{NOON}\rangle, \hat{J}_z] = 4(\Delta\hat{J}_z)^2 = N^2$, and thus $\Delta\theta_{\mathrm{QCR}} = \Delta\theta_{\mathrm{HL}}$ for the NOON state. Note that the relative spin probability distribution of the NOON state $P(m_y) = |\langle m_y|e^{-i\theta\hat{J}_z}|\mathrm{NOON}\rangle|^2$, see Fig. 5(d) (right), shows a comblike structure as a function of m. These substructures change quickly with θ: for $\theta = 2\pi n/N$ only even values of m are populated, for $\theta = \pi(1 + 2n)/N$ only odd values of m are populated, with $n = 0, 1, \ldots, N-1$. This quick change of parity with θ can be exploited in order to reach the Heisenberg limit of phase sensitivity with the NOON state (Bollinger *et al.*, 1996); see also Sec. VI.B.2.

8. Further notions of spin squeezing and their relation to entanglement

When it is not possible to address individual qubits, or in the presence of low counting statistics, entanglement criteria based on the measurement of collective properties—as the condition $\xi_{\mathrm{R}} < 1$ introduced in Sec. II.C.5—are experimentally important. Moreover, states of a large number of particles cannot be characterized via full state tomography: the reconstruction of the full density matrix is hindered and finally prevented by the exponential increase in the required number of measurements. In the literature, different definitions of spin squeezing for collective angular momentum operators can be found (Ma *et al.*, 2011; Tóth and Apellaniz, 2014). In the following we review the ones most relevant for the present context.

a. Squeezing parameter of Kitagawa and Ueda

A spin-1/2 particle is characterized by isotropic spin fluctuations, equal to 1/4, along any direction $\perp$ orthogonal to the mean spin direction $\boldsymbol{s}$. By adding N uncorrelated spins all pointing along $\boldsymbol{s}$ (as in a coherent spin state), we have $(\Delta\hat{J}_\perp)^2 = N/4$. Quantum correlations between spins may result in reduced fluctuations in one direction $(\Delta\hat{J}_\perp)^2 < N/4$ at the expense of enhanced fluctuations along the other direction orthogonal to $\boldsymbol{s}$. This suggests the introduction of the spin-squeezing parameter (Kitagawa and Ueda, 1993)

$$\xi_{\mathrm{S}}^2 = \frac{4\min_\perp(\Delta\hat{J}_\perp)^2}{N}, \quad (51)$$

where $\xi_{\mathrm{S}}^2 < 1$ is the spin-squeezing condition. Equation (51) is related to metrological spin squeezing via $\min_\perp \xi_{\mathrm{R}}^2 = [N/(2\langle\hat{J}_s\rangle)]^2\xi_{\mathrm{S}}^2$. Since $|\langle\hat{J}_s\rangle| \le N/2$, we obtain

$$\xi_{\mathrm{S}}^2 \le \xi_{\mathrm{R}}^2. \quad (52)$$

In other words, metrological spin squeezing $\xi_{\mathrm{R}}^2 < 1$ implies spin squeezing $\xi_{\mathrm{S}}^2 < 1$ according to the definition of Kitagawa and Ueda. The converse is not true: there is no direct relation between $\xi_{\mathrm{S}}^2 < 1$ and the improvement of metrological sensitivity, as illustrated in Fig. 8. It is worth noting that the minimum in Eq. (51) is given by the smallest eigenvalue of the covariance matrix $\mathrm{Cov}(\hat{J}_{\boldsymbol{n}_i}, \hat{J}_{\boldsymbol{n}_j}) = \langle\{\hat{J}_{\boldsymbol{n}_i}, \hat{J}_{\boldsymbol{n}_j}\}\rangle/2 - \langle\hat{J}_{\boldsymbol{n}_i}\rangle\langle\hat{J}_{\boldsymbol{n}_j}\rangle$, where $\boldsymbol{n}_1$ and $\boldsymbol{n}_2$ are two mutually orthogonal directions in the plane perpendicular to $\boldsymbol{s}$ and $\{\hat{J}_{\boldsymbol{n}_1}, \hat{J}_{\boldsymbol{n}_2}\} = \hat{J}_{\boldsymbol{n}_1}\hat{J}_{\boldsymbol{n}_2} + \hat{J}_{\boldsymbol{n}_2}\hat{J}_{\boldsymbol{n}_1}$. Taking, without loss of generality, $\langle\hat{J}_{\boldsymbol{n}_1}\rangle = \langle\hat{J}_{\boldsymbol{n}_2}\rangle = 0$, we have (Wang and Sanders, 2003b)

$$\xi_{\mathrm{S}}^2 = \frac{\langle\hat{J}_{\boldsymbol{n}_1}^2 + \hat{J}_{\boldsymbol{n}_2}^2\rangle - \sqrt{\langle\hat{J}_{\boldsymbol{n}_1}^2 - \hat{J}_{\boldsymbol{n}_2}^2\rangle^2 + \langle\{\hat{J}_{\boldsymbol{n}_1}, \hat{J}_{\boldsymbol{n}_2}\}\rangle^2}}{N/2}. \quad (53)$$

b. Entanglement witnessed by mean values and variances of spin operators

For separable states (29), the inequalities

$$N(\Delta\hat{J}_{\boldsymbol{n}_1})^2 \geq \langle\hat{J}_{\boldsymbol{n}_2}\rangle^2 + \langle\hat{J}_{\boldsymbol{n}_3}\rangle^2, \tag{54a}$$

$$(\Delta\hat{J}_{\boldsymbol{n}_1})^2 + (\Delta\hat{J}_{\boldsymbol{n}_2})^2 + (\Delta\hat{J}_{\boldsymbol{n}_3})^2 \geq \frac{N}{2}, \tag{54b}$$

$$(N-1)(\Delta\hat{J}_{\boldsymbol{n}_1})^2 \geq \langle\hat{J}^2_{\boldsymbol{n}_2}\rangle + \langle\hat{J}^2_{\boldsymbol{n}_3}\rangle - \frac{N}{2}, \tag{54c}$$

$$(N-1)[(\Delta\hat{J}_{\boldsymbol{n}_1})^2 + (\Delta\hat{J}_{\boldsymbol{n}_2})^2] \geq \langle\hat{J}^2_{\boldsymbol{n}_3}\rangle + \frac{N(N-2)}{4} \tag{54d}$$

are all fulfilled, where $\boldsymbol{n}_1$, $\boldsymbol{n}_2$, and $\boldsymbol{n}_3$ are three mutually orthogonal directions. The violation of at least one of these inequalities signals that the state is entangled. Equation (54a) is equivalent to $\xi^2_{\mathrm{R}} \geq 1$, see Sec. II.C.5, and was introduced by Sørensen *et al.* (2001). The inequalities (54b)–(54d) were introduced by Tóth *et al.* (2007, 2009). A violation of the condition (54b) can be used to detect entanglement in singlet states (Tóth and Mitchell, 2010; Behbood *et al.*, 2014). The third condition, Eq. (54c), can be rewritten as $\xi^2_{\mathrm{D}} \geq 1$, where

$$\xi^2_{\mathrm{D}} = \frac{N(\Delta\hat{J}_{\boldsymbol{n}_1})^2}{\langle\hat{\boldsymbol{J}}^2\rangle - N/2 - \langle\hat{J}_{\boldsymbol{n}_1}\rangle^2}. \tag{55}$$

In particular, the condition $\xi^2_{\mathrm{D}} < 1$ can be used to detect entanglement close to Dicke states (Tóth *et al.*, 2007); see also Raghavan *et al.* (2001). The detection of multiparticle entanglement close to Dicke states for spin-1/2 particles was studied by Duan (2011) and Lücke *et al.* (2014) and for spin-J particles with $J > 1/2$ by Vitagliano *et al.* (2017). The inequalities (54b)–(54d) and the further inequality $\langle\hat{\boldsymbol{J}}^2\rangle \leq (N/2)(N/2+1)$, which is valid for all quantum states (not only for separable states), form a system of conditions that defines a polytope in the three-dimensional space with coordinates $\langle\hat{J}^2_{\boldsymbol{n}_1}\rangle$, $\langle\hat{J}^2_{\boldsymbol{n}_2}\rangle$, and $\langle\hat{J}^2_{\boldsymbol{n}_3}\rangle$ (Tóth *et al.*, 2007, 2009). The polytope encloses all separable states. It was demonstrated that Eqs. (54) form a complete set (Tóth *et al.*, 2007, 2009), meaning that it is not possible to add new entanglement conditions based only on mean values and variances of spin moments that detect more entangled states. The inequalities (54) have been generalized to arbitrary spin systems (Vitagliano *et al.*, 2011, 2014) and to systems of fluctuating numbers of particles (He *et al.*, 2012; Hyllus, Pezzè *et al.*, 2012). Furthermore, Korbicz, Cirac, and Lewenstein (2005) and Korbicz *et al.* (2006) have shown that, if the inequality

$$\left(\langle\hat{J}^2_{\boldsymbol{n}_1}\rangle + \frac{N(N-2)}{4}\right)^2 < \left(\langle\hat{J}^2_{\boldsymbol{n}_2}\rangle + \langle\hat{J}^2_{\boldsymbol{n}_3}\rangle - \frac{N}{2}\right)^2 + (N-1)^2\langle\hat{J}_{n_1}\rangle^2 \tag{56}$$

holds, then the state possesses pairwise entanglement, i.e., entanglement in the two-qubit reduced density matrix $\hat{\rho}_{i,j} = \mathrm{Tr}_{\{1,\ldots,N\}\setminus\{i,j\}}[\hat{\rho}]$ obtained by tracing the N qubit state $\hat{\rho}$ over all particles except the ith and jth.

c. Spin squeezing and entanglement of symmetric states

We emphasize that none of the above entanglement witnesses require any assumptions on the symmetry of the state. For states that are symmetric under particle exchange, we have $\langle\hat{\boldsymbol{J}}^2\rangle = (N/2)(N/2+1)$. In this case, Eq. (56) can be rewritten as

$$\xi^2_{\mathrm{N}} = \frac{4(\Delta\hat{J}_{\boldsymbol{n}})^2}{N} < 1 - \frac{4\langle\hat{J}_{\boldsymbol{n}}\rangle^2}{N^2}, \tag{57}$$

where ξ^2_{N} is called the number-squeezing parameter. The inequality (57) is necessary and sufficient for pairwise entanglement (Korbicz, Cirac, and Lewenstein, 2005; Korbicz *et al.*, 2006). It should be noted that if $\xi^2_{\mathrm{S}} < 1$ holds, then the inequality (57) is satisfied as well (taking $\boldsymbol{n} = \perp$ and $\langle\hat{J}_{\boldsymbol{n}}\rangle = 0$). Hence, symmetric spin-squeezed states possess two-qubit entanglement. The converse is not true: since $\boldsymbol{n}$ in Eq. (57) is not necessarily orthogonal to the mean spin direction $\boldsymbol{s}$, number squeezing ($\xi^2_{\mathrm{N}} < 1$) does not imply spin squeezing ($\xi^2_{\mathrm{S}} < 1$).

The relationship between Kitagawa-Ueda spin squeezing and pairwise entanglement has also been studied by Ulam-Orgikh and Kitagawa (2001) and Wang and Sanders (2003b). For an arbitrary symmetric state of N qubits, the spin-squeezing parameter (51) can be written in terms of the two-spin correlation function (Ulam-Orgikh and Kitagawa, 2001)

$$\xi^2_{\mathrm{S}} = 1 + (N-1)\langle\hat{\sigma}^{(i)}_{\perp} \otimes \hat{\sigma}^{(j)}_{\perp}\rangle, \qquad i \neq j. \tag{58}$$

This equation shows that spin squeezing $\xi^2_{\mathrm{S}} < 1$ is equivalent to negative pairwise spin-spin correlations that, in turn, are sufficient for pairwise entanglement.[9] Furthermore, for symmetric pure states of two qubits, there is a direct correspondence between ξ^2_{S} and the concurrence $\mathcal{C}$ (Ulam-Orgikh and Kitagawa, 2001; Wang and Sanders, 2003b): $\xi^2_{\mathrm{S}} = 1 - \mathcal{C}$. We recall that $\mathcal{C} > 0$ is a necessary and sufficient condition of, and quantifies, entanglement of a pair of qubits (Hill and Wootters, 1997; Wootters, 1998). Symmetric pure states of two qubits are entangled if and only if they satisfy $\xi^2_{\mathrm{S}} < 1$ (Ulam-Orgikh and Kitagawa, 2001). For symmetric states of N qubits that fulfill $\xi^2_{\mathrm{S}} \leq 1$ and other conditions,[10] the equality

$$\xi^2_{\mathrm{S}} = 1 - (N-1)\mathcal{C} \tag{59}$$

[9]The two-qubit reduced density matrix of a separable symmetric state of N qubits has positive pairwise correlations: $\langle\hat{\sigma}^{(i)}_{\perp} \otimes \hat{\sigma}^{(j)}_{\perp}\rangle > 0$ for any $i \neq j$ (Wang and Sanders, 2003b).

[10]Equation (59) was derived in Wang and Sanders (2003b) for symmetric states having $\langle\hat{J}_{\boldsymbol{s}}\rangle \neq 0$ and $\langle\hat{J}_{\boldsymbol{n}_i}\rangle = \langle\hat{J}_{\boldsymbol{s}}\hat{J}_{\boldsymbol{n}_i}\rangle = \langle\hat{J}_{\boldsymbol{n}_i}\hat{J}_{\boldsymbol{s}}\rangle = 0$, $i = 1, 2$, where $\boldsymbol{n}_1$ and $\boldsymbol{n}_2$ are vectors orthogonal to the mean spin direction $\boldsymbol{s}$.

holds (Wang and Sanders, 2003b), where $\mathcal{C}$ is calculated from the two-particle reduced density matrix. Equantion (59) tells us that $\xi_S^2 < 1$ implies $\mathcal{C} > 0$ and thus pairwise entanglement. When $\xi_S^2 > 1$, Eq. (59) breaks down and we cannot draw any conclusion about pairwise entanglement: for example, Dicke states can be pairwise entangled even though they are not spin squeezed (Wang and Mølmer, 2002).

d. Planar spin-squeezed states

While many useful spin-squeezed states have reduced quantum fluctuations along a single spin direction (with a corresponding increase in fluctuations along a perpendicular direction), the spin commutation relations make it possible to reduce the fluctuations along two orthogonal spin directions simultaneously while increasing those along a third direction. Specifically, an initially coherent state along the $\boldsymbol{n}_3$ direction can be squeezed in the perpendicular plane such that simultaneously $(\Delta\hat{J}_{\boldsymbol{n}_1})^2 < J/2$ and $(\Delta\hat{J}_{\boldsymbol{n}_2})^2 < J/2$ (Puentes *et al.*, 2013), which does not violate Heisenberg's uncertainty relation, Eq. (42), if $\langle\hat{J}_{\boldsymbol{n}_3}\rangle$ is reduced at the same time. In general, such planar spin-squeezed states reduce the variance sum $(\Delta\hat{J}_{\parallel})^2 = (\Delta\hat{J}_{\boldsymbol{n}_1})^2 + (\Delta\hat{J}_{\boldsymbol{n}_2})^2$ below the coherent-state value of $(\Delta\hat{J}_{\parallel}^{\mathrm{coh}})^2 = J$, ultimately limited by (He, Peng *et al.*, 2011)

$$(\Delta\hat{J}_{\parallel})^2 \geq C_J \approx 0.595\,275 J^{2/3} + \mathcal{O}(J^{1/3}). \tag{60}$$

Planar spin-squeezed states are useful for interferometric phase measurements where the phase fluctuations and the number fluctuations are squeezed simultaneously (see Sec. V.A.1), while the spin length fluctuates significantly. Note that not all planar spin-squeezed states are entangled (He *et al.*, 2012; Puentes *et al.*, 2013; Vitagliano *et al.*, 2018); see Eqs. (54b) and (54d) for relevant entanglement criteria.

9. Einstein-Podolsky-Rosen entanglement and Bell correlations

a. Continuous variable and Einstein-Podolsky-Rosen entanglement

Let us consider two bosonic modes $|a_+\rangle$ and $|a_-\rangle$ and introduce the corresponding annihilation $\hat{a}_{\pm1}$ and creation $\hat{a}_{\pm1}^\dagger$ operators. Mode-separable quantum states are defined as $\hat{\rho}_{\mathrm{msep}} = \sum_q p_q \hat{\rho}_q^{(+1)} \otimes \hat{\rho}_q^{(-1)}$, where $p_q > 0$, $\sum_q p_q = 1$, and $\hat{\rho}_q^{(\pm1)}$ is the state of the $|a_{\pm1}\rangle$ mode. Mode entanglement, i.e., $\hat{\rho} \neq \hat{\rho}_{\mathrm{msep}}$, can be revealed by correlations between bosonic position $\hat{X}_{\pm1}(\phi) = (\hat{a}_{\pm1}e^{-i\phi} + \hat{a}_{\pm1}^\dagger e^{i\phi})/\sqrt{2}$ and momentum $\hat{P}_{\pm1}(\phi) = \hat{X}_{\pm1}(\phi + \pi/2)$ quadratures (Reid *et al.*, 2009). Mode-separable states fulfill (Duan, Giedke *et al.*, 2000; Simon, 2000)

$$V_{X(\phi)}^{\pm} + V_{P(\phi)}^{\mp} \geq 2, \tag{61}$$

where $V_{X(\phi)}^{\pm} = \mathrm{Var}[\hat{X}_{+1}(\phi) \pm \hat{X}_{-1}(\phi)]$ and $V_{P(\phi)}^{\mp} = \mathrm{Var}[\hat{P}_{+1}(\phi) \mp \hat{P}_{-1}(\phi)]$ are variances. A violation of this condition detects entanglement between the $|a_{\pm1}\rangle$ modes. It is also a necessary and sufficient condition for mode entanglement in Gaussian states (Duan, Giedke *et al.*, 2000; Simon, 2000); see also Giovannetti *et al.* (2003), Shchukin and Vogel (2005), Walborn *et al.* (2009), and Gessner, Pezzè, and Smerzi (2016, 2017) for further (and sharper) conditions. Mode entanglement finds several applications in quantum technologies (Braunstein and van Loock, 2005).

Correlations between quadrature variances are at the heart of the Einstein-Podolsky-Rosen (EPR) paradox (Einstein, Podolsky, and Rosen, 1935). When the quadratures $\hat{X}_{+1}$ and $\hat{P}_{+1}$ are measured in independent realizations of the same state, the correlations allow for a prediction of $\hat{X}_{-1}$ and $\hat{P}_{-1}$ with inferred variances violating the Heisenberg uncertainty relation $\Delta\hat{X}_{-1}^{\mathrm{inf}}\Delta\hat{P}_{-1}^{\mathrm{inf}} < 1/2$, known as the EPR criterion (Reid, 1989; Reid *et al.*, 2009). This extends the original EPR discussion (Einstein, Podolsky, and Rosen, 1935) that was limited to perfect quadrature correlations. Nonsteerable states, including separable states, fulfill (Reid, 1989)

$$V_{X(\phi)}^{-} V_{P(\phi)}^{+} \geq 1/4. \tag{62}$$

The violation of this condition witnesses a strong form of entanglement ("EPR entanglement") necessary to fulfill the EPR criterion. With atoms, continuous-variable entanglement was first proven with room-temperature vapor cells (Julsgaard, Kozhekin, and Polzik, 2001). With spinor Bose-Einstein condensates, mode entanglement (Gross *et al.*, 2011) and EPR entanglement (Peise *et al.*, 2015) were demonstrated; see Sec. IV.C.

b. Bell correlations

The strongest form of correlations between particles are those that violate a Bell inequality (Bell, 1964). The existence of Bell correlations has profound implications for the foundations of physics and underpins quantum technologies such as quantum key distribution and certified randomness generation (Brunner *et al.*, 2014). Bell correlations have been observed in systems of at most a few (usually two) particles (Freedman and Clauser, 1972; Aspect, Grangier, and Roger, 1982; Eibl *et al.*, 2003; Zhao *et al.*, 2003; Matsukevich *et al.*, 2008; Hofmann *et al.*, 2012; Lanyon *et al.*, 2014; Giustina *et al.*, 2015; Hensen *et al.*, 2015; Shalm *et al.*, 2015; Rosenfeld *et al.*, 2017), but their role in many-body systems is largely unexplored (Tura *et al.*, 2014).

Entanglement is necessary but not sufficient for Bell correlations (Werner, 1989; Brunner *et al.*, 2014). Therefore, entanglement criteria such as those discussed cannot be used to determine whether a system could violate a Bell inequality. Schmied *et al.* (2016) derived a criterion in the spirit of a spin-squeezing parameter to determine whether Bell correlations are present in an N-particle quantum system. For any two axes $\boldsymbol{n}_1$ and $\boldsymbol{n}_2$, the inequality

$$\mathcal{W} = -\frac{|\langle\hat{\boldsymbol{J}}_{\boldsymbol{n}_2}\rangle|}{N/2} + (\boldsymbol{n}_1\cdot\boldsymbol{n}_2)^2\frac{\langle\hat{J}_{\boldsymbol{n}_1}^2\rangle}{N/4} + 1 - (\boldsymbol{n}_1\cdot\boldsymbol{n}_2)^2 \geq 0 \tag{63}$$

is satisfied for all states that are not Bell correlated. States that satisfy $\mathcal{W} < 0$ can violate the many-particle Bell inequality of Tura *et al.* (2014), which is a statement about the strength of two-body correlations, but does not imply the violation of a

two-particle Bell inequality for every pair of particles. By optimizing Eq. (63) over the angle between the two axes, a criterion follows that facilitates comparison with well-known spin-squeezing criteria: for any two axes $\boldsymbol{n}_1$ and $\boldsymbol{n}_2$ perpendicular to each other,

$$\frac{\langle \hat{J}^2_{\boldsymbol{n}_1}\rangle}{N/4} \geq \frac{1}{2}\left[1-\sqrt{1-\left(\frac{\langle \hat{J}_{\boldsymbol{n}_2}\rangle}{N/2}\right)^2}\right] \tag{64}$$

is satisfied for all states that are not Bell correlated. A similar criterion that is violated more easily was derived by Wagner *et al.* (2017),

$$\frac{\langle \hat{J}^2_{\boldsymbol{n}_1}\rangle}{N/4} \geq 1-\left(\frac{\langle \hat{J}_{\boldsymbol{n}_2}\rangle}{N/2}\right)/\operatorname{artanh}\left(\frac{\langle \hat{J}_{\boldsymbol{n}_2}\rangle}{N/2}\right). \tag{65}$$

Detecting Bell correlations by violating inequalities (63), (64), or (65) requires only collective manipulations and measurements on the entire N-particle system. While this does not provide a loophole-free and device-independent Bell test, it is a powerful tool for characterizing correlations in many-body systems state independently. Bell correlations according to Eqs. (63), (64), and (65) have been observed with Bose-Einstein condensates; see Sec. III.B.3.

D. Tomography of spin states

1. Spin-noise tomography

Spin-noise tomography is a widely used technique to gain information about spin-squeezed states, whose main characteristics are captured by their second spin moments along the squeezing and antisqueezing directions. For this tomography, the state is rotated by an angle ϑ using resonant Rabi rotations, followed by projective spin measurements along the z axis: $\hat{J}_z$ defined in Eqs. (3) is measured by counting the numbers of particles in the two modes; see Sec. II.E. The kth moment of these spin projections can be fit to a linear combination of $\cos(n\vartheta)$ and $\sin(n\vartheta)$ with $n \in \{k, k-2, k-4, \ldots\}$, which allows interpolating these projective measurements to arbitrary angles ϑ. Also, technical noise sources can be characterized and their influence subtracted from the resulting moments; any spin squeezing concluded after noise subtraction will be called inferred spin squeezing (see open circles in Fig. 2). Since this method estimates spin projection moments separately, they do not necessarily fulfill all consistency criteria imposed by the positive semidefiniteness of the density operator (Schmied, 2016). In practical situations concerning spin-squeezed states, however, this restriction is often irrelevant. The information captured from low-order spin moments through spin-noise tomography may be insufficient to characterize and visualize general spin states. Different techniques have been developed for full state tomography (Paris and Řeháček, 2004; Blume-Kohout, 2010; Schmied and Treutlein, 2011), estimating all spin moments up to order N.

2. Visualizing spin states

State representations on the Bloch sphere are very useful to gain an intuition about the properties of quantum states and their sensitivity to rotations. In the following we consider symmetric states of N spin-1/2 particles (see Sec. II.A). There are various representations in the form of pseudoprobability densities (Schleich, 2001). These are based on the decomposition of a general density operator $\hat{\rho} = \sum_{k=0}^{2J}\sum_{q=-k}^{k}\rho_{kq}\hat{T}^{(J)}_{kq}$ into the orthonormalized spherical tensor (or multipole) operators $\hat{T}^{(J)}_{kq} = \sum_{\mu,\mu'=-J}^{J}(-1)^{J-\mu'}\langle J,\mu;J,-\mu'|k,q\rangle|J,\mu_z\rangle\langle J,\mu'_z|$ defined in terms of Clebsch-Gordan coefficients, with $\rho_{kq} = \mathrm{Tr}[\hat{\rho}(\hat{T}^{(J)}_{kq})^\dagger]$ (Arecchi *et al.*, 1972; Agarwal, 1981; Dowling, Agarwal, and Schleich, 1994; Schmied and Treutlein, 2011). This decomposition has properties similar to the Fourier transform in Euclidean space: it separates low-frequency components (small k) from high-frequency components (large k), which are affected very differently by experimental noise. Further, it allows us to define the family of spherical functions (Agarwal, 1981)

$$f(\vartheta,\varphi) = \sqrt{\frac{N+1}{4\pi}}\sum_{k=0}^{N} f_k \sum_{q=-k}^{k}\rho_{kq}Y_{kq}(\vartheta,\varphi) \tag{66}$$

in terms of spherical harmonics $Y_{kq}(\vartheta,\varphi)$. All of these functions are linear in the density operator. The following representations (corresponding to different choices for the coefficients f_k) are often used, with examples given in Table I and Fig. 9.

a. Wigner distribution

The Wigner quasiprobability distribution $W(\vartheta,\varphi)$ (Wigner, 1932) corresponds to the case $f_k = 1$ in Eq. (66). It is found by replacing the spherical tensor operators in the decomposition of $\hat{\rho}$ by spherical harmonics of the same order, which obey the same orthonormalization. Because of this close similarity, the Wigner quasiprobability distribution is equivalent to the density operator. $W(\vartheta,\varphi)$ is not a true probability density, as it can take negative values (Leibfried *et al.*, 1996; Lvovsky *et al.*, 2001; McConnell *et al.*, 2015). For continuous variables, this is often understood as a sign of nonclassical behavior. Note however that in the present finite-dimensional space, even the Wigner distribution of a coherent spin state has negative parts of amplitude $\sim 2^{-N}$, exponentially decreasing with the number of particles.

TABLE I. Distributions of a coherent spin state. Different representations of a coherent spin state with mean spin direction $\boldsymbol{s}$; the last column is the approximate expression for $N \gg 1$. Here $x = \{\sin\vartheta\cos\varphi, \sin\vartheta\sin\varphi, \cos\vartheta\}\cdot\boldsymbol{s}$, $P_k(x)$ are Legendre polynomials, $J_1(x)$ is a Bessel function of the first kind, and $\zeta = \cos^{-1}(x)$.

Exact	$N \gg 1$
$P(x) = \sum_{k=0}^{N}\frac{2k+1}{4\pi}P_k(x)$	$\approx \frac{(N+1)^2}{2\pi}\frac{J_1[(N+1)\zeta]}{(N+1)\zeta}$
$W(x) = \sum_{k=0}^{N}\frac{2k+1}{4\pi}\sqrt{\frac{N!(N+1)!}{(N-k)!(N+k+1)!}}P_k(x)$	$\approx \frac{N+3/2}{2\pi}\exp[-\frac{N+3/2}{2}\zeta^2]$
$Q(x) = \frac{N+1}{4\pi}\left(\frac{1+x}{2}\right)^N$	$\approx \frac{N+2}{4\pi}\exp[-\frac{N+2}{4}\zeta^2]$

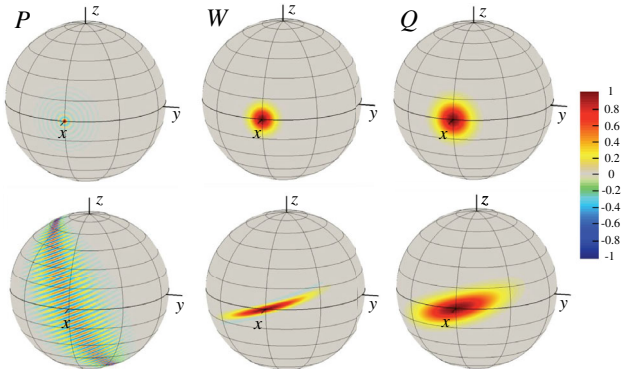

FIG. 9. Quasiprobability representations. Upper row: P, W, and Q representations of a coherent state pointing in the $+x$ direction (see Table I), with $\boldsymbol{s}=\{1,0,0\}$. Lower row: P, W, and Q representations of a spin-squeezed state reached by one-axis twisting with $\chi t=0.01\pi$ (see Sec. III.B). The color scale for each panel is normalized to its maximum value. Here $N=100$.

b. Husimi-Kano representation

The Husimi-Kano Q representation (Husimi, 1940; Haas *et al.*, 2014; Barontini *et al.*, 2015)

$$Q(\vartheta,\varphi)=\frac{N+1}{4\pi}\langle\vartheta,\varphi,N|\hat{\rho}|\vartheta,\varphi,N\rangle$$

corresponds to the case

$$f_k=\sqrt{\frac{N!(N+1)!}{(N-k)!(N+k+1)!}}$$

in Eq. (66). It is non-negative and proportional to the probability of finding the system in the coherent spin state $|\vartheta,\varphi,N\rangle$. Since $Q(\vartheta,\varphi)$ is the convolution of $W(\vartheta,\varphi)$ with the Wigner distribution of a coherent spin state (Agarwal, 1981), in practice the former contains much less information than the latter. Furthermore, recovering the Wigner distribution (and hence the density matrix) from an experimentally determined Q representation is generally not feasible.

c. Glauber-Sudarshan representation

The Glauber-Sudarshan P representation $P(\vartheta,\varphi)$ (Glauber, 1963; Sudarshan, 1963; Kiesel *et al.*, 2008) is obtained for

$$f_k=\sqrt{\frac{(N-k)!(N+k+1)!}{N!(N+1)!}}$$

in Eq. (66). It is the deconvolution of $W(\vartheta,\varphi)$ with the Wigner distribution of a coherent spin state (Agarwal, 1981) and serves to construct the density operator from coherent spin states: $\hat{\rho}=\int_0^{\pi}d\vartheta\sin\vartheta\int_0^{2\pi}d\varphi P(\vartheta,\varphi)|\vartheta,\varphi,N\rangle\langle\vartheta,\varphi,N|$. While in infinite-dimensional Hilbert spaces the P representation is often of limited practical use because of its singular behavior (Scully and Zubairy, 1997), this is not the case for the representation of a spin. Indeed, in this case, partial-wave contributions are limited to angular momenta (spherical harmonics) $k\leq N$ in Eq. (66) in order to match the number of degrees of freedom of the density operator; the amplitudes of the partial waves with $k>N$ are not determined by the density matrix and may be set to zero. However, if higher-order partial waves ($k>N$) are added, then the P representation of any symmetric separable state can be chosen non-negative (Korbicz, Cirac, and Lewenstein, 2005). In this case, the entanglement condition (37) is sufficient for nonclassicality (Rivas and Luis, 2010). In general, the indeterminacy of the P representation does not allow the conclusion that a given P representation with negative regions implies either nonclassicality or entanglement: separable states may have a P representation with negative parts as can be seen in Table I.

E. Detection of atomic states

Quantum metrology requires the detection of large ensembles of N atoms with a resolution in atom number that is significantly better than $\sqrt{N}$. In particular, reaching the Heisenberg limit requires counting the N atoms with single-atom resolution (we note that this requirement can be relaxed by nonlinear detection, see Sec. VII.A.6). Traditionally, techniques that provide single-atom detection have been applied only to systems with at most a few atoms: for quantum metrology, single-atom detectivity must be combined with a much larger dynamic range.

1. Atom counting

For atomic qubits, there are two principal destructive methods using (near-)resonant light for counting the number of atoms in one level.

a. Resonant absorption imaging

The absorption of a narrow-linewidth laser beam is measured quantitatively and converted to an absolute atom number (Reinaudi *et al.*, 2007). The precision of this technique on mesoscopic ensembles is currently at the level of four atoms (Ockeloen *et al.*, 2010; Muessel *et al.*, 2013, 2015; Schmied *et al.*, 2016) (standard deviation on the detection of hundreds of atoms). However, it is state selective and can be used to measure both N_a and N_b in a single atomic ensemble, i.e., in a single run of the experiment.

b. Resonant fluorescence imaging

The intensity of atomic fluorescence is converted to an absolute atom number. This method is used especially for ions (Rowe *et al.*, 2001) but also finds application for atomic ensembles. In free space, single-atom resolution has been achieved in ensembles of up to about $N=1200$ (Hume *et al.*, 2013); however, it is challenging to measure N_a and N_b separately (Stroescu, Hume, and Oberthaler, 2015). Very high sensitivity in fluorescence detection of many atoms has been shown by spatially resolving each atom in an optical lattice (Nelson, Li, and Weiss, 2007; Bakr *et al.*, 2009; Sherson *et al.*, 2010). This technique can image and count individual atoms but does not determine the exact atom number as atom pairs are quickly lost due to light-assisted collisions.

In order to count the atom numbers N_a and N_b in the two modes separately, different strategies have been employed.

If the two modes $|a\rangle$ and $|b\rangle$ are localized at different points in space, then spatially resolved imaging can yield mode-selective atom counts (Stroescu, Hume, and Oberthaler, 2015). Spatial separation can also be achieved by time-of-flight imaging if two initially overlapping modes are given different momentum kicks, usually by a state-selective force as in a Stern-Gerlach experiment (Lücke *et al.*, 2011). This method is often used when the two modes are hyperfine levels with equal total angular momentum F but different projections M_F. If the modes are spectrally separated by more than the atomic linewidth, they can be addressed individually with a laser and counted separately by absorption or fluorescence. Particularly for states in different hyperfine F levels this option is used frequently (Gross *et al.*, 2010; Riedel *et al.*, 2010). The detection of level $|b\rangle$ can occur at a different time than level $|a\rangle$ by the same absorption or fluorescence technique. The population of one level is counted first, followed by a population exchange or transfer between the levels $|a\rangle$ and $|b\rangle$, after which the same level is counted again but now representing the original population of the other level.

2. Quantum nondemolition measurements of atom number

Off-resonant light can be used to perform nondestructive measurements of the atom numbers (Hammerer, Sørensen, and Polzik, 2010; Ritsch *et al.*, 2013). In atomic clocks, nondestructive atom counting can reduce the loading (dead) time and thus dramatically improve the clock frequency stability (Lodewyck, Westergaard, and Lemond, 2009; Norcia and Thompson, 2016). Quantum nondemolition measurement can also be used to entangle the atoms (see Sec. V.A). Specific techniques are as follows.

a. Faraday effect

A probe-light beam's polarization rotates slowly around the polarization direction of an atomic ensemble (Wasilewski *et al.*, 2010; Sewell *et al.*, 2012). By measuring the effected rotation angle, the ensemble's polarization and thus its value of $\hat{J}_z$ is determined.

b. Dispersion

The refractive index of an atomic ensemble depends on the atomic populations; an off-resonant probe-light beam thus picks up a $\hat{J}_z$-dependent phase shift (Kuzmich, Mandel, and Bigelow, 2000; Appel *et al.*, 2009) that can be measured in an optical interferometer (usually of Mach-Zehnder type).

c. Cavity-enhanced detection

Atoms that are coupled to a high-finesse optical cavity make its transmission depend on the atoms' internal state (Kimble, 1998) and allow $\hat{J}_z$ of the atoms to be measured (Schleier-Smith, Leroux, and Vuletić, 2010b; Zhang *et al.*, 2012; McConnell *et al.*, 2015; Hosten, Engelsen *et al.*, 2016). For small atom numbers, this method can resolve single excitations (Haas *et al.*, 2014).

3. Inhomogeneous spin coupling and effective spin

The definition in Eq. (1) assumes that each atom contributes to the collective spin with the same weight. This assumption is not always satisfied: in experiments exploiting atom-light interactions, the coupling is inhomogeneous if the atoms are trapped in a standing wave whose wavelength is incommensurate with that of the probe field (Leroux, Schleier-Smith, and Vuletić, 2010b; Tanji-Suzuki *et al.*, 2011; McConnell *et al.*, 2015), if the atoms are trapped in a large volume that samples the spatial profile of the probe field (Appel *et al.*, 2009), or if the atoms move in space (Hammerer, Sørensen, and Polzik, 2010). In these situations, Eq. (1) is modified so that each atom contributes to the collective spin with a weight given by its coupling g_i to the cavity mode. The internal-state dynamics of the effectively addressed atoms can be described by an effective spin operator

$$\hat{\boldsymbol{J}}_{\rm eff} = \sum_i \frac{g_i}{g_{\rm eff}} \frac{\hat{\boldsymbol{\sigma}}_i}{2} \tag{67}$$

and an effective atom number

$$N_{\rm eff} = \sum_i \frac{g_i}{g_{\rm eff}} = \frac{(\sum_i g_i)^2}{\sum_i g_i^2}, \tag{68}$$

where $g_{\rm eff} = (\sum_i g_i^2)/(\sum_i g_i)$ is the effective coupling strength (Hu *et al.*, 2015). $\hat{\boldsymbol{J}}_{\rm eff}$ satisfies the usual angular momentum commutation and uncertainty relations as long as the average total spin remains large ($\|\langle \hat{\boldsymbol{J}}_{\rm eff}\rangle\| \approx N_{\rm eff}/2 \gg 1$) and the detection does not resolve single spins, i.e., in the limit where the Holstein-Primakoff approximation is valid. In this limit, the effective spin can be treated in the same way as a real spin of length $N_{\rm eff}/2$, and the metrological methods described remain valid. Special care is required for conclusions about the correlations between real (not effective) atoms, such as the entanglement depth (Hu *et al.*, 2015; McConnell *et al.*, 2015).

III. ENTANGLEMENT VIA ATOMIC COLLISIONS: THE BOSONIC JOSEPHSON JUNCTION

Tunable elastic atom-atom collisions are naturally present in Bose-Einstein condensates and represent a well-established method to generate metrologically useful entanglement in these systems. Furthermore, Bose-Einstein condensates have a weak coupling to the environment and can be restricted to occupy two modes only. These can be two "internal" hyperfine atomic states or two "external" spatial states of a trapping potential; see Fig. 10. Two-mode Bose-Einstein condensates can be described by the bosonic Josephson junction model[11]

[11]The Hamiltonian (69) maps to a class of models first introduced by Lipkin, Meshkov and Glick in nuclear physics (Lipkin, Meshkov, and Glick, 1965); see Ulyanov and Zaslavskii (1992) for a review. This corresponds to a fully connected Ising Hamiltonian of spin-1/2 particles where each spin interacts with all the other spins. While in the Lipkin-Meshkov-Glick model the spins are distinguishable, the bosonic Josephson junction considers undistinguishable bosons occupying two modes.

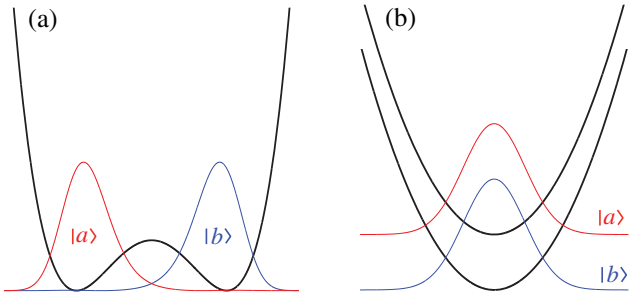

FIG. 10. (a) External bosonic Josephson junction realized by a Bose-Einstein condensate trapped in a double-well potential (thick black line). The thin colored lines are the amplitudes of the mean-field wave functions (see text) localized on the left and right wells. (b) Internal bosonic Josephson junction made by a trapped Bose-Einstein condensate in two different hyperfine states. For each state, the thick black line is the harmonic trap and the thin colored line is the condensate wave function.

$$\hat{H}_{\mathrm{BJJ}} = -\hbar\Omega\hat{J}_x + \hbar\chi\hat{J}_z^2 + \hbar\delta\hat{J}_z. \tag{69}$$

Here $\hat{J}_x$ and $\hat{J}_z$ describe a linear coupling and an energy imbalance between the two modes, respectively. The term $\hat{J}_z^2$ accounts for the interaction of each atom with all the other particles in the system. The parameters χ and Ω (in the following we assume $\Omega \geq 0$, without loss of generality) can be precisely and independently tuned and, in particular, switched on and off at will (Pethick and Smith, 2002). Furthermore, Bose-Einstein condensates offer the possibility to control the trapping geometry and to count atoms using established techniques such as absorption or fluorescence imaging. Useful entanglement for quantum metrology can be found in the ground state of Eq. (69) for $\chi \neq 0$ (either positive or negative); see Sec. III.A. The ground state can be experimentally addressed by adiabatically tuning interaction and/or coupling parameters. The nonlinear interaction can also be exploited for the dynamical generation of entanglement starting from particles prepared in a separable state; see Secs. III.B and III.C. In particular, for $\Omega, \delta = 0$, Eq. (69) is equivalent to the one-axis twisting Hamiltonian first introduced by Kitagawa and Ueda (1993). A limitation is that the contact interaction, which is the ingredient to entangle the atoms, is also—via particle losses induced by nonelastic scattering—a main source of decoherence in these systems.

The external bosonic Josephson junction can be realized with a dilute Bose-Einstein condensate confined in a double-well potential $V_{\mathrm{dw}}(\boldsymbol{r})$ (Javanainen, 1986; Milburn *et al.*, 1997; Smerzi *et al.*, 1997; Zapata, Sols, and Leggett, 1998); see Fig. 10(a). For a sufficiently high barrier and weak interaction, we can describe the system in a two-mode approximation. The two modes are given by the first spatially symmetric $|\psi_{\mathrm{g}}\rangle$ and first antisymmetric $|\psi_{\mathrm{e}}\rangle$ solutions of the Gross-Pitaevskii equation in the double-well trap (Raghavan *et al.*, 1999; Ananikian and Bergeman, 2006). Spatial modes localized in the left and right wells are given by $|a\rangle = (|\psi_{\mathrm{g}}\rangle + |\psi_{\mathrm{e}}\rangle)/\sqrt{2}$ and $|b\rangle = (|\psi_{\mathrm{g}}\rangle - |\psi_{\mathrm{e}}\rangle)/\sqrt{2}$, respectively; see Fig. 10(a). The parameters in Eq. (69) are then identified as

$$\hbar\Omega = \mu_{\mathrm{e}} - \mu_{\mathrm{g}}, \tag{70a}$$

$$\hbar\chi = 2g\int d^3\boldsymbol{r}\psi_{\mathrm{g}}^2(\boldsymbol{r})\psi_{\mathrm{e}}^2(\boldsymbol{r}), \tag{70b}$$

where

$$\mu_{\mathrm{g}} = \int d^3\boldsymbol{r}\psi_{\mathrm{g}}(\boldsymbol{r})\left[-\frac{\hbar^2}{2M}\nabla^2 + V_{\mathrm{dw}}(\boldsymbol{r})\right]\psi_{\mathrm{g}}(\boldsymbol{r}) + gN\psi_{\mathrm{g}}^4(\boldsymbol{r}) \tag{71}$$

is the chemical potential (and analogous definition for μ_{e}), $g = 4\pi\hbar^2 a_{\mathrm{s}}/M$, a_{s} is the s-wave scattering length (positive for repulsive interactions and negative for attractive interactions), and M is the atomic mass. In the derivation of Eq. (69) we have taken $\psi_{\mathrm{g,e}}(\boldsymbol{r})$ real and normalized to 1, and assumed $\int d^3\boldsymbol{r}\psi_{\mathrm{g}}^2\psi_{\mathrm{e}}^2 \approx \int d^3\boldsymbol{r}\psi_{\mathrm{g}}^4 \approx \int d^3\boldsymbol{r}\psi_{\mathrm{e}}^4$, which is valid for a sufficiently high tunneling barrier. Experimentally, the external bosonic Josephson junction has been realized on atom chips (Schumm *et al.*, 2005; Hall *et al.*, 2007; Jo, Choi *et al.*, 2007; Maussang *et al.*, 2010; LeBlanc *et al.*, 2011) as well as in optical traps (Shin *et al.*, 2004; Albiez *et al.*, 2005; Hadzibabic *et al.*, 2006). The spatial separation allows for sensing of a variety of fields and forces (Cronin, Schmiedmayer, and Pritchard, 2009; Inguscio and Fallani, 2013). The experimental challenges are the required high degree of stability of the external potential as well as the precise control of the tunneling coupling between the two wells (Gati *et al.*, 2006; Levy *et al.*, 2007; Spagnolli *et al.*, 2017).

The internal bosonic Josephson junction is created with a trapped Bose-Einstein condensate in two different hyperfine states (Cirac *et al.*, 1998; Steel and Collett, 1998); see Fig. 10(b). The Josephson-like coupling is provided by an electromagnetic field that coherently transfers particles between the two states via Rabi rotations (Hall, Matthews, Ensher *et al.*, 1998; Hall, Matthews, Wieman, and Cornell, 1998; Böhi *et al.*, 2009). Assuming that the external motion of the atoms is not influenced by the internal dynamics, one can apply a single-mode approximation for each atomic species. The many-body Hamiltonian becomes Eq. (69) with coefficients

$$\hbar\Omega = \hbar\Omega_{\mathrm{R}}\int d^3\boldsymbol{r}\psi_a^*(\boldsymbol{r})\psi_b(\boldsymbol{r}), \tag{72a}$$

$$\hbar\chi = U_{aa} + U_{bb} - 2U_{ab}, \tag{72b}$$

$$U_{ij} = \frac{2\pi\hbar^2 a_s^{(i,j)}}{M}\int d^3\boldsymbol{r}|\psi_i(\boldsymbol{r})|^2|\psi_j(\boldsymbol{r})|^2, \tag{72c}$$

where Ω_{R} is the Rabi frequency, $a_{\mathrm{s}}^{(a,a)}$, $a_{\mathrm{s}}^{(b,b)}$ and $a_{\mathrm{s}}^{(a,b)}$ are the intraspecies and interspecies s-wave scattering lengths, and $\psi_{a,b}(\boldsymbol{r})$ are mode functions of the two internal states ($|a\rangle = |\psi_a\rangle$ and $|b\rangle = |\psi_b\rangle$ here), which can be determined in a mean-field description from the Gross-Pitaevskii equation. A more accurate value for χ is obtained if one also takes into account the change of the mode functions with particle number; see Smerzi and Trombettoni (2003) and Li *et al.* (2009). Since the phase and amplitude of the coupling field Ω_{R} can be switched on and off on nanosecond time scales, it is

possible to implement arbitrary rotations on the Bloch sphere that are helpful to read out and characterize the internal state. Furthermore, during Rabi coupling pulses it is possible to reach the regime $\Omega \gg N\chi$, where interaction effects can be neglected.

A. Metrologically useful entanglement in the ground state of the bosonic Josephson junction

Several approaches to the bosonic Josephson junction model Hamiltonian (69) have been discussed in the literature. A semiclassical mean-field approximation provides useful insight (Smerzi *et al.*, 1997; Raghavan *et al.*, 1999). It is obtained by replacing mode operators with complex numbers $\hat{a} \mapsto \sqrt{N_a}e^{-i\varphi_a}$ and $\hat{b} \mapsto \sqrt{N_b}e^{-i\varphi_b}$, where $N_{a,b}$ and $\varphi_{a,b}$ are the numbers of particles and phases of the condensate in the $|a\rangle$ and $|b\rangle$ modes, respectively. The spin operators are replaced by $\hat{J}_x \to (N/2)\sqrt{1-z^2}\cos\varphi$, $\hat{J}_y \to (N/2)\sqrt{1-z^2}\sin\varphi$, and $\hat{J}_z \to (N/2)z$, where $\varphi = \varphi_a - \varphi_b$ is the relative phase between the two condensate modes, and $z = (N_a - N_b)/N$ is the fractional population difference $(-1 \le z \le 1)$. The Hamiltonian (69) becomes

$$H(z,\varphi) = \frac{\Lambda z^2}{2} - \sqrt{1-z^2}\cos\varphi + \Delta E z, \tag{73}$$

where energies are in units of $N\hbar\Omega/2$, $\Lambda = N\chi/\Omega$, and $\Delta E = \delta/\Omega$. In the following we mainly focus on the case $\Delta E = 0$ unless explicitly stated.

A common method to extend the analysis beyond the mean-field approximation consists in quantizing the conjugate number and phase semiclassical variables (Leggett and Sols, 1991), i.e., replacing z and φ with operators $\hat{z}$ and $\hat{\varphi}$ obeying the commutation relation $[\hat{z},\hat{\varphi}] = 2i/N$, where $2/N$ plays the role of the Planck constant. We can thus write $\hat{\varphi} = -(2i/N)\hat{\partial}_z$ and $\hat{z} = (2i/N)\hat{\partial}_\varphi$ by canonical quantization. Note that a rigorous phase operator is lacking (Carruthers and Nieto, 1968; Lynch, 1995), and the above phase quantization may break down for large phase fluctuations. Series expanding Eq. (73) to second order in z and φ we have

$$H(z,\varphi) = \frac{\Lambda+1}{2}z^2 + \frac{\varphi^2}{2}. \tag{74}$$

By quantizing the conjugate variables we obtain

$$\hat{H}_z = -\frac{2}{N^2}\hat{\partial}_z^2 + \frac{\Lambda+1}{2}\hat{z}^2 \tag{75}$$

in number representation, and

$$\hat{H}_\varphi = -\frac{2(\Lambda+1)}{N^2}\hat{\partial}_\varphi^2 + \frac{1}{2}\hat{\varphi}^2 \tag{76}$$

in phase representation. Equations (75) and (76) predict Gaussian number and phase ground state wave functions with variances

$$\sigma_z^2 = \frac{1}{N\sqrt{1+\Lambda}} \quad \text{and} \quad \sigma_\varphi^2 = \frac{\sqrt{1+\Lambda}}{N}, \tag{77}$$

respectively (Smerzi and Raghavan, 2000; Paraoanu *et al.*, 2001). Improvements over Eqs. (75) and (76) have been discussed in the literature. Considering a second-order expansion in phase around $\varphi = 0$ of Eq. (73) one obtains the Hermitian Hamiltonian

$$\hat{H}_z = -\frac{2}{N^2}\hat{\partial}_z\sqrt{1-\hat{z}^2}\hat{\partial}_z + W_0(\hat{z}), \tag{78}$$

describing a fictitious quantum particle with z-dependent effective mass moving in an anharmonic one-dimensional potential

$$W_0(z) = \frac{\Lambda z^2}{2} - \sqrt{1-z^2} + \Delta E z. \tag{79}$$

Shchesnovich and Trippenbach (2008) derived the Hamiltonian (78) using a continuous approximation of the relative population difference and avoiding phase-number commutation relations; see also Javanainen and Ivanov (1999) and Spekkens and Sipe (1999). For $\Delta E = 0$, the effective potential (79) changes from harmonic, for $\Lambda > -1$, to quartic, at $\Lambda = -1$, to a double-well shape with wells centered at $z_\pm = \pm\sqrt{1-1/\Lambda^2}$, for $\Lambda < -1$. The fictitious quantum particle description is expected to give accurate results for large N, provided that the wave function is sufficiently smooth and vanishes at the boundaries of z (Juliá-Díaz, Zibold *et al.*, 2012), and phase fluctuations remain small. Anglin, Drummond, and Smerzi (2001) proposed a complementary approach consisting of a projection of the Hamiltonian (69) over the overcomplete Bargmann basis

$$|\varphi\rangle = \sum_{m=-N/2}^{N/2} \frac{e^{im\varphi}}{\sqrt{(N/2+m)!(N/2-m)!}}|m_z\rangle. \tag{80}$$

This leads to an exact quantum phase model

$$\hat{H}_{\rm BJJ}|\psi\rangle = \int_{-\pi}^{\pi}\frac{d\varphi}{2\pi}|\varphi\rangle e^{(N/2\Lambda)\cos\varphi}\hat{H}_{\rm EQPM}\psi(\varphi), \tag{81}$$

where $|\psi\rangle$ is an arbitrary two-mode state, $\psi(\varphi)$ is an effective phase wave function, and

$$\hat{H}_{\rm EQPM} = -\frac{2\Lambda}{N^2}\partial_\varphi^2 - \left(1+\frac{1}{N}\right)\cos(\varphi) - \frac{1}{4\Lambda}\cos(2\varphi). \tag{82}$$

The first two terms in Eq. (82) give the quantum phase model Hamiltonian that is widely used to study superconducting Josephson junctions (Barone and Paternò, 1982). The quantum phase model is relevant in the Josephson and Fock regimes; see below. The additional term proportional to $\cos(2\varphi)$ is important for weak interactions in the Rabi regime. Equation (82) is exact in the sense that the lowest $N+1$ frequencies in its eigenspectrum are exactly the spectrum of Eq. (69) (Anglin, Drummond, and Smerzi, 2001).

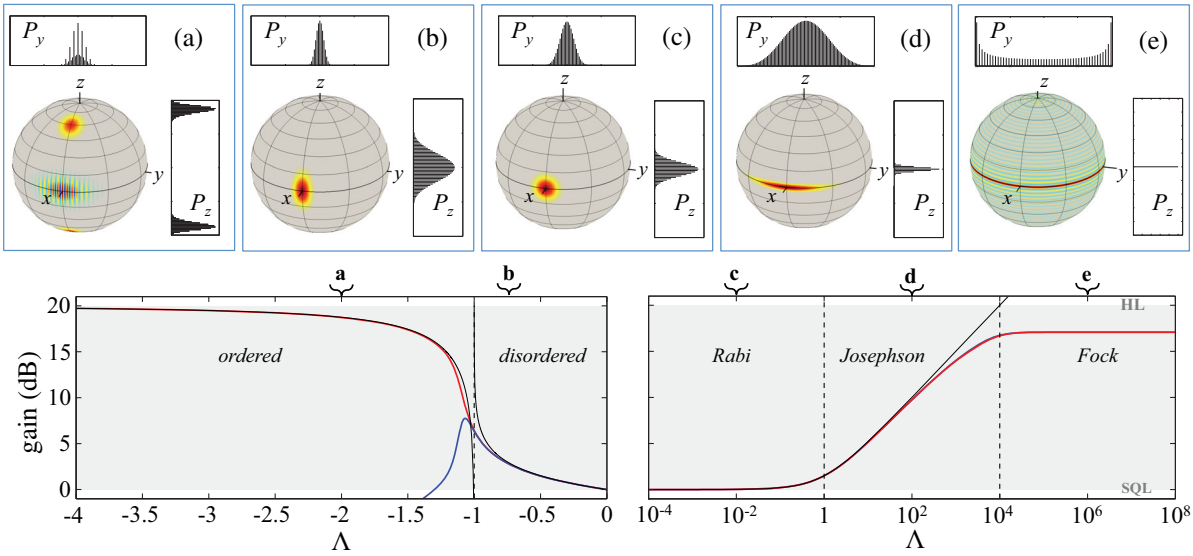

FIG. 11. Entanglement in the ground states of the bosonic Josephson junction. Upper panels: Normalized Wigner distributions of the ground state $|\psi_\Lambda\rangle$ of the Hamiltonian (69) in different regimes and for $\delta = 0$. The histograms are probability distributions $P_y(m) = |\langle m_y|\psi_\Lambda\rangle|^2$ and $P_z(m) = |\langle m_z|\psi_\Lambda\rangle|^2$. Crossing from the Rabi to the Fock regime (for positive nonlinearities), P_z narrows while P_y broadens. In the Fock regime, P_y vanishes for odd values of m. In the transition from the disordered to the ordered phase (for negative nonlinearities), P_y narrows while P_z broadens and splits when crossing the critical value $\Lambda = -1$. Lower panels: Normalized quantum Fisher information (F_Q/N, red line) and inverse spin-squeezing parameter ($1/\xi_R^2$, blue line) as a function of Λ. For $\Lambda > 0$, the solid black line is Eq. (83). For $\Lambda < 0$, the solid black lines are Eq. (87) in the disordered regime and Eq. (88) in the ordered regime. Here $N = 100$ and the color scale of the Wigner distributions is as in Fig. 5.

Finally, it is worth pointing out that the spectrum of Eq. (69)—and of the more general Lipkin-Meshkov-Glick model—is analytically known within a Bethe ansatz (Pan and Draayer, 1999; Morita *et al.*, 2006) and in the thermodynamic limit (Ribeiro, Vidal, and Mosseri, 2007, 2008).

1. Ground state for positive nonlinearities

A positive effective nonlinearity ($\Lambda > 0$) makes number fluctuations between the two modes energetically unfavorable. The ground state $|\psi_\Lambda\rangle$ of Eq. (69) with $\delta = 0$ is thus characterized by a squeezed atom number distribution at the expense of increased phase fluctuations (Leggett and Sols, 1998; Steel and Collett, 1998; Javanainen and Ivanov, 1999; Spekkens and Sipe, 1999). Following Leggett (2001), we distinguish three regimes; see Fig. 11.

a. Rabi regime, $0 < \Lambda \ll 1$

At $\Lambda = 0$ the ground state is given by the coherent spin state pointing in the positive-x direction (for $\Omega > 0$), $|\psi_{\Lambda=0}\rangle \propto (\hat{a}^\dagger + \hat{b}^\dagger)^N|\text{vac}\rangle$, with binomial occupation of each mode, where $|\text{vac}\rangle$ is the vacuum. In the Rabi regime, the Josephson junction is dominated by tunneling, which keeps a well-defined relative phase between the two modes. The coherence is high, $\langle \hat{J}_x\rangle \approx N/2$, and number (phase) fluctuations slightly decrease (increase) with respect to the noninteracting case. Using $(\Delta\hat{J}_y)^2 = N^2\sigma_\varphi^2/4$, $(\Delta\hat{J}_z)^2 = N^2\sigma_z^2/4$, and Eq. (77), we find

$$\xi_R^2 = \frac{1}{\sqrt{1+\Lambda}} \quad \text{and} \quad \frac{F_Q[|\psi_\Lambda\rangle, \hat{J}_y]}{N} = \sqrt{\Lambda+1}. \tag{83}$$

In particular, $F_Q/N = 1/\xi_R^2$ in this regime.[12] The ground state of Eq. (69) is spin squeezed along the z axis and useful for sensing rotations around the y axis.

b. Josephson regime, $1 \ll \Lambda \ll N^2$

In the Josephson regime number (phase) fluctuations are further reduced (increased) while the coherence remains high. The approximations leading to Eq. (77) are still very good. We thus expect Gaussian number and phase distributions with width $\sigma_z^2 = 1/(N\sqrt{\Lambda})$ and $\sigma_\varphi^2 = \sqrt{\Lambda}/N$, respectively, giving (Pezzè *et al.*, 2005)

$$\xi_R^2 = \frac{1}{\sqrt{\Lambda}} \quad \text{and} \quad \frac{F_Q[|\psi_\Lambda\rangle, \hat{J}_y]}{N} = \sqrt{\Lambda}. \tag{84}$$

For a fixed ratio $\chi/\Omega = \Lambda/N$, we have $F_Q/N = 1/\xi_R^2 = \sqrt{\chi/\Omega}\sqrt{N}$, predicting a scaling of phase sensitivity $(\Delta\theta_{QCR})^2 \sim N^{-3/2}$, intermediate between the standard quantum limit and the Heisenberg limit.

[12] In Eqs. (83)–(86), i.e., for positive nonlinearities, the spin squeezing is calculated as $\xi_R^2 = N(\Delta\hat{J}_z)^2/\langle\hat{J}_x\rangle^2$. For negative nonlinearities, Eq. (87), as $\xi_R^2 = N(\Delta\hat{J}_y)^2/\langle\hat{J}_x\rangle^2$.

c. Fock regime, $\Lambda \gg N^2$

In the Fock regime interaction dominates over tunneling, giving rise to a fragmented Bose-Einstein condensate (Spekkens and Sipe, 1999; Jääskeläinen, Zhang, and Meystre, 2004). Phase fluctuations become of the order of 2π and the approach leading to Eq. (77) breaks down. The ground state is approximately obtained by putting an equal number of particles in both modes with vanishing number fluctuations. For $\Lambda \to \infty$ and even values of N, we have $|\psi_\Lambda\rangle = (\hat{a}^\dagger)^N(\hat{b}^\dagger)^N|\text{vac}\rangle = |N/2\rangle_a|N/2\rangle_b$. In the limit of large but finite Λ, we find

$$\xi_R^2 = \frac{2}{N+2} \quad \text{and} \quad \frac{F_Q[|\psi_\Lambda\rangle, \hat{J}_\perp]}{N} = \frac{N+2}{2}, \tag{85}$$

where $\perp$ is any axis on the equatorial plane of the Bloch sphere. In this limit, both $(\Delta\hat{J}_z)^2$ and $\langle\hat{J}_x\rangle$ vanish, such the ratio $\xi_R^2 = N(\Delta\hat{J}_z)^2/\langle\hat{J}_x\rangle$ is finite but very sensitive to experimental noise. For odd values of N, the ground state is given by

$$|\psi_\Lambda\rangle = \frac{1}{\sqrt{2}}\left(\left|\frac{N+1}{2}\right\rangle_a\left|\frac{N-1}{2}\right\rangle_b + \left|\frac{N-1}{2}\right\rangle_a\left|\frac{N+1}{2}\right\rangle_b\right),$$

which is spin squeezed with

$$\xi_R^2 = \frac{4N}{N(N+2)+1} \quad \text{and} \quad \frac{F_Q[|\psi_\Lambda\rangle, \hat{J}_\perp]}{N} = \frac{(N^2-1)}{2N} + 1. \tag{86}$$

2. Ground state for negative nonlinearities

A negative effective nonlinearity ($\Lambda < 0$) favors localization of particles in one mode and, in a symmetric Josephson junction ($\delta = 0$), enhances number fluctuations between the two modes. The interplay of linear coupling and nonlinear interaction in the Hamiltonian (69) gives rise to a second-order quantum phase transition with discrete symmetry breaking and mean-field critical exponents (Gilmore and Feng, 1978; Botet, Jullien, and Pfeuty, 1982; Ulyanov and Zaslavskii, 1992). The quantum phase transition occurs in the thermodynamic limit $N \to \infty$ and $\chi \to 0$ such that $\Lambda = -1$. The order parameter is given by the absolute value of the population imbalance $|z|$ with $W_0(z)$ in Eq. (79) playing the role of an effective Ginzburg-Landau potential. Entanglement (Vidal, Palacios, and Mosseri, 2004; Orús, Dusuel, and Vidal, 2008; Ma and Wang, 2009; Mazzarella *et al.*, 2011; Buonsante *et al.*, 2012) and fluctuations of the order parameter (Zin *et al.*, 2008) approaching the critical point have been extensively studied. This quantum phase transition has been experimentally investigated by Trenkwalder *et al.* (2016) in a double-well potential with potassium atoms of tunable interaction. The dynamics following the sudden quench into the vicinity of the quantum critical point (in a two-component Bose gas) has been studied by Nicklas *et al.* (2015).

a. Disordered phase, $-1 < \Lambda < 0$

The approximations leading to Eq. (77) remain valid also for weak attractive interactions. This equation predicts phase squeezing and number antisqueezing (Steel and Collett, 1998):

$$\xi_R^2 = \sqrt{1+\Lambda} \quad \text{and} \quad \frac{F_Q[|\psi_\Lambda\rangle, \hat{J}_z]}{N} = \frac{1}{\sqrt{1+\Lambda}}. \tag{87}$$

The ground state is entangled and useful for sensing rotations around the z axis; see Fig. 11. At $\Lambda \to -1$ the harmonic oscillator approximation breaks down and Eq. (77) predicts a divergence of number fluctuations. At the transition point one finds $F_Q/N \approx 1/\xi_R^2 = \mathcal{O}(N^{1/3})$ (Hauke *et al.*, 2016; Gabbrielli, Smerzi, and Pezzè, 2018).

b. Ordered phase, $\Lambda < -1$

This phase is characterized by the presence of macroscopic-superposition states (Cirac *et al.*, 1998; Ho and Ciobanu, 2004; Huang and Moore, 2006; Lee, 2006). Soon after crossing the quantum phase transition critical point, the mean spin length $\|\langle\hat{\boldsymbol{J}}\rangle\|$ vanishes and spin squeezing is lost for $\Lambda < -\sqrt{(1+\sqrt{5})/2}$ (Gabbrielli, Smerzi, and Pezzè, 2018); see Fig. 11. For strong nonlinearities $\Lambda \ll -1$ and unbalanced modes (with $\Delta E = 0$), the ground state is given by the symmetric superposition (i.e., a Schrödinger-cat-like state, see Fig. 11) of distinguishable states localized on the right and left wells of the effective double-well Ginzburg-Landau potential $W_0(z)$ in Eq. (79) (Shchesnovich and Trippenbach, 2008), giving

$$\frac{F_Q[|\psi_\Lambda\rangle, \hat{J}_z]}{N} = N\left(1 - \frac{1}{\Lambda^2}\right). \tag{88}$$

In this regime, the quantum Fisher information has thus a Heisenberg scaling with N. Finally, for $\Lambda \ll -\sqrt{N}$, the ground state is approximatively given by a NOON state (Shchesnovich and Trippenbach, 2008). The macroscopic superposition states are lost for an infinitesimally small energy imbalance $\Delta E \neq 0$, breaking the symmetry of $W_0(z)$.

3. Adiabatic splitting

Experimentally, the Rabi and Josephson regimes for repulsive interactions, and the disordered phase for attractive interactions, can be reached by adiabatically splitting a Bose-Einstein condensate initially prepared in the ground state of the strong-tunneling (Rabi) regime (Javanainen and Ivanov, 1999; Menotti *et al.*, 2001; Isella and Ruostekoski, 2005; Pezzè *et al.*, 2005; Streltsov, Alon, and Cederbaum, 2007; Bodet *et al.*, 2010). By varying the plasma frequency $\omega_p = \Omega\sqrt{1+\Lambda}$ adiabatically in time, the system follows its ground state if (Javanainen and Ivanov, 1999; Schaff, Langen, and Schmiedmayer, 2014)

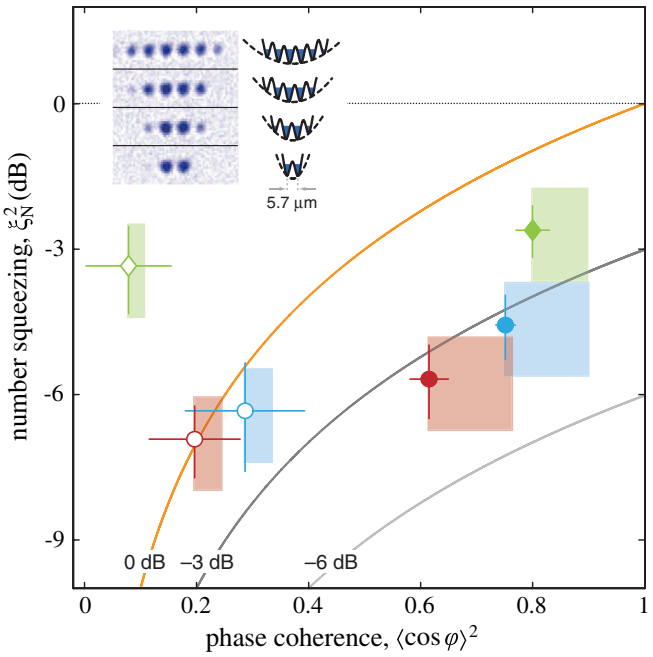

FIG. 12. Spin squeezing in the ground states of the bosonic Josephson junction. Symbols report number squeezing (with photon shot-noise subtracted) and phase coherence obtained by splitting a Bose-Einstein condensate. Open and filled symbols correspond to different barrier heights (larger for the open symbols). The shaded areas show systematic error bounds. Solid lines are reference values for ξ^2_R, the orange (0 dB) line being the standard quantum limit. Measurements are shown for the two main well pairs of a six-well lattice [red (dark) and blue (light) circles] and for a double-well potential (green diamonds). The total atom number in each pair is approximately $N = 2200$ in the six-well case and $N = 1600$ in the double-well case. The inset shows single-site-resolving absorption images of atoms trapped in an optical lattice superposed on an atomic dipole trap. Adapted from Estève *et al.*, 2008.

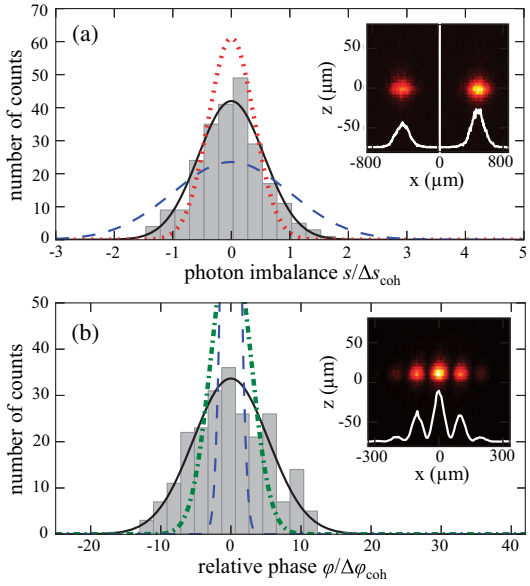

FIG. 13. Number and phase distributions after the adiabatic splitting of a Bose-Einstein condensate in a double-well potential. (a) Distribution of photon imbalance $s = s_L - s_R$ between fluorescence images of the left and right clouds (inset), proportional to the imbalance of atom numbers in the two wells. The solid black line is the normal distribution corresponding to the measured number-squeezing factor, the dotted red line is the expected distribution when detection noise is subtracted, and the dashed blue line is the distribution expected for a coherent spin state in the absence of detection noise. (b) The curves indicate a normal distribution with the measured $\Delta\varphi$ (solid black line) and the distributions expected for a coherent state in the absence (dashed blue line) and in the presence (dash-dotted green line) of detection noise. The inset shows a typical matter-wave interference pattern from which the phase is extracted. Adapted from Berrada *et al.*, 2013.

$$\left|\frac{d\omega_p}{dt}\right| \lesssim \omega_p^2. \tag{89}$$

Increasing the height of the potential barrier in order to reach the Fock regime, the required time scale for adiabaticity eventually diverges, setting a limit to the attainable entanglement. A shortcut to adiabaticity (Juliá-Díaz, Torrontegui *et al.*, 2012; Lapert, Ferrini, and Sugny, 2012; Yuste *et al.*, 2013) and optimal control techniques (Huang and Moore, 2008; Grond, Schmiedmayer, and Hohenester, 2009; Pichler *et al.*, 2016) for the fast production of highly entangled states have also been studied. It should be noted that Eq. (89) assumes that the gas is prepared in the ground state configuration. Experimentally, the finite temperature of the gas is the main factor limiting the squeezing via the adiabatic-splitting technique (Estève *et al.*, 2008).

4. Experimental spin squeezing in the ground state of the BJJ

Estève *et al.* (2008) reported the first direct experimental demonstration of spin squeezing and entanglement in the ground state of the bosonic Josephson junction. A ^{87}Rb Bose-Einstein condensate confined in a shallow harmonic trap is split adiabatically by ramping up a one-dimensional optical lattice. The particles are distributed over two and six lattice sites; see the inset of Fig. 12. Direct atom detection better than atomic shot noise is implemented by absorption imaging of the atomic density, with a spatial resolution well below the lattice spacing. This gives direct access to the number-squeezing parameter $\xi^2_N = 4(\Delta\hat{J}_z)^2/N$. Additionally, the phase coherence $\langle\cos\varphi\rangle^2$ is directly obtained from the interference pattern observed after releasing the atomic cloud from the trap. Noticing that $\langle\hat{J}_x\rangle^2 = \langle\hat{N}_a\rangle\langle\hat{N}_b\rangle\langle\cos\varphi\rangle^2$ (valid for $\langle\hat{N}_a\rangle, \langle\hat{N}_b\rangle \approx N/2 \gg 1$, and $\sigma^2_\varphi \ll 2\pi$), metrological spin squeezing is given by $\xi^2_R = \xi^2_N/\langle\cos\varphi\rangle^2$. The simultaneous presence of number squeezing and high phase coherence allowed one to reach an inferred spin squeezing of $\xi^2_R = -3.8$ dB for the two main well pairs of a six-well lattice, and $\xi^2_R = -2.3$ dB for the double-well configuration. The results are summarized in Fig. 12.

More recent experiments studied number squeezing (Maussang *et al.*, 2010) and spin squeezing (Berrada *et al.*, 2013) when splitting a Bose-Einstein condensate in a double-well trap on an atom chip. Maussang *et al.* (2010) realized purely magnetic double-well potential. This experiment reports a detailed investigation of the optimal splitting time,

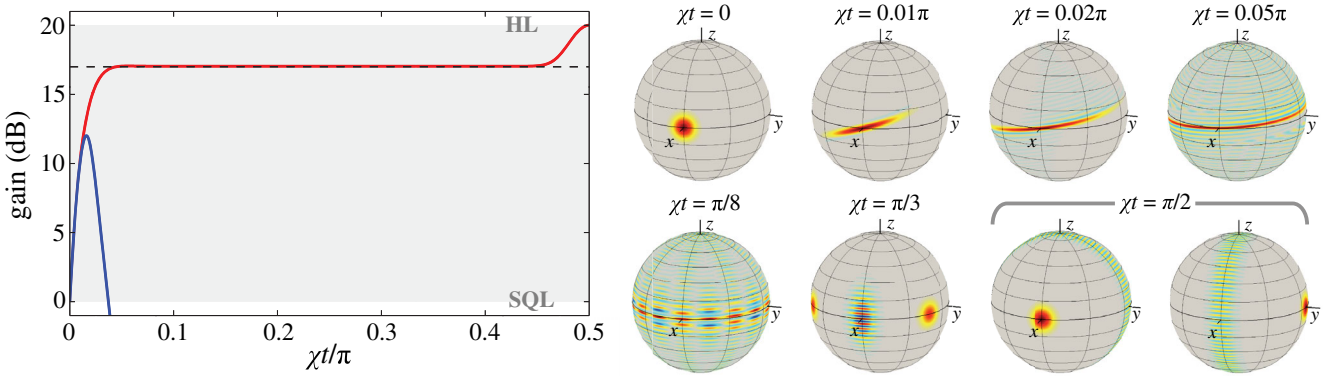

FIG. 14. One-axis twisting dynamics. The left panel reports the inverse spin-squeezing parameter ($1/\xi_R^2$, blue, lower line) and normalized quantum Fisher information (F_Q/N, red, upper line) as a function of $\chi t/\pi$. The right panels show snapshots of the Wigner distribution at different times. For $\chi t = \pi/2$ we plot both the Wigner distributions for $N = 100$ (left) and $N = 101$ (right). In all plots $N = 100$ (unless specified) and the color scale is as in Fig. 5.

given by the interplay of the barrier raising rate (which must be slow in order to avoid excitations to higher modes), heating effects, and atom loss. Berrada *et al.* (2013) based the splitting on a radio-frequency dressing (Hofferberth *et al.*, 2006) that dynamically deforms the static magnetic trap into a double-well potential (Schumm *et al.*, 2005). A split Bose-Einstein condensate of $N = 1200$ ^{87}Rb atoms is characterized via the measurement of the number of particles in each well and the relative phase, see Fig. 13, showing number squeezing and phase antisqueezing. From these results, using $\xi_R^2 = \xi_N^2/\langle\cos\varphi\rangle^2$, it is possible to obtain $\xi_R^2 = -5.6$ dB ($\xi_R^2 = -7.8$ dB inferred). This corresponds to a metrologically useful entanglement depth of 150 atoms, excluding useful entanglement of less than 67 particles with 90% probability. Berrada *et al.* (2013) also investigated the reduced phase diffusion associated with number squeezing (Lewenstein and You, 1996; Castin and Dalibard, 1997; Javanainen and Wilkens, 1997) and the fast recombination (Negretti and Henkel, 2004; Jo, Choi *et al.*, 2007; Negretti, Henkel, and Mølmer, 2008; Scott, Judd, and Fromhold, 2008; Berrada *et al.*, 2016) of the condensates in the two wells.

B. One-axis twisting dynamics

One-axis twisting is a benchmark model for studying the generation of spin-squeezed states (Kitagawa and Ueda, 1993), Schrödinger cats (Mølmer and Sørensen, 1999), and useful entanglement for quantum metrology (Pezzè and Smerzi, 2009). The one-axis twisting Hamiltonian (here along the z axis) is

$$\hat{H}_{\rm OAT} = \hbar\chi\hat{J}_z^2. \tag{90}$$

This model can be realized via atom-atom elastic collisions in a Bose-Einstein condensate (Sørensen *et al.*, 2001), trapped ions, see Sec. VI.B, and cold atoms in an optical cavity, see Sec. V.B.

The quantum dynamics $e^{-i\hat{H}_{\rm OAT}t/\hbar}$ of a localized spin wave packet can be roughly viewed as a rotation $e^{-i\chi t\langle\hat{J}_z\rangle\hat{J}_z}$ around the z axis. The $\langle\hat{J}_z\rangle$-dependent angular velocity (whose sign differs on the two hemispheres of the Bloch sphere) leads to a twisting of the state on the Bloch sphere. To analyze this effect quantitatively, let us consider the dynamical evolution of an initial coherent spin state pointing along the positive x axis, $|\psi_{\rm OAT}(\chi t)\rangle = e^{-i\chi t\hat{J}_z^2}|\pi/2, 0, N\rangle$; see Fig. 14. The coherent spin state initially stretches in the y-z plane tangential to the Bloch sphere. Kitagawa and Ueda (1993) identified the squeezing angle $\delta = (1/2)\arctan(B/A)$ in terms of $A = 1 - \cos^{N-2}(2\chi t)$ and $B = 4\sin(\chi t)\cos^{N-2}(\chi t)$, as well as the squeezed and antisqueezed spin components $\hat{J}_s = \hat{J}_z\cos(\delta) - \hat{J}_y\sin(\delta)$ and $\hat{J}_{as} = \hat{J}_y\cos(\delta) + \hat{J}_z\sin(\delta)$, respectively. Squeezing is accompanied by loss of contrast $\langle\hat{J}_x\rangle = (N/2)\cos^{N-1}(\chi t)$ as the state spreads on the Bloch sphere. The spin squeezing $\xi_R^2 = N(\Delta\hat{J}_s)^2/\langle\hat{J}_x\rangle^2$ and the quantum Fisher information $F_Q[|\psi_{\rm OAT}(\chi t)\rangle, \hat{J}_{as}] = 4(\Delta\hat{J}_{as})^2$ are readily calculated, giving (Kitagawa and Ueda, 1993; Sørensen *et al.*, 2001)

$$\xi_R^2 = \frac{4 + (N-1)(A - \sqrt{A^2 + B^2})}{4\cos^{2N-2}(\chi t)}, \tag{91}$$

and (Pezzè and Smerzi, 2009)

$$\frac{F_Q[|\psi_{\rm OAT}(t)\rangle, \hat{J}_{as}]}{N} = 1 + \frac{(N-1)}{4}(A + \sqrt{A^2 + B^2}), \tag{92}$$

respectively.[13] For $\chi t \lesssim 1/\sqrt{N}$ the state is spin squeezed, $\xi_R^2 < 1$, reaching $\xi_R^2 = \mathcal{O}(N^{-2/3})$ at an optimal time $\chi t = \mathcal{O}(N^{-2/3})$. For $\chi t \gtrsim 1/\sqrt{N}$ the states wraps around the Bloch sphere and spin squeezing is lost, $\xi_R^2 > 1$. Yet, the state is still entangled. The quantum Fisher information reaches a plateau $F_Q[|\psi_{\rm OAT}(\chi t)\rangle, \hat{J}_{as}] = N(N+1)/2$ for $2/\sqrt{N} \lesssim \chi t \lesssim \pi/2 - 2/\sqrt{N}$ signaling entanglement in the oversqueezed state (Pezzè and Smerzi, 2009), according to Eq. (37). The state

[13]The quantum Fisher information optimized over rotation directions in the Bloch sphere is given by the maximum between $F_Q[|\psi_{\rm OAT}(\chi t)\rangle, \hat{J}_{as}]/N$, Eq. (92), and $F_Q[|\psi_{\rm OAT}(\chi t)\rangle, \hat{J}_x]/N = N[1 - \cos^{2N-2}(\chi t)] - (N-1)A/2$.

evolves at time $\chi t = \pi/n$ into a coherent superposition of $2 \leq n \lesssim \pi\sqrt{N}/2$ coherent spin states distributed evenly on the equator of the Bloch sphere (Agarwal, Puri, and Singh, 1997); see Fig. 14. At $\chi t = \pi/2$ we observe the dynamical creation of a NOON state along the x axis $|\psi_{\mathrm{OAT}}(\pi/2)\rangle = e^{-i(\pi/2)\hat{J}_y}|\mathrm{NOON}\rangle$ if N is even and along the y axis $|\psi_{\mathrm{OAT}}(\pi/2)\rangle = e^{-i(\pi/2)\hat{J}_x}|\mathrm{NOON}\rangle$ if N is odd (Agarwal, Puri, and Singh, 1997; Mølmer and Sørensen, 1999). For the NOON state, the quantum Fisher information, optimized over the spin direction, reaches its maximum value $F_{\mathrm{Q}} = N^2$; see Sec. II.C.7. For even (odd) values of N, the dynamics is reversed for $\chi t \geq \pi/2$ ($\chi t \geq \pi$) and we have a complete revival of the initial condition at $\chi t = \pi$ ($\chi t = 2\pi$). The one-axis twisting dynamics is modified by particle loss (Li, Castin, and Sinatra, 2008; Sinatra *et al.*, 2011; Sinatra, Witkowska, and Castin, 2012; Sinatra, Castin, and Witkowska, 2013; Spehner *et al.*, 2014) and other imperfections such as phase noise (Ferrini, Minguzzi, and Hekking, 2008; Ferrini *et al.*, 2011) and finite temperature of the Bose gas (Sinatra *et al.*, 2011), limiting the achievable squeezing. We further comment on these works in Sec. VII.

1. Spin squeezing and particle entanglement

Spin squeezing obtained via one-axis twisting dynamics in a Bose-Einstein condensate was first experimentally demonstrated by Gross *et al.* (2010) and Riedel *et al.* (2010). These experiments used a ^{87}Rb condensate prepared in a coherent spin state with equal mean populations in two hyperfine states. With ^{87}Rb atoms, the interaction parameter $\hbar\chi = U_{aa} + U_{bb} - 2U_{ab}$, see Eq. (72b), is small due to an almost perfect compensation of interspecies and intraspecies collisional interactions, i.e., $2U_{ab} \approx U_{aa} + U_{bb}$. Different approaches have been used to increase χ artificially.

Riedel *et al.* (2010) used a spatially inhomogeneous microwave field to manipulate the trapping potentials of the atom cloud in the two hyperfine states $|a\rangle = |F = 1, m_F = -1\rangle$ and $|b\rangle = |2, 1\rangle$ by microwave level shifts (Treutlein *et al.*, 2006; Böhi *et al.*, 2009). The trapping potential for atoms in one state is suddenly shifted by such a state-selective force, and the states coherently demix and begin to oscillate in space. In this way the overlap of the wave functions of the two states changes dynamically and modulates collisional effects (Li *et al.*, 2009): according to Eq. (72c), when the two components are spatially separated, the interspecies interaction U_{ab} vanishes. The parameter χ is then determined solely by intraspecies interactions and reaches sufficiently high values to induce fast spin-squeezing dynamics. After each full oscillation, the two states coherently remix and the collisional squeezing dynamics stops. Spin-noise tomography and the reconstructed Wigner distribution of the squeezed state are shown in Fig. 15. The results demonstrate a squeezing parameter $\xi_{\mathrm{R}}^2 = -1.2$ dB ($\xi_{\mathrm{R}}^2 = -2.5$ dB inferred). More recent experiments using this technique achieved up to $\xi_{\mathrm{R}}^2 = -7.0$ dB with detection noise subtracted (Ockeloen *et al.*, 2013; Schmied *et al.*, 2016).

Gross *et al.* (2010) used a Bose-Einstein condensate of $N \approx 400$ atoms in the $|a\rangle = |1, 1\rangle$ and $|b\rangle = |2, -1\rangle$ hyperfine levels of the electronic ground state of rubidium. A bias magnetic field is used to bring the system near a Feshbach resonance (Chin *et al.*, 2010) in order to reduce the interspecies s-wave scattering length $a_s^{(a,b)}$. This enhances the effective nonlinearity χ leading to squeezing and entanglement. Spin-noise tomography leads to an inferred $\xi_{\mathrm{R}}^2 = -8.2$ dB, predicting an entanglement depth excluding less than 80 particles within 3 standard deviations (and a mean of 170 entangled atoms).

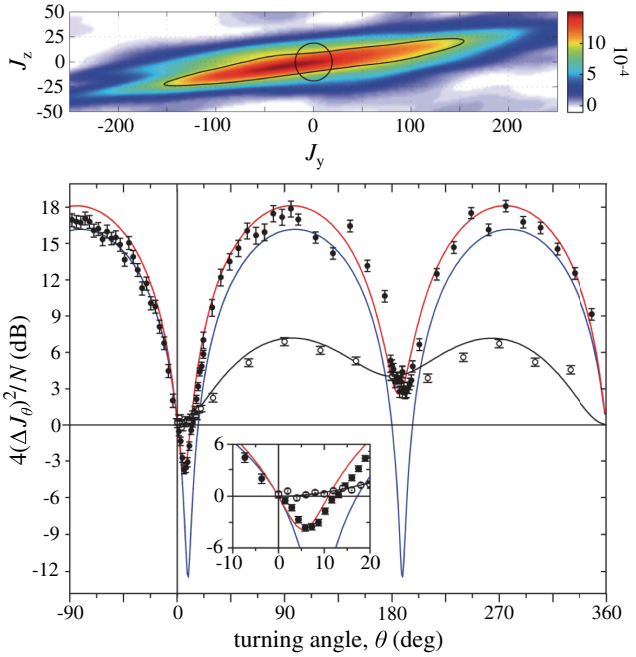

FIG. 15. Spin-noise tomography and reconstructed Wigner function of a spin-squeezed Bose-Einstein condensate. Top: Reconstructed Wigner distribution of a spin-squeezed state of $N \approx 1250$ atoms. The black contour line indicates where the Wigner distribution has fallen to $1/e$ of its maximum. For comparison, the circular $1/e$ contour of an ideal coherent spin state is shown. Bottom: Observed spin fluctuations of a spin-squeezed state (solid circles) and of a coherent spin state (open circles), as a function of the turning angle of the Bloch sphere. Solid lines are results of dynamical simulations including losses and technical noise: blue (lowest), spin-squeezed state with losses but without technical noise; red (highest), spin-squeezed state with losses and technical noise; and black, coherent state with losses and technical noise. Adapted from Riedel *et al.*, 2010.

2. Quantum interferometry

Gross *et al.* (2010) also demonstrated a full Ramsey interferometer sequence with spin-squeezed states; see Fig. 16. The squeezed-state creation is followed by a rotation around the x axis to prepare a phase-squeezed state (i.e., squeezed along the y axis)—in effect constructing a nonlinear beam splitter. After a short interrogation time $\chi t \ll 1$, during which the interaction is still active, a second $\pi/2$ beam splitter closes the Ramsey sequence. The directly measured phase sensitivity gain is $(\Delta\theta/\Delta\theta_{\mathrm{SQL}})^2 = -1.4$ dB, corresponding to a reduction of phase variance 15% below the standard quantum limit. In a more recent experiment, Muessel *et al.* (2014) were able to scale the generation of spin-squeezed

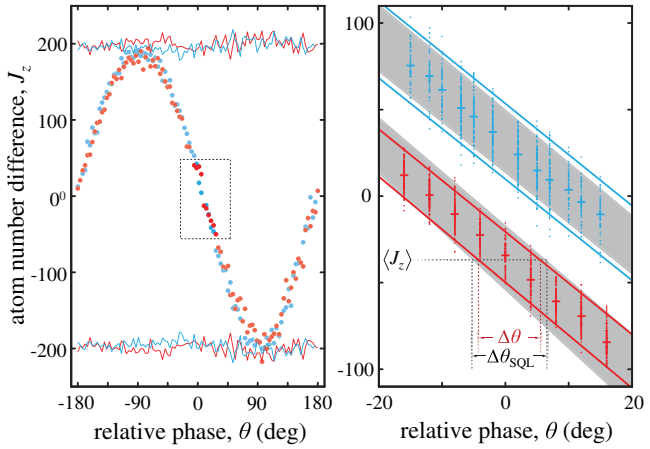

FIG. 16. Direct experimental demonstration of a phase sensitivity beyond the standard quantum limit using an atomic spin-squeezed state. Left: Ramsey fringe scanned over a full 2π period. The blue (lighter) data are obtained with a coherent spin state, the red (darker) data with a spin-squeezed state showing a visibility of 92%. Solid lines are $\pm N/2$, measured for each phase setting, as a reference. Right: Ramsey fringe around the maximum-slope optimal point. The solid lines are fits through the lower and upper ends of the 2 standard deviation error bars. The gray shaded areas are the uncertainty regions for an ideal coherent spin state; they correspond to the standard quantum limit. Red (darker) data show a phase error 15% below the standard quantum limit. Adapted from Gross *et al.*, 2010.

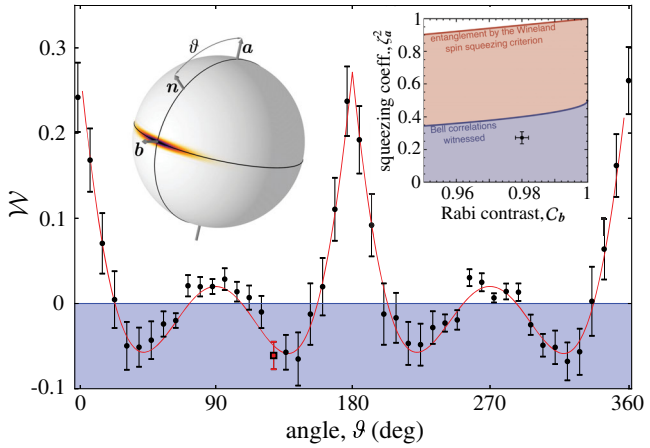

FIG. 17. Bell correlations in a Bose-Einstein condensate. Measurement of the Bell correlation witness $\mathcal{W}$ of Eq. (63) on a spin-squeezed state as a function of the angle ϑ between the squeezing axis a and the axis n lying in the squeezing plane, with 1σ error bars. The continuous red line is the value of $\mathcal{W}$ computed from the measurement of $\zeta_a^2 = 4\langle \hat{J}_a^2 \rangle / N$ and the fitted Rabi oscillation $\mathcal{C}_n = \mathcal{C}_b \sin(\vartheta)$ with $\mathcal{C}_b = 2\langle \hat{J}_b \rangle / N$. Bell correlations are present in the blue shaded region. Right inset: Representation of the same data (ζ_a^2 and $\mathcal{C}_b$) as a single black point, with 1σ error bars. Red shaded region: Entanglement detected by spin squeezing $\xi_{\rm R}^2 < 1$, Eq. (41). Blue shaded region: Bell correlations detected by violation of the witness inequality (64). Adapted from Schmied *et al.*, 2016.

states up to $N = 12\,500$ particles using a chain of trapped independent condensates and exploiting a differential estimation of the phase. They demonstrated a spin squeezing $\xi_{\rm R}^2 = -3.4$ dB and a sensitivity 24% below the standard quantum limit. Ramsey interferometry using spin-squeezed states generated via one-axis twisting in Bose-Einstein condensate has recently found application to sense magnetic fields (Ockeloen *et al.*, 2013; Muessel *et al.*, 2014), as discussed in more detail in Sec. VII.

3. Bell correlations

Schmied *et al.* (2016) observed Bell correlations in spin-squeezed Bose-Einstein condensates of about $N = 480$ ^{87}Rb atoms trapped on an atom chip. Following the generation of the spin-squeezed state by one-axis twisting, the Bell correlation witness $\mathcal{W}$ of Eq. (63) is determined by measuring the second spin moment along the squeezed direction and combining it with spin contrast measurements along other projection axes; see Fig. 17. The measured values of $\mathcal{W}$ violate the inequality (63) and thus also the inequalities (64) and (65). This proves the presence of Bell correlations and implies that the spin-squeezed states can violate the many-particle Bell inequality of Tura *et al.* (2014). The detection of Bell correlations indicates that spin-squeezed states are useful beyond quantum metrology: they also contain the resource for quantum-information tasks such as certified randomness generation or quantum key distribution (Brunner *et al.*, 2014).

While Schmied *et al.* (2016) observed Bell correlations in a spin-squeezed Bose-Einstein condensate, Engelsen *et al.* (2017) confirmed Bell correlations in a spin-squeezed thermal ensemble. The interpretation of these experiments relies on the common assumption that atoms do not communicate through unknown channels. This assumption can be relaxed if the atoms are spatially separated in an optical lattice potential, as proposed by Pelisson, Pezzè, and Smerzi (2016). Many-body Bell tests with Bose-Einstein condensates have also been proposed by Mullin and Laloë (2008) and Laloë and Mullin (2009). In Sec. III.D we discuss proposals to create entanglement between spatially separated condensates, which could also be employed for Bell tests.

C. Twist-and-turn dynamics

The creation of entanglement in the one-axis twisting model is enriched, and accelerated to some extent (Muessel *et al.*, 2015; Sorelli, Pezzè, and Smerzi, 2015), by the dynamical evolution using the turning term $\hat{J}_x$ simultaneously with the twisting term J_z^2 in the Hamiltonian (69). The resulting twist-and-turn dynamics is experimentally studied from the starting point of a coherent spin state pointing in the $+x$ or $-x$ direction. The interaction is suddenly switched to a finite value of Λ in presence of linear coupling.

The twist-and-turn dynamics can be described as the evolution of an effective relative-number wave packet (Juliá-Díaz, Zibold *et al.*, 2012). For an initial coherent spin state polarized along the positive x axis, the effective Hamiltonian is given by Eq. (78). $W_0(z)$ can be well approximated as a harmonic potential of frequency $\omega_0 = \Omega\sqrt{1+\Lambda}$. Suddenly switching the interaction from $\Lambda = 0$ to a positive value (corresponding to a tighter harmonic

oscillator potential, i.e., $\omega_0/\Omega > 1$) gives rise to a breathing mode of the effective wave packet with periodic squeezing of the relative population. For a coherent spin state polarized along the negative x axis, the effective potential is

$$W_\pi(z) = -\frac{\Lambda z^2}{2} - \sqrt{1-z^2}. \tag{93}$$

For $0 < \Lambda < 1$, $W_\pi(z)$ is harmonic with frequency $\omega_\pi = \Omega\sqrt{1-\Lambda}$. Since $\omega_\pi/\Omega < 1$, in this case a sudden switch of the interaction leads to a breathing motion predicting number antisqueezing (and phase squeezing). Damping of the oscillations is observed for increasing values of Λ (Gordon and Savage, 1999; Choi and Bigelow, 2005) corresponding to the wave packet feeling the anharmonicity of the effective potential.

These predictions are recovered for $0 < \Lambda \ll 1$ by a frozen-spin approximation (Law, Ng, and Leung, 2001) that consists of neglecting fluctuations of the mean spin $\hat{J}_x$ being replaced by $\pm N/2$. The variances

$$(\Delta\hat{J}_z)^2 = \frac{N}{4}\left(\cos^2(\omega t) + \frac{\Omega^2}{\omega^2}\sin^2(\omega t)\right), \tag{94a}$$

$$(\Delta\hat{J}_y)^2 = \frac{N}{4}\left(\cos^2(\omega t) + \frac{\omega^2}{\Omega^2}\sin^2(\omega t)\right), \tag{94b}$$

show periodic oscillations and the spin-squeezing parameter reaches $\xi_R^2 = 1/(1+\Lambda)$ ($\xi_R^2 = 1-\Lambda$) for the coherent spin state pointing along the positive (negative) x axis.

The situation changes completely if $\Lambda > 1$ (Gordon and Savage, 1999; Micheli *et al.*, 2003). The potential $W_\pi(z)$, Eq. (93), turns from a single-well to a double-well shape, with minima at $z_\pm = \pm\sqrt{1-1/\Lambda^2}$. The repulsive potential tends to split the initial Gaussian wave packet sitting at the top of the barrier, see Fig. 18, corresponding to a coherent spin state. This splitting gives rise to a macroscopic superposition corresponding to the wave packet localized in the left and right wells of $W_\pi(z)$. The semiclassical equations of motion $\dot{z} = -\partial H(z,\varphi)/\partial\varphi$ and $\dot{\varphi} = \partial H(z,\varphi)/\partial z$, where $H(z,\varphi)$ is given by Eq. (73), offer an alternative view (Smerzi *et al.*, 1997; Raghavan *et al.*, 1999). The fixed point $\Upsilon_\pi \equiv (z=0, \varphi=\pi)$ becomes unstable for $\Lambda > 1$ and two new stable fixed points $\Upsilon_\pm \equiv (z_\pm, \pi)$ appear. The exact quantum dynamics shows that, at short times, the state stretches along the semiclassical separatrix passing through Υ_π; see Fig. 18. At longer times the quantum state wraps around $\Upsilon_\pm$. In this regime, spin squeezing is lost, while the quantum Fisher information, sensitive to the creation of macroscopic superposition states, continues increasing. For $\Lambda = 2$ the semiclassical separatrix reaches the poles of the Bloch sphere: the dynamics creates NOON-like states on a time scale $\chi t \approx \ln(8N)/N$ (Micheli *et al.*, 2003). For $\Lambda > 2$ the separatrix winds around the Bloch sphere, the maximum distance between the separatrix and the equator decreases, and the dynamics resembles that of the one-axis twisting.

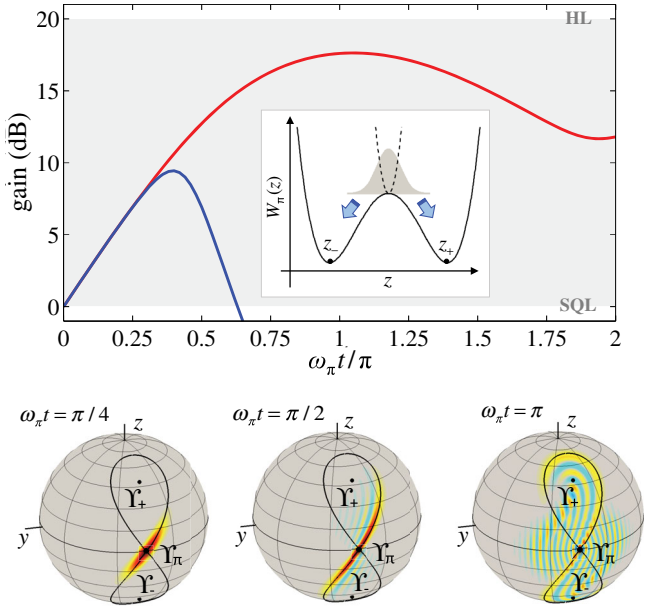

FIG. 18. Twist-and-turn dynamics. Top: Normalized quantum Fisher information (F_Q/N, red upper line) and inverse spin-squeezing parameter ($1/\xi_R^2$, blue lower line) as a function of $\omega_\pi t/\pi$, where $\omega_\pi = \Omega\sqrt{\Lambda-1}$. The inset shows the effective potential $W_\pi(z)$ initially (dotted line, $\Lambda = 0$) and after a quench to a finite Λ (solid line, $\Lambda = 1.5$). The initial coherent spin state corresponds to a Gaussian wave packet located at the top of the barrier. Bottom: Snapshots of the Wigner distribution at different times. The solid black lines are the mean-field separatrices and the dots are fixed points of the semiclassical model. Here $N = 100$ and the color scale is as in Fig. 5.

1. Entanglement beyond spin squeezing

Twist-and-turn dynamics has been first experimentally investigated by Strobel *et al.* (2014) using two internal hyperfine levels $|b\rangle = |F=1, m_F=1\rangle$ and $|a\rangle = |2,-1\rangle$ of ^{87}Rb atoms. A narrow Feshbach resonance is used to reduce the interspecies interaction. Coupling between the internal levels is provided by radio frequency and microwave drive. The experiments start with $N \approx 400$ atoms in the $|b\rangle$ mode, followed by a $\pi/2$ Rabi pulse that prepares a coherent spin state aligned with the x axis. Subsequently, the Rabi coupling is decreased to reach $\Lambda \approx 1.5$, and its phase adjusted to orient it along the negative x axis. Strobel *et al.* (2014) and Muessel *et al.* (2015) have investigated the short-time spin-squeezing dynamics. For an evolution of 15 ms, Strobel *et al.* (2014) demonstrated $\xi_R^2 = -4.5$ dB [and inferred $\xi_R^2 = -7.1$ dB (Muessel *et al.*, 2015)]. Muessel *et al.* (2015) also demonstrated a spin squeezing $\xi_R^2 = -4$ dB using ~30 independent condensates in parallel (each condensate experiencing independently a twist-and-turn dynamics), with a total of $N = 10^4$ particles. For longer times, spin squeezing is quickly lost and the experimental Husimi distribution of the reconstructed state shows the characteristic S shape; see Fig. 19. Strobel *et al.* (2014) extracted the Fisher information reporting values $F > N$ and thus demonstrating that the state is entangled. The experimental extraction of the Fisher information requires one to rotate the state around the y axis and to

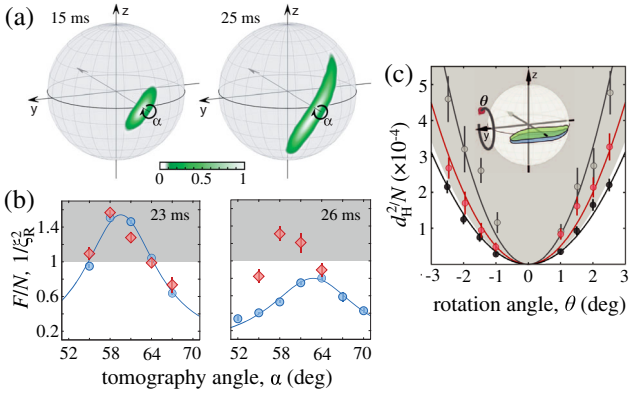

FIG. 19. Entanglement of non-spin-squeezed states. (a) Experimental Husimi distributions at different evolution times of the twist-and-turn dynamics. (b) Normalized Fisher information (F/N, red diamonds) and inverse spin-squeezing parameter ($1/\xi_R^2$, blue circles) as a function of the tomography angle [identified by the rotation angle α in (a)]. The gray shaded area is accessible only by entangled states. At 26 ms, spin squeezing cannot witness the entanglement that is detected by the Fisher information. (c) Squared Hellinger distance as a function of the rotation angle θ [see inset for the rotation of the initial (blue) state to a final (green) one] at three evolution times: $t = 0$ corresponding to a separable state (black points), $t = 15$ ms corresponding to an optimal spin-squeezed state (light gray points), and $t = 26$ ms corresponding to a state that is entangled but not spin squeezed (red points). The curvature of the quadratic fits (solid lines) is proportional to F/N. Adapted from Strobel *et al.*, 2014.

collect the probability distributions of the relative particle number in $|a\rangle$ and $|b\rangle$ at different rotation angles. The Fisher information is obtained according to Eq. (19) from a quadratic fit of the Hellinger distance (18) between a reference distribution (at $\theta = 0$) and the distribution obtained at a finite θ. Experimental results are shown in Fig. 19.

D. Entanglement of two spatially separated Bose-Einstein condensates

Creating entanglement between two spatially separated, individually addressable, Bose-Einstein condensates offers interesting possibilities: in such a system, local manipulations and measurements can be performed on the spin state of each condensate separately and nonlocal quantum correlations between the measurement results can be directly observed. This is particularly relevant for experiments on EPR entanglement and Bell tests, where the spatial separation can be used to rule out unknown causal influences between the clouds.

Bar-Gill *et al.* (2011), He, Reid *et al.* (2011), and Kurkjian *et al.* (2013) proposed schemes to generate EPR entanglement between two spatially separated Bose-Einstein condensates using elastic collisions. The condensates represent collective spins $\hat{J}^{(1)}$ and $\hat{J}^{(2)}$, respectively, which can be individually addressed and prepared in a coherent spin state. Bar-Gill *et al.* (2011) and He, Reid *et al.* (2011) considered schemes where EPR entanglement is generated by first spin squeezing each condensate and then interfering the squeezed states on a beam splitter. In the scheme of Kurkjian *et al.* (2013), on the other hand, a state-dependent potential is turned on such that the wave function of state $|a\rangle$ of the first condensate overlaps with the wave function of state $|b\rangle$ of the second condensate, picking up a collisional phase shift. Dropping constant and linear terms in $\hat{J}^{(i)}$, this realizes the Hamiltonian $H_{2\mathrm{BEC}} = \chi_1(\hat{J}_z^{(1)})^2 + \chi_2(\hat{J}_z^{(2)})^2 - \chi_{12}\hat{J}_z^{(1)}\hat{J}_z^{(2)}$, which generates entanglement between the two condensates in addition to spin squeezing in each condensate. After an interaction time, the state-dependent potential is turned off and the condensates are spatially separated again for detection, revealing EPR entanglement between them (Kurkjian *et al.*, 2013). For long interaction times, macroscopic entangled states can be created, as also analyzed by Byrnes (2013), who investigated applications of entangled Bose-Einstein condensates in quantum-information processing (Byrnes, Wen, and Yamamoto, 2012). While such experiments have not yet been reported, we note that continuous-variable entanglement has been created between spatially separated atomic vapor cells using a measurement-based scheme (Julsgaard, Kozhekin, and Polzik, 2001).

IV. ENTANGLEMENT VIA ATOMIC COLLISIONS: SPIN-MIXING DYNAMICS

The generation of correlated photon pairs via spontaneous parametric down-conversion in nonlinear crystals (Kwiat *et al.*, 1995) is one of the most widely used sources of entangled quantum states in optics (O'Brien, Furusawa, and Vučović, 2009). When postselecting n photons in the pair distribution (let us indicate with $|\pm 1\rangle$ the signal and idler modes), the corresponding state is a twin Fock $|n\rangle_{+1}|n\rangle_{-1}$. The twin-Fock state has been used to overcome the standard quantum limit in an optical interferometer using up to $n = 2$ photons per pair (Nagata *et al.*, 2007; Krischek *et al.*, 2011; Xiang *et al.*, 2011). Without postselection, parametric down-conversion creates quadrature-squeezed light (Walls, 1983; Slusher *et al.*, 1985; Wu *et al.*, 1986; Ou *et al.*, 1992; Breitenbach, Schiller, and Mlynek, 1997). Following the proposal of Caves (1981), squeezed light has been successfully used for optical interferometry beyond the standard quantum limit (Vahlbruch *et al.*, 2005, 2016), with direct application to gravitational wave detectors (Schnabel *et al.*, 2010; Aasi *et al.*, 2013). In the same spirit, the generation of correlated pairs of atoms has thus attracted large interest: many experiments have been proposed and performed. In the following, we review the most successful of these techniques, namely, spin-mixing dynamics in a spinor Bose-Einstein condensate (Kawaguchi and Ueda, 2012; Stamper-Kurn and Ueda, 2013); see Sec. IV.A. We discuss the creation of twin-Fock states in Sec. IV.B and quadrature squeezing in Sec. IV.C. Finally, in Sec. IV.D we review alternative protocols for the creation of atom pairs.

A. Spinor Bose-Einstein condensates

1. Spin-changing collisions

When a Bose-Einstein condensate is confined in a far-off resonant optical dipole trap, the spin degree of freedom of the atoms evolves freely. Spin-changing s-wave collisions, see Fig. 20, give rise to a coherent redistribution of atomic populations among Zeeman sublevels while preserving the

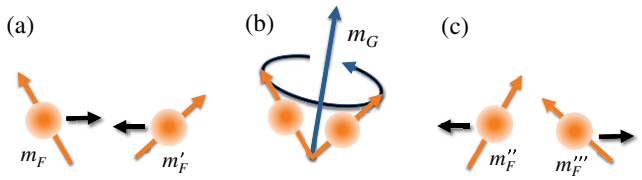

FIG. 20. Binary s-wave collision of two spin-F bosons. (a) When two spin-F bosons in internal states $|F, m_F\rangle$ and $|F, m'_F\rangle$ approach each other (here F is the hyperfine spin and m_F, $m'_F = -F, -F+1, \ldots, F$ the magnetic quantum number), they couple to form a total spin $G = F + F'$. (b) The combined internal state is given by $|G, m_G\rangle$. For bosons undergoing elastic s-wave scattering, G is restricted to even values satisfying $0 \le G \le 2F$, e.g., $G = 0, 2$ for two $F = 1$ particles. (c) After the collision the atoms fly apart and their internal states are again well described by the hyperfine spins F. However, the magnetic quantum numbers may have changed: $|F, m_F\rangle|F, m'_F\rangle \mapsto |F, m''_F\rangle|F, m'''_F\rangle$. The conservation of total angular momentum imposes $m_F + m'_F = m''_F + m'''_F$.

total magnetization (Ho, 1998; Ohmi and Machida, 1998). The quantum description of an ultracold gas of spin-F bosons requires introducing a vector order parameter with $2F+1$ components, $\{\hat{\Psi}_{-F}, \hat{\Psi}_{-F+1}, \ldots, \hat{\Psi}_F\}$ (Kawaguchi and Ueda, 2012; Stamper-Kurn and Ueda, 2013). Here $\hat{\Psi}_{m_F}$ is the atomic field annihilation operator associated with the hyperfine spin state $|F, m_F\rangle$. The single-mode approximation (Law, Pu, and Bigelow, 1998) assumes that the spatial atomic density distribution of all spin components is approximately equal and not affected by the spin dynamics. The common scalar wave function $\phi(\boldsymbol{r})$ defining the spatial mode of the condensate is determined as the solution of the Gross-Pitaevskii equation, neglecting contributions from the spin-dependent interactions. In this approximation, the field operators are $\hat{\Psi}_{m_F}(\boldsymbol{r}) = \phi(\boldsymbol{r})\hat{a}_{m_F}$, where $\hat{a}_{m_F}$ are annihilation operators that obey the usual bosonic commutation relations. Let $\hat{N}_{m_F} = \hat{a}^\dagger_{m_F}\hat{a}_{m_F}$ be the number of particles in the mode $|F, m_F\rangle$, and $\hat{N} = \sum_{m_F=-F}^{F} \hat{N}_{m_F}$ the total number of particles. The many-body Hamiltonian for a $F = 1$ Bose-Einstein condensate is (Law, Pu, and Bigelow, 1998; Pu *et al.*, 1999)

$$\hat{H}_{\rm SM} = [q + \lambda(2\hat{N}_0 - 1)](\hat{N}_{+1} + \hat{N}_{-1}) + 2\lambda(\hat{a}^\dagger_{-1}\hat{a}^\dagger_{+1}\hat{a}_0\hat{a}_0 + \hat{a}^\dagger_0\hat{a}^\dagger_0\hat{a}_{-1}\hat{a}_{+1}), \quad (95)$$

where we neglected terms proportional to the conserved magnetization (we assume $\hat{N}_{+1} - \hat{N}_{-1} = 0$ in the following) and total number of atoms. Here $q = (\Delta E_1 + \Delta E_{-1})/2$ is an effective quadratic Zeeman shift, where $\Delta E_{m_F} = E_{m_F} - E_0$ is the relative energy shift of the $m_F = \pm 1$ mode, which can be tuned by a magnetic field (q being proportional to the square of the magnetic field) and/or near-resonant microwave dressing. The interaction parameter is

$$\lambda = \frac{g_2}{2}\int d^3\boldsymbol{r}|\phi(\boldsymbol{r})|^4, \quad (96)$$

with $g_2 = 4\pi\hbar^2(a_2 - a_0)/(3M)$, and a_G the scattering lengths for s-wave collisions in the $G = 0, 2$ allowed channels. The single-mode approximation is valid if the system size is much smaller than the spin healing length $\sqrt{\hbar^2/2M|g_2|\rho_0}$, where ρ_0 is the density of the $m_F = 0$ component, giving the minimum size of a spin domain (Stamper-Kurn and Ueda, 2013). The last term in Eq. (95) describes the coherent and reversible creation of a pair of atoms in the magnetic sublevels $m_F = \pm 1$ from the scattering of two atoms in $m_F = 0$.

It is useful to rewrite the Hamiltonian (95) in terms of the spin operators

$$\hat{\mathcal{S}}_x = \frac{\hat{a}^\dagger_0\hat{\mathfrak{z}} + \hat{a}_0\hat{\mathfrak{z}}^\dagger}{2}, \qquad \hat{\mathcal{A}}_x = \frac{\hat{a}^\dagger_0\hat{\mathfrak{a}} + \hat{a}_0\hat{\mathfrak{a}}^\dagger}{2}, \quad (97a)$$

$$\hat{\mathcal{S}}_y = \frac{\hat{a}^\dagger_0\hat{\mathfrak{z}} - \hat{a}_0\hat{\mathfrak{z}}^\dagger}{2\mathrm{i}}, \qquad \hat{\mathcal{A}}_y = \frac{\hat{a}^\dagger_0\hat{\mathfrak{a}} - \hat{a}_0\hat{\mathfrak{a}}^\dagger}{2\mathrm{i}}, \quad (97b)$$

$$\hat{\mathcal{S}}_z = \frac{\hat{a}^\dagger_0\hat{a}_0 - \hat{\mathfrak{z}}^\dagger\hat{\mathfrak{z}}}{2}, \qquad \hat{\mathcal{A}}_z = \frac{\hat{a}^\dagger_0\hat{a}_0 - \hat{\mathfrak{a}}^\dagger\hat{\mathfrak{a}}}{2}, \quad (97c)$$

where $\hat{\mathfrak{z}} = (\hat{a}_{+1} + \hat{a}_{-1})/\sqrt{2}$ and $\hat{\mathfrak{a}} = (\hat{a}_{+1} - \hat{a}_{-1})/\sqrt{2}$ are symmetric and antisymmetric combinations of $\hat{a}_{+1}$ and $\hat{a}_{-1}$. The spin operators $\hat{\boldsymbol{\mathcal{S}}} = \{\hat{\mathcal{S}}_x, \hat{\mathcal{S}}_y, \hat{\mathcal{S}}_z\}$ and $\hat{\boldsymbol{\mathcal{A}}} = \{\hat{\mathcal{A}}_x, \hat{\mathcal{A}}_y, \hat{\mathcal{A}}_z\}$ do not commute with each other and define two SU(2) subspaces. With these operators, the Hamiltonian (95) takes the compact form (Duan, Cirac, and Zoller, 2002)

$$\hat{H}_{\rm SM} = \left(4\hbar\lambda\hat{\mathcal{S}}_x^2 - \frac{2\hbar q}{3}\hat{\mathcal{S}}_z\right) + \left(4\hbar\lambda\hat{\mathcal{A}}_y^2 - \frac{2\hbar q}{3}\hat{\mathcal{A}}_z\right), \quad (98)$$

which highlights the presence of nonlinear spin terms. It should be noted that a symmetric radio-frequency coupling between the $m_F = 0, \pm 1$ modes with Rabi frequency $\Omega_{\rm rf}$ corresponds to a rotation of the $\hat{\boldsymbol{\mathcal{S}}}$ vector around the x axis,

$$\hat{H}_{\rm rf} = \frac{\hbar\Omega_{\rm rf}}{2\sqrt{2}}(\hat{a}^\dagger_0\hat{a}_{+1} + \hat{a}^\dagger_0\hat{a}_{-1} + \text{H.c.}) = \hbar\Omega_{\rm rf}\hat{\mathcal{S}}_x. \quad (99)$$

A relative phase shift between the $m_F = 0$ and ± 1 modes corresponds to a rotation of both $\hat{\boldsymbol{\mathcal{S}}}$ and $\hat{\boldsymbol{\mathcal{A}}}$ around the z axis, $e^{-i\theta(\hat{N}_0 - \hat{N}_{+1})/2}e^{-i\theta(\hat{N}_0 - \hat{N}_{-1})/2} = e^{-i\theta\hat{\mathcal{S}}_z}e^{-i\theta\hat{\mathcal{A}}_z}$.

Another popular expression of Eq. (95) is (Law, Pu, and Bigelow, 1998; Zhang and Duan, 2013)

$$\hat{H}_{\rm SM} = \lambda\hat{\boldsymbol{L}} - q\hat{N}_0, \quad (100)$$

where $\hat{\boldsymbol{L}} = \{\hat{L}_x, \hat{L}_y, \hat{L}_z\}$, $\hat{L}_x = 2\hat{\mathcal{S}}_x$, $\hat{L}_y = 2\hat{\mathcal{A}}_y$, and $\hat{L}_z = \hat{N}_{-1} - \hat{N}_{+1}$ obey angular momentum commutation relations.[14]

[14]Some authors have also studied spin-1 condensates using the a quadrupole tensor operator $\hat{\boldsymbol{Q}}$ (Müstecaplıoğlu, Zhang, and You, 2002; Sau *et al.*, 2010; Hamley *et al.*, 2012) with components related to Eq. (97) as $\hat{Q}_{yz} = -2\hat{\mathcal{S}}_y$, $\hat{Q}_{xz} = 2\hat{\mathcal{A}}_x$, $\hat{Q}_{zz} - \hat{Q}_{yy} = -4\hat{\mathcal{S}}_z$, $\hat{Q}_{xx} - \hat{Q}_{zz} = 4\hat{\mathcal{A}}_z$, and $\hat{Q}_{xy} = i(\hat{a}^\dagger_{-1}\hat{a}_{+1} - \hat{a}^\dagger_{+1}\hat{a}_{-1})$.

2. Metrologically useful entanglement in the ground state of the spin-mixing Hamiltonian

The ground state of the Hamiltonian (95) is characterized by the competition between the energy shift, proportional to q, and the spin-dependent collisional interaction, proportional to λ (Sadler *et al.*, 2006; Lamacraft, 2007; Murata, Saito, and Ueda, 2007). The mean-field limit of Eq. (95), obtained by replacing $\hat{a}_{m_F}=\sqrt{N_{m_F}}e^{-i\phi_{m_F}}$ and assuming $N_{+1}=N_{-1}$, gives $E_{\rm SM}=-qN_0+4\hbar N_0(N-N_0)\cos^2(\phi/2)$, where $\phi=2\phi_0-\phi_{+1}-\phi_{-1}$ (Zhang *et al.*, 2005; Stamper-Kurn and Ueda, 2013). In a full quantum treatment, the system is conveniently studied in the Fock basis $\{|k\rangle_{-1}|N-2k\rangle_0|k\rangle_{+1}\}_{k=0,1,\ldots,N/2}$, where $|n\rangle_{m_F}$ indicates a state of n particles in the mode m_F, or in terms of the eigenstates $|l,m\rangle$ (here $m=0$) of $\hat{\boldsymbol{L}}$ and $\hat{L}_z$ (Law, Pu, and Bigelow, 1998).

For a ferromagnetic condensate $\lambda<0$ (e.g., ^{87}Rb) there are two quantum phase transitions with order parameter given by the mean population of the $m_F=0$ mode. For $q>4N|\lambda|$, the ground state is $|0\rangle_{-1}|N\rangle_0|0\rangle_{+1}$, corresponding to a polar phase with all particles in $m_F=0$ ($N_0=N$). For $|q|<4N|\lambda|$, the minimization of $E_{\rm SM}$ leads to $\phi=0$ and $N_0=(4|\lambda|N+q)/(8|\lambda|)$, corresponding to the so-called broken asymmetry phase. The population of N_0 decreases linearly with q and the modes $m_F=\pm1$ are equally populated. For $q<-4N|\lambda|$, we have a twin-Fock phase with $N_0=0$ and the ground state given by the twin-Fock state $|N/2\rangle_{-1}|0\rangle_0|N/2\rangle_{+1}$. Entanglement in the ground state for the spin-1 system was studied by Zhang and Duan (2013). Feldmann *et al.* (2018) studied the quantum Fisher information of the ground state $|\psi_{\rm gs}\rangle$ of the Hamiltonian (95) for different operators. In particular, $F_Q[|\psi_{\rm gs}\rangle,\hat{\mathcal{S}}_x]=F_Q[|\psi_{\rm gs}\rangle,\hat{\mathcal{A}}_y]=N(N+1)/2$ at $q=0$ (Feldmann *et al.*, 2018; Zou *et al.*, 2018), associated with the presence of macroscopic superposition states (Pezzè *et al.*, 2017). Furthermore, $F_Q[|\psi_{\rm gs}\rangle,\hat{J}_{x,y}]=N(N+2)/2$ in the twin-Fock phase, see Fig. 21, where $\hat{J}_x=(\hat{a}^\dagger_{+1}\hat{a}_{-1}+\hat{a}_{+1}\hat{a}^\dagger_{-1})/2$ and $\hat{J}_y=(\hat{a}^\dagger_{+1}\hat{a}_{-1}-\hat{a}_{+1}\hat{a}^\dagger_{-1})/2i$.

For an antiferromagnetic condensate $\lambda>0$ (e.g., ^{23}Na), the mean-field energy is minimized by taking $\phi=\pi$ and $N_0=N$ for $q>0$, and $N_0=N$ for $q<0$. There is a quantum phase transition at $q=0$: in the limit $N\to\infty$, for $q>0$ the ground state is given by the fully polarized state $|0\rangle_{-1}|N\rangle_0|0\rangle_{+1}$, while for $q<0$ by the twin-Fock state $|N/2\rangle_{-1}|0\rangle_0|N/2\rangle_{+1}$. See Wu and You (2016) for a calculation of the quantum Fisher information of the ground state for $q=0$ and nonzero magnetization.

3. Quantum spin-mixing dynamics in the low-depletion limit

The spin dynamics of an initial condensate in $m_F=0$ is formally analogous to optical spontaneous four-wave mixing (Goldstein and Meystre, 1999): atom-atom interaction plays the role of the nonlinear Kerr medium, the $m_F=0$ condensate is equivalent to a coherent pump field with the external trapping potential corresponding to a high-finesse cavity, and the condensates in $m_F=\pm1$ can be identified as signal and idler. Remarkably, spin-changing collisions are unaffected by the linear Zeeman shift from a homogeneous magnetic field. Only higher-order effects, such as a quadratic Zeeman shift or a linear Zeeman shift from an inhomogeneous magnetic field, affect it.

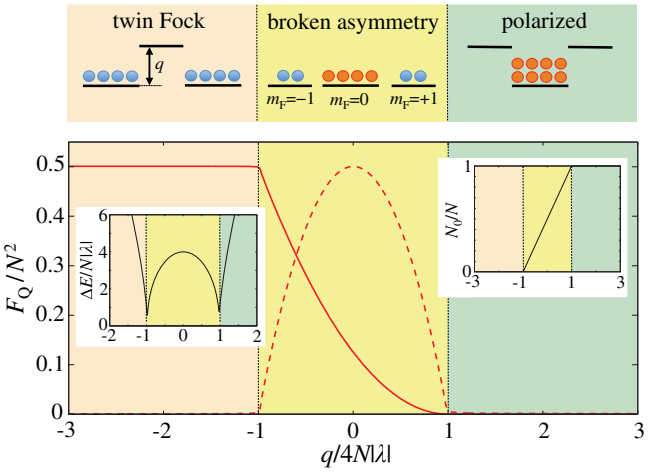

FIG. 21. Entanglement in the ground state of the spin-mixing Hamiltonian. The upper panel reports a schematic representation of the different phases obtained as a function of q (linear Zeeman shifts are not shown). The lower panel shows $F_Q[|\psi_{\rm gs}\rangle,\hat{J}_x]/N^2$ (solid line) and $F_Q[|\psi_{\rm gs}\rangle,\hat{\mathcal{S}}_x]/N^2$ (dashed line) as a function of $q/4N|\lambda|$. The left inset shows the energy gap ΔE between the ground state and the first excited state, closing at $q_c=\pm4N|\lambda|$. The right inset shows the normalized population of the $m_F=0$ mode N_0/N. Here $\lambda<0$ and $N=1000$.

The low-depletion limit, i.e., $N_0\approx N\gg1$, is analyzed by replacing the mode operator $\hat{a}_0$ in Eq. (95) with $\sqrt{N_0}$. In this approximation, the condensate serves as an unlimited resource of particles for the parametric amplification of the $m_F=\pm1$ modes. We obtain the quadratic Hamiltonian $\hat{H}_{\rm SM}=\alpha(\hat{a}^\dagger_{+1}\hat{a}_{+1}+\hat{a}^\dagger_{-1}\hat{a}_{-1})+\beta(\hat{a}^\dagger_{-1}\hat{a}^\dagger_{+1}+\hat{a}_{-1}\hat{a}_{+1})$, where $\alpha=q+\lambda(2N_0-1)$ and $\beta=2\lambda N_0$. This Hamiltonian can be diagonalized by a Bogoliubov transformation (Duan, Sørensen *et al.*, 2000; Pu and Meystre, 2000); see also Truax (1985). The unitary evolution $|\psi_{\rm SM}(t)\rangle=e^{-i\hat{H}_{\rm SM}t/\hbar}|{\rm vac}\rangle$ can be calculated exactly, giving

$$|\psi_{\rm SM}(t)\rangle=\sum_{n=0}^{+\infty}\frac{[-i(\beta\tau/\hbar)\sin(t/\tau)]^n}{[\cos(t/\tau)+i(\alpha\tau/\hbar)\sin(t/\tau)]^{n+1}}|n\rangle_{+1}|n\rangle_{-1}, \tag{101}$$

where $\tau=\hbar/\sqrt{\alpha^2-\beta^2}$, and $|{\rm vac}\rangle=|0\rangle_{+1}|0\rangle_{-1}$ indicates empty $m_F=\pm1$ modes. This state has a vanishing population difference $\Delta^2(\hat{N}_{+1}-\hat{N}_{-1})=0$, while the $m_F=\pm1$ modes are nonempty,

$$\langle\hat{N}_{\pm1}\rangle=\frac{\beta^2}{\alpha^2-\beta^2}\sin^2\left(t\sqrt{\alpha^2-\beta^2}/\hbar\right), \tag{102}$$

and characterized by large (super-Poissonian) population fluctuations $\Delta^2\hat{N}_{\pm1}=\langle\hat{N}_{\pm1}\rangle(\langle\hat{N}_{\pm1}\rangle+1)$. It is also interesting to consider the quadratures

$$2(\Delta\hat{Q}_\jmath)^2 = V_Q\cos^2(\phi-\phi_Q)+\frac{1}{V_Q}\sin^2(\phi-\phi_Q), \tag{103a}$$

$$2(\Delta\hat{Q}_\imath)^2 = V_Q\sin^2(\phi-\phi_Q)+\frac{1}{V_Q}\cos^2(\phi-\phi_Q), \tag{103b}$$

where $\hat{Q}_\jmath = \cos\phi\hat{X}_\jmath + \sin\phi\hat{P}_\jmath$, $\hat{X}_\jmath = (\hat{\jmath}+\hat{\jmath}^\dagger)/\sqrt{2}$, $\hat{P}_\jmath = (\hat{\jmath}-\hat{\jmath}^\dagger)/(i\sqrt{2})$, and an analogous definition of $\hat{Q}_\imath$ in terms of the operators $\hat{\imath}$ and $\hat{\imath}^\dagger$. The time-dependent coefficients are $V_Q = 1+2\langle\hat{N}_{\pm1}\rangle - 2\Delta\hat{N}_{\pm1}$ and $\cos(2\phi_Q) = \alpha\langle\hat{N}_{\pm1}\rangle/(\beta\Delta\hat{N}_{\pm1})$.

For $\alpha^2<\beta^2$, τ is imaginary and the condensate is dynamically unstable. The instability is characterized by the exponential increase of population in the $m_F=\pm1$ modes,

$$\langle\hat{N}_{\pm1}\rangle = \frac{\beta^2}{\beta^2-\alpha^2}\sinh^2\left(t\sqrt{\beta^2-\alpha^2}/\hbar\right). \tag{104}$$

On resonance ($\alpha=0$) the spin-mixing Hamiltonian becomes $\hat{H}_{\rm SM} = 2\lambda N_0(\hat{a}_{-1}^\dagger\hat{a}_{+1}^\dagger + \hat{a}_{-1}\hat{a}_{+1})$, which generates the familiar two-mode squeezed-vacuum state (Walls and Milburn, 1994),

$$|\psi_{\rm SM}(t)\rangle = \sum_{n=0}^{+\infty}\frac{(-i\tanh r)^n}{\cosh r}|n\rangle_{+1}|n\rangle_{-1}, \tag{105}$$

where $r=|\beta|t/\hbar = 2|\lambda|N_0t/\hbar$ and $\langle\hat{N}_{\pm1}\rangle = \sinh^2 r$. The Hamiltonian $\hat{H}_{\rm SM}$ (for $\alpha=0$) can be rewritten as $\hat{H}_{\rm SM} = 2\lambda[(\hat{\mathcal{S}}_x^2-\hat{\mathcal{S}}_y^2)-(\hat{\mathcal{A}}_x^2-\hat{\mathcal{A}}_y^2)]$, corresponding to two-axis countertwisting (Kitagawa and Ueda, 1993; Duan, Cirac, and Zoller, 2002; Anders *et al.*, 2018) for the $\boldsymbol{\mathcal{S}}$ and $\boldsymbol{\mathcal{A}}$ spins. Note that $\hat{\boldsymbol{\mathcal{S}}}$ and $\hat{\boldsymbol{\mathcal{A}}}$ commute in the low-depletion limit. For $\alpha=0$, Eqs. (103a) and (103b) reduce to

$$2(\Delta\hat{Q}_\jmath)^2 = e^{2r}\sin^2\left(\phi-\frac{\pi}{4}\right)+e^{-2r}\cos^2\left(\phi-\frac{\pi}{4}\right), \tag{106a}$$

$$2(\Delta\hat{Q}_\imath)^2 = e^{2r}\cos^2\left(\phi-\frac{\pi}{4}\right)+e^{-2r}\sin^2\left(\phi-\frac{\pi}{4}\right), \tag{106b}$$

respectively. The quadrature $(\Delta\hat{Q}_\jmath)^2$ [$(\Delta\hat{Q}_\imath)^2$] is squeezed by a factor e^{-2r} below the vacuum level at an optimal angle $\phi=\pi/4$ ($\phi=3\pi/4$), and antisqueezed by a factor e^{2r} at $\phi=3\pi/4$ ($\phi=\pi/4$). For a sufficiently long evolution time, $t\gtrsim\hbar/(2|\lambda|N_0)$ spin dynamics is modified by the depletion of the condensate. The initially exponential growth of population in $m_F=\pm1$ slows down and finally stops (Law, Pu, and Bigelow, 1998; Mias, Cooper, and Girvin, 2008).

For $\alpha^2\geq\beta^2$ the spin-mixing dynamics is stable and the population of $m_F=\pm1$ oscillates in time,

$$\langle\hat{N}_{\pm1}\rangle = \frac{\beta^2}{\alpha^2-\beta^2}\sin^2\left(t\sqrt{\alpha^2-\beta^2}/\hbar\right). \tag{107}$$

For $\alpha^2\gg\beta^2$ the amplitude of this oscillation becomes negligible and the system remains stable in $m_F=0$.

Typical experiments exploring the quantum spin-mixing dynamics (Schmaljohann *et al.*, 2004; Chang *et al.*, 2005; Leslie *et al.*, 2009; Liu *et al.*m 2009; Klempt *et al.*, 2010; Peise, Lücke *et al.*, 2015) start with a condensate in the stable configuration. A sudden quench of parameters brings the condensate in the dynamical unstable configuration. After spin-mixing dynamics, the trap is turned off and a Stern-Gerlach field is used to separate the m_F components during a time-of-flight expansion.

Finally, it is worth recalling that the discussion so far has been focused on one spatial eigenmode. A rich resonance structure is expected when taking into account many spatial modes as experimentally shown by Klempt *et al.* (2010) and Scherer *et al.* (2010).

B. Population correlations and twin-Fock state

Several experiments have explored the creation of the twin-Fock state $|n\rangle_{+1}|n\rangle_{-1}$ in the $m_F=\pm1$ Zeeman modes. This can be accessed either by quantum spin-mixing dynamics (which can turn a large fraction of an atomic Bose-Einstein condensate into a mixture of perfectly correlated pairs of atom, with large fluctuations of n) or by adiabatic preparation. The twin-Fock state is particle entangled and useful in a Ramsey interferometer to reach sensitivities beyond the standard quantum limit; see Sec. II.C.6.

1. Number squeezing

The presence of correlations in the populations of $m_F=\pm1$ modes after spin dynamics was first demonstrated by Bookjans, Hamley, and Chapman (2011), Gross *et al.* (2011), and Lücke *et al.* (2011). Number squeezing $\xi_{\rm N}^2 = \Delta^2(\hat{N}_{+1}-\hat{N}_{-1})/(N_{+1}+N_{-1})$ up to $\xi_{\rm N}^2\approx-7$ dB [$\xi_{\rm N}^2=-12.4$ dB in the more recent experiment of Lücke *et al.* (2014)] below the projection noise level has been reported; see Fig. 22. The main limitation is given by detection noise for short-time evolutions and particles losses for long time.

2. Quantum interferometry with twin-Fock states

Lücke *et al.* (2011) have investigated the phase sensitivity of the paired atoms generated by the spin-mixing dynamics of a ^{87}Rb condensate prepared in $|F=2,m_F=0\rangle$. The generated atom pairs in $|2,\pm1\rangle$ (due to the short evolution time, the populations in $|2,\pm2\rangle$ can be neglected due to the quadratic Zeeman shift detuning) are coupled via a series of microwave pulses of variable duration; see Fig. 23. This forms an internal-state beam splitter $e^{-i\theta\hat{J}_x}$, where the rotation angle θ is estimated via the measurement of $\hat{J}_z^2 = (\hat{N}_{+1}-\hat{N}_{-1})^2/4$. The output state is postselected to a total number $N_{+1}+N_{-1}\approx10^4$. Ideally, this postselection would correspond to a twin-Fock state as input of the beam splitter operation. Applying error propagation $\Delta\theta = (\Delta\hat{J}_z^2)/|d\langle\hat{J}_z^2\rangle/d\theta|$, it was possible to demonstrate a phase variance 1.61 dB below the standard quantum limit at an optimal rotation angle; see Fig. 23.

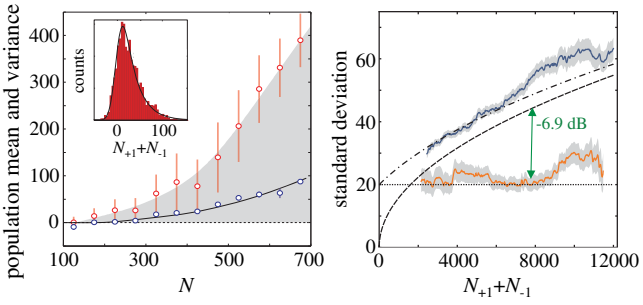

FIG. 22. Population correlations after spin-mixing dynamics. Left panel: $\langle \hat{N}_{+1} + \hat{N}_{-1} \rangle$ (red, light circles) and $\Delta^2(\hat{N}_{+1} - \hat{N}_{-1})$ (blue, dark circles) as a function of the total atom number N. Error bars are fluctuations (1 standard deviation) and the gray area corresponds to the sub-Poisson regime. The black line is a theoretical model including particle loss due to spin relaxation. The inset shows the distribution of $N_{+1} + N_{-1}$ for $250 < N < 300$, where the black line is a fitted squeezed-vacuum distribution corresponding to $r \approx 2$. Adapted from Gross *et al.*, 2011. Right panel: Standard deviation of the population difference $(\hat{N}_{+1} - \hat{N}_{-1})/2$ (red, lower line), compared to the projection noise $\sqrt{N_{+1} + N_{-1}}/2$ (dashed line), and $\sqrt{(N_{+1} + N_{-1})/4 + \sigma_{\mathrm{dn}}^2}$ (dot-dashed line) taking into account a number-independent detection noise $\sigma_{\mathrm{dn}} = 20$ (dotted line). The blue, upper line is the experimental result for unentangled atoms. The shaded area indicates the standard deviation. Adapted from Lücke *et al.*, 2011.

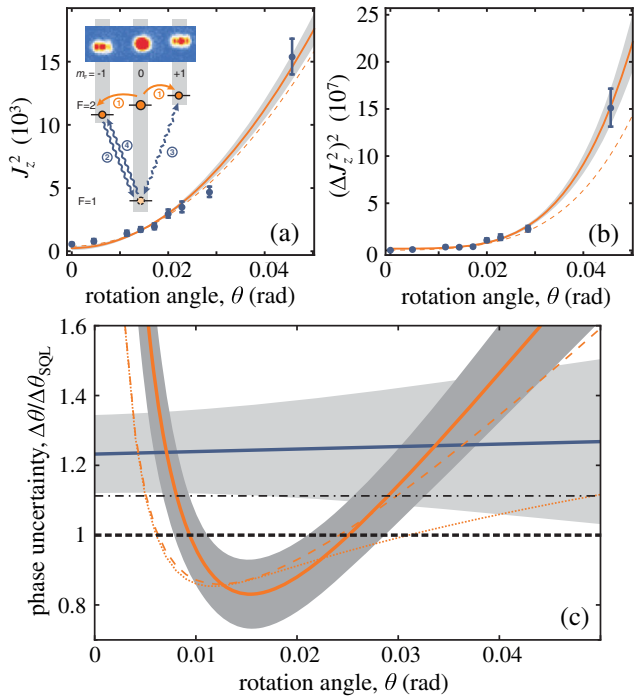

FIG. 23. Twin-Fock interferometry. The inset of (a) shows the experimental operations: (1) spin dynamics, (2) a resonant microwave π pulse between $|2,-1\rangle$ and $|1,0\rangle$, (3) a pulse of variable duration, defining θ, and (4) a second π pulse. (a) Second moment $\langle \hat{J}_z^2 \rangle$ of the population imbalance $\hat{J}_z = (\hat{N}_{+1} - \hat{N}_{-1})/2$ as a function of θ (dots with error bars) for postselected numbers of atoms between 6400 and 7600. The solid line is a polynomial fit (with gray uncertainty region); the dotted line is the theoretical prediction including detection noise. (b) Same for $(\Delta \hat{J}_z^2)^2 = \langle \hat{J}_z^4 \rangle - \langle \hat{J}_z^2 \rangle^2$. (c) Phase estimation uncertainty obtained via error propagation $\Delta\theta = (\Delta \hat{J}_z^2)/|d\langle \hat{J}_z^2 \rangle/d\theta|$ (solid orange line with gray uncertainty region) compared to the theoretical prediction (dashed orange line) and Cramér-Rao bound (dotted orange line) including detection noise only. Around $\theta = 0.015$ rad the phase variance lies 1.61 dB below the standard quantum limit (black dashed line). Adapted from Lücke *et al.*, 2011.

3. Particle entanglement

The experiment of Lücke *et al.* (2014) demonstrated the generation of (metrologically useful) entanglement in an atomic twin-Fock state. This has been further investigated by Lücke *et al.* (2014). In this experiment, entanglement (in a postselected twin-Fock state of $N \approx 8000$ atoms in $m_F = \pm 1$ modes) is witnessed by the inequality $\xi_{\mathrm{D}}^2 < 1$, Eq. (55), additionally extended to detect an arbitrary k-particle entanglement (Lücke *et al.*, 2014). Experimental data exclude an entanglement depth of less than 28 atoms with 2 standard deviations of confidence and show an average entanglement depth of 68 atoms. It should be noted that $\xi_{\mathrm{D}}^2 < 1$ signals entanglement independently from its metrological usefulness. Useful k-particle entanglement is a more demanding resource than algebraic k-particle entanglement. With experimental data similar to those reported by Lücke *et al.* (2014), Apellaniz *et al.* (2015) reported a useful entanglement depth of about three atoms.

4. Adiabatic state preparation

Twin-Fock states can be accessed via an adiabatic passage through the quantum phase transition(s) (Zhang and Duan, 2013; Luo *et al.*, 2017), as discussed in Sec. IV.A.2. The ferromagnetic condensate is favorable since the energy gap at the critical points closes as $\Delta E_{\mathrm{SM}}/N\hbar|\lambda| = \mathcal{O}(N^{-1/3})$, while the energy gap for the antiferromagnetic condensate closes as $\Delta E_{\mathrm{SM}}/N\hbar\lambda = \mathcal{O}(N^{-1})$. The condensate is initially prepared via optical pumping with all N atoms in $m_F = 0$ and, ideally, an adiabatic ramp of q would transform the polarized state to a twin-Fock state with $N/2$ atoms in $m_F = \pm 1$ (Zhang and Duan, 2013). Hoang *et al.* (2016) characterized the amplitude excitations and measured the energy gap at the critical point in a ^{87}Rb condensate. The entangled state preparation was experimentally investigated by Luo *et al.* (2017). This experiment demonstrates, despite the diabatic ramp of the parameter and the finite loss rate, the deterministic and almost perfect preparation of a twin-Fock state in $m_F = \pm 1$ modes $[(N_{+1} + N_{-1})/N = 96 \pm 2\%$ at the end of the ramp], with high number squeezing ($\xi_N^2 = -10.7$ dB) and high coherence. The measurements demonstrate an average entanglement depth of 910 atoms with more than 450 atoms at the confidence level of 1 standard deviation. In a successive experiment, Zou *et al.* (2018) investigated the adiabatic preparation of the ground state at $q = 0$, corresponding to a spin-1 Dicke state $|l = N, m = 0\rangle$ of the $\hat{\boldsymbol{L}}$ manifold. The prepared state has been used to estimate the angle of a Rabi rotation with a sensitivity of 2.42 dB beyond the standard quantum limit.

C. Quadrature squeezing and squeezed-vacuum state

1. Quadrature squeezing

The experiments of Gross *et al.* (2011), Hamley *et al.* (2012), and Peise *et al.* (2015) investigated quadrature squeezing in the state generated via spin-mixing dynamics in the low-depletion limit. In this regime, the quadrature variance Eq. (103a) can be rewritten as $2(\Delta\hat{Q}_\vartheta)^2 = N\Delta^2(\hat{\mathcal{S}}_x\cos\phi + \hat{\mathcal{S}}_y\sin\phi)/\langle\hat{\mathcal{S}}_z\rangle^2$, where $\langle\hat{\mathcal{S}}_z\rangle \approx N/2$ [and analogous relation between Eq. (103b) and the $\hat{\boldsymbol{\mathcal{A}}}$ spin]: quadrature squeezing thus corresponds to spin squeezing; see Sec. II.C.5.b. Experimentally, the quadrature modes are accessed via atomic homodyne detection, as first realized by Gross *et al.* (2011); see also Peise *et al.* (2015). In analogy to standard techniques in quantum optics (Ou *et al.*, 1992; Scully and Zubairy, 1997), atomic homodyne consists of a symmetric radio-frequency coupling between the condensate in $m_F = 0$, used as a local oscillator, and the $m_F = \pm 1$ modes. In the limit of low transfer and $N_0 \gg N_{\pm 1}$, this corresponds to a displacement operation $e^{-i\Omega_{\rm rf}t\hat{\mathcal{S}}_x} = e^{-i\Omega_{\rm rf}t\sqrt{N}(\hat{\vartheta}+\hat{\vartheta}^\dagger)/2}$. Hamley *et al.* (2012) demonstrated quadrature squeezing using $N = 4.5\times10^4$ ^{87}Rb atoms and characterized the spin-squeezed states via noise tomography; see Fig. 24. Values up to $\xi_{\rm R}^2 = -8.3$ dB (-10.3 dB inferred) below the SQL are reported.

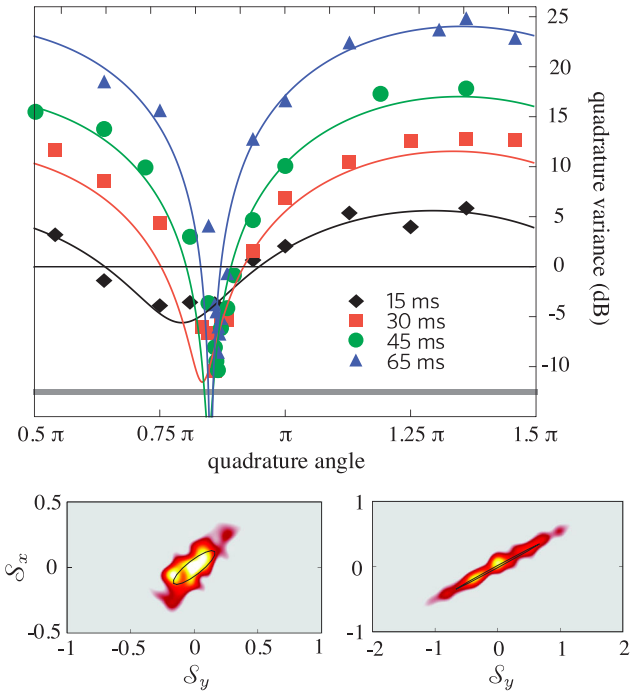

FIG. 24. Top: Quadrature variance $4\Delta^2(\hat{\mathcal{S}}_x\cos\phi + \hat{\mathcal{S}}_y\sin\phi)/N$ of the state generated after variable duration of the spin-mixing dynamics (colored lines and symbols), as functions of the quadrature angle ϕ. Symbols are experimental results obtained via state tomography, whereas the solid lines are theoretical predictions. Bottom: Reconstructed phase space distributions at $t = 15$ ms (left) and $t = 45$ ms (right); the black ellipses are the $1/\sqrt{e}$ uncertainty ellipse predicted theoretically. Adapted from Hamley *et al.*, 2012.

2. Continuous variable and EPR entanglement

The two-mode squeezed-vacuum state (105) realizes, in field modes, the position-momentum correlations that are at the heart of the Einstein-Podolsky-Rosen criterion (Reid, 1989); see Sec. II.C.9.a. Recall that[15] $V^{\pm}_{\hat{X}(\phi)} = \cosh(2r) \mp \sin(2\phi)\sinh(2r)$. As the angle ϕ is varied, these quadrature variances oscillate between a maximum value e^{2r} and a minimum value e^{-2r}, which is below the value of 1 of the unsqueezed vacuum state. In the limit $r\to\infty$, at $\phi = 3\pi/4$ ($\phi = \pi/4$), we have perfect correlations between $\hat{X}_{+1}$ and $\hat{X}_{-1}$ ($\hat{X}_{+1}$ and $-\hat{X}_{-1}$), as well as between $\hat{P}_{+1}$ and $-\hat{P}_{-1}$ ($\hat{P}_{+1}$ and $\hat{P}_{-1}$), where $\hat{P}_{\pm1}(\phi) = \hat{X}_{\pm1}(\phi+\pi/2)$. According to Eqs. (61) and (62) discussed in Sec. II.C.9, the two-mode squeezed-vacuum state produced via spin-mixing dynamics in spinor condensates (Duan, Sørensen *et al.*, 2000; Pu and Meystre, 2000) is mode entangled for $r > 0$ and fulfills the EPR criterion for $r > \ln\sqrt{2}$ (Reid *et al.*, 2009).[16] The quadratures $X_\pm(\phi)$ are proportional to the number of particles $\hat{N}_{+1} \pm \hat{N}_{-1}$ measured after a radio-frequency pulse coupling $m_F = 0$ with $m_F = \pm1$ (Gross *et al.*, 2011). With spinor condensates (Duan, Cirac, and Zoller, 2002), continuos variable entanglement, e.g., the violation of Eq. (61), was first demonstrated by Gross *et al.* (2011), while EPR entanglement, e.g., the violation of Eq. (62) was observed by Peise *et al.* (2015); see Fig. 25. The experimental violation of Eq. (62) demonstrates a form of entanglement intrinsically connected with local realism. The demonstration of the continuous-variable EPR paradox with massive particles would additionally require spacelike separation of measurements to rule out causal influences, which has not yet been experimentally achieved.

3. Interferometry with squeezed vacuum

Quadrature squeezing is a resource for quantum interferometry; see Sec. II.C.5.b (Caves, 1981). Within spin-mixing dynamics, squeezing occurs in the quadratures corresponding to the symmetric $|s\rangle = (|1,+1\rangle + |1,-1\rangle)/\sqrt{2}$ and the antisymmetric $|a\rangle = (|1,+1\rangle - |1,-1\rangle)/\sqrt{2}$ combinations of the $|F=1, m_F=\pm1\rangle$ modes. Kruse *et al.* (2016) realized an atomic clock that exploits the squeezed-vacuum states created in the $|s\rangle$ mode. An initial condensate of $N\approx10^4$ atoms undergoes spin-mixing dynamics in the $F=1$ manifold of ^{87}Rb in the low-depletion regime ($\langle\hat{N}_0\rangle \gg \langle\hat{N}_{\pm1}\rangle$ after spin dynamics). The interferometer consists of a rf coupling (corresponding to a balanced beam splitter between the condensate in $|1,0\rangle$ and the squeezed vacuum in $|s\rangle$,

[15] Note the relations $\hat{Q}_\vartheta(\phi) = [\hat{X}_{+1}(\phi) + \hat{X}_{-1}(\phi)]/\sqrt{2}$ and $\hat{Q}_\varepsilon(\phi) = [\hat{X}_{+1}(\phi) - \hat{X}_{-1}(\phi)]/\sqrt{2}$, where $\hat{X}_{\pm1}(\phi) = (\hat{a}_{\pm1}e^{-i\phi} + \hat{a}^\dagger_{\pm1}e^{i\phi})/\sqrt{2}$. In particular $V^+_{\hat{X}(\phi)} = \mathrm{Var}[\hat{X}_{+1}(\phi) + \hat{X}_{-1}(\phi)] = 2(\Delta\hat{Q}_\vartheta)^2$ and $V^-_{\hat{X}(\phi)} = \mathrm{Var}[\hat{X}_{+1}(\phi) - \hat{X}_{-1}(\phi)] = 2(\Delta\hat{Q}_\varepsilon)^2$.

[16] In the case of a finite number of particles in the local oscillator ($m_F = 0$ mode), the inequalities (61) and (62) generalize to $V^{\pm}_{\hat{X}(\phi)} + V^{\mp}_{\hat{P}(\phi)} \geq 2 - (N_{+1}+N_{-1})/N_0$, and $V^-_{\hat{X}(\phi)}V^+_{\hat{P}(\phi)} \geq (1/4)\times(1 - N_{-1}/N_0)^2$, respectively (Raymer *et al.*, 2003; Ferris *et al.*, 2008).

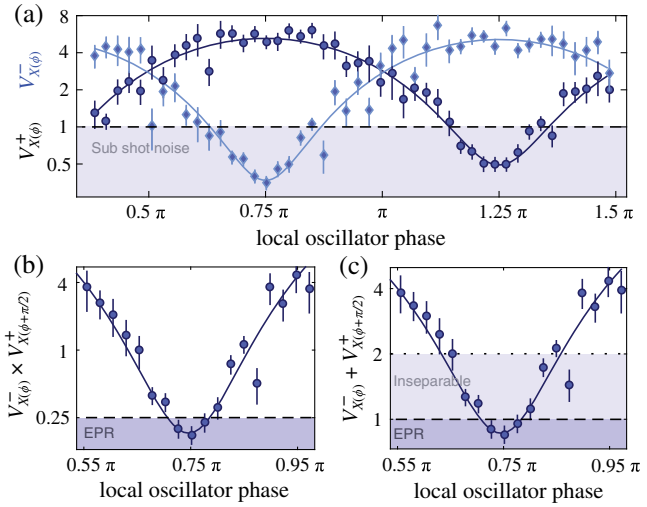

FIG. 25. Einstein-Podolsky-Rosen entanglement with spinor condensates. (a) Experimental variances $V^{+}_{X(\phi)}$ and $V^{-}_{X(\phi)}$ as functions of the local oscillator phase ϕ. The dashed line is the quadrature variance for the vacuum state. The lowest measured quadrature variance is $V^{-}_{X} = 0.42$, corresponding to a squeezing of 3.77 dB below the vacuum limit. (b) Product $V^{-}_{X(\phi)} \times V^{+}_{X(\phi+\pi/2)}$: data points below the dashed line violate the inequality (62) and thus signal Einstein-Podolsky-Rosen entanglement. Data reach $V^{-}_{X(\phi)} \times V^{+}_{X(\phi+\pi/2)} = 0.18(3)$, which is 2.4 standard deviations below the limit of 1/4. (c) Sum $V^{+}_{X(\phi)} + V^{-}_{X(\phi+\pi/2)}$: Data points below the dotted line violate the inequality (61) and thus signal entanglement between the $m_F = \pm 1$ modes, and data below the dashed line signal Einstein-Podolsky-Rosen entanglement. Data reach $V^{+}_{X(\phi)} + V^{-}_{X(\phi+\pi/2)} = 0.85(8)$. Adapted from Peise *et al.*, 2015.

$\hat{H}_{\rm rf} = \hbar\Omega_{\rm rf}\hat{\mathcal{S}}_x$), a relative phase shift θ implemented by a detuned π pulse between $|1,0\rangle$ and $|2,0\rangle$, and a second balanced beam splitter between $|1,0\rangle$ and $|s\rangle$. The antisymmetric mode $|a\rangle$ is left unchanged by the interferometer transformation (up to an overall phase), while the $|s\rangle$ is rotated in the Bloch sphere identified by the $\hat{\boldsymbol{\mathcal{S}}}$ manifold. The experiment of Kruse *et al.* (2016) reported Ramsey fringes as a function of θ reaching a clock sensitivity 2.05 dB below $\Delta\theta_{\rm SQL} = 1/\sqrt{N}$. In the absence of noise, the expected sensitivity is $\Delta\theta = e^{-r}/\sqrt{N}$ (Caves, 1981) in the low squeezing regime and can reach the Heisenberg limit $\Delta\theta_{\rm HL} = 1/N$ when the input states in each mode of the interferometer have the same population on average (Pezzè and Smerzi, 2008).

4. Nonlinear SU(1,1) interferometry

Spin-mixing dynamics can also be used to realize a SU(1,1) interferometer as first proposed by Yurke, McCall, and Klauder (1986) in optics[17] and further analyzed by Marino, Corzo Trejo, and Lett (2012) and Gabbrielli, Pezzè, and Smerzi (2015) for spinor condensates. The basic idea of this interferometric scheme is to replace the linear beam splitters of a standard Mach-Zehnder scheme with nonlinear beam splitters that create or annihilate pairs of particles, as implemented via spin-mixing dynamics. Let us indicate with $\mathcal{N}$ the total average number of atoms transferred in pairs from a condensate prepared in $m_F = 0$ to the initially empty $m_F = \pm 1$ modes. After spin mixing, the system acquires a relative phase $\theta = 2\theta_0 - (\theta_{+1} + \theta_{-1})$ between $m_F = 0$ and ± 1 modes. A second spin-mixing dynamics closes the interferometer. The final populations in $m_F = 0, \pm 1$ depend on θ. When treating the condensate in $m_F = 0$ as an undepletable source of atomic pairs, the predicted phase sensitivity is (Yurke, McCall, and Klauder, 1986)

$$\Delta\theta = \sqrt{\frac{\mathcal{N}(\mathcal{N}+2)\cos^2(\theta/2)+1}{\mathcal{N}(\mathcal{N}+2)\sin^2(\theta/2)}}. \tag{108}$$

Equation (108) reaches $\Delta\theta = 1/\sqrt{\mathcal{N}(\mathcal{N}+2)}$ at the optimal working point $\theta = \pi$ (a dark fringe, where no particle is found in the output $m_F = \pm 1$ states) and shows that only the particles outcoupled from the $m_F = 0$ mode contribute to the phase sensitivity.

An analysis beyond the low-depletion limit shows that the SU(1,1) interferometer scheme can overcome the standard quantum limit with respect to the total number of particles N in the initial condensate (Gabbrielli, Pezzè, and Smerzi, 2015) and reach $\Delta\theta = \mathcal{O}(1/N)$. The sensitivity can be further enhanced by an additional linear coupling of the three modes before and after phase imprinting, a scheme called "pumped-up" SU(1,1) interferometer (Szigeti, Lewis-Swan, and Haine, 2017).

Linnemann *et al.* (2016) experimentally realized a nonlinear SU(1,1) interferometer within the $F = 2$ manifold of ^{87}Rb. The experiment is performed in the low-depletion regime with $\mathcal{N} = 2.8$, using $N \approx 400$ atoms. The interferometer is probed by tuning the relative phase between the $m_F = 0$ condensate and the $m_F = \pm 1$ modes to the dark fringe. The phase θ is imprinted via a second-order Zeeman shift by applying a magnetic field for varying times and is read out from the mean total number of atoms in the $m_F = \pm 1$ modes. Results demonstrate a sensitivity $\Delta\theta$ close to the theoretical prediction of Eq. (108).

D. Other protocols to create correlated atomic pairs

Spin-mixing dynamics is not the only possibility to create correlated atom pairs. Alternative methods have been studied and implemented experimentally. Relative number squeezing between two Bose-Einstein condensates with opposite momenta has been obtained in the collisional deexcitation of a one-dimensional quasicondensate, where the reduced dimensionality restricted the number of available modes (Bücker *et al.*, 2011). The atoms were initially prepared in a highly nonequilibrium state such that the only allowed deexcitation channel is a two-particle collision process, emitting atom pairs. Bücker *et al.* (2011) observed a number squeezing of up to −4.3 dB. Jaskula *et al.* (2010) observed sub-Poissonian atom number fluctuations, with 0.5 dB of

[17] SU(1,1) interferometers have been recently realized with a bright laser source by Hudelist *et al.* (2014) and with a hybrid atom-light system by Bing Chen *et al.* (2015).

number squeezing, between atoms of opposing momenta in the halo produced by the *s*-wave scattering of two Bose-Einstein condensates of metastable ^{4}He. The amount of detected squeezing was limited by the large number of collisional modes (isotropically distributed over the scattering sphere) and the correspondingly small number of atoms per mode. With the same scheme (Lewis-Swan and Kheruntsyan, 2014) it was possible to demonstrate Hong-Ou-Mandel interference (Hong, Ou, and Mandel, 1987). Each atom of the pair in the motional degree of freedom is sent to the input channel of a beam splitter realized using Bragg scattering on an optical lattice (Bonneau *et al.*, 2013). When two inputs are indistinguishable, they emerge together in one of the output channels, demonstrating two-particle interference (Lopes *et al.*, 2015).

V. ENTANGLEMENT CREATION VIA ATOM-LIGHT INTERACTION

The light-matter quantum interface finds important applications in several areas of quantum-information processing (Kimble, 2008; Hammerer, Sørensen, and Polzik, 2010). Here we review the many successful experiments and proposals that exploit the coupling between atoms and light for the creation of useful entangled states for quantum metrology. This quest started in the late 1990s with pioneering experiments using room-temperature vapor cells (Kuzmich *et al.*, 1999; Kuzmich, Mandel, and Bigelow, 2000) and laser-cooled atomic gases (Hald *et al.*, 1999), which demonstrated the reduction of atomic spin (or pseudospin) fluctuations. In these experiments, the atom-light interface was implemented in free space using optically thick atomic ensembles (Kuzmich and Polzik, 2003). Optical cavities can be used to effectively increase the optical depth of the atomic sample and represent a versatile system with rich possibilities for creating entanglement between atoms (Miller *et al.*, 2005; Tanji-Suzuki *et al.*, 2011; Ritsch *et al.*, 2013). These techniques have allowed the demonstration of metrological spin-squeezing, squeezed-state atomic clocks and the creation of highly nonclassical states.

Key theoretical proposals and experiments on atom-light interfaces for quantum metrology can be classified into three broad categories: (a) nondestructive measurements, including quantum nondemolition measurements and Zeno dynamics, Sec. V.A; (b) light-mediated coherent interaction between distant atoms, Sec. V.B; and (c) the transfer of squeezing to atoms via absorption of nonclassical light, Sec. V.C. Atom-light interaction currently represents the most successful method for producing large amounts of squeezing and entanglement in atomic ensembles.

A. Quantum state preparation using nondestructive measurements

1. Quantum nondemolition measurements in free space

In a quantum nondemolition (QND) measurement, a system (e.g., an atomic ensemble) and a meter (a measurement degree of freedom, e.g., a light beam) are coupled, such that a direct measurement of the meter provides indirect information about an observable of the system (Braginsky, Vorontsov, and Thorne, 1980; Braginsky and Khalili, 1992; Grangier, Levenson, and Poizat, 1998). The measurement is called QND if the system and the measured value of the observable are conserved after the measurement. QND measurements are a resource for quantum metrology as they allow the preparation of entangled and spin-squeezed states of many atoms. This is well illustrated by a model Hamiltonian describing a far-off resonant dispersive interaction between the collective spin of an ensemble of atoms and a two-mode light beam in free space (Kuzmich, Bigelow, and Mandel, 1998; Takahashi *et al.*, 1999):

$$\hat{H}_{\mathrm{QND}} = (\hbar k/t_{\mathrm{p}})\hat{S}_z\hat{J}_z. \tag{109}$$

Here t_{p} is the light pulse duration, $\hat{\boldsymbol{J}} = \{\hat{J}_x, \hat{J}_y, \hat{J}_z\}$ is the atomic collective spin, and $\hat{\boldsymbol{S}} = \{\hat{S}_x, \hat{S}_y, \hat{S}_z\}$ is the Stokes vector operator of the light, with components $\hat{S}_x = (\hat{a}_+^\dagger\hat{a}_- + \hat{a}_-^\dagger\hat{a}_+)/2$, $\hat{S}_y = (\hat{a}_+^\dagger\hat{a}_- - \hat{a}_-^\dagger\hat{a}_+)/(2i)$, and $\hat{S}_z = (\hat{a}_+^\dagger\hat{a}_+ - \hat{a}_-^\dagger\hat{a}_-)/2$. The operators $\hat{a}_\pm$ can refer to two polarization modes (Takahashi *et al.*, 1999; Hammerer *et al.*, 2004), in which case Eq. (109) describes the paramagnetic Faraday rotation of light; or to two spatial modes of an optical Mach-Zehnder interferometer where atoms are placed in one arm and phase shift the light (Oblak *et al.*, 2005; Chaudhury *et al.*, 2006; Windpassinger *et al.*, 2008). The dimensionless interaction strength in Eq. (109) is $k \propto (\sigma/A)\Gamma/\Delta$, where σ is the resonant photon scattering cross section of the probe transition, Γ is the spontaneous emission rate, A is the spatial cross section of the atomic ensemble illuminated by the pulse, and Δ is the detuning of the light from resonance (Hammerer, Sørensen, and Polzik, 2010). The Hamiltonian (109) satisfies the backaction evasion condition $[\hat{J}_z, \hat{H}_{\mathrm{QND}}] = 0$ such that $\hat{J}_z$ is a constant of motion. During the interaction, $\hat{\boldsymbol{S}}$ precesses around the z axis by an angle $k\hat{J}_z$. To lowest order in this angle, we have

$$\hat{S}_x^{\mathrm{out}} \approx \hat{S}_x^{\mathrm{in}} - k\hat{S}_y^{\mathrm{in}}\hat{J}_z^{\mathrm{in}}, \qquad \hat{J}_x^{\mathrm{out}} \approx \hat{J}_x^{\mathrm{in}} - k\hat{J}_y^{\mathrm{in}}\hat{S}_z^{\mathrm{in}}, \tag{110a}$$

$$\hat{S}_y^{\mathrm{out}} \approx \hat{S}_y^{\mathrm{in}} + k\hat{S}_x^{\mathrm{in}}\hat{J}_z^{\mathrm{in}}, \qquad \hat{J}_y^{\mathrm{out}} \approx \hat{J}_y^{\mathrm{in}} + k\hat{J}_x^{\mathrm{in}}\hat{S}_z^{\mathrm{in}}, \tag{110b}$$

$$\hat{S}_z^{\mathrm{out}} = \hat{S}_z^{\mathrm{in}}, \qquad \hat{J}_z^{\mathrm{out}} = \hat{J}_z^{\mathrm{in}}. \tag{110c}$$

A measurement of $\hat{S}_x^{\mathrm{out}}$ or $\hat{S}_y^{\mathrm{out}}$ thus realizes a QND measurement of $\hat{J}_z$ while preserving the system's quantum coherence. As an illustration, we take atomic and optical systems both initially prepared in coherent spin states polarized along the x axis. Assuming $\langle\hat{S}_y^{\mathrm{in}}\rangle = 0$ and $\langle\hat{J}_z\rangle = 0$, the average phase precession is zero, $\langle\hat{S}_y^{\mathrm{out}}\rangle = 0$, while the variance $(\Delta\hat{S}_y^{\mathrm{out}})^2 = n(1+\kappa^2)/4$ increases with $\kappa^2 = nNk^2/4$, where N is the number of atoms and n is the number of photons in the pulse. The mean value and variance of $\hat{J}_z$ after the measurement of the light spin $\hat{S}_y$ (with result m_y) are

$$\langle\hat{J}_z^{\mathrm{out}}\rangle|_{m_y} = \frac{\kappa}{1+\kappa^2}\sqrt{\frac{N}{n}}m_y, \tag{111a}$$

$$(\Delta\hat{J}_z^{\mathrm{out}})^2|_{m_y} = \frac{1}{1+\kappa^2}\frac{N}{4}, \tag{111b}$$

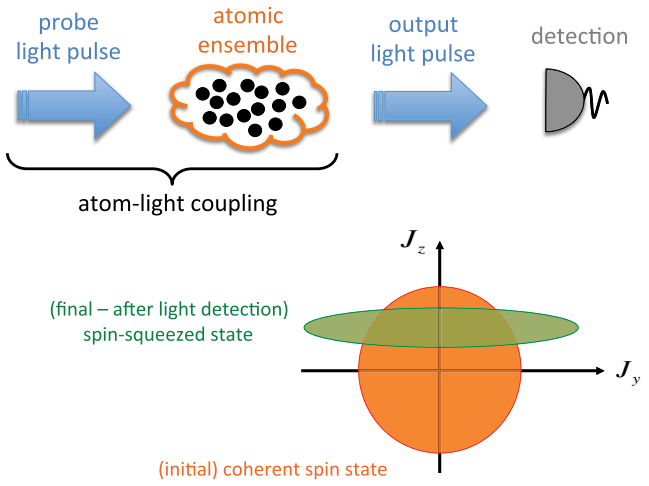

FIG. 26. Conditional spin squeezing via QND measurements. A light beam (blue arrows) propagates through the atomic ensemble. By measuring the output light field, one gains information about the atomic state. The initial coherent spin state (orange circle) changes after the detection of the light beam (green ellipse). It becomes squeezed in $\hat{J}_z$ and shifted (conditioned by the measurement result), according to Eqs. (111a) and (111b).

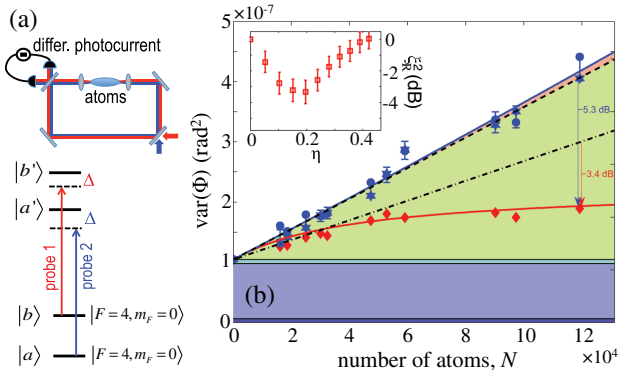

FIG. 27. Spin squeezing via quantum nondemolition measurements in free space. (a) A cloud of cold Cs atoms is confined in an elongated dipole trap placed in one arm of an optical Mach-Zehnder interferometer and aligned with the largest resonant optical depth. The relative populations of the clock levels $|a\rangle$ and $|b\rangle$ are measured via the phase shift ϕ accumulated by two detuned probe beams propagating through the atomic cloud. (b) Red diamonds are $\mathrm{Var}(\Phi)$ (with $\Phi=\phi_1-\zeta\phi_2$) obtained after two consecutive QND measurements of covariance ζ. Blue symbols are $\mathrm{Var}(\Phi)$ obtained for a coherent spin state ($\Phi=\phi_1$, dots, and $\Phi=\phi_2$, stars). The solid line is a quadratic fit and the dashed line is the expected linear scaling with the atom number N due to projection noise. The dot-dashed line is the projection noise scaled down by the factor $(1-\eta)^2=0.64$, corresponding to the reduction by the measured observed loss of atomic coherence. Different color regions are the optical shot noise (light blue), detector noise (dark blue), and projection noise (green, light). The inset illustrates the trade-off between spin squeezing ξ_R^2 and loss of coherence η due to spontaneous emission. Adapted from Appel *et al.*, 2009.

respectively; see Fig. 26. Although the final atomic state depends on the result of the measurement of the light beam (and it is thus termed conditional), the reduction in spin noise according to Eq. (111b) is completely deterministic, with no postselection necessary. Unconditional spin squeezing can be achieved by an additional spin rotation that compensates the stochastic shift of $\langle\hat{J}_z\rangle$ in Eq. (111a) (Berry and Sanders, 2002; Thomsen, Mancini, and Wiseman, 2002). Inoue *et al.* (2013) and Cox *et al.* (2016) experimentally demonstrated such unconditional spin squeezing via feedback control; see also Vanderbruggen *et al.* (2013). In the QND scheme, the squeezing is due to the projective measurement of the atomic state upon detection of the light, and its efficacy is determined by the performance of the detector. Yet, this discussion is highly idealized: far-off resonant dispersive probing is unavoidably accompanied by decoherence due to Raman spin flips.[18] Note that $\kappa^2=\eta\alpha_0$, where $\alpha_0\propto N\sigma/A$ is the resonant optical depth and $\eta\propto n(\sigma/A)(\Gamma/\Delta)^2$ is the average photon scattering rate per atom during the probe pulse. Scattered photons carry information about the spin state of the atoms: these photons reduce the spin length as $|\langle\hat{J}_x^{\mathrm{out}}\rangle|\approx(1-\eta)|\langle\hat{J}_x\rangle|$ for $\eta\ll 1$ (Hammerer *et al.*, 2004) and add noise that counteracts the reduction of spin variance (Hammerer *et al.*, 2004; Madsen and Mølmer, 2004; de Echaniz *et al.*, 2005). A suitable choice of atomic levels may be used to avoid this effect (Saffman *et al.*, 2009; Chen *et al.*, 2014). The successful implementation of QND measurements is thus based on the proper choice of light power (increasing n reduces the photon shot noise of light detection but increases Raman scattering) and detuning [exploiting the favorable scaling of $k\propto\Gamma/\Delta$ over $\eta\propto(\Gamma/\Delta)^2$]. The most important figure of merit of an atom-light interface is the resonant optical depth α_0, which should be much larger than unity.

Appel *et al.* (2009) reported the first experimental demonstration of metrological spin squeezing (reaching $\xi_R<1$) via QND measurements in free space. This experiment used $N=1.2\times10^5$ Cs atoms (with measured $\kappa^2\approx3.2$ and optical depth $\alpha_0\approx16$). Two equally intense and linearly polarized laser beams of different frequencies enter the arms of an optical Mach-Zehnder interferometer; see Fig. 27(a). The beams off resonantly probe different atomic transitions and experience phase shifts proportional to the number of atoms in the probed levels (Saffman *et al.*, 2009). The detection of the relative phase shift ϕ accumulated in the optical path performs a QND measurement of the relative population in the two atomic levels (Kuzmich, Bigelow, and Mandel, 1998; Saffman *et al.*, 2009). Spin squeezing is quantified by correlations between two consecutive QND measurements. One finds

$$\mathrm{Var}(\phi_2-\zeta\phi_1)=\frac{1}{n}+\frac{\kappa^2}{1+\kappa^2}\frac{N}{4}, \tag{112}$$

where ϕ_1 and ϕ_2 refer to the first and second phase shift detections, respectively, and the covariance

[18] In the literature, nonideal measurements are still termed QND provided that the loss of coherence in the atomic ensemble remains small.

$$\zeta = \mathrm{Cov}(\phi_1, \phi_2)/\mathrm{Var}(\phi_1) = \frac{\kappa^2}{1+\kappa^2} \tag{113}$$

expresses the correlations between the two measurements. The results reveal a spin squeezing $\xi_R^2 = -3.4$ dB; see Fig. 27(b). Furthermore, Louchet-Chauvet *et al.* (2010) used a similar apparatus to perform a Ramsey sequence (between the two QND measurements) and demonstrated an atomic clock with a measured phase sensitivity 1.1 dB below the standard quantum limit.

Spin squeezing has also been experimentally obtained by measuring the polarization rotation of probe light passing through a cloud of atoms. This technique was pioneered by Kuzmich *et al.* (1999) and Kuzmich, Mandel, and Bigelow (2000), and more recently investigated in ensembles of spin-1/2 ^{171}Yb (Takano *et al.*, 2009, 2010; Inoue *et al.*, 2013) and spin-1 ^{87}Rb atoms (Sewell *et al.*, 2012, 2013, 2014). Sewell *et al.* (2012, 2014) achieved spin squeezing using a two-polarization probing technique (Koschorreck *et al.*, 2010a, 2010b). These experiments demonstrated $\xi_R^2 = -1.5$ dB (Sewell *et al.*, 2014) [$\xi_R^2 = -2$ dB inferred (Sewell *et al.*, 2012)] using $N \approx 6 \times 10^5$ atoms, limited mainly by the photon shot noise of the readout light. Polarization-based QND measurements find direct application in entanglement-assisted optical magnetometry; see Sec. VII.C.

Puentes *et al.* (2013) proposed to generate planar spin squeezing (see Sec. II.C.8.d) in spin-1 atomic ensembles via sequential QND measurements of two orthogonal spin components. Measurements by Colangelo, Martin Ciurana, Puentes *et al.* (2017) and Colangelo, Martin Ciurana, Bianchet *et al.* (2017) in cold $F = 1$ ^{87}Rb atoms show phase and amplitude squeezing simultaneously, as well as entanglement between the atoms' spins (Vitagliano *et al.*, 2018).

2. Cavity-based quantum nondemolition measurements in the dispersive regime

The strength of the interaction between the light and the atomic ensemble is usually weak, but can be enhanced by placing the atoms inside an optical cavity. This method is very promising as the squeezing factor increases with the cavity finesse, which can be pushed to large values. Moreover, a small single-pass optical depth is advantageous for applications in atomic clocks, since it allows one to reduce atomic-density-dependent atom losses, dephasing, and systematic errors.

The essential features of dispersive atom-light interaction in a cavity (Vernac, Pinard, and Giacobino, 2000; Bouchoule and Mølmer, 2002a; Madsen and Mølmer, 2004; Nielsen and Mølmer, 2008) are captured by a simplified model comprising N three-level atoms; see Fig. 28(a). Each atom has two hyperfine levels $|a\rangle$ and $|b\rangle$ of energy difference $\hbar\omega$, and an excited state $|e\rangle$ with linewidth Γ (spontaneous decay rate into free space). The atoms are placed in an optical cavity with resonance frequency ω_c and linewidth κ_c, driven resonantly with a single-atom–single-photon effective intracavity Rabi frequency $2g$. The detuning of the cavity from the $|a\rangle \leftrightarrow |e\rangle$ and $|b\rangle \leftrightarrow |e\rangle$ transitions is chosen of equal magnitude $\Delta = \pm\omega/2$. Assuming homogeneous interaction (see Sec. II.E.3), low intracavity photon number ($n_c = \langle \hat{c}^\dagger \hat{c} \rangle \ll \Delta^2/g^2$), and large detuning ($\Delta \gg \kappa_c, \Gamma, \sqrt{N}g$), the

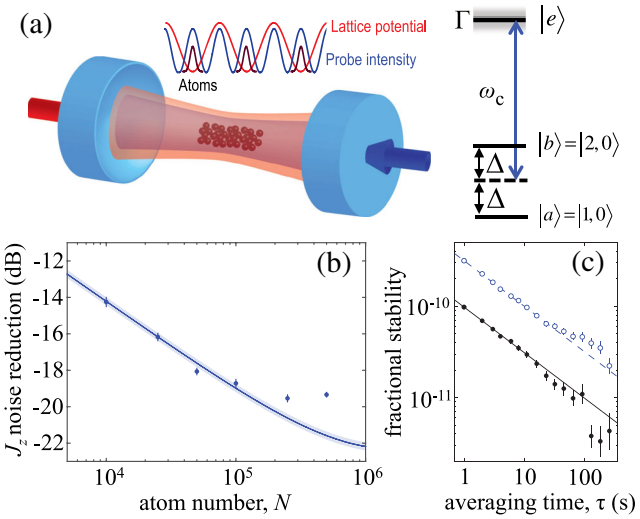

FIG. 28. Spin squeezing via cavity-based quantum nondemolition measurements in the dispersive regime. (a) Laser-cooled atoms are optically trapped in a standing wave (red, lighter line) inside an optical resonator. The cavity resonance is shifted in proportion to the relative population of two clock levels. The shift is measured from the transmission of a probe beam (blue, darker line). Uniform atom-light coupling is achieved using trapping and probe beams of commensurate frequencies. (b) Measured spin-noise reduction $4(\Delta \hat{J}_z)^2/N$ (dots) normalized to the coherent spin state projection noise. The solid line is a model fit. (c) Allan deviation of a clock that uses the generated squeezed states (black dots; the solid line indicates 9.7×10^{-11} $\mathrm{s}^{1/2}/\sqrt{\tau}$) or coherent spin states (blue circles; the dashed line is the standard quantum limit). Adapted from Hosten, Engelsen *et al.*, 2016.

coupling Hamiltonian is (Schleier-Smith, Leroux, and Vuletić, 2010a)

$$\hat{H} = \hbar\omega_c \hat{c}^\dagger \hat{c} + \hbar \frac{2g^2}{\Delta} \hat{c}^\dagger \hat{c} \hat{J}_z + \hbar\omega \hat{J}_z, \tag{114}$$

where $\hat{c}$ and $\hat{c}^\dagger$ are cavity mode operators. The effect of the light on the atoms is an ac Stark shift of the transition frequency $\delta\omega = (2g^2/\Delta)n_c$ between $|a\rangle$ and $|b\rangle$. Atoms in $|a\rangle$ ($|b\rangle$) increase (decrease) the index of refraction seen by the probe light, so that the net effect is a shift of the cavity resonance by

$$\delta\omega_c = \frac{2g^2}{\Delta} \frac{N_a - N_b}{2} = \frac{2g^2}{\Delta} J_z, \tag{115}$$

where N_a and N_b are the numbers of atoms in $|a\rangle$ and $|b\rangle$, respectively. This shift can be probed by injecting a laser into the cavity, providing a QND measurement of $\hat{J}_z$. A detailed analysis including decoherence associated with free-space scattering of the probe light shows the possibility to achieve (Chen *et al.*, 2014; Hosten, Engelsen *et al.*, 2016)

$$\xi_R^2 \approx \frac{1 + NC(\Gamma/\omega)^2}{\sqrt{NC}}, \tag{116}$$

where $C = (2g)^2/(\kappa_c \Gamma)$ is the single-atom cavity cooperativity. C is the ratio between the number of photons scattered

into the cavity mode and those scattered into free space and quantifies the optical depth of an atom with respect to the cavity mode (Tanji-Suzuki *et al.*, 2011). Note that C depends on the cavity geometry and is proportional to the cavity finesse (Tanji-Suzuki *et al.*, 2011).

Spin squeezing via a cavity-based QND measurement was first demonstrated by Schleier-Smith, Leroux, and Vuletić (2010b) using magnetically insensitive clock states of ^{87}Rb atoms. This experiment reported a spin squeezing $\xi_R^2 = -1.45$ dB with respect to the standard quantum limit $(\Delta\theta_{SQL})^2 = 1/N_{eff}$, referring to $N_{eff} \approx 0.66N$ uncorrelated atoms (N_{eff} accounts for spatial variation in the atom-light coupling due to the trapping lattice being incommensurate with the cavity mode used for probing, and $N = 5 \times 10^4$). This result is mainly limited by inhomogeneous dephasing due to the cavity locking light. Hosten, Engelsen *et al.* (2016) used a cavity of higher cooperativity and exploited probing and trapping beams of commensurate frequencies, achieving a uniform atom-light coupling; see Fig. 28(a). This avoids the need for spin-echo techniques required for nonuniformly coupled systems. This experiment demonstrated 10.5 dB of improved phase sensitivity with respect to $(\Delta\theta_{SQL})^2 = 1/N$, with $N = 1 \times 10^5$ ^{87}Rb atoms, and a spin squeezing $\xi_R^2 = -18.5$ dB (-20.1 dB inferred); see Figs. 28(b) and 28(c). This represents the highest value in expected metrological spin squeezing and measured phase sensitivity gain to date.

3. Heralded atomic entanglement created by single-photon detection

In the preceding sections we discussed the interaction of an atomic ensemble with an intense laser pulse (10^5–10^7 photons in typical experiments), which is subsequently detected by a standard linear photodetector that does not resolve individual photons. The light in these experiments is effectively a continuous-variable quantum system. A different approach uses weak laser pulses in combination with single-photon counting, in close analogy to the techniques developed for atomic ensemble-based quantum repeaters (Duan *et al.*, 2001; Sangouard *et al.*, 2011). These techniques allow one to create a range of highly nonclassical states of a large number of atoms in a heralded way, i.e., conditioned on the detection of a single photon. The interaction of a linearly polarized photon with the atoms according to Eq. (109) produces a weak Faraday rotation of the photon polarization. Denoting $|\mathrm{v}\rangle$ and $|\mathrm{h}\rangle$ the vertical and horizontal polarizations, respectively, an atom-light system initialized in $|\mathrm{v}\rangle \otimes |\vartheta, \varphi, N\rangle$ (where $|\vartheta, \varphi, N\rangle$ is a coherent spin state, see Sec. II.C) evolves by the QND interaction (109) to the state (McConnell *et al.*, 2013)

$$|\psi\rangle = \tfrac{1}{2}|\mathrm{v}\rangle \otimes (|\vartheta, \varphi_+, N\rangle + |\vartheta, \varphi_-, N\rangle) + \tfrac{1}{2}|\mathrm{h}\rangle \otimes (|\vartheta, \varphi_+, N\rangle - |\vartheta, \varphi_-, N\rangle), \quad (117)$$

where $\varphi_\pm = \varphi \pm \phi$ and ϕ is the phase accumulated during the interaction. The detection of a vertically polarized photon projects the atomic ensemble to $|\psi_\mathrm{v}\rangle \propto |\vartheta, \varphi_+, N\rangle + |\vartheta, \varphi_-, N\rangle$, whereas the detection of a horizontally polarized photon prepares $|\psi_\mathrm{h}\rangle \propto |\vartheta, \varphi_+, N\rangle - |\vartheta, \varphi_-, N\rangle$. The entanglement properties strongly depend on the phase ϕ, and the quantum Fisher information is (without loss of generality we assume here that $\vartheta = \pi/2$ and $\varphi = 0$)

$$\frac{F_Q[|\psi_{\mathrm{h,v}}\rangle, \hat{J}_y]}{N} = \frac{1 + (N-1)\sin^2\phi \pm \cos^N\phi}{1 \pm \cos^N\phi}, \quad (118)$$

where the plus (minus) sign holds for the detection of a vertically (horizontally) polarized photon. To the leading order in N, we have $F_Q[|\psi_\mathrm{v}\rangle, \hat{J}_y]/N = 1 + N\phi^2/2 + \mathcal{O}(N^2\phi^4)$ and $F_Q[|\psi_\mathrm{h}\rangle, \hat{J}_y]/N = 3 + N\phi^2/2 + \mathcal{O}(N^2\phi^4)$: for $|\phi| \lesssim 2/\sqrt{N}$, the state $|\psi_\mathrm{h}\rangle$ is metrologically more useful than $|\psi_\mathrm{v}\rangle$. In particular, for $|\phi| \ll 1/\sqrt{N}$, the (rare) detection of a horizontally polarized photon heralds the generation of $|\psi_\mathrm{h}\rangle = |(N/2-1)_x\rangle$, which is the one-excitation Dicke state. For $|\phi| \gtrsim 2/\sqrt{N}$, we have $\cos^N\phi \approx 0$ in Eq. (118) and the two states approximately give the same quantum Fisher information. At $\phi = \pm\pi/2$, we get the NOON state $|\psi_{\mathrm{h,v}}\rangle = [|(N/2)_y\rangle \pm |(-N/2)_y\rangle]/\sqrt{2}$. In the realistic scenario $|\phi| \ll 1/\sqrt{N}$, the detection of a sequence of photons conditionally prepares more and more entanglement. For instance, disregarding losses and decoherence, the detection of n_h h-polarized photons prepares the NOON state $[|(N/2)_z\rangle + |(-N/2)_z\rangle]/\sqrt{2}$ when $n_\mathrm{h}|\phi| \gtrsim \sqrt{N}$. Finally, W. Chen *et al.* (2015) generalized this method showing the possibility to generate a broad class of entangled states of many atoms using single photons having a tailored frequency spectrum and time-resolved detection.

Experimentally, the use of single-photon detection for preparing entangled states of an atomic ensemble was pioneered by Christensen *et al.* (2013, 2014). These experiments reported the expected increase of spin fluctuations above projection noise. McConnell *et al.* (2015) demonstrated the generation of entanglement in an atomic ensemble of $N = 3100$ laser-cooled ^{87}Rb atoms prepared in an optical cavity and probed with an off-resonant weak pulse (of about 200 photons) of vertically polarized light; see Fig. 29(a). The accumulated phase is $\phi = 4g^2/(\kappa_c\Delta)$, being $2/\kappa_c$ the characteristic atom-photon interaction time [$\phi\sqrt{N} \approx 0.03$ in the experiment of McConnell *et al.* (2015)]. This experiment investigated the entangled state produced by the detection of a horizontally polarized photon, while the detection of vertically polarized photons gives, for these experimental parameters, only a slight spin squeezing. From the tomographic reconstructed density matrix it is possible to obtain a Wigner distribution with negative areas, see Fig. 29(b), and an entanglement depth (not related to metrological usefulness) of 2900 atoms. This work demonstrates how the information carried by a single (or a few) photon(s) can create entanglement in a large atomic ensemble. Hu *et al.* (2017) reanalyzed the experimental data of McConnell *et al.* (2015) to show that the generated atomic state violates classical physics even if no assumptions related to quantum mechanics are made. This conclusion (Kot *et al.*, 2012), similarly to Bell inequalities (Brunner *et al.*, 2014), observes that marginal probability distributions measured for noncommuting observables do not always come from a joint probability distribution identified with a classical state. As in Schmied *et al.* (2016) (see Fig. 17),

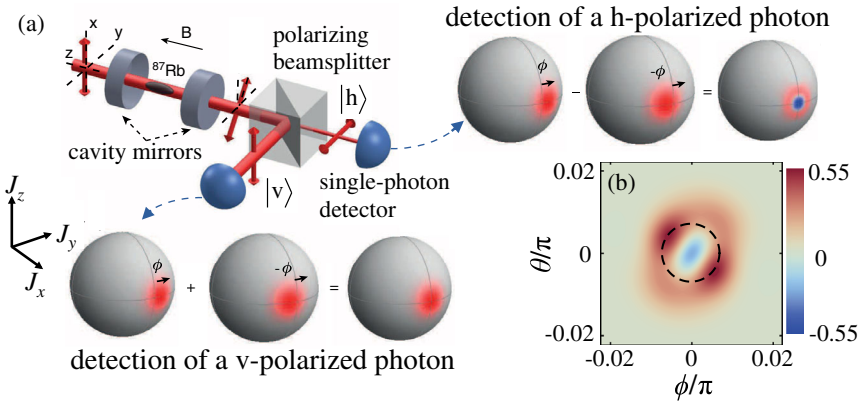

FIG. 29. Entangled states generated by the detection of a single photon. (a) An atomic ensemble confined in a cavity interacts with vertically polarized light. The detection of an outgoing horizontally (vertically) polarized single photon projects the atoms into a state with a negative (positive) Wigner distribution. (b) Experimental Wigner distribution of the heralded atomic state obtained from the least-squares-fitted atomic density matrix via Eq. (66). It shows negative parts. The dashed line is the contour at which the Wigner distribution of an N-atom coherent spin state is equal to $1/\sqrt{e}$ of its maximum value. Adapted from McConnell *et al.*, 2015.

Hu *et al.* (2017) showed that classical physics is insufficient for describing mesoscopic entangled states of atoms.

4. Cavity-based quantum nondemolition measurements in the normal mode splitting regime

The experiments discussed in the previous sections operate in the dispersive regime, where the cavity is far detuned from atomic resonance. In this section, we discuss quantum state preparation schemes where the cavity is tuned near an atomic resonance with respect to the atomic transition $|b\rangle \leftrightarrow |e\rangle$; see Fig. 30(a). Let us assume that atoms in $|a\rangle$ do not interact with the cavity mode, the number of atoms in $|b\rangle$ is $N_b \gg 1$, and the system is driven weakly so that the mean number of atoms in $|e\rangle$ is small with respect to N_b. We have that atoms in $|b\rangle$ cause a splitting $\omega_c \to \omega_c^{\pm}$ of the cavity resonance frequency (Chen *et al.*, 2014) that depends on N_b:

$$\omega_c^{\pm} = \omega_c - \frac{\delta_c \pm \sqrt{\delta_c^2 + 4g^2 N_b}}{2}, \tag{119}$$

where $\delta_c = \omega_c - \omega_{be}$ is the cavity detuning from the atomic transition ω_{be}, ω_c is the bare cavity frequency, and g is the single-atom–single-photon coupling rate (uniform coupling is assumed). At $\delta_c = 0$, the appearance of two well-resolved resonances separated by $2g\sqrt{N_b}$ is referred to as collective vacuum Rabi splitting. In the limit of collective strong coupling $g\sqrt{N_b} \gg \kappa_c, \Gamma$ the normal modes of the coupled system are well resolved: a measurement of $\omega_c^{\pm}$ thus allows one to determine N_b.

In the experiments of Chen *et al.* (2011), Bohnet *et al.* (2014), and Cox *et al.* (2016), the atom number N_b is measured nondestructively by probing the cavity resonant frequency with an additional probe laser injected into the cavity. The number of particles in level $|a\rangle$ can be probed by first applying a resonant π pulse between $|a\rangle$ and $|b\rangle$ and then repeating the QND measurement. A detailed analysis of the impact of decoherence in this system (mainly due to scattering of cavity photons into free space) can be found in Chen *et al.* (2014). Chen *et al.* (2011) tuned the optical cavity to resonance $\delta_c = 0$ with $NC \approx 1400$. This experiment reported a spin squeezing $\xi_R^2 = -1$ dB ($\xi_R^2 = -3.3$ dB inferred) relative to the standard quantum limit using $N_{\text{eff}} = 7 \times 10^5$ ^{87}Rb atoms (N_{eff} is an effective atom number taking into account inhomogeneous coupling in the cavity, see Sec. II.E.3). Bohnet *et al.* (2014) and Cox *et al.* (2016) considerably reduced noise effects taking advantage of a cycling transition (Saffman *et al.*, 2009; Chen *et al.*, 2014), and a higher collective cooperativity $NC \approx 6000$ was reached. Experimental results demonstrate $\xi_R^2 = -10.2$ dB (Bohnet *et al.*, 2014), see Fig. 30, and $\xi_R^2 = -17.7$ dB (Cox *et al.*, 2016), using $N_{\text{eff}} = 4 \times 10^5$ ^{87}Rb atoms. The achieved spin squeezing witnesses the presence of useful 170 ± 30 particle entanglement (Cox *et al.*, 2016). This squeezing technique was further combined with quantum feedback reaching $\xi_R^2 = -7.4$ dB of deterministic spin squeezing (Cox *et al.*, 2016).

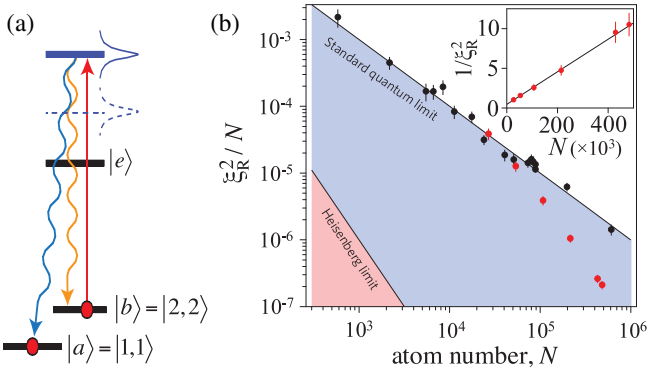

FIG. 30. Spin squeezing obtained via quantum nondemolition measurements in the normal mode splitting regime. (a) Energy-level diagram showing the cavity shift due to atoms in level $|b\rangle$. (b) ξ_R^2/N as a function of atom number N for uncorrelated particles (black dots) and spin-squeezed states [red (gray) dots]. The inset shows $1/\xi_R^2$ of the spin-squeezed state (red dots) as a function of N. The black line is a fit to the data according to a $1/N^2$ scaling. Adapted from Bohnet *et al.*, 2014.

Resonant atom-light coupling in an optical cavity also offers the possibility to create entangled states beyond spin squeezing. Haas *et al.* (2014) used an atom chip integrated with a high-finesse fiber-optical cavity in the strong-coupling regime (Volz *et al.*, 2011) to prepare a generalized W state of $N \approx 40$ cold ^{87}Rb atoms. In this experiment the cavity and probe laser tuned on resonance with the $|b\rangle \leftrightarrow |e\rangle$ transition. The single-atom strong coupling $g \gg \kappa_c, \Gamma$ guarantees that the cavity transmits light only if all N atoms are in level $|a\rangle$: a single atom in $|b\rangle$ is sufficient to block the cavity transmission. The experiment of Haas *et al.* (2014) starts with all atoms in level $|a\rangle$, and a weak microwave pulse coupling $|a\rangle$ and $|b\rangle$ prepares the state $\sqrt{1-p}|N\rangle_a|0\rangle_b + \sqrt{p}|N-1\rangle_a|1\rangle_b$, where $p \ll 1$ to avoid multiparticle excitations. The cavity transmission is then measured with a probe-light beam. A low transmission heralds the QND preparation of the W state $|N-1\rangle_a|1\rangle_b$. The resulting state is characterized by state tomography from which it is possible to extract an entanglement depth of 13 atoms, at least.

5. Quantum state preparation via quantum Zeno dynamics

Quantum Zeno dynamics combines the coherent evolution of a system with the measurement of an initially unoccupied quantum state (Facchi and Pascazio, 2008): if the measurement is performed with high enough frequency, the measured state remains unoccupied. This profoundly modifies the system dynamics and allows engineering specific entangled states. Barontini *et al.* (2015) used a cavity-based measurement in the regime of high cooperativity $C \gg 1$ (Volz *et al.*, 2011) to prepare a generalized W state of 36 ^{87}Rb atoms via quantum Zeno dynamics. The N atoms are all initialized in level $|b\rangle$ and coupled to the $|a\rangle$ level by a microwave drive at Rabi frequency Ω. The cavity is in resonance with the $|b\rangle \leftrightarrow |e\rangle$ transition and transmits only if there are no atoms in level $|b\rangle$. The cavity transmission is probed at a rate much larger than Ω. When no measurement is performed, the microwave Rabi coupling prepares the state $|N\rangle_a|0\rangle_b$ after a time $T = \pi/\Omega$. In the presence of the cavity measurement, the quantum Zeno effect forbids the preparation of $|N\rangle_a|0\rangle_b$ and deterministically prepares the W state $|N-1\rangle_a|1\rangle_b$; see Fig. 31. From the density matrix extracted via state tomography, it is possible to obtain a lower bound to the quantum Fisher information, $F_Q/N \geq 1.51$ (Barontini *et al.*, 2015).

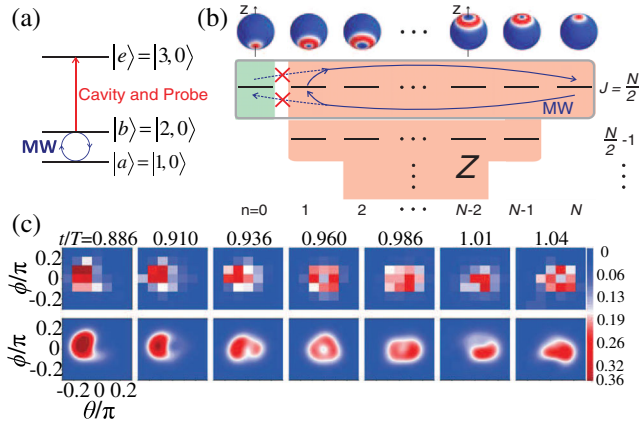

FIG. 31. State engineering via quantum Zeno dynamics. (a) $|a\rangle$ and $|b\rangle$ are coupled by a microwave field at Rabi frequency Ω, while the optical cavity transition $|b\rangle \leftrightarrow |e\rangle$ is probed with a coupling rate much faster than Ω. (b) Starting with all atoms in $|b\rangle$, microwave Rabi coupling and simultaneous measurement of the cavity transmission leads to a coherent evolution restricted to the subspace highlighted by the orange (right shaded) area. The preparation of the state with no atoms in $|b\rangle$ (green, left shaded area) is forbidden by the quantum Zeno effect. The upper row shows the Husimi distributions of symmetric Dicke states. (c) Experimental Husimi distributions for different evolution times t/T, where $T = \pi/\Omega$ is the time for a Rabi π pulse in the absence of cavity probing. The upper row shows direct measurements, while the lower row shows the reconstructed density matrix. Adapted from Barontini *et al.*, 2015.

B. Light-mediated coherent interaction between distant atoms

In contrast to the measurement-based scheme of Sec. V.A, off-resonant atom-light coupling can also be used to realize a light-mediated coherent interaction between distant atoms. When the light Stokes operator $\hat{S}_z$ is proportional to the atomic $\hat{J}_z$, the Hamiltonian $\hat{H} \propto \hat{S}_z\hat{J}_z$ describing atom light interaction [see Eq. (109)] becomes $\hat{H} \propto \hat{J}_z^2$ (Agarwal, Puri, and Singh, 1997; Zhang, Peng, and Braunstein, 2003), corresponding to an effective one-axis twisting nonlinearity that generates unconditional spin squeezing (Kitagawa and Ueda, 1993). As a main difference with respect to contact interaction discussed in Sec. III.B, this light-mediated interaction can be applied to a dilute atomic sample, which is preferred for minimizing systematic errors in precision measurements. Moreover, in contrast to spin squeezing obtained from QND measurements, it deterministically produces known entangled states, independently from the detector performance. Furthermore, atom-cavity coupling can be easily switched on and off.

There are different proposals for the realization of an effective interaction between distant atoms. Takeuchi *et al.* (2005) studied a double-pass Faraday interaction in free space where a polarized light beam passes twice through an atomic ensemble (after the first passage the polarization is properly rotated such that $\hat{S}_z \propto \hat{J}_z$ at the second passage). An improved version of this proposal was discussed by Trail, Jessen, and Deutsch (2010) using a quantum eraser to remove residual spin-probe entanglement. Schleier-Smith, Leroux, and Vuletić (2010a) and Zhang *et al.* (2015) proposed the realization of light-induced atom-atom interaction in an optical cavity (also called cavity squeezing or cavity feedback); see Fig. 32(a). This relies on the dispersive interaction between one mode of the cavity and an ensemble of three-level atoms. As shown by Eq. (114) the atoms modify the cavity resonance frequency by an amount proportional to $\hat{J}_z$. When the cavity is driven by a probe laser of frequency ω_p tuned to the slope of the cavity resonance ($\omega_p = \kappa_c$), the intracavity photon number $n_c = \langle \hat{c}^\dagger \hat{c} \rangle$ in Eq. (114), being detuning dependent, changes linearly with the index of refraction of the atomic cloud (which, in turn, is proportional to $\hat{J}_z$); see Fig. 32(b). Note that tracing out the light field (which carries information about the atomic spin) yields a dissipative dynamics that

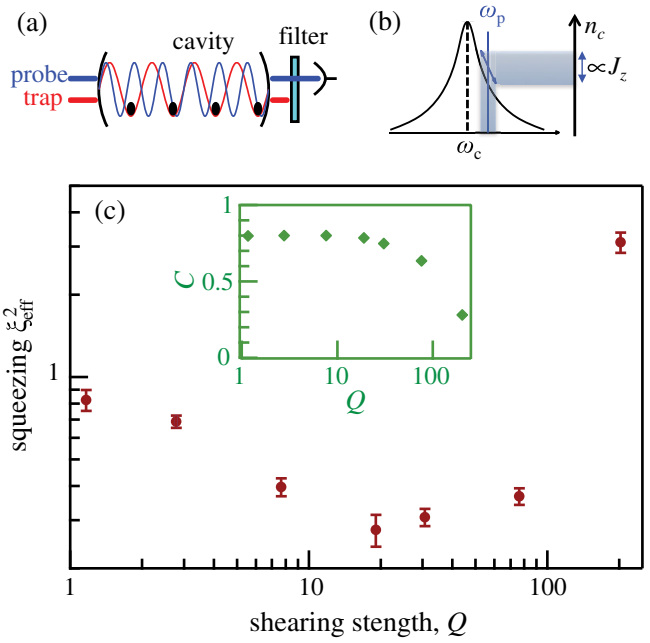

FIG. 32. Squeezing via light-mediated effective interaction between atoms. (a) The atoms are trapped in a standing-wave dipole trap inside an optical resonator. (b) The probe laser is detuned from cavity resonance by half a linewidth, so that atom-induced shifts of the cavity frequency change the transmitted power by an amount proportional to J_z. (c) Effective spin squeezing $\xi^2_{\rm eff} = \sigma^2(Q)\mathcal{C}(0)/\mathcal{C}(Q)^2$ giving the gain with respect to the sensitivity experimentally achieved in the absence of entanglement, as a function of the shearing strength Q (proportional to the photon number in the cavity). Here $\sigma^2(Q) = (\Delta\hat{J}_z)^2/(N_{\rm eff}/4)$, and $\mathcal{C}(Q)$ is the contrast of Rabi oscillations of the sheared state, shown in the inset. The effective spin squeezing is related to the metrological spin squeezing Eq. (41) as $\xi^2_{\rm eff} = \mathcal{C}(0)\xi^2_{\rm R}$. An effective squeezing $\xi^2_{\rm eff} = -5.6$ dB is reached, corresponding to $\xi^2_{\rm R} = -4.6$ dB. Adapted from Leroux, Schleier-Smith, and Vuletić, 2010a.

limits the attainable squeezing (Leroux *et al.*, 2012). See also Pawłowski *et al.* (2016) for an analysis of the spin squeezing reachable with the cavity feedback method in the presence of cavity losses and spontaneous emission. Finally, an alternative proposal to realize an effective one-axis twisting atomic Hamiltonian uses a four-wave Raman scheme to directly drive the atomic ensemble, where atoms communicate with one another by exchanging photons via a weakly occupied cavity mode (Sørensen, 2002).

One-axis twisting by light-mediated coherent interaction has been experimentally implemented in an optical cavity (Leroux, Schleier-Smith, and Vuletić, 2010a, 2010b), using an effective number $N_{\rm eff} = 3 \times 10^4$ of ^{87}Rb atoms. The experiment realizes the scheme of Schleier-Smith, Leroux, and Vuletić (2010a). The squeezed state is characterized via spin-noise tomography and the contrast of Rabi oscillations. The results of Leroux, Schleier-Smith, and Vuletić (2010a) are summarized in Fig. 32(c) and demonstrate a gain $\xi^2_{\rm R} = -4.6$ dB over $(\Delta\theta_{\rm SQL})^2 = 1/N_{\rm eff}$ ($\xi^2_{\rm eff} = -5.6$ dB over the sensitivity experimentally reached in the absence of entanglement). Leroux, Schleier-Smith, and Vuletić (2010b) used the squeezed states generated with this method to realize an atomic clock with short-time fractional frequency stability a factor 2.8 (corresponding to 4.5 dB) in variance below the standard quantum limit; see Sec. VII.

C. Quantum state transfer from nonclassical light to atoms

Spin-squeezed states can be also created by transferring quadrature squeezing of light to atomic spin squeezing (Agarwal and Puri, 1990; Kuzmich, Mølmer, and Polzik, 1997; Hammerer, Sørensen, and Polzik, 2010). This effect can be understood from the Jaynes-Cummings model Hamiltonian

$$\hat{H}_{\rm JC} = \hbar\Omega(\hat{c}\hat{J}_+ + \hat{c}^\dagger\hat{J}_-), \tag{120}$$

describing the interaction of nondecaying two-level atoms with a light mode. Here $\hat{c}^\dagger$ and $\hat{c}$ are the light creation and annihilation operators, respectively, $\hat{J}_\pm$ are spin rising and lowering operators, see Sec. II.A, and Ω is a coupling constant. The Heisenberg equations of motion for $\hat{c}$ and $\hat{J}_\pm$ can be found analytically within a frozen-spin approximation, assuming $\hat{J}_z$ constant and equal to $N/2$. We obtain (Wineland *et al.*, 1992, 1994)

$$\xi^2_{\rm R}(t) = \xi^2_{\rm R}(0)\cos^2(\Omega_N t) + \xi^2_p(0)\sin^2(\Omega_N t), \tag{121a}$$

$$\xi^2_p(t) = \xi^2_p(0)\cos^2(\Omega_N t) + \xi^2_{\rm R}(0)\sin^2(\Omega_N t), \tag{121b}$$

where $\xi^2_p = 2(\Delta\hat{P}_c)^2$, $\hat{P}_c = (\hat{c} - \hat{c}^\dagger)/(i\sqrt{2})$, $\xi^2_{\rm R} = N(\Delta\hat{J}_x)^2/\langle\hat{J}_z\rangle^2$, and $\Omega_N = k\sqrt{N}$. Similar expressions can be obtained relating $\xi^2_{\rm R} = N(\Delta\hat{J}_y)^2/\langle\hat{J}_z\rangle^2$ with $\xi^2_x = 2(\Delta\hat{X}_c)^2$, where $\hat{X}_c = (\hat{c} + \hat{c}^\dagger)/\sqrt{2}$. These equations predict that atomic spin squeezing $\xi_{\rm R} < 1$ can be achieved by first squeezing the light field $\xi^2_p < 1$ and then transferring this quadrature squeezing onto the spins. Optimal spin squeezing is reached at $t = \pi/(2\Omega_N)$. For strong squeezing the contrast $\langle\hat{J}_z\rangle$ decreases, and the frozen-spin approximation breaks down. Since the squeezed light is the source of spin squeezing in this method, the degree of squeezing is determined by the quality of the quadrature squeezed light.

Quantum state transfer from light to atoms was first experimentally demonstrated by Hald *et al.* (1999) using an ensemble of 10^7 cold Cs atoms, following the theoretical proposal of Kuzmich, Mølmer, and Polzik (1997). This experiment used a V-level scheme consisting of three atomic hyperfine levels (Hald *et al.*, 1999, 2000). The reduction of atomic spin noise below the projection noise of uncorrelated atoms is generated by the absorption of polarized coherent and squeezed vacuum light with opposite circular polarizations.

An alternative approach mapping a quantum state of light onto an atomic state via electromagnetically induced transparency was proposed by Fleischhauer and Lukin (2000); see also Liu *et al.* (2001) and Phillips *et al.* (2001). Further studies include the mapping quantum states of light into a Bose-Einstein condensate with application to atom interferometers (Szigeti *et al.*, 2014) and atom lasers (Fleischhauer and Gong, 2002; Haine and Hope, 2005).

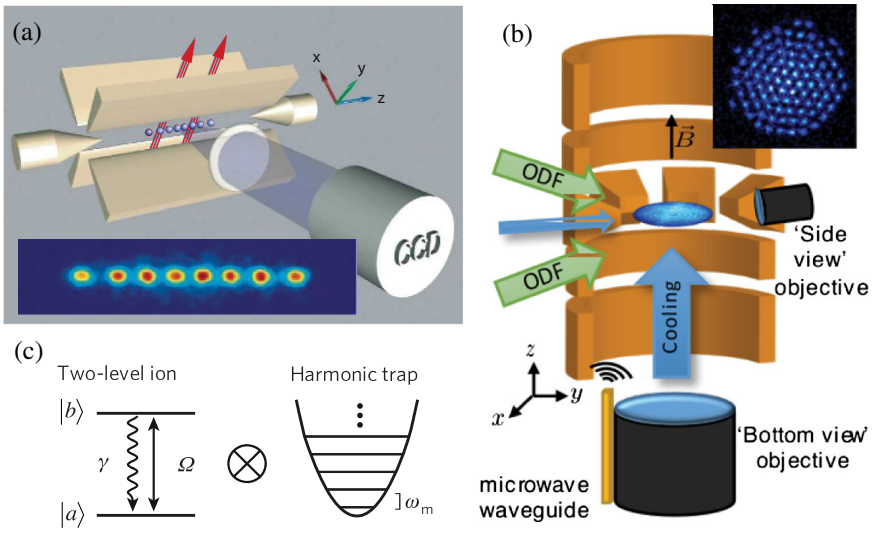

FIG. 33. Common ion-trapping setups. (a) Linear Paul trap. Ions are trapped using radio-frequency oscillating electric fields combined with static electric control fields. In tight radial confinement, laser-cooled ions form a linear string (see the inset image for eight ions) with a spacing determined by the balance between external confining fields and ion-ion Coulomb repulsion. From Blatt and Wineland, 2008. (b) Penning trap. Ions are confined in the x-y plane with a strong homogeneous magnetic field and axially by a quadrupole electric field. The green ODF arrows indicate bichromatic light fields used to generate entanglement. The inset shows an image of a 2D crystal of 91 ions. From Bohnet *et al.*, 2016. (c) Each trapped ion can be modeled as an effective internal two-level system, $|a\rangle$ and $|b\rangle$ interacting with a radiation characterized by Rabi frequency Ω and decay rate γ, and a shared external harmonic oscillator potential with equally spaced energy levels of mode frequency ω_m.

VI. ENTANGLED STATES OF TRAPPED IONS

Ensembles of trapped ions confined in electromagnetic traps and manipulated with laser beams are one of the most successful systems to generate and exploit entanglement (Blatt and Wineland, 2008; Wineland, 2013). Direct applications include quantum information and computation (Häffner, Roos, and Blatt, 2008; Roos, 2014), quantum networks (Duan and Monroe, 2010), quantum simulations (Blatt and Roos, 2012; Schneider, Porras, and Schaetz, 2012; Martinez *et al.*, 2016) and, as reviewed here, quantum metrology. Trapped ions are well isolated from the environment, can be coherently manipulated, individually addressed, and detected with almost unit efficiency (Leibfried, Blatt *et al.*, 2003).

Typical experiments (Leibfried, Blatt *et al.*, 2003) confine ions in linear Paul traps [Fig. 33(a)], surface-electrode Paul traps (Sterling *et al.*, 2014; Mielenz *et al.*, 2016), or Penning traps [Fig. 33(b)]. One- and two-dimensional ion arrangements are well suited for individually controlling and reading out internal states of the ions. We note that individual particle manipulation and detection are crucial for many quantum-computation and quantum information tasks, but they are not necessary for quantum-enhanced metrology. Interesting metrological experiments can thus also be performed in Penning traps (where local manipulation is currently not available), which are well suited to store, manipulate, and entangle large numbers of ions (Britton *et al.*, 2012; Bohnet *et al.*, 2016).

In trapped ion experiments, the qubit is formed by two internal (usually hyperfine) states $|a\rangle$ and $|b\rangle$ of each ion. This internal qubit can be coupled by an electromagnetic field to external (motional, vibrational) degrees of freedom; see Fig. 33(c). A key aspect is the local detection of the internal ion's state with extremely high efficiency. This is usually achieved by resonant fluorescence. Detection errors arise if the qubit changes its state during the detection interval or if photons scattered off trap electrodes are mistaken for fluorescence photons. Myerson *et al.* (2008) and Harty *et al.* (2014) reported qubit detection errors smaller than 10^{-4}.

A. Generation of metrologically useful entangled states of many ions

The generation of entanglement between different qubits is one major challenge in quantum-information processing with trapped ions (Wineland *et al.*, 1998). The Coulomb force pushes the ions apart to a distance much larger than the Bohr radius and thus prevents state-dependent ion-ion interactions in the absence of external electromagnetic fields. However, as a consequence of the Coulomb force, the normal modes of motion in the trap are shared among all ions and can provide a means for entangling the qubits. Most of the schemes for entangling trapped ion qubits are based on internal-state-dependent forces acting on the ions, generated by external electromagnetic fields. These forces can be arranged in time and frequency in such a way that an effective entangling operation is carried out between two or more qubits and no entanglement persists between the qubits and the vibrational degrees of freedom.

The entangling gates can be broadly classified in three categories, according to the way the electromagnetic fields interact with the ions: (i) Quantum gates induced by a laser beam that interacts with a single ion at a time as originally proposed by Cirac and Zoller (1995). The ion is entangled with a vibrational mode of the ion string and the entanglement

is subsequently transferred from the vibrational mode to the internal state of a second ion. (ii) Quantum gates induced by an electromagnetic field that simultaneously addresses two or more ions, either through optical ac Stark shifts (Mølmer and Sørensen, 1999; Solano, de Matos Filho, and Zagury, 1999; Sørensen and Mølmer, 1999, 2000; Milburn, Schneider, and James, 2000; Leibfried *et al.*, 2003; García-Ripoll, Zoller, and Cirac, 2005; Lee *et al.*, 2005; Kim *et al.*, 2009, 2010), through static magnetic-field gradients in combination with homogeneous radio-frequency fields (Mintert and Wunderlich, 2001; Johanning *et al.*, 2009; Johanning, Varón, and Wunderlich, 2009; Welzel *et al.*, 2011), or with radio-frequency field gradients (Ospelkaus *et al.*, 2008, 2011). As an important advantage, these gates do not require one to cool all ion normal modes to their ground states, but only the ion motion to be well within the Lamb-Dicke regime $\langle \hat{z}^2 \rangle \ll (\lambda/2\pi)^2$, where z is the displacement of an ion along the laser propagation direction and λ is the laser wavelength. The basic idea is to drive a phonon (normal) mode of frequency ν by a periodic state-dependent force with frequency ω. In the rotating-wave approximation, the Hamiltonian describing this conditional interaction is (Roos, 2014)

$$\hat{H} = i\hbar k(\hat{c}^\dagger e^{i\delta t} - \hat{c}e^{-i\delta t})\hat{O}, \tag{122}$$

where $\hat{O}$ is an operator acting on the (internal) qubit states, $\hat{c}^\dagger$ and $\hat{c}$ are the harmonic oscillator creation and annihilation operators of the addressed normal mode, respectively, k is a coupling strength, and $\delta = \omega - \nu$. The propagator $\hat{U}$ corresponding to this time-dependent Hamiltonian is

$$\hat{U}(t) = \exp[\alpha(t)\hat{O}\hat{c}^\dagger - \alpha^*(t)\hat{O}^\dagger\hat{c}]\exp[i\phi(t)\hat{O}^2], \tag{123}$$

where $\alpha(t) = i(k/\delta)(1 - e^{i\delta t})$ and $\phi(t) = (k/\delta)^2(\delta t - \sin\delta t)$. If the interaction time $t = \tau$ is chosen such that $\alpha(\tau) = 0$, then the propagator reduces to $U(\tau) = \exp[i\phi(\tau)\hat{O}^2]$. A vibrational mode becomes transiently entangled with the qubits before getting disentangled at the end of the gate operation, resulting in an effective nonlocal operation capable of entangling the ions. The conditional phase gate (Leibfried *et al.*, 2003) is obtained by setting $\hat{O} = \sum_{i=1}^N \hat{\sigma}_z^{(i)}/2 = \hat{J}_z$ in Eq. (123), and is realized by placing the ions in a qubit-state-dependent potential created by two counterpropagating laser beams. The Mølmer-Sørensen gate (Mølmer and Sørensen, 1999; Sørensen and Mølmer, 2000) is obtained by setting $\hat{O} = \sum_{i=1}^N \hat{\sigma}_y^{(i)}/2 = \hat{J}_y$ (or $\hat{O} = \hat{J}_x$). This gate is realized by a bichromatic laser field tuned close to the upper and lower motional sidebands of the qubit transition (Sackett *et al.*, 2000; Benhelm *et al.*, 2008). In both gates, the propagator is the one-axis twisting $\hat{U} = \exp[i\phi(\tau)\hat{J}_{\boldsymbol{n}}^2]$; see Sec. III.B. Spin-dependent optical dipole forces generated by a pair of off-resonance laser beams with different frequencies, addressing many normal modes simultaneously, have been recently used to engineer tunable Ising spin-spin coupling (Lee *et al.*, 2005; Porras and Cirac, 2006; Kim *et al.*, 2009). The resulting propagator is (Porras and Cirac, 2006)

$$\hat{U}(t) = \exp\left[i\sum_{i,j=1}^N V_{i,j}\hat{\sigma}_z^{(i)}\hat{\sigma}_z^{(j)}\right], \tag{124}$$

where $V_{ij} \propto d_{ij}^{-\alpha}$, d_{ij} is the distance between the ith and jth ions, and α can be tuned by adjusting the laser frequencies in the range $0 \le \alpha \le 3$ (Schmied, Wesenberg, and Leibfried, 2011; Britton *et al.*, 2012). Ising spin-spin couplings have been implemented in a linear Paul trap with up to ∼20 ions (Islam *et al.*, 2013; Jurcevic *et al.*, 2014; Richerme *et al.*, 2014) and in a Penning trap forming a 2D Coulomb crystal of ∼200 ions (Britton *et al.*, 2012; Bohnet *et al.*, 2016); see Fig. 33(b). (iii) A third way to generate ion entanglement is based on performing joint measurements on photons that are first entangled with ion qubits (Moehring *et al.*, 2007; Stute *et al.*, 2012; Casabone *et al.*, 2013). This scheme enables the generation of entanglement between ions separated by large distances and does not require the ions to be in the Lamb-Dicke regime.

B. Quantum metrology with trapped ions

1. Quantum metrology with two ions

The first deterministic generation of entanglement of two trapped ions was reported by Turchette *et al.* (1998). This experiment was readily followed by the demonstration of a phase sensitivity below the standard quantum limit (Sackett *et al.*, 2000; Meyer *et al.*, 2001). Meyer *et al.* (2001) reported the creation of the state

$$|\psi\rangle = \cos\beta|a\rangle^{\otimes 2} + i\sin\beta|b\rangle^{\otimes 2} \tag{125}$$

of two $^9Be^+$ ions via a Mølmer-Sørensen gate in a linear Paul trap. Here β is a tunable parameter proportional to the laser pulse duration. The state (125) is spin squeezed,

$$\xi_R^2 = \frac{N(\Delta\hat{J}_\perp)^2}{\langle\hat{J}_z\rangle^2} = \frac{1-\sin 2\beta}{\cos^2 2\beta} < 1 \tag{126}$$

for $0 < \beta < \pi/2$. It reaches the Heisenberg limit $\xi_R^2 = 1/2$ at $\beta = \pi/4$, corresponding to a maximally entangled state. However, at $\beta = \pi/4$, $\langle\hat{J}_z\rangle = 0$ and any technical noise prevents detecting the maximally entangled state as spin squeezed. The experiment of Meyer *et al.* (2001) reached $\xi_R^2 = 0.85$ at the experimentally optimal working point $\beta = \pi/10$. A phase estimation with sensitivity below $\Delta\theta_{SQL}$ with the maximally entangled state was demonstrated by applying a spin rotation $\exp(-i\theta\hat{J}_z)$ followed by $\exp[-i(\pi/2)\hat{J}_x]$. Measuring the parity $\hat{\Pi} = \hat{\sigma}_z^{(1)}\hat{\sigma}_z^{(2)}$ led to a sensitivity $(\Delta\theta)^2/(\Delta\theta_{SQL})^2 = 0.7$, where $\Delta\theta = \Delta\hat{\Pi}/|d\langle\hat{\Pi}\rangle/d\theta|$ (Meyer *et al.*, 2001). Many experiments with two ions have reported parity oscillations from which it is possible to extract the phase sensitivity; see Fig. 34. These experiments have been performed in magnetic-field-insensitive clock states of $^{111}Cd^+$ (Haljan *et al.*, 2005) and using an optical transition in $^{40}Ca^+$ (Home *et al.*, 2006; Monz *et al.*, 2011; Noguchi, Toyoda, and Urabe, 2012)

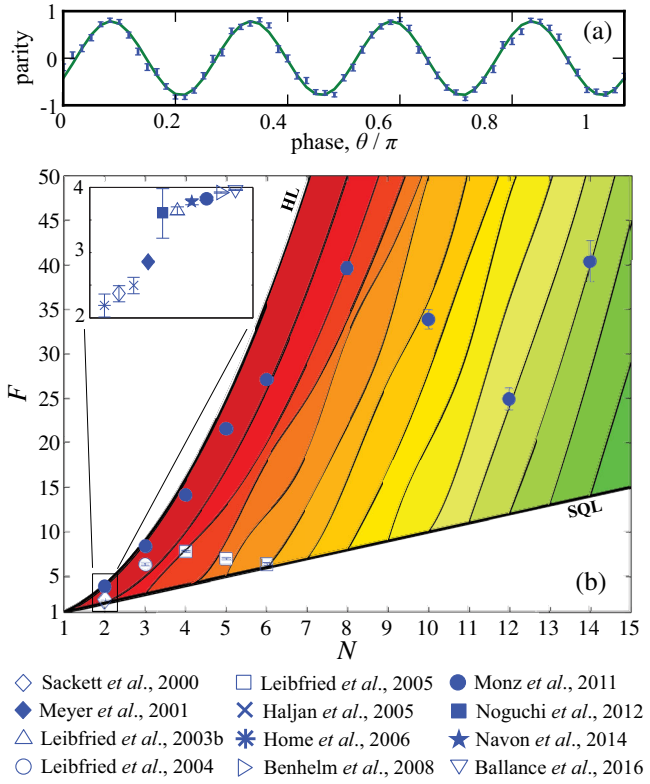

FIG. 34. Phase sensitivity of ion Schrödinger cat states. (a) Typical parity oscillations obtained with cat states, Eq. (127). These oscillations have a characteristic period $2\pi/N$ (here for $N = 8$). From Monz *et al.*, 2011. (b) Summary of the experimental achievements (symbols). Here we show the Fisher information $F = V^2N^2$ as a function of the number of qubits N, obtained from the extracted experimental visibilities V. The upper thick line is the Heisenberg limit $F = N^2$, and the lower thick line is the standard quantum limit $F = N$. The thin lines are bounds for useful k-particle entanglement, Eq. (38): they delimit from below a shaded region corresponding to $(k+1)$-particle entanglement. In particular, the darker red region stands for useful genuine N-particle entanglement. The next lighter red region stands for useful $(N-1)$-particle entanglement, and so on. For instance, the point at $N = 10$ reveals useful 4-particle entanglement. The inset summarizes experimental results obtained with Schrödinger cat states of $N = 2$ ions. Adapted from Pezzè *et al.*, 2016.

and $^{88}Sr^+$ (Navon *et al.*, 2014) ions. A very high visibility of the parity signal has been reported with $^{40}Ca^+$ (Benhelm *et al.*, 2008) and $^{43}Ca^+$ (Ballance *et al.*, 2016) ions; see also Gaebler *et al.* (2016) for the high-fidelity generation of the two-qubit GHZ states with $^9Be^+$ ions (Leibfried *et al.*, 2003). Finally, Meyer *et al.* (2001) also reported a full Ramsey sequence, where the maximally entangled state is generated between two Ramsey pulses and the phase θ is proportional to the interrogation time. In this case, the initial probe state was a symmetric Dicke state $|\psi\rangle = (|a\rangle|b\rangle + |b\rangle|a\rangle)/\sqrt{2}$. By measuring the parity, it was possible to reach a spectroscopic sensitivity $(\Delta\theta)^2/(\Delta\theta_{\rm SQL})^2 = 0.77$. Noguchi, Toyoda, and Urabe (2012) reported the creation of symmetric Dicke states of two and four $^{40}Ca^+$ ions.

2. Quantum metrology with GHZ states of several ions

The maximally entangled (or Schrödinger cat) state

$$|\psi_{N,\rm cat}\rangle = \frac{|a\rangle^{\otimes N} + |b\rangle^{\otimes N}}{\sqrt{2}} \tag{127}$$

has been created with up to $N = 6$ $^9Be^+$ ions (Leibfried *et al.*, 2005) and $N = 14$ $^{40}Ca^+$ ions (Monz *et al.*, 2011) in a linear Paul trap. This state is formally obtained from $\hat{U}_{\rm cat}|b\rangle^{\otimes N}$, where

$$\hat{U}_{\rm cat} = \exp\left(-i\frac{N\pi}{2}\hat{J}_x\right)\exp\left(i\frac{\pi}{2}\hat{J}_x^2\right), \tag{128}$$

see Sec. III.B. When applying a spin rotation $\exp(-i\theta\hat{J}_z)$, the state (127) transforms as $|\psi_{N,\rm cat}(\theta)\rangle = [\exp(i\theta N/2)|a\rangle^{\otimes N} + \exp(-i\theta N/2)|b\rangle^{\otimes N}]/\sqrt{2}$, such that the relative phase between $|a\rangle^{\otimes N}$ and $|b\rangle^{\otimes N}$ is $N\theta$. The state can be detected after a $\pi/2$ Rabi rotation around the x axis. The probability to obtain N_a atoms in level a and $N_b = N - N_a$ atoms in level b is $P(N_a|N,\theta) = 2^{-N}\binom{N}{N_a}\{1 + (-1)^{N_a}\cos[N(\theta+\pi/2)]\}$. These probabilities oscillate with a frequency N times faster than that of a single qubit. Therefore, most observable properties of these states feature these rapid oscillations (Bollinger *et al.*, 1996). Notably, applying the nonlinear transformation $\hat{U}_{\rm cat}$ again after phase encoding, one obtains only two detection events (N atoms in level a or b) that can be experimentally distinguished with high efficiency (Leibfried *et al.*, 2004, 2005). Experiments exploring quantum metrology with states (127) generally report dichotomic events—the parity of the relative atom number, in Leibfried *et al.* (2004) and Monz *et al.* (2011), or the detection of all atoms in the same level in Leibfried *et al.* (2004, 2005). Figure 34(a) shows an example of parity oscillations

$$P(\pm|\theta) = \frac{1 \pm V\cos N\theta}{2}, \tag{129}$$

where the visibility $0 \le V \le 1$ accounts for experimental noise and imperfect state preparation. The corresponding Fisher information is

$$F(\theta) = \frac{V^2N^2\sin^2 N\theta}{1 - V^2\cos^2 N\theta}. \tag{130}$$

It reaches the maximum value $F = V^2N^2$ when $\sin N\theta = \pm 1$. It is thus possible to detected useful entanglement and obtain sensitivities below the standard quantum limit when $V^2 > 1/N$ (corresponding to $F > N$). Metrologically useful N-partite entangled states are detected when

$$V^2 > \left(1 - \frac{1}{N}\right)^2 + \frac{1}{N^2} \tag{131}$$

corresponding to $F > (N-1)^2 + 1$, obtained from Eq. (38) with $k = N - 1$. Figure 34(b) gives an overview of the experimental results obtained with cat states of trapped ions.

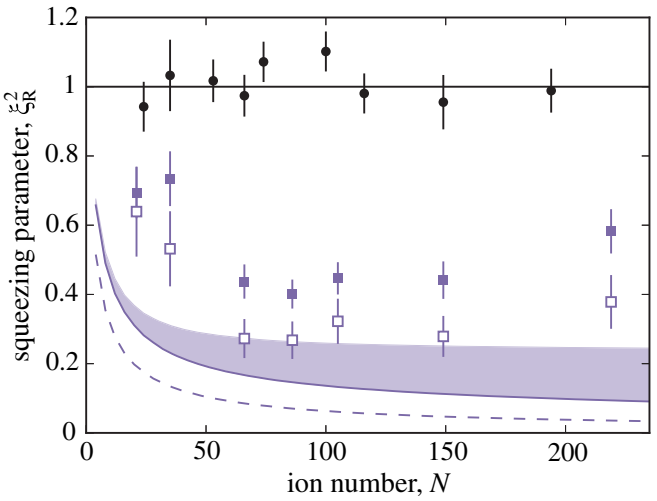

FIG. 35. Metrological spin-squeezing parameter as a function of the number of ions. The black points are obtained for a coherent spin state. The purple symbols are obtained with spin-squeezed states (optimized over probe preparation time): with (open squares) and without (solid squares) subtraction of photon shot noise. The dashed (solid) line is a theoretical prediction (including spontaneous emission). From Bohnet *et al.*, 2016.

In Monz *et al.* (2011) the fringe visibility of parity oscillations was sufficiently high that the Fisher information witnesses metrologically useful genuine N-particle entanglement up to $N = 6$ ions (Pezzè *et al.*, 2016).

Note that the fast oscillations of the output probabilities obtained with the state (127) seem to prevent the unambiguous estimate of a phase larger than $2\pi/N$ (Boto *et al.*, 2000; Mitchell, 2005; Pezzè and Smerzi, 2007; Berry *et al.*, 2009). A phase estimation at the Heisenberg limit with no constraint on θ in $[-\pi, \pi]$ can be obtained using states with different numbers of particles. The optimal sequence $N = 1, 2, 4, \ldots, 2^p$ provides $\Delta\theta = 2.55/N_T$ (at $\theta = 0$), where $N_T = \sum_{n=0}^{p} 2^n = 2^{p+1} - 1$ is the total number of particles used (Pezzè and Smerzi, 2007).

It is finally worth pointing out that W states (that are less useful than ideal cat states for metrological applications) have been created experimentally with up to eight ions (Roos *et al.*, 2004; Häffner *et al.*, 2005).

3. Spin squeezing and useful entanglement of many ions

Recently, entanglement and metrological spin squeezing of hundreds of trapped $^9Be^+$ ions have been demonstrated in a Penning trap (Bohnet *et al.*, 2016). The experiment realized a homogeneous Ising spin-spin interaction (Kitagawa and Ueda, 1993), i.e., $\alpha \approx 0$ in Eq. (124) corresponding to the one-axis twisting model; see Sec. III.B. Figure 35 shows ξ^2_R, optimized over the evolution time, as a function of the number of ions ranging from $N = 20$ to 220. For long evolution times, the state wraps around the Bloch sphere and spin squeezing is lost (see Sec. III.B). In this case, Bohnet *et al.* (2016) inferred (with noise subtraction) $F_Q/N > 2.1$, where the bound has been extracted following the Hellinger method of Strobel *et al.* (2014). For an analysis of decoherence in this system see Foss-Feig *et al.* (2013).

VII. WORKING ENTANGLEMENT-ENHANCED INTERFEROMETERS AND PROSPECTS FOR APPLICATIONS

Atomic ensembles are routinely used as precision sensors of inertial forces or external fields, or as atomic clocks, which usually operate as Ramsey interferometers (Bordè, 2002; Wynands and Weyers, 2005; Cronin, Schmiedmayer, and Pritchard, 2009; Wynands, 2009; Kitching, Knappe, and Donley, 2011; Barrett, Bertoldi, and Bouyer, 2016). The accumulated phase is $\theta = \omega T_R$, where T_R is the Ramsey interrogation time and ω is the parameter to be estimated. In an atomic sensor $\omega = \Delta E/\hbar$, where ΔE is the energy shift between the two interferometer modes, induced by an external field, an acceleration, a rotation, or a force. In an atomic clock $\omega = \omega_{LO} - \omega_0$, where ω_{LO} is the frequency of a local oscillator to be locked to the transition frequency ω_0 between the two atomic levels that define the clock. The standard quantum limit for the estimation of the frequency ω is, from Eq. (33),

$$\Delta\omega_{SQL} = \frac{1}{T_R\sqrt{N\nu}} = \frac{1}{T_R\sqrt{N}}\sqrt{\frac{T_{cycle}}{\tau}}, \tag{132}$$

where we expressed the number of measurements $\nu = \tau/T_{cycle}$ in terms of the total averaging time τ and the cycle time T_{cycle} of the experiment, with $T_{cycle} \geq T_R$. Using separable states, if quantum noise dominates over technical noise and $T_{cycle} \approx T_R$ is optimized, the sensitivity can thus be increased only by increasing the interrogation time T_R, the number N of particles, and/or the total averaging time τ. In realistic setups this is not always possible: every sensor has an optimal working range for T_R and N, and drifts always limit the duration τ over which identical state preparation can be assumed (Bak, Tang, and Wiesenfeld, 1987). In general, increasing the atom number leads to systematic errors due to collisions that spoil the sensitivity. Ramsey interrogation times are limited by mechanical restrictions (e.g., the limited ballistic flight time in fountain clocks), by the desired temporal resolution (e.g., when measuring high-frequency magnetic fields in broadband magnetometers), or decoherence (e.g., the phase coherence time of the local oscillator in atomic clocks). Can entangled states improve the performance of atomic sensors and, if so, under what conditions?

Entangled states are typically more susceptible to decoherence than separable states during phase encoding. Thus their gain (i.e., their more favorable scaling of phase sensitivity with N) may be counterbalanced by the requirement of shorter interrogation times. Whether or not an improvement is possible can be decided only after a detailed analysis of the specific sensor taking its actual limitations into account, and ultimately hinges on an experimental demonstration. As an example we note that squeezing of light has recently been used to improve the performance of a laser-interferometer gravitational wave observatory (The LIGO Scientific Collaboration, 2011; Aasi *et al.*, 2013). The aim of this section is to review the state of the art of entanglement-enhanced measurements with atomic ensembles beyond proof-of-concept demonstrations and to discuss prospects for applications.

A. The influence of noise and decoherence

A common and central aspect of quantum-enhanced metrology is the fragility of useful entangled states when coupled to the environment. Noise affects the preparation of the probe state, phase encoding, and detection. The literature has focused mainly on specific noise models and only few general results are available. An important challenge is to devise protocols (e.g., differential schemes, or error correction), special phase sensing situations (e.g., non-Markovian, or transverse noise), and detection schemes that make metrology below the standard quantum limit robust against noise.

1. General results

Phase encoding in the presence of noise can be formally described by a θ-dependent completely positive trace-preserving map Λ_θ (Rivas and Huelga, 2012), such that $\hat{\rho}_\theta = \Lambda_\theta[\hat{\rho}_0]$, where $\hat{\rho}_0$ and $\hat{\rho}_\theta$ are the probe and output state, respectively. The evolution from $\hat{\rho}_0$ to $\hat{\rho}_\theta$ can be conveniently studied by introducing additional degrees of freedom that are not under control and play the role of an "environment." The action of any quantum channel Λ_θ can be described via its Kraus representation $\hat{\rho}_\theta = \sum_\ell \hat{K}_\ell \hat{\rho}_0 \hat{K}_\ell^\dagger$ (Nielsen and Chuang, 2000), where $\hat{K}_\ell \equiv \langle \ell_{\rm E}|\hat{U}_{\rm SE}(\theta)|0_{\rm E}\rangle$ are Kraus operators, $|\ell_{\rm E}\rangle$ is an orthonormal and complete set of states ($\sum_\ell |\ell_{\rm E}\rangle\langle \ell_{\rm E}| = \mathbb{1}_{\rm E}$ guarantees $\sum_\ell \hat{K}_\ell \hat{K}_\ell^\dagger = 1$), and $|0_{\rm E}\rangle$ is the initial state of the environment (taken pure, without loss of generality). We recall that a Krauss representation is not unique: we can generate a new set by a unitary (eventually θ-dependent) transformation (Nielsen and Chuang, 2000).

In the enlarged Hilbert space $\mathcal{H}_{\rm S} \otimes \mathcal{H}_{\rm E}$, given by the product of the Hilbert space of the system and of the environment, phase encoding is modeled by a unitary operation $\hat{U}_{\rm SE}(\theta)$. Decoherence is taken into account by tracing over the environment $\hat{\rho}_\theta = {\rm Tr}_{\rm E}[|\psi_\theta^{\rm SE}\rangle\langle\psi_\theta^{\rm SE}|]$, where $|\psi_\theta^{\rm SE}\rangle = \hat{U}_{\rm SE}(\theta)|\psi_0^{\rm SE}\rangle$ is a purification of $\hat{\rho}_\theta$ and $|\psi_0^{\rm SE}\rangle$ a purification of the probe state $\hat{\rho}_0 = {\rm Tr}_{\rm E}[|\psi_0^{\rm SE}\rangle\langle\psi_0^{\rm SE}|]$. We recall that two purifications $|\psi_\theta^{\rm SE}\rangle$ and $|\tilde{\psi}_\theta^{\rm SE}\rangle$ of the same state are related via unitary operations acting only on the environment space (Nielsen and Chuang, 2000), $|\psi_\theta^{\rm SE}\rangle = \hat{U}_{\rm E}(\theta)|\tilde{\psi}_\theta^{\rm SE}\rangle$. Discarding part of the information regarding the unitary phase encoding in $\mathcal{H}_{\rm S} \otimes \mathcal{H}_{\rm E}$ motivates the inequality

$$F_{\rm Q}[\hat{\rho}_\theta] \leq F_{\rm Q}[|\psi_\theta^{\rm SE}\rangle], \tag{133}$$

valid for all purifications $|\psi_\theta^{\rm SE}\rangle$ of $\hat{\rho}_\theta$, where

$$F_{\rm Q}[|\psi_\theta^{\rm SE}\rangle] = 4(\langle\partial_\theta\psi_\theta^{\rm SE}|\partial_\theta\psi_\theta^{\rm SE}\rangle - |\langle\partial_\theta\psi_\theta^{\rm SE}|\psi_\theta^{\rm SE}\rangle|^2). \tag{134}$$

Equation (133) suggests to search for the minimum of $F_{\rm Q}[|\psi_\theta^{\rm SE}\rangle]$ over all purifications of $\hat{\rho}_\theta$ (Escher, de Matos Filho, and Davidovich, 2011; Escher *et al.*, 2012). Following Uhlmann's theorem (Uhlmann, 1976), Escher, de Matos Filho, and Davidovich (2011) indeed showed that

$$F_{\rm Q}[\hat{\rho}_\theta] = \min_{\{|\psi_\theta^{\rm SE}\rangle\}} F_{\rm Q}[|\psi_\theta^{\rm SE}\rangle], \tag{135}$$

see also Fujiwara and Imai (2008). In other words, there is always an environment that, when monitored together with the system, does not lead to more information about θ than monitoring the system alone. In particular, for an initial pure state $\hat{\rho}_0 = |\psi_0\rangle\langle\psi_0|$, Eq. (135) can be rewritten as (Escher, de Matos Filho, and Davidovich, 2011)

$$F_{\rm Q}[\hat{\rho}_\theta] = 4\min_{\{\hat{K}_\ell\}} \sum_\ell \langle(\partial_\theta\hat{K}_\ell^\dagger)(\partial_\theta\hat{K}_\ell)\rangle - \left(i\sum_\ell \langle\hat{K}_\ell^\dagger\partial_\theta\hat{K}_\ell\rangle\right)^2, \tag{136}$$

where the mean values are calculated over $|\psi_0\rangle$ and the minimization runs over all Kraus representations of the quantum channel. It is worth pointing out that, even if the optimal purification in Eq. (135) or the optimal set of Kraus operators in Eq. (136) are difficult to find, specific choices may yield nontrivial upper bounds to the quantum Fisher information (Escher, de Matos Filho, and Davidovich, 2011).

A special case of this formalism is that of a θ-independent quantum channel Λ where noise acts after phase encoding. In this case the quantum Fisher information never increases (Petz, 1996; Petz and Ghinea, 2011):

$$F_{\rm Q}[\Lambda(\hat{\rho}_\theta)] \leq F_{\rm Q}[\hat{\rho}_\theta]. \tag{137}$$

For example, the partial trace operation can only decrease the quantum Fisher information, consistent with the intuition that ignoring part of a system can only decrease the information about the estimated parameter. The equality in Eq. (137) is always obtained if Λ is unitary, because unitary θ-independent transformations can be absorbed into a redefinition of the optimal measurement saturating the quantum Fisher information.

2. Uncorrelated decoherence

A typical example illustrating the fragility of frequency estimation with respect to noise follows from Huelga *et al.* (1997). Let us consider a single atom prepared in the superposition $(|a\rangle + |b\rangle)/\sqrt{2}$. It evolves freely for a time $T_{\rm R}$, according to the Hamiltonian $\hbar\omega\hat{\sigma}_z$, and acquires a phase $\omega T_{\rm R}$ in the presence of local Markovian dephasing. The probability of finding the probe in its initial state is $P = [1 + e^{-\gamma T_{\rm R}}\cos(\omega T_{\rm R})]/2$, where $\gamma \geq 0$ is the dephasing rate. From this probability it is possible to estimate the frequency ω. The corresponding Fisher information is $F(\omega) = (\partial_\omega P)^2/(P - P^2) = T_{\rm R}^2 e^{-2\gamma T_{\rm R}}\sin^2(\omega T_{\rm R})/[1 - e^{-2\gamma T_{\rm R}}\cos^2(\omega T_{\rm R})]$, which is optimal at $\omega_{\rm opt} T_{\rm R} = \pi/2$. To calculate the sensitivity we take into account that the experiment can be repeated using N uncorrelated atoms in parallel, $\nu = T/T_{\rm R}$ times, where T is the total duration of the experiment (neglecting dead times). The Cramér-Rao bound is thus $\Delta\omega_{\rm CR} = \sqrt{T_{\rm R}/[F(\omega_{\rm opt})NT]} = 1/\sqrt{NTT_{\rm R}e^{-2\gamma T_{\rm R}}}$. We can further optimize this sensitivity over $T_{\rm R}$, giving $\Delta\omega_{\rm CR} = \sqrt{2\gamma e/(NT)}$ at the optimal Ramsey time $T_{\rm R} = 1/(2\gamma)$. If we now take a GHZ state $(|a\rangle^{\otimes N} + |b\rangle^{\otimes N})/\sqrt{2}$ in the presence of the same source of single-particle dephasing, the probability of finding the probe in the initial state is $P = [1 + e^{-\gamma N T_{\rm R}}\cos(\omega N T_{\rm R})]/2$: it oscillates N times faster than in the single-particle case (this is typical for GHZ states, see Sec. II.C.7), but the visibility of these oscillations decays N

times quicker. The Fisher information at the optimal point $N\omega_{\rm opt}T_{\rm R}=\pi/2$ is given by $F(\omega_{\rm opt})=N^2T_{\rm R}^2e^{-2N\gamma T_{\rm R}}$. Again, the experiment is repeated $\nu=T/T_{\rm R}$ times, and the Cramér-Rao bound is $\Delta\omega_{\rm CR}=\sqrt{T_{\rm R}/[F(\omega_{\rm opt})T]}=1/\sqrt{N^2TT_{\rm R}e^{-2N\gamma T_{\rm R}}}$. The optimal Ramsey time is now $T_{\rm R}=1/(2N\gamma)$ and we find $\Delta\omega_{\rm CR}=\sqrt{2\gamma e/(NT)}$. We recover exactly the same bound as in the case of uncorrelated atoms. In this example, the ideal sensitivity enhancement offered by GHZ states for $\gamma=0$ disappears in the presence of arbitrarily small uncorrelated dephasing ($\gamma>0$). Although the overall absolute sensitivity is not improved, the GHZ state reaches the sensitivity limit N times faster than using the uncorrelated atoms: this may be of practical interest when experimental constraints require $T_{\rm R}\ll 1/\gamma$ (Huelga *et al.*, 1997; Shaji and Caves, 2007). An optimization over probe states shows that at most a constant factor of $1/\sqrt{e}$ in the absolute frequency error can be gained in the presence of single-particle dephasing (Huelga *et al.*, 1997; Ulam-Orgikh and Kitagawa, 2001; Escher, de Matos Filho, and Davidovich, 2011).

Bounds to the quantum Fisher information in the presence of more general models of uncorrelated decoherence have been discussed in the literature. Let us consider N particles prepared in a state $\hat{\rho}_0$ and a noisy channel Λ_θ that acts independently on each particle, such that $\hat{\rho}_\theta=\Lambda_\theta^{\otimes N}(\hat{\rho}_0)$. The maximum of the quantum Fisher information over all possible probe states is bounded as (Fujiwara and Imai, 2008)

$$\max_{\hat{\rho}_0}F_{\rm Q}[\Lambda_\theta^{\otimes N}(\hat{\rho}_0)]\leq 4\min_{\{\hat{K}_\ell\}}\{N\|\alpha_K\|+N(N-1)\|\beta_K\|^2\},\quad(138)$$

where $\alpha_K=\sum_\ell(\partial_\theta\hat{K}_\ell^\dagger)(\partial_\theta\hat{K}_\ell)$, $\beta_K=i\sum_\ell(\partial_\theta\hat{K}_\ell^\dagger)\hat{K}_\ell$, $\|\cdot\|$ denotes the operator norm, and the minimization runs over all equivalent Kraus representations of the channel Λ_θ. In particular, if there exists a Kraus representation such that $\beta_K=0$, then the second term in Eq. (138) vanishes and $F_{\rm Q}[\Lambda_\theta^{\otimes N}(\hat{\rho}_0)]$ has asymptotically in N a bound that scales linearly with N. Relevant single-particle quantum channels fulfill the condition[19] $\beta_K=0$ (Escher, de Matos Filho, and Davidovich, 2011; Demkowicz-Dobrzański, Kołodyński, and Guţă, 2012; Kołodyński and Demkowicz-Dobrzański, 2013).

[19]A notable class of channels that fulfills $\beta_K=0$ is that of *quantum simulable* channels (Kołodyński and Demkowicz-Dobrzański, 2013), i.e., those that can be written as $\Lambda_\theta(\hat{\rho})=\Phi(\hat{\rho}\otimes\hat{\sigma}_\theta)$, where Φ is a θ-independent channel (Matsumoto, 2010). Φ acts on an enlarged space including the auxiliary state $\hat{\sigma}_\theta$ that contain all information about the parameter. We have $F_{\rm Q}[\Lambda_\theta^{\otimes N}(\hat{\rho})]\leq F_{\rm Q}[\hat{\sigma}_\theta^{\otimes N}]=NF_{\rm Q}[\hat{\sigma}_\theta]$ that follows from Eq. (137) and the additivity of the quantum Fisher information. A quantum simulable channel may admit several decompositions, the optimal one being that giving the smallest value $F_{\rm Q}[\hat{\sigma}_\theta]$. When $\hat{\sigma}_\theta$ has a diagonal form $\hat{\sigma}_\theta=\sum_i p_{\theta,i}|e_i\rangle\langle e_i|$, where $|e_i\rangle$ is some basis of the enlarged Hilbert space, the channels is said to be *classical simulable* (Matsumoto, 2010). In this case we have $F_{\rm Q}[\hat{\sigma}_\theta]=1/\epsilon_+\epsilon_-$ (Demkowicz-Dobrzański, Kołodyński, and Guţă, 2012), where $\epsilon_\pm$ can be found from the geometric properties of the convex space of quantum channels (Bengtsson and Zyczkowski, 2006). In particular, $\epsilon_\pm>0$ for channels that lie in the set of completely positive trace-preserving maps away from its boundary, including full-rank channels.

This means that, for those channels, the phase sensitivity achievable with an arbitrary probe state is $\Delta\theta\geq 1/\sqrt{\nu\alpha N}$, with $\alpha=4\min_{\{\hat{K}_\ell\};\beta_K=0}\|\alpha_K\|$. Therefore, asymptotically in the number of particles, the optimal achievable phase sensitivity has a scaling $N^{-1/2}$ and the possible gain over the standard quantum limit is only limited to a prefactor (when $\alpha>1$). We notice however that this is an asymptotic result for $N\to\infty$: entangled states may still provide a scaling of phase sensitivity better than the standard quantum limit, up to the Heisenberg limit, even for relatively large N.

According to Eq. (138) a necessary condition to overcome the asymptotic scaling $N^{-1/2}$ of precision is to have $\beta_K\neq 0$. It has been shown that this condition can be achieved for relatively short interrogation times in the case of non-Markovian noise (Matsuzaki, Benjamin, and Fitzsimons, 2011; Chin, Huelga, and Plenio, 2012) and also when considering dephasing noise perpendicular to phase-encoding evolution (Chaves *et al.*, 2013). In these cases, quantum-enhanced frequency estimation can be found in the limit $N\to\infty$. In particular, Matsuzaki, Benjamin, and Fitzsimons (2011) and Chin, Huelga, and Plenio (2012) showed that a frequency variance $(\Delta\omega)^2=\mathcal{O}(N^{-3/2})$ can be reached for an interrogation time $T_{\rm R}=\mathcal{O}(N^{-1/2})$ under general models of non-Markovian phase noise; see also Berrada (2013), Szańkowski, Trippenbach, and Chwedeńczuk (2014), Macieszczak (2015), and Smirne *et al.* (2016). Moreover, Chaves *et al.* (2013) showed that if Markovian dephasing is acting along a spin direction perpendicular to the phase encoding, in the limit $N\to\infty$ a sensitivity $(\Delta\omega)^2=\mathcal{O}(N^{-5/3})$ can be obtained for interrogation times $T_{\rm R}=\mathcal{O}(N^{-1/3})$. The possibility of reaching the Heisenberg limit $(\Delta\omega)^2=\mathcal{O}(N^{-1})$ in this case was discussed by Dür *et al.* (2014) and Kessler, Lovchinsky *et al.* (2014) when making use of quantum error correction techniques (see later). The orientation-dependent lifetime of spin-squeezed states was investigated experimentally by Leroux, Schleier-Smith, and Vuletić (2010b).

3. Correlated phase noise, differential interferometry, and decoherence-free subspaces

The above discussion regards uncorrelated noise, acting on each atom separately. Yet, in many experimental systems, a significant source of noise is correlated dephasing, where all atoms are subject to the same stochastic fluctuation of the phase shift. For instance, correlated dephasing is relevant in experiments with ions stored in linear Paul traps (Roos *et al.*, 2006; Monz *et al.*, 2011): phase fluctuations are caused by noisy stray fields inducing random energy shifts of the atomic levels. Correlated phase noise is modeled as

$$\hat{\rho}_\theta=\int d\varphi P(\varphi|\theta)\hat{U}_\varphi\hat{\rho}_0\hat{U}_\varphi^\dagger,\quad(139)$$

where $P(\varphi|\theta)$ describes the phase fluctuations around θ and $\hat{U}_\varphi$ is the phase-encoding unitary tramsformation. The probability of a generic detection event (being $|\mu\rangle$ the corresponding eigenstate) is

$$P_{\rm pn}(\mu|\theta) = \int d\varphi P(\mu|\varphi)P(\varphi|\theta), \tag{140}$$

where $P(\mu|\varphi) = \langle\mu|\hat{U}_\varphi\hat{\rho}_0\hat{U}_\varphi^\dagger|\mu\rangle$. Inserting $P_{\rm pn}(\mu|\theta)$ into Eq. (7) allows one to calculate the Cramér-Rao bound in the presence of arbitrary phase noise. Taking $P(\varphi|\theta) = e^{-(\varphi-\theta)^2/(2\sigma_{\rm pn}^2)}/\sqrt{2\pi\sigma_{\rm pn}^2}$ for $\sigma_{\rm pn} \ll 2\pi$, $\hat{U}_\varphi = e^{-i\varphi\hat{J}_z}$, and considering probe states symmetric under particle exchange, we obtain

$$\langle m_z|\hat{\rho}_\theta|n_z\rangle = \langle m_z|\hat{\rho}_0|n_z\rangle e^{-(\sigma_{\rm pn}^2/2)(m-n)^2} e^{-i\theta(m-n)}, \tag{141}$$

where $|m_z\rangle$ is an eigenstate of $\hat{J}_z$ with eigenvalue m. As a consequence of correlated phase noise, off-diagonal elements $\langle m|\hat{\rho}_\theta|n\rangle$ are exponentially suppressed at a rate proportional to $(m-n)^2$. Equation (141) predicts that the coherence of a N-qubit GHZ state decays faster than that of a single qubit by a factor N^2. This effect, also known as superdecoherence, has been demonstrated experimentally with maximally entangled states of $^{40}Ca^+$ ions by adding a variable delay time between creation and coherence investigation (Monz *et al.*, 2011). Correlated phase noise is more dramatic than uncorrelated dephasing. Indeed, taking the sum of the smallest possible quantum and phase noise [see also Genoni, Olivares, and Paris (2011) and Escher *et al.* (2012)], we have

$$\Delta\theta \geq \frac{1}{\sqrt{\nu}}\sqrt{\sigma_{\rm pn}^2 + \frac{1}{N^2}}, \tag{142}$$

which does not scale with N for $N \gg 1/\sigma_{\rm pn}$ in contrast with uncorrelated dephasing.

However, correlated phase noise can be counteracted by a differential interferometer scheme (Roos *et al.*, 2006; Dorner, 2012; Landini *et al.*, 2014), see Fig. 36(a), that consists of two interferometers running in parallel. The phase shift in the first interferometer is $\theta + \varphi_1$, while that in the second interferometer is φ_2, where θ is the signal phase to be estimated and $\varphi_{1,2}$ are shot-to-shot random phases. Taking a Gaussian $P(\varphi_{1,2}|\theta)$ as before, $\hat{U}_\varphi = e^{-i\varphi_1\hat{J}_z^{(1)}} \otimes e^{-i\varphi_2\hat{J}_z^{(2)}}$ and perfectly correlated interferometers with $\varphi = \varphi_1 = \varphi_2$, we have

$$\langle \boldsymbol{m}_z|\hat{\rho}_\theta|\boldsymbol{n}_z\rangle = \langle \boldsymbol{m}_z|\hat{\rho}_0|\boldsymbol{n}_z\rangle e^{-(\sigma_{\rm pn}^2/2)(m_1+m_2-n_1-n_2)^2} e^{-i\theta(m_1-n_1)}, \tag{143}$$

where $|\boldsymbol{m}_z\rangle = |m_z^{(1)}\rangle \otimes |m_z^{(2)}\rangle$ and $|m_z^{(1,2)}\rangle$ are eigenstates of $\hat{J}_z^{(1,2)}$ with eigenvalues $m_{1,2}$. Components with $m_1 + m_2 = n_1 + n_2$ are insensitive to phase noise and define a decoherence-free subspace (Zanardi and Rasetti, 1997; Lidar, Chuang, and Whaley, 1998). This condition is met by nontrivial states achieving the Heisenberg limit of phase sensitivity (Dorner, 2012; Jeske, Cole, and Huelga, 2014; Landini *et al.*, 2014). Figure 36(b) illustrates examples showing the superior performance of a differential scheme (thick solid lines) with respect to that of a single interferometer (dashed lines) affected by the phase noise with the same amplitude $\sigma_{\rm pn}$. For a differential scheme where each interferometer is fed with NOON states, the Fisher information saturates to $F_{\rm Q} = N^2/4$ for $N\sigma_{\rm pn} \gtrsim 1$ (Landini *et al.*, 2014). Finally, noise correlations between the two interferometers are crucial: achieving the Heisenberg limit in a differential interferometer requires $\Delta(\varphi_1 - \varphi_2) \ll 1/N$ (Landini *et al.*, 2014). Roos *et al.* (2006) experimentally demonstrated the preparation of a designed entangled state of two ion qubits in a decoherence-free subspace and proved its robustness by measuring the electric field quadrupole shift while removing sensitivity to a noisy magnetic-field environment. Monz *et al.* (2011) constructed decoherence-free states with up to eight ions, achieving long coherence times; see also Pruttivarasin *et al.* (2015). In specific cases, entanglement can be preserved in the presence of correlated dephasing even if the state is not in a decoherence-free subspace (Carnio, Buchleitner, and Gessner, 2015).

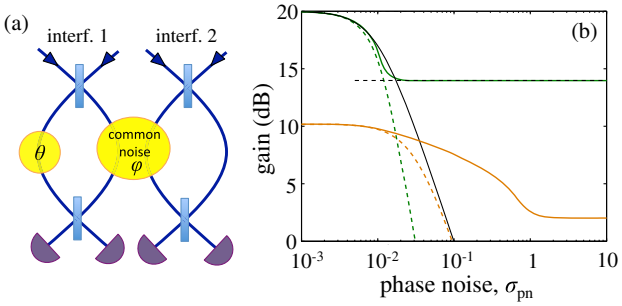

FIG. 36. Differential interferometry scheme (a): two Mach-Zehnder interferometers working in parallel are coupled to the shot-to-shot fluctuating phase noise φ. The signal to be estimated is θ. (b) Normalized Fisher information (F/N, gain over the shot noise) as a function of the phase noise, modeled according to Eq. (139) with $P(\varphi|\theta) \sim e^{-(\varphi-\theta)^2/(2\sigma_{\rm pn}^2)}$. The green (darker) lines refer to NOON states in each interferometer, while the orange (lighter) lines refer to spin-squeezed states obtained via Kitagawa-Ueda evolution $e^{-i\chi t\hat{J}_z^2}|0,\pi/2\rangle$ of a coherent spin state $|0,\pi/2\rangle$, with $\chi t = 0.01\pi$. The thick solid lines are obtained with a differential interferometer, while the dashed lines are obtained with a single interferometer. The thin black solid line is Eq. (142). The horizontal dashed line is $N^2/4$. Here $N = 100$.

4. Error correction

Quantum error correction techniques are crucial in quantum computing (Shor, 1995; Steane, 1996; Nielsen and Chuang, 2000) and can be used to counteract the effect of noise in quantum metrology (Ozeri, 2013; Arrad *et al.*, 2014; Dür *et al.*, 2014; Kessler, Lovchinsky *et al.*, 2014; Herrera-Martí *et al.*, 2015; Plenio and Huelga, 2016). These schemes correct the imprinting of phase information in a quantum state against decoherence by employing ancilla qubits that neither interact with the parameter nor are subject to noise. Noise operators map the state to ancilla Hilbert subspaces orthogonal to the phase-encoding subspace. Error correction is accomplished by projective measurements into the orthogonal subspaces and then applying a correction sequence. These techniques can be used to extend the coherence time and/or to achieve the Heisenberg limit for certain noise models (Ozeri, 2013; Arrad *et al.*, 2014; Dür *et al.*, 2014; Kessler, Lovchinsky *et al.*,

2014). Lu, Yu, and Oh (2015) provided conditions under which the quantum Fisher information, rather than the full quantum state, can be protected under a class of noisy channels.

Finally, it was shown that entanglement between the probe and an ancillary system in the preparation and measurement stage can be useful in the presence of uncorrelated noise (Demkowicz-Dobrzański and Maccone, 2014; Haine and Szigeti, 2015; Haine *et al.*, 2015; Huang, Macchiavello, and Maccone, 2016).

5. Particle losses

The incoherent loss of particles can strongly impact the usefulness of a state for quantum metrology. A paradigmatic example is the NOON state: the loss of a single particle transforms Eq. (49) into the incoherent mixture

$$\tfrac{1}{2}|N-1\rangle_a\langle N-1|\otimes|0\rangle_b\langle 0|+\tfrac{1}{2}|0\rangle_a\langle 0|\otimes|N-1\rangle_b\langle N-1|,$$

which is useless for phase sensing. Losses can be modeled by a beam splitter of transmission coefficient $0\le\eta\le 1$ that equally couples each interferometer arm to environment modes. This leads to the bound of sensitivity

$$\Delta\theta\ge\frac{1}{\sqrt{\nu N}}\sqrt{1+\frac{1-\eta}{\eta}N}, \tag{144}$$

that is valid for any probe state (Escher, de Matos Filho, and Davidovich, 2011): when $N\ll\eta/(1-\eta)$, $\Delta\theta$ is bounded by the Heisenberg limit, while for $N\gg\eta/(1-\eta)$ one recovers the $1/\sqrt{N}$ scaling with a prefactor that is $\sqrt{(1-\eta)/\eta}<1$ for $\eta>1/2$.

For ultracold atoms, collisional losses are especially relevant. One-body losses are due to collisions of trapped atoms with residual hot atoms due to imperfect vacuum, whereas two- and three-body losses are caused by inelastic collisions within the trapped cloud and are relevant in dense samples. For instance, Li, Castin, and Sinatra (2008) studied the impact of atom losses during the preparation of spin-squeezed states via one-axis twisting (see Sec. III.B) and showed that $\xi_R^2=\mathcal{O}(N^{-4/15})$ for one-body losses, assuming $N\to\infty$ and an optimal evolution time. For two-body losses, the optimal ξ_R^2 does not depend on N, while for three-body losses $\xi_R^2=\mathcal{O}(N^{4/15})$ and there is a finite optimal number of particles for squeezing.

6. Finite detection efficiency and interaction-based readout

Low efficiency in the detection of large atom numbers is one of the main limitations in many current entanglement-enhanced metrology experiments. Finite detection efficiency blurs the interferometer signal and thus degrades the phase sensitivity. A noisy detector can be modeled as a beam splitter of transmission coefficient η followed a perfect detector. In this case (assuming equal efficiency for both detectors), the bound (144) applies. More generally, we can model an imperfect detection by replacing ideal probabilities $P(\mu|\theta)=\langle\mu|\hat{\rho}_\theta|\mu\rangle$—here μ is the result of a measurement (we restrict for simplicity to projective measurements but the discussion can be straightforwardly extended to generalized measurements, see footnote [2])—with

$$P_{\rm dn}(\mu|\theta)=\sum_{\tilde{\mu}}P(\mu|\tilde{\mu})P(\tilde{\mu}|\theta), \tag{145}$$

where $P(\mu|\tilde{\mu})$ is a convolution function giving the probability to obtain the result μ when the "true" value is $\tilde{\mu}$. In practice, one can use a normalized Gaussian $P(\mu|\tilde{\mu})=e^{-(\mu-\tilde{\eta}\,\tilde{\mu})^2/(2\sigma_{\rm dn}^2)}/\sum_\mu e^{-(\mu-\tilde{\eta}\,\tilde{\mu})^2/(2\sigma_{\rm dn}^2)}$, where $\sigma_{\rm dn}$ accounts for the detection noise (independent of the detection signal, for simplicity) and $0\le\tilde{\eta}\le 1$ for the attenuation of the signal. Finite detection efficiency limits the distinguishability of the probability distribution when changing the parameter and thus decreases the Fisher information; see Sec. II.B.4.

An interaction-based readout can make phase estimation robust against detection noise, removing the requirement of single-atom resolution to reach a precision approaching the Heisenberg limit (Davis, Bentsen, and Schleier-Smith, 2016; Fröwis, Sekatski, and Dür, 2016; Nolan, Szigeti, and Haine, 2017; Anders *et al.*, 2018). In an interaction-based readout, some nonlinear unitary evolution $\hat{U}_{\rm nl}$ (e.g., generated by the interaction between the particles) is applied before the readout measurement, such that the probability of a result μ is given by $P(\mu|\theta)=\langle\mu|\hat{U}_{\rm nl}\hat{\rho}_\theta\hat{U}_{\rm nl}^\dagger|\mu\rangle$. For instance, $\hat{U}_{\rm nl}$ can be the inverse of the nonlinear transformation that generates the entangled probe state, thus realizing an echo sequence (Macrì, Smerzi, and Pezzè, 2016; Garttner *et al.*, 2017). Note that SU(1,1) interferometers, see Sec. IV.C.4, take advantage of an interaction-based readout and their robustness to detection noise was emphasized by Marino, Corzo Trejo, and Lett (2012), Ou (2012), and Gabbrielli, Pezzè, and Smerzi (2015). An example of the advantage offered by the interaction-based readout is illustrated in Fig. 37(a). This effect can be understood as a phase magnification (Hosten, Krishnakumar *et al.*, 2016): output probability distributions of phase-shifted states can become more distinguishable (and thus less prone to detection noise) when applying a nonlinear evolution prior to readout. As a simple example, following Leibfried *et al.* (2005), let us consider phase estimation using the NOON state (49). Applying a phase encoding $\exp(-i\theta\hat{J}_z)$ followed by a $\pi/2$ Rabi rotation around the x axis, one can measure the relative number of particles in $|a\rangle$ and $|b\rangle$. The phase information is included in fine structure of this probability distribution. These structures are washed out by the detection noise of just one atom; see Fig. 37(b). However, applying the transformation $e^{-i(\pi/2)\hat{J}_x^2}$ after phase encoding, only two detection events are possible (N atoms in $|a\rangle$ or $|b\rangle$) that can be experimentally distinguished even for a large detection noise (e.g., $\sigma_{\rm dn}\approx\sqrt{N}$); see Fig. 37(c).

A nonlinear readout was exploited by Leibfried *et al.* (2004, 2005) for quantum-enhanced metrology with GHZ states of $N\lesssim 6$ trapped ions (see Sec. VI.B), and more recently by Linnemann *et al.* (2016) for the realization of a SU(1,1) interferometer with a spinor Bose-Einstein condensate (see Sec. IV.C.4). In the experiment of Hosten, Krishnakumar *et al.* (2016) the collective spin of $N=5\times10^5$ ^{87}Rb atoms is first squeezed via a light-mediated interaction in an optical cavity (see Sec. V.B), and then rotated by an angle θ. After a second

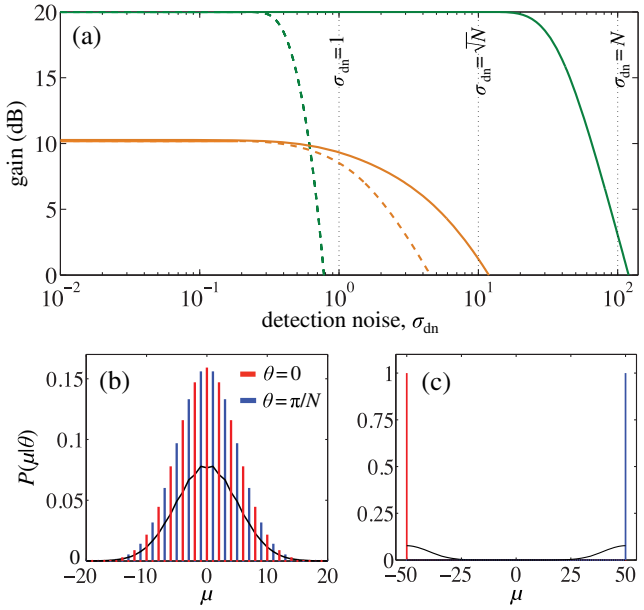

FIG. 37. Interaction-based readout. (a) Normalized Fisher information (F/N, gain over the shot noise) as a function of the detection noise, modeled according to Eq. (145) with a Gaussian $P(\mu|\tilde{\mu})$ of width $\sigma_{\rm dn}$ and $\tilde{\eta}=1$. The green (darker) lines refer to a NOON state, and the orange (lighter) lines to a spin-squeezed state obtained via Kitagawa-Ueda evolution $e^{-i\tau\hat{J}_z^2}|0,\pi/2\rangle$ of a coherent spin state $|0,\pi/2\rangle$, with $\tau=0.01\pi$. The solid lines are obtained with an interaction-based readout, and the dashed lines with a standard particle number detection. (b) Probability distributions of a NOON state $P(\mu|\theta)=|\langle\mu_z|e^{i(\pi/2)\hat{J}_x}e^{-i\theta\hat{J}_z}|\text{NOON}\rangle|^2$ for $\theta=0$ (red, lighter histogram) and $\theta=\pi/N$ (blue, darker histogram). Substructures that characterize the probability distributions are washed out by a detection noise of just one atom ($\sigma=1$, black line). (c) Probability distribution for an interaction-based readout $P(\mu|\theta)=|\langle\mu_z|e^{-i(\pi/2)\hat{J}_x^2}e^{-i[\theta+\pi/(2N)]\hat{J}_z}|\text{NOON}\rangle|^2$. The distribution for $\theta=0$ [$P(\mu|\theta)=\delta_{\mu,-N/2}$, red, lighter histogram] and that for $\theta=\pi/N$ [$P(\mu|\theta)=\delta_{\mu,N/2}$, blue, darker histogram] are maximally distinguishable and thus robust against detection noise: the thick and thin black lines are $P_{\rm dn}(\mu|\theta)$ for $\sigma_{\rm dn}=\sqrt{N}$ for $\theta=0$ and π/N, respectively, showing that the two distributions do not overlap even in the presence of large detection noise. Here $N=100$.

period of collective spin interactions in the cavity, the state is detected via fluorescence imaging, demonstrating a phase sensitivity 8 dB below the standard quantum limit, using a detection with a technical noise floor 10 dB above the projection noise of uncorrelated atoms.

B. Atomic clocks

Passive atomic clocks operate by locking, via a feedback loop, the frequency of a local oscillator to the transition frequency ω_0 between two levels $|a\rangle$ and $|b\rangle$ of an atom (Wynands and Weyers, 2005; Wynands, 2009; Kohlhaas *et al.*, 2015; Ludlow *et al.*, 2015). The standard clock configuration (e.g., for fountain clocks) is based on Ramsey spectroscopy (Ramsey, 1963). Atoms are initially prepared in the clock state $|a\rangle$. A near-resonant $\pi/2$ pulse from the local oscillator prepares a superposition of $|a\rangle$ and $|b\rangle$. Finally, after a time $T_{\rm R}$ of free evolution (Ramsey interrogation time), a second $\pi/2$ pulse is applied to the atoms. The accumulated phase, $\int_0^{T_{\rm R}}dt[\omega_{\rm LO}(t)-\omega_0]$, where $\omega_{\rm LO}(t)$ is the instantaneous local oscillator frequency, is estimated from a measurement of the atom number in the two levels and used for a feedback loop that steers the $\omega_{\rm LO}$ toward ω_0. Atomic clocks are characterized by their accuracy and stability (Vanier and Audoin, 1992; Rihele, 2004). Accuracy refers to the frequency offset from the ideal value, whereas stability describes the fluctuations of the instantaneous frequency $\omega_{\rm LO}(t)$ from ω_0. Improving the stability of time keeping is one of the primary targets of quantum-enhanced metrology. It also allows for faster evaluation of systematic errors, which in turn can improve the accuracy (Nicholson *et al.*, 2015).

The standard figure of merit for quantifying the stability of a clock is the Allan standard deviation of the relative frequency fluctuations $y(t)=[\omega_{\rm LO}(t)-\omega_0]/\omega_0$ (Vanier and Audoin, 1992; Rihele, 2004),

$$\sigma(\tau)=\sqrt{\frac{\sum_{k=1}^{\nu-1}(y_{k+1}-y_k)^2}{2(\nu-1)}},\quad\text{with}\quad y_k=\int_{t_k}^{t_k+\tau}\frac{dt}{\tau}y(t),\tag{146}$$

where $y_{k+1}-y_k$ is the relative change of the clock frequency between two successive averaging bins of duration τ. The Allan deviation quantifies the discrepancy between two consecutive observations of the clock frequency averaged for a time τ, including dead times in preparation of the sample and data acquisition. For an atomic clock operating at the standard quantum limit with uncorrelated (shot-to-shot) measurements, we have

$$\sigma_{\rm SQL}(\tau)=\frac{1}{\omega_0 T_{\rm R}\sqrt{N}}\sqrt{\frac{T_{\rm cycle}}{\tau}},\tag{147}$$

where $T_{\rm cycle}\geq T_{\rm R}$ is the clock cycle duration ($\tau/T_{\rm cycle}$ being the number of measurements performed in a time τ). Currently, the stability of atomic clocks is nearly (Nicholson *et al.*, 2012; Hinkley *et al.*, 2013; Bloom *et al.*, 2014) or already, as in the case of ion spectroscopy (Itano *et al.*, 1993) and fountain clocks (Santarelli *et al.*, 1999), limited by Eq. (147). In principle, the clock stability is optimized by extending the interrogation time until atomic decoherence dominates in the interferometer output signal. In practice, the main limitations of current clocks, in particular, of optical clocks using trapped atoms, are random fluctuations of the local oscillator frequency that induce fringe hopping for sufficiently long interrogation times. These limit the stability of frequency comparisons to interrogation times of the order of a second, well short of the limits imposed by atomic decoherence, such as excited-state decay (Wineland *et al.*, 1998).

Theoretical studies of entanglement-enhanced atomic clocks have focused on the impact of collective dephasing caused by fluctuations of the local oscillator frequency, taking into account temporal noise correlations as well as the

feedback mechanism that controls the local oscillator frequency. State and measurement optimization (Bužek, Derka, and Massar, 1999; André, Sørensen, and Lukin, 2004; Rosenband, 2011) as well as adaptive schemes (Borregaard and Sørensen, 2013; Kessler, Kómár *et al.*, 2014) have been considered. André, Sørensen, and Lukin (2004) showed the possibility of achieving an entanglement-enhanced stability $\sigma(\tau) \propto 1/(N^{2/3}\sqrt{\tau})$ by optimizing over a family of moderately squeezed states. This provides the gain of a factor $N^{1/3}$ (in variance) over the standard quantum limit. One of the main limitations in using squeezed states is the strong dependence of the sensitivity with the estimated phase. Borregaard and Sørensen (2013) showed that this problem can be overcome by using nondestructive measurements to steer the squeezed state toward the optimal phase sensitivity point, before the final distructive measurement; see also Shiga and Takeuchi (2012). They demonstrated the possibility to achieve $\sigma(\tau) \propto 1/(N\sqrt{\tau})$, thus reaching the Heisenberg scaling. Rosenband (2011), Mullan and Knill (2014), Kessler, Kómár *et al.* (2014), and Leroux *et al.* (2017) have studied different adaptive schemes for optimal state preparation and measurement in the presence of local oscillator fluctuations. Overall, these protocols show that entangled states can be useful to track and stabilize the fluctuations of the local oscillator over long time scales. Finally, quantum bounds of frequency stability were discussed by Chabuda, Leroux, and Demkowicz-Dobrzański (2016) and Fraas (2016).

1. Entanglement-assisted atomic clocks

Atomic clocks with a performance beating the standard quantum limit have been experimentally demonstrated with two trapped ions (Meyer *et al.*, 2001), ensembles of cold thermal atoms (Leroux, Schleier-Smith, and Vuletić, 2010b; Louchet-Chauvet *et al.*, 2010; Hosten, Engelsen *et al.*, 2016), and Bose-Einstein condensates (Gross *et al.*, 2010; Ockeloen *et al.*, 2013; Kruse *et al.*, 2016). The neutral-atom experiments have realized microwave-frequency clocks on magnetic field-insensitive hyperfine transitions with spin-squeezed states as input.[20] Leroux, Schleier-Smith, and Vuletić (2010b) measured an Allan deviation of $\sigma(\tau) = 1.1 \times 10^{-9}\ \mathrm{s}^{1/2}/\sqrt{\tau}$ for their squeezed clock, corresponding to an improvement of 4.5 dB in variance beyond the standard quantum limit; see Fig. 38. More recently, Hosten, Engelsen *et al.* (2016) performed a similar measurement, reaching $\sigma(\tau) = 9.7 \times 10^{-11}\ \mathrm{s}^{1/2}/\sqrt{\tau}$, or 10.5 dB in variance beyond the standard quantum limit; see Fig. 28(c). While these experiments are impressive proof-of-principle demonstrations of entanglement-enhanced atomic clocks, they do not yet reach the frequency stability of state-of-the-art fountain clocks. This is mostly due to a much shorter Ramsey interrogation time of $T_R \sim 200\ \mu\mathrm{s}$, limited by the noise of the microwave local oscillator. For comparison, current fountain clocks using uncorrelated atoms operate with $T_R \sim 1$ s and reach $\sigma(\tau) \sim 10^{-14}\ \mathrm{s}^{1/2}/\sqrt{\tau}$ (Wynands, 2009).

[20]Note that, to date, squeezing has not yet been realized on an optical transition. Monz *et al.* (2011) created GHZ states on the optical clock transition of $^{40}Ca^{+}$ ions.

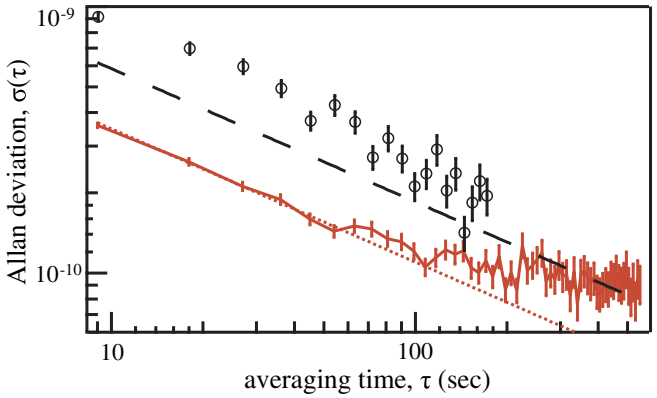

FIG. 38. Stability of an atomic clock beating the standard quantum limit. Allan deviation of an atomic clock with a spin-squeezed input state (red data with error bars, the solid red line being a guide to the eye), with $T_R = 200\ \mu$s, $N = 3.5 \times 10^4$, and $T_{\mathrm{cycle}} = 9$ s. The red dotted line $\sigma(\tau) = 1.1 \times 10^{-9}\ \mathrm{s}^{1/2}/\sqrt{\tau}$ is a factor of 2.8 in variance (corresponding to 4.5 dB) below the standard quantum limit [black dashed line $\sigma(\tau) = 1.85 \times 10^{-9}\ \mathrm{s}^{1/2}/\sqrt{\tau}$]. Open black circles: reference measurements with uncorrelated atoms. From Leroux, Schleier-Smith, and Vuletić, 2010b.

2. Proposals for entanglement-assisted lattice clocks and atom interferometers

Optical atomic clocks that interrogate narrow optical transitions in ensembles of atoms trapped in an optical lattice are currently the most precise and accurate measurement devices (Ye, Kimble, and Katori, 2008; Ludlow *et al.*, 2015), reaching stabilities of $\sigma(\tau) \sim 10^{-16}\ \mathrm{s}^{1/2}/\sqrt{\tau}$, integrating down to the lower 10^{-18} level after a few thousand seconds of averaging (Nicholson *et al.*, 2015). Their stability is within a factor of 2 above the quantum projection noise limit (Ludlow *et al.*, 2008; Hinkley *et al.*, 2013; Bloom *et al.*, 2014). Since, in these systems, there is a limit to the exploitable number of atoms, using entanglement to increase the sensitivity is of considerable interest. So far only theoretical studies are available. Meiser, Ye, and Holland (2008) studied the creation of spin-squeezed states in a neutral-atom optical lattice clock through a cavity-based QND measurement. Weinstein, Beloy, and Derevianko (2010) considered the creation of GHZ states through the on-site interaction of an atom moving across the lattice. A further interesting possibility is to exploit long-range Rydberg-dressing interactions between atoms at different lattice sites induced by laser excitations (Bouchoule and Mølmer, 2002b; Henkel, Nath, and Pohl, 2010; Pupillo *et al.*, 2010; Opatrný and Mølmer, 2012; Mohammadsadegh *et al.*, 2016) [see Saffman, Walker, and Mølmer (2010) and Browaeys, Barredo, and Lahaye (2016) for reviews] to generate spin-squeezed (Gil *et al.*, 2014) and non-Gaussian entangled states (Macrì, Smerzi, and Pezzè, 2016).

For precision sensing applications in atom interferometers it would be highly desirable to generate strongly squeezed states of the atomic center-of-mass motion. At present, this remains a challenging and experimentally unexplored task (Hosten, Engelsen *et al.*, 2016). For a recent theoretical proposal see Salvi *et al.* (2018).

C. Optical magnetomenters

Optical magnetometers (Budker and Romalis, 2007; Budker and Kimball, 2013) exploit the interaction of light with a spin-polarized atomic ensemble (either thermal atoms in a vapor cell at room temperature or laser-cooled atoms in an optical trap[21]) to measure the strength of a magnetic field (Budker *et al.*, 2002). Generally, the device consists of N spin-F atoms initially optically pumped into a fully polarized state (pointing along the x axis, for instance), such that the collective spin of the ensemble has length $\langle \hat{J}_x \rangle = FN$. A weak magnetic field along the y axis causes the precession of the collective spin in the x-z plane at a rate $g\mu_B B/\hbar$, where g is the gyromagnetic ratio, μ_B is the Bohr magneton, and B is the magnetic field strength. The atomic spin precession is measured by observing the polarization rotation of the probe light transmitted through the atomic sample. The interrogation time is limited by spin relaxation due to collisions of the atoms with the cell walls that enclose the vapor or, for high density gases, due to spin-exchange collisions (Budker and Romalis, 2007). The sensitivity of current optical magnetometers is fundamentally limited by quantum noise in the form of atomic projection noise and photon (polarization) shot noise. The backaction of light onto the atoms is a further limiting factor. Current optical magnetometers are approaching quantum noise limits (Kominis *et al.*, 2003; Wasilewski *et al.*, 2010).

Polarization squeezing of the probe light (Wolfgramm *et al.*, 2010; Horrom *et al.*, 2012) or spin squeezing of the atomic ensemble (Geremia *et al.*, 2003; Auzinsh *et al.*, 2004; Petersen, Madsen, and Mølmer, 2005; Sewell *et al.*, 2012) can be used to reduce the quantum noise. Spin squeezing induced by continuous quantum nondemolition measurements (Auzinsh *et al.*, 2004) can enhance the sensitivity, and a scaling $N^{-3/4}$ is predicted when using shot-noise-limited light. This can be further pushed to the Heisenberg limit $1/N$ if squeezed light is used. However, single-atom spin relaxation modifies this picture, and a reduction of quantum noise below the standard quantum limit is expected only for interrogation times shorter than the spin coherence time (Auzinsh *et al.*, 2004). Spin-squeezed states can thus increase the measurement bandwidth (i.e., they are useful for short interrogation times) without loss of sensitivity, with important applications in biology and medicine. For long interrogation times, entanglement-enhanced sensitivity using spin-squeezed states is expected for high-density ensembles due to the suppression of spin-relaxation noise (Kominis, 2008; Vasilakis, Shah, and Romalis, 2011).

1. Entanglement-assisted optical magnetometers

An improvement in magnetic-field sensing via the reduction of the optical polarization noise was demonstrated by Wolfgramm *et al.* (2010) and Horrom *et al.* (2012) using squeezed probe light. Atomic projection noise limited and entanglement-assisted magnetometry was demonstrated in the experiment of Wasilewski *et al.* (2010), who realized a pulsed rf magnetometer made of two atomic ensembles (two vapor cells with opposite atomic polarizations) with $N = 3.6 \times 10^{12}$ Cs atoms. The first light pulse is used to entangle the two ensembles via a quantum nondemolition measurement as first demonstrated by Julsgaard, Kozhekin, and Polzik (2001). This is a useful resource to improve the sensitivity of the magnetometer for large bandwidths as shown in Fig. 39(a). The improvement is observed for interrogation times shorter than the entanglement lifetime of 4 ms. The increase of the measurement bandwidth in dc magnetometers was shown by Shah, Vasilakis, and Romalis (2010) using continuous quantum nondemolition measurements. Sewell *et al.* (2012) generated spin-squeezed states in ensembles of cold spin-1 ^{87}Rb atoms via quantum nondemolition measurements (Koschorreck *et al.*, 2010a, 2010b) and applied them to optical magnetometry. Results corresponding to interrogation pulses of 5 μs (giving a measurement bandwidth of 200 kHz) are shown in Fig. 39(b).

D. Scanning probe magnetometers using Bose-Einstein condensates

Trapped Bose-Einstein condensates are particularly well suited for sensing applications requiring high spatial resolution, taking advantage of their small size, high degree of coherence, and the availability of sophisticated techniques for precise positioning of the atoms. Current Bose-Einstein condensate magnetometers reach sensitivities of the order of 10 pT/$\sqrt{\text{Hz}}$ with probe volumes of 10^2–10^4 μm^3 (Wildermuth *et al.*, 2006; Vengalattore *et al.*, 2007; Aigner *et al.*, 2008; Eto *et al.*, 2013). In these systems, the required small probe size gives rise to an upper bound on the atom number due to density-dependent collisional trap losses. It is

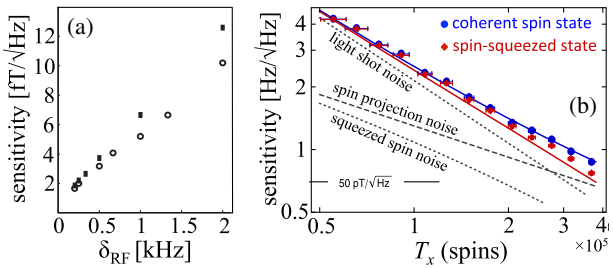

FIG. 39. Entanglement-assisted optical magnetometry. (a) Measurement sensitivity obtained in the absence (squares) and the presence (open circles) of entanglement between atomic ensembles in a two-cell radio-frequency magnetometer. An improvement was demonstrated for short radio-frequency pulse durations τ, where $\delta_{RF} = 1/\tau$. From Wasilewski *et al.*, 2010. (b) Measurement sensitivity as a function of the number of atoms with a coherent spin state (blue circles) and spin-squeezed (red diamonds) probe. Solid lines are predictions obtained from an independent analysis of the probe state, while dashed lines are different noise contributions to the sensitivity. From Sewell *et al.*, 2012.

[21]Vapor cell magnetometers are currently the most sensitive measuring devices for low-frequency magnetic fields, reaching sensitivity levels below 1 fT/$\sqrt{\text{Hz}}$ with probe volumes of 10^6–10^{12} μm^3 and large atom numbers $N = 10^{11}$–10^{15}. Laser-cooled atoms in an optical trap contain a much smaller number of atoms $N = 10^5$–10^8 but are more compact and better suited for field measurements with high spatial resolution.

thus crucial to use entangled states to increase the sensitivity without increasing the atom number.

Ockeloen *et al.* (2013) demonstrated a scanning probe atom interferometer operating beyond the standard quantum limit. Bose-Einstein condensates of ^{87}Rb atoms were prepared on an atom chip and spin squeezed by means of collisions in a spin-dependent trapping potential (see Sec. III.B). Using the spin-squeezed state as input, a Ramsey interferometer sequence was implemented, achieving a performance of 4 dB below the standard quantum limit with $N = 1400$ atoms for interrogation times up to $T_R = 10$ ms; see Fig. 40. This interferometer is sensitive to microwave magnetic fields, with a sensitivity of 77 pT/$\sqrt{\text{Hz}}$ using a small probe volume of 20 μm^3. The interferometer was operated as a scanning probe, by translating the Bose-Einstein condensate on the atom chip to measure the spatial dependence of an on-chip microwave near field.

The magnetometer of Muessel *et al.* (2014) consists of ~30 independent Bose-Einstein condensates in a one-dimensional optical lattice each containing about $N = 400$ ^{87}Rb atoms. Spin squeezing is created via one-axis twisting (see Sec. III.B), with interactions tuned by a Feshbach resonance. Subsequently, a microwave π pulse transfers the squeezing to a magnetic-field-sensitive hyperfine transition. This experiment demonstrated sub-SQL magnetometry (3.4 dB below the standard quantum limit) with interrogation times up to 340 μs, reaching a sensitivity of 1.9 nT/$\sqrt{\text{Hz}}$ for static magnetic fields. The array configuration is particularly well suited for differential measurements and magnetic-field gradiometry.

Taking the small probe volume into account, the experiments of Ockeloen *et al.* (2013) and Muessel *et al.* (2014) already achieved state-of-the-art sensitivity (Budker and Kimball, 2013).

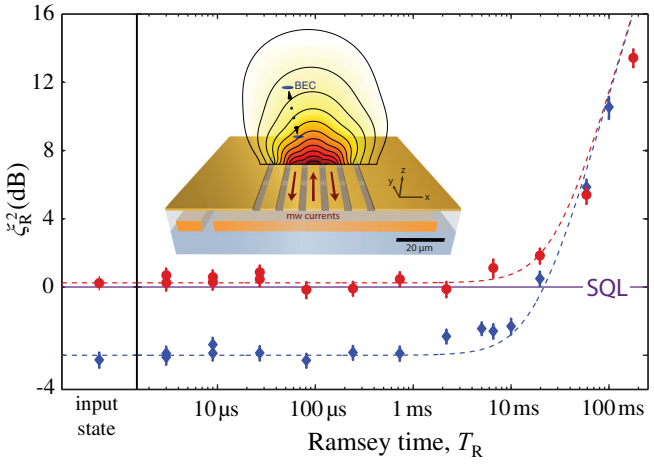

FIG. 40. Performance of a spin-squeezed Bose-Einstein condensate magnetometer expressed in terms of ξ_R^2 as a function of varying interrogation times T_R for squeezed (blue diamonds) and coherent (red circles) input states. Dashed lines model the constant performance of $\xi_R^2 = -4.0$ dB (squeezed state) and +0.2 dB (coherent state) plus technical noise due to shot-to-shot frequency fluctuations. Inset: Scanning probe measurements of microwave fields. The Bose-Einstein condensate (blue) is translated near the surface of an atom chip to measure the spatial dependence of microwave magnetic near fields. Adapted from Ockeloen *et al.*, 2013.

E. Nonlocal phase encoding

Usually, the coupling between an atomic ensemble and an external field is local in the particles. The phase-encoding transformation of standard (or linear) interferometers is thus modeled by $\exp(-i\theta\sum_{i=1}^{N}\hat{\sigma}_{\boldsymbol{n}}^{(i)}/2)$, where $\hat{\sigma}_{\boldsymbol{n}}^{(i)}$ is a single-particle Pauli operator (see Sec. II). Yet in some cases the coupling between the atoms and the external field to be measured may be associated with a nonlocal Hamiltonian that involves interactions between the particles. Nonlinear interferometry was first proposed by Luis (2004) and extensively studied in the literature (Boixo *et al.*, 2007, 2008; Luis, 2007; Choi and Sundaram, 2008; Roy and Braunstein, 2008; Rivas and Luis, 2010). In this case, the notions of a standard quantum limit (i.e., the highest phase sensitivity achievable by separable states) and a Heisenberg limit (i.e., the ultimate allowed phase sensitivity) discussed in Sec. II.C still hold. However, the scalings of these bounds with the number of particles in the probe state depend on the specific phase-encoding Hamiltonian. For instance, Boixo *et al.* (2007, 2008) and Choi and Sundaram (2008) considered phase encoding of the kind $\exp[-i\theta(\sum_{i=1}^{N}\hat{\sigma}_{\boldsymbol{n}}^{(i)}/2)^k]$. For $N \gg 1$, the standard quantum limit and Heisenberg limit become

$$\Delta\theta_{\text{SQL}} = \frac{\alpha_k}{N^{k-1/2}\sqrt{\nu}} \quad \text{and} \quad \Delta\theta_{\text{HL}} = \frac{\beta_k}{N^k\sqrt{\nu}}, \tag{148}$$

respectively, where α_k and β_k are constant prefactors. For $k > 1$ these bounds have faster scalings of phase sensitivity with the number of particles than $\Delta\theta_{\text{SQL}} = 1/\sqrt{N\nu}$ and $\Delta\theta_{\text{HL}} = 1/(N\sqrt{\nu})$, discussed in Sec. II for linear interferometers. Several systems were proposed to observe these scalings of phase sensitivity, including Kerr nonlinearities (Beltrán and Luis, 2005), collisions in Bose-Einstein condensates (Rey, Jiang, and Lukin, 2007; Boixo *et al.*, 2008, 2009; Choi and Sundaram, 2008), nonlinearities in nanomechanical resonators (Woolley, Milburn, and Caves, 2008), double-pass effective nonlinearities with a cold atomic ensemble (Chase *et al.*, 2009), topological excitations in nonlinear systems (Negretti, Henkel, and Mølmer, 2008), and atom-photon interactions in cold atom systems (Napolitano and Mitchell, 2010). Nonlinear interferometers find applications in optical magnetometry (Chase *et al.*, 2009; Sewell *et al.*, 2014) and in the measurement of atomic scattering properties (Rey, Jiang, and Lukin, 2007).

Napolitano *et al.* (2011) engineered an effective atom-light Hamiltonian $\hat{H}_{\text{eff}} = \alpha\hat{J}_z\hat{S}_z + \beta\hat{J}_z\hat{S}_z N_{\text{ph}}/2$ using an optical pulse passing through a cold atom ensemble of ^{87}Rb atoms. Here $\hat{\boldsymbol{J}}$ is a collective atomic spin, $\hat{\boldsymbol{S}}$ is the Stokes vector of the light, and N_{ph} is the photon number. $\hat{H}_{\text{eff}}$ describes a paramagnetic (nonlinear) Faraday rotation of the light beam (Napolitano and Mitchell, 2010) with rotation angle proportional to $\langle\hat{J}_z\rangle$. The coefficients α and β strongly depend on the detuning of the light beam and experimental conditions for which $\alpha = 0$ can be achieved (Napolitano and Mitchell,

2010). The second term in $\hat{H}_{\rm eff}$ accounts for nonlinear photon-photon interactions. The measurement uncertainty achieved with unentangled photons is $\Delta J_z = 1/(AN_{\rm ph}^{1/2} + BN_{\rm ph}^{3/2})$, where $A \propto \alpha$ and $B \propto \beta$. A scaling $\Delta J_z \propto N_{\rm ph}^{-3/2}$ obtained by varying the photon number between 5×10^5 and 5×10^7 was demonstrated by Napolitano *et al.* (2011). Sewell *et al.* (2014), using a nonlinear Faraday rotation based on alignment-to-orientation conversion (Budker *et al.*, 2000), demonstrated $\Delta J_z \propto N_{\rm ph}^{-3/2}$, surpassing the sensitivity achievable by a linear measurement with the same photon number.

VIII. OUTLOOK

The possibility to achieve phase sensitivities beyond the standard quantum limit using atomic ensembles is fueling a vivid and exciting research activity that focuses on the engineering, characterization, and manipulation of entangled many-body quantum states. On the theoretical side, a comprehensive and convincing conceptual framework was developed for quantum metrology with entangled states, centered around key concepts such as spin squeezing and Fisher information. Connections between the concepts of quantum metrology and other fields of quantum information (such as Bell correlations, quantum Zeno dynamics, and Einstein-Podolsky-Rosen entanglement) can shed new light on quantum technologies. Current active research trends are centered on quantum-enhanced metrology taking into account relevant experimental imperfections and searching for protocols where the fragile entanglement is protected against noise sources. On the experimental side, many of the key concepts that were proposed during the past decades, such as entanglement created via particle-particle or atom-light interactions, have recently been implemented in proof-of-principle experiments. The progress in terms of sensitivity gain with respect to the standard quantum limit has been extremely fast, in particular, when compared to squeezing of light. In atomic ensembles, less than ten years after the first spin-squeezing experiments, impressive gains up to 20 dB have been achieved. The field is now at the verge of moving from proof-of-principle experiments to technological applications in entanglement-enhanced precision measurements of time, external fields, and forces.

ACKNOWLEDGMENTS

We are indebted to our colleagues and collaborators with whom we have shared many useful discussions over the past years. In particular, we thank B. Allard, M. Fadel, M. Fattori, C. Klempt, W. Muessel, L. Santos, H. Strobel, G. Tóth, and T. Zibold. R. S. and P. T. acknowledge funding from the Swiss National Science Foundation through NCCR QSIT.

REFERENCES

Aasi, J., *et al.*, 2013, "Enhanced sensitivity of the ligo gravitational wave detector by using squeezed states of light," Nat. Photonics **7**, 613–619.

Agarwal, G. S., 1981, "Relation between atomic coherent-state representation, state multipoles, and generalized phase-space distributions," Phys. Rev. A **24**, 2889–2896.

Agarwal, G. S., and R. R. Puri, 1990, "Cooperative behavior of atoms irradiated by broadband squeezed light," Phys. Rev. A **41**, 3782–3791.

Agarwal, G. S., and R. R. Puri, 1994, "Atomic states with spectroscopic squeezing," Phys. Rev. A **49**, 4968–4971.

Agarwal, G. S., R. R. Puri, and R. P. Singh, 1997, "Atomic Schrödinger cat states," Phys. Rev. A **56**, 2249–2254.

Aigner, S., L. Della Pietra, Y. Japha, O. Entin-Wohlman, T. David, R. Salem, R. Folman, and J. Schmiedmayer, 2008, "Long-range order in electronic transport through disordered metal films," Science **319**, 1226–1229.

Albiez, M., R. Gati, J. Fölling, S. Hunsmann, M. Cristiani, and M. K. Oberthaler, 2005, "Direct observation of tunneling and nonlinear self-trapping in a single bosonic Josephson junction," Phys. Rev. Lett. **95**, 010402.

Amico, L., R. Fazio, A. Osterloh, and V. Vedral, 2008, "Entanglement in many-body systems," Rev. Mod. Phys. **80**, 517–576.

Ananikian, D., and T. Bergeman, 2006, "Gross-Pitaevskii equation for Bose particles in a double-well potential: Two-mode models and beyond," Phys. Rev. A **73**, 013604.

Anders, F., L. Pezzè, A. Smerzi, and C. Klempt, 2018, "Phase magnification by two-axis countertwisting for detection-noise robust interferometry," Phys. Rev. A **97**, 043813.

André, A., A. S. Sørensen, and M. D. Lukin, 2004, "Stability of atomic clocks based on entangled atoms," Phys. Rev. Lett. **92**, 230801.

Anglin, J. R., P. Drummond, and A. Smerzi, 2001, "Exact quantum phase model for mesoscopic Josephson junctions," Phys. Rev. A **64**, 063605.

Apellaniz, I., M. Kleinmann, O. Gühne, and G. Tóth, 2017, "Optimal witnessing of the quantum fisher information with few measurements," Phys. Rev. A **95**, 032330.

Apellaniz, I., B. Lücke, J. Peise, C. Klempt, and G. Toth, 2015, "Detecting metrologically useful entanglement in the vicinity of Dicke states," New J. Phys. **17**, 083027.

Appel, J., P. J. Windpassinger, D. Oblak, N. Hoff, U. B. Kjærgaard, and E. S. Polzik, 2009, "Mesoscopic atomic entanglement for precision measurements beyond the standard quantum limit," Proc. Natl. Acad. Sci. U.S.A. **106**, 10960.

Aragone, C., G. Guerri, S. Salamo, and J. L. Tani, 1974, "Intelligent spin states," J. Phys. A **7**, L149.

Arecchi, F. T., E. Courtens, R. Gilmore, and H. Thomas, 1972, "Atomic coherent states in quantum optics," Phys. Rev. A **6**, 2211–2237.

Arrad, G., Y. Vinkler, D. Aharonov, and A. Retzker, 2014, "Increasing sensing resolution with error correction," Phys. Rev. Lett. **112**, 150801.

Aspect, A., P. Grangier, and G. Roger, 1982, "Experimental realization of Einstein-Podolsky-Rosen-Bohm Gedankenexperiment: A new violation of Bell's inequalities," Phys. Rev. Lett. **49**, 91–94.

Auzinsh, M., D. Budker, D. F. Kimball, S. M. Rochester, J. E. Stalnaker, A. O. Sushkov, and V. V. Yashchuk, 2004, "Can a quantum nondemolition measurement improve the sensitivity of an atomic magnetometer?" Phys. Rev. Lett. **93**, 173002.

Bak, P., C. Tang, and K. Wiesenfeld, 1987, "Self-organized criticality: An explanation of the $1/f$ noise," Phys. Rev. Lett. **59**, 381–384.

Bakr, W. S., J. I. Gillen, A. Peng, S. Fölling, and M. Greiner, 2009, "A quantum gas microscope for detecting single atoms in a Hubbard-regime optical lattice," Nature (London) **462**, 74–77.

Ballance, C. J., T. P. Harty, N. M. Linke, M. A. Sepiol, and D. M. Lucas, 2016, "High-fidelity quantum logic gates using trapped-ion hyperfine qubits," Phys. Rev. Lett. **117**, 060504.

Bar-Gill, N., C. Gross, I. Mazets, M. Oberthaler, and G. Kurizki, 2011, "Einstein-Podolsky-Rosen correlations of ultracold atomic gases," Phys. Rev. Lett. **106**, 120404.

Barone, A., and G. Paternò, 1982, *Physics and Applications of the Josephson Effect* (John Wiley & Sons, New York).

Barontini, G., L. Hohmann, F. Haas, J. Estève, and J. Reichel, 2015, "Deterministic generation of multiparticle entanglement by quantum Zeno dynamics," Science **349**, 1317–1321.

Barrett, B., A. Bertoldi, and P. Bouyer, 2016, "Inertial quantum sensors using light and matter," Phys. Scr. **91**, 053006.

Behbood, N., F. Martin Ciurana, G. Colangelo, M. Napolitano, G. Tóth, R. J. Sewell, and M. W. Mitchell, 2014, "Generation of macroscopic singlet states in a cold atomic ensemble," Phys. Rev. Lett. **113**, 093601.

Bell, J. S., 1964, "On the Einstein Podolsky Rosen paradox," Physics Physique Fizika **1**, 195–200.

Beltrán, J., and A. Luis, 2005, "Breaking the Heisenberg limit with inefficient detectors," Phys. Rev. A **72**, 045801.

Bengtsson, I., and K. Zyczkowski, 2006, *Geometry of Quantum States: An Introduction to Quantum Entanglement* (Cambridge University Press, Cambridge).

Benhelm, J., G. Kirchmair, C. F. Roos, and R. Blatt, 2008, "Towards fault-tolerant quantum computing with trapped ions," Nat. Phys. **4**, 463–466.

Berrada, K., 2013, "Non-Markovian effect on the precision of parameter estimation," Phys. Rev. A **88**, 035806.

Berrada, T., S. van Frank, R. Bücker, T. Schumm, J.-F. Schaff, and J. Schmiedmayer, 2013, "Integrated Mach-Zehnder interferometer for Bose-Einstein condensates," Nat. Commun. **4**, 2077.

Berrada, T., S. van Frank, R. Bücker, T. Schumm, J.-F. Schaff, J. Schmiedmayer, B. Julía-Díaz, and A. Polls, 2016, "Matter-wave recombiners for trapped Bose-Einstein condensates," Phys. Rev. A **93**, 063620.

Berry, D. W., B. L. Higgins, S. D. Bartlett, M. W. Mitchell, G. J. Pryde, and H. M. Wiseman, 2009, "How to perform the most accurate possible phase measurements," Phys. Rev. A **80**, 052114.

Berry, D. W., and B. C. Sanders, 2002, "Near-optimal two-mode spin squeezing via feedback," Phys. Rev. A **66**, 012313.

Bhattacharyya, A., 1943, "On a measure of divergence between two statistical populations defined by their probability distributions," Bull. Calcutta Math. Soc. **35**, 99.

Biederharn, L. G., and J. C. Louck, 1981, *Angular Momentum in Quantum Physics: Theory and Applications* (Addison-Wesley, Reading, MA).

Blatt, R., and C. F. Roos, 2012, "Quantum simulations with trapped ions," Nat. Phys. **8**, 277.

Blatt, R., and D. J. Wineland, 2008, "Entangled states of trapped atomic ions," Nature (London) **453**, 1008.

Bloom, B. J., T. L. Nicholson, J. R. Williams, S. L. Campbell, M. Bishof, X. Zhang, W. Zhang, S. L. Bromley, and J. Ye, 2014, "An optical lattice clock with accuracy and stability at the 10^{-18} level," Nature (London) **506**, 71–75.

Blume-Kohout, R., 2010, "Optimal, reliable estimation of quantum states," New J. Phys. **12**, 043034.

Bodet, C., J. Estève, M. K. Oberthaler, and T. Gasenzer, 2010, "Two-mode Bose gas: Beyond classical squeezing," Phys. Rev. A **81**, 063605.

Böhi, P., M. F. Riedel, J. Hoffrogge, J. Reichel, T. W. Hänsch, and P. Treutlein, 2009, "Coherent manipulation of Bose-Einstein condensates with state-dependent microwave potentials on an atom chip," Nat. Phys. **5**, 592–597.

Bohnet, J. G., K. C. Cox, M. A. Norcia, J. M. Weiner, Z. Chen, and J. K. Thompson, 2014, "Reduced spin measurement back-action for a phase sensitivity ten times beyond the standard quantum limit," Nat. Photonics **8**, 731–736.

Bohnet, J. G., B. C. Sawyer, J. W. Britton, M. L. Wall, A. M. Rey, M. Foss-Feig, and J. J. Bollinger, 2016, "Quantum spin dynamics and entanglement generation with hundreds of trapped ions," Science **352**, 1297–1301.

Boixo, S., A. Datta, M. J. Davis, A. Shaji, A. B. Tacla, and C. M. Caves, 2009, "Quantum-limited metrology and Bose-Einstein condensates," Phys. Rev. A **80**, 032103.

Boixo, S., A. Datta, S. T. Flammia, A. Shaji, E. Bagan, and C. M. Caves, 2008, "Quantum-limited metrology with product states," Phys. Rev. A **77**, 012317.

Boixo, S., S. T. Flammia, C. M. Caves, and J. M. Geremia, 2007, "Generalized limits for single-parameter quantum estimation," Phys. Rev. Lett. **98**, 090401.

Bollinger, J. J., Wayne M. Itano, D. J. Wineland, and D. J. Heinzen, 1996, "Optimal frequency measurements with maximally correlated states," Phys. Rev. A **54**, R4649–R4652.

Bondurant, R. S., and J. H. Shapiro, 1984, "Squeezed states in phase-sensing interferometers," Phys. Rev. D **30**, 2548–2556.

Bonneau, M., J. Ruaudel, R. Lopes, J.-C. Jaskula, A. Aspect, D. Boiron, and C. I. Westbrook, 2013, "Tunable source of correlated atom beams," Phys. Rev. A **87**, 061603.

Bookjans, E. M., C. D. Hamley, and M. S. Chapman, 2011, "Strong quantum spin correlations observed in atomic spin mixing," Phys. Rev. Lett. **107**, 210406.

Bordè, Ch. J., 2002, "Atomic clocks and inertial sensors," Metrologia **39**, 435–463.

Borregaard, J., and A. S. Sørensen, 2013, "Near-Heisenberg-limited atomic clocks in the presence of decoherence," Phys. Rev. Lett. **111**, 090801.

Botet, R., R. Jullien, and P. Pfeuty, 1982, "Size scaling for infinitely coordinated systems," Phys. Rev. Lett. **49**, 478–481.

Boto, A. N., P. Kok, D. S. Abrams, S. L. Braunstein, C. P. Williams, and J. P. Dowling, 2000, "Quantum interferometric optical lithography: Exploiting entanglement to beat the diffraction limit," Phys. Rev. Lett. **85**, 2733–2736.

Bouchoule, I., and K. Mølmer, 2002a, "Preparation of spin-squeezed atomic states by optical-phase-shift measurement," Phys. Rev. A **66**, 043811.

Bouchoule, I., and K. Mølmer, 2002b, "Spin squeezing of atoms by the dipole interaction in virtually excited Rydberg states," Phys. Rev. A **65**, 041803.

Braginsky, V. B., and F. Y. Khalili, 1992, *Quantum Measurement* (Cambridge University Press, Cambridge).

Braginsky, V. B., Y. I. Vorontsov, and K. S. Thorne, 1980, "Quantum nondemolition measurements," Science **209**, 547–557.

Braunstein, S. L., and C. M. Caves, 1994, "Statistical distance and the geometry of quantum states," Phys. Rev. Lett. **72**, 3439–3443.

Braunstein, S. L., C. M. Caves, and G. J. Milburn, 1996, "Generalized uncertainty relations: Theory, examples, and Lorentz invariance," Ann. Phys. (N.Y.) **247**, 135–173.

Braunstein, S. L., A. S. Lane, and C. M. Caves, 1992, "Maximum-likelihood analysis of multiple quantum phase measurements," Phys. Rev. Lett. **69**, 2153–2156.

Braunstein, S. L., and P. van Loock, 2005, "Quantum information with continuous variables," Rev. Mod. Phys. **77**, 513–577.

Breitenbach, G., S. Schiller, and J. Mlynek, 1997, "Measurement of the quantum states of squeezed light," Nature (London) **387**, 471–475.

Brif, C., and A. Mann, 1996, "Nonclassical interferometry with intelligent light," Phys. Rev. A **54**, 4505–4518.

Britton, J. W., B. C. Sawyer, A. C. Keith, C. C. J. Wang, J. K. Freericks, H. Uys, M. J. Biercuk, and J. J. Bollinger, 2012, "Engineered two-dimensional Ising interactions in a trapped-ion quantum simulator with hundreds of spins," Nature (London) **484**, 489–492.

Browaeys, A., D. Barredo, and T. Lahaye, 2016, "Experimental investigations of dipole–dipole interactions between a few Rydberg atoms," J. Phys. B **49**, 152001.

Brunner, N., D. Cavalcanti, S. Pironio, V. Scarani, and S. Wehner, 2014, "Bell nonlocality," Rev. Mod. Phys. **86**, 419–478.

Bücker, R., J. Grond, S. Manz, T. Berrada, T. Betz, C. Koller, U. Hohenester, T. Schumm, A. Perrin, and J. Schmiedmayer, 2011, "Twin-atom beams," Nat. Phys. **7**, 608.

Budker, D., W. Gawlik, D. F. Kimball, S. M. Rochester, V. V. Yashchuk, and A. Weis, 2002, "Resonant nonlinear magneto-optical effects in atoms," Rev. Mod. Phys. **74**, 1153–1201.

Budker, D., D. F. Kimball, S. M. Rochester, and V. V. Yashchuk, 2000, "Nonlinear magneto-optical rotation via alignment-to-orientation conversion," Phys. Rev. Lett. **85**, 2088–2091.

Budker, D., and D. F. J. Kimball, 2013, Eds., *Optical Magnetometry* (Cambridge University Press, Cambridge).

Budker, D., and M. V. Romalis, 2007, "Optical magnetometry," Nat. Phys. **3**, 227.

Buonsante, P., R. Burioni, E. Vescovi, and A. Vezzani, 2012, "Quantum criticality in a bosonic Josephson junction," Phys. Rev. A **85**, 043625.

Bures, D., 1969, "An extension of Kakutani's theorem on infinite product measures to the tensor product of semifinite w^*-algebras," Trans. Am. Math. Soc. **135**, 199.

Bužek, V., R. Derka, and S. Massar, 1999, "Optimal quantum clocks," Phys. Rev. Lett. **82**, 2207–2210.

Byrnes, T., 2013, "Fractality and macroscopic entanglement in two-component Bose-Einstein condensates," Phys. Rev. A **88**, 023609.

Byrnes, T., K. Wen, and Y. Yamamoto, 2012, "Macroscopic quantum computation using Bose-Einstein condensates," Phys. Rev. A **85**, 040306.

Campos, R. A., Christopher C. Gerry, and A. Benmoussa, 2003, "Optical interferometry at the Heisenberg limit with twin Fock states and parity measurements," Phys. Rev. A **68**, 023810.

Carnio, E. G., A. Buchleitner, and M. Gessner, 2015, "Robust asymptotic entanglement under multipartite collective dephasing," Phys. Rev. Lett. **115**, 010404.

Carruthers, P., and M. M. Nieto, 1968, "Phase and angle variables in quantum mechanics," Rev. Mod. Phys. **40**, 411–440.

Casabone, B., A. Stute, K. Friebe, B. Brandstätter, K. Schüppert, R. Blatt, and T. E. Northup, 2013, "Heralded entanglement of two ions in an optical cavity," Phys. Rev. Lett. **111**, 100505.

Castin, Y., and J. Dalibard, 1997, "Relative phase of two Bose-Einstein condensates," Phys. Rev. A **55**, 4330–4337.

Caves, C. M., 1981, "Quantum-mechanical noise in an interferometer," Phys. Rev. D **23**, 1693–1708.

Chabuda, K., I. D. Leroux, and R. Demkowicz-Dobrzański, 2016, "The quantum allan variance," New J. Phys. **18**, 083035.

Chang, M.-S., Q. Qin, W. Zhang, L. You, and M. S. Chapman, 2005, "Coherent spinor dynamics in a spin-1 bose condensate," Nat. Phys. **1**, 111–116.

Chase, B. A., B. Q. Baragiola, H. L. Partner, B. D. Black, and J. M. Geremia, 2009, "Magnetometry via a double-pass continuous quantum measurement of atomic spin," Phys. Rev. A **79**, 062107.

Chaudhury, S., G. A. Smith, K. Schulz, and P. S. Jessen, 2006, "Continuous nondemolition measurement of the Cs clock transition pseudospin," Phys. Rev. Lett. **96**, 043001.

Chaves, R., J. B. Brask, M. Markiewicz, J. Kołodyński, and A. Acín, 2013, "Noisy metrology beyond the standard quantum limit," Phys. Rev. Lett. **111**, 120401.

Chen, B., C. Qiu, S. Chen, J. Guo, L. Q. Chen, Z. Y. Ou, and W. Zhang, 2015, "Atom-light hybrid interferometer," Phys. Rev. Lett. **115**, 043602.

Chen, W., J. Hu, Y. Duan, B. Braverman, H. Zhang, and V. Vuletić, 2015, "Carving complex many-atom entangled states by single-photon detection," Phys. Rev. Lett. **115**, 250502.

Chen, Z., J. G. Bohnet, S. R. Sankar, J. Dai, and J. K. Thompson, 2011, "Conditional spin squeezing of a large ensemble via the vacuum Rabi splitting," Phys. Rev. Lett. **106**, 133601.

Chen, Z., J. G. Bohnet, J. M. Weiner, K. C. Cox, and J. K. Thompson, 2014, "Cavity-aided nondemolition measurements for atom counting and spin squeezing," Phys. Rev. A **89**, 043837.

Chin, A. W., S. F. Huelga, and M. B. Plenio, 2012, "Quantum metrology in non-Markovian environments," Phys. Rev. Lett. **109**, 233601.

Chin, C., R. Grimm, P. Julienne, and E. Tiesinga, 2010, "Feshbach resonances in ultracold gases," Rev. Mod. Phys. **82**, 1225–1286.

Choi, S., and N. P. Bigelow, 2005, "Quantum squeezing and entanglement in a two-mode Bose-Einstein condensate with time-dependent Josephson-like coupling," Phys. Rev. A **72**, 033612.

Choi, S., and B. Sundaram, 2008, "Bose-Einstein condensate as a nonlinear Ramsey interferometer operating beyond the Heisenberg limit," Phys. Rev. A **77**, 053613.

Christensen, S. L., J.-B. Béguin, E. Bookjans, H. L. Sørensen, J. H. Müller, J. Appel, and E. S. Polzik, 2014, "Quantum interference of a single spin excitation with a macroscopic atomic ensemble," Phys. Rev. A **89**, 033801.

Christensen, S. L., J.-B. Béguin, H. L. Sørensen, E. Bookjans, D. Oblak, J. H. Müller, J. Appel, and E. S. Polzik, 2013, "Toward quantum state tomography of a single polariton state of an atomic ensemble," New J. Phys. **15**, 015002.

Chwedeńczuk, J., P. Hyllus, F. Piazza, and A. Smerzi, 2012, "Sub-shot-noise interferometry from measurements of the one-body density," New J. Phys. **14**, 093001.

Cirac, J. I., M. Lewenstein, K. Mølmer, and P. Zoller, 1998, "Quantum superposition states of Bose-Einstein condensates," Phys. Rev. A **57**, 1208–1218.

Cirac, J. I., and P. Zoller, 1995, "Quantum computations with cold trapped ions," Phys. Rev. Lett. **74**, 4091–4094.

Cohen, M., 1968, "The Fisher information and convexity," IEEE Trans. Inf. Theory **14**, 591–592.

Colangelo, G., F. Martin Ciurana, G. Puentes, M. W. Mitchell, and R. J. Sewell, 2017, "Entanglement-enhanced phase estimation without prior phase information," Phys. Rev. Lett. **118**, 233603.

Colangelo, G., F. Martin Ciurana, L. C. Bianchet, R. J. Sewell, and M. W. Mitchell, 2017, "Simultaneous tracking of spin angle and amplitude beyond classical limits," Nature (London) **543**, 525–528.

Cox, K. C., G. P. Greve, J. M. Weiner, and J. K. Thompson, 2016, "Deterministic squeezed states with collective measurements and feedback," Phys. Rev. Lett. **116**, 093602.

Cramér, H., 1946, *Mathematical Methods of Statistics* (Princeton University Press, Princeton, NJ).

Cronin, A. D., J. Schmiedmayer, and D. E. Pritchard, 2009, "Optics and interferometry with atoms and molecules," Rev. Mod. Phys. **81**, 1051–1129.

Davis, E., G. Bentsen, and M. Schleier-Smith, 2016, "Approaching the Heisenberg limit without single-particle detection," Phys. Rev. Lett. **116**, 053601.

de Echaniz, S. R., M. W. Mitchell, M. Kubasik, M. Koschorreck, H. Crepaz, J. Eschner, and E. S. Polzik, 2005, "Conditions for spin squeezing in a cold ^{87}Rb ensemble," J. Opt. B **7**, S548.

Demkowicz-Dobrzański, R., J. Kołodyński, and M. Guţă, 2012, "The elusive Heisenberg limit in quantum-enhanced metrology," Nat. Commun. **3**, 1063.

Demkowicz-Dobrzański, R., and L. Maccone, 2014, "Using entanglement against noise in quantum metrology," Phys. Rev. Lett. **113**, 250801.

Dicke, R. H., 1954, "Coherence in spontaneous radiation processes," Phys. Rev. **93**, 99–110.

Dorner, U., 2012, "Quantum frequency estimation with trapped ions and atoms," New J. Phys. **14**, 043011.

Dowling, J. P., 1998, "Correlated input-port, matter-wave interferometer: Quantum-noise limits to the atom-laser gyroscope," Phys. Rev. A **57**, 4736–4746.

Dowling, J. P., G. S. Agarwal, and W. P. Schleich, 1994, "Wigner distribution of a general angular-momentum state: Applications to a collection of two-level atoms," Phys. Rev. A **49**, 4101–4109.

Duan, L.-M., 2011, "Entanglement detection in the vicinity of arbitrary Dicke states," Phys. Rev. Lett. **107**, 180502.

Duan, L.-M., J. I. Cirac, and P. Zoller, 2002, "Quantum entanglement in spinor Bose-Einstein condensates," Phys. Rev. A **65**, 033619.

Duan, L.-M., G. Giedke, J. I. Cirac, and P. Zoller, 2000, "Inseparability criterion for continuous variable systems," Phys. Rev. Lett. **84**, 2722–2725.

Duan, L.-M., M. D. Lukin, J. I. Cirac, and P. Zoller, 2001, "Long-distance quantum communication with atomic ensembles and linear optics," Nature (London) **414**, 413.

Duan, L.-M., and C. Monroe, 2010, "*Colloquium*: Quantum networks with trapped ions," Rev. Mod. Phys. **82**, 1209–1224.

Duan, L.-M., A. Sørensen, J. I. Cirac, and P. Zoller, 2000, "Squeezing and entanglement of atomic beams," Phys. Rev. Lett. **85**, 3991–3994.

Dür, W., M. Skotiniotis, F. Fröwis, and B. Kraus, 2014, "Improved quantum metrology using quantum error correction," Phys. Rev. Lett. **112**, 080801.

Dür, W., G. Vidal, and J. I. Cirac, 2000, "Three qubits can be entangled in two inequivalent ways," Phys. Rev. A **62**, 062314.

Eibl, M., S. Gaertner, M. Bourennane, C. Kurtsiefer, M. Żukowski, and H. Weinfurter, 2003, "Experimental observation of four-photon entanglement from parametric down-conversion," Phys. Rev. Lett. **90**, 200403.

Einstein, A., B. Podolsky, and N. Rosen, 1935, "Can quantum-mechanical description of physical reality be considered complete?" Phys. Rev. **47**, 777–780.

Engelsen, N. J., R. Krishnakumar, O. Hosten, and M. A. Kasevich, 2017, "Bell correlations in spin-squeezed states of 500 000 atoms," Phys. Rev. Lett. **118**, 140401.

Escher, B. M., L. Davidovich, N. Zagury, and R. L. de Matos Filho, 2012, "Quantum metrological limits via a variational approach," Phys. Rev. Lett. **109**, 190404.

Escher, B. M., R. L. de Matos Filho, and L. Davidovich, 2011, "General framework for estimating the ultimate precision limit in noisy quantum-enhanced metrology," Nat. Phys. **7**, 406.

Estève, J., C. Gross, A. Weller, S. Giovanazzi, and M. K. Oberthaler, 2008, "Squeezing and entanglement in a Bose-Einstein condensate," Nature (London) **455**, 1216–1219.

Eto, Y., H. Ikeda, H. Suzuki, S. Hasegawa, Y. Tomiyama, S. Sekine, M. Sadgrove, and T. Hirano, 2013, "Spin-echo-based magnetometry with spinor Bose-Einstein condensates," Phys. Rev. A **88**, 031602.

Facchi, P., and S. Pascazio, 2008, "Quantum Zeno dynamics: mathematical and physical aspects," J. Phys. A **41**, 493001.

Feldmann, P., M. Gessner, M. Gabbrielli, C. Klempt, L. Santos, L. Pezzè, and A. Smerzi, 2018, "Interferometric sensitivity and entanglement by scanning through quantum phase transitions in spinor bose-einstein condensates," Phys. Rev. A **97**, 032339.

Ferrini, G., A. Minguzzi, and F. W. J. Hekking, 2008, "Number squeezing, quantum fluctuations, and oscillations in mesoscopic Bose Josephson junctions," Phys. Rev. A **78**, 023606.

Ferrini, G., D. Spehner, A. Minguzzi, and F. W. J. Hekking, 2011, "Effect of phase noise on quantum correlations in Bose-Josephson junctions," Phys. Rev. A **84**, 043628.

Ferris, A. J., M. K. Olsen, E. G. Cavalcanti, and M. J. Davis, 2008, "Detection of continuous variable entanglement without coherent local oscillators," Phys. Rev. A **78**, 060104.

Fisher, R. A., 1922, "On the mathematical foundations of theoretical statistics," Phil. Trans. R. Soc. A **222**, 309–368.

Fisher, R. A., 1925, "Theory of statistical estimation," Math. Proc. Cambridge Philos. Soc. **22**, 700.

Fleischhauer, M., and M. D. Lukin, 2000, "Dark-state polaritons in electromagnetically induced transparency," Phys. Rev. Lett. **84**, 5094–5097.

Fleischhauer, M., and S. Gong, 2002, "Stationary source of nonclassical or entangled atoms," Phys. Rev. Lett. **88**, 070404.

Foss-Feig, M., K. R. A. Hazzard, J. J. Bollinger, and A. M. Rey, 2013, "Nonequilibrium dynamics of arbitrary-range Ising models with decoherence: An exact analytic solution," Phys. Rev. A **87**, 042101.

Fraas, M., 2016, "An analysis of the stationary operation of atomic clocks," Commun. Math. Phys. **348**, 363–393.

Fréchet, M., 1943, "Sur l'extension de certaines evaluations statistiques au cas de petits échantillons," Revue de l'Institut International de Statistique **11**, 182–205.

Freedman, S. J., and J. F. Clauser, 1972, "Experimental test of local hidden-variable theories," Phys. Rev. Lett. **28**, 938–941.

Frérot, I., and T. Roscilde, 2016, "Quantum variance: A measure of quantum coherence and quantum correlations for many-body systems," Phys. Rev. B **94**, 075121.

Fröwis, F., P. Sekatski, and W. Dür, 2016, "Detecting large quantum Fisher information with finite measurement precision," Phys. Rev. Lett. **116**, 090801.

Fuchs, C. A., and C. M. Caves, 1995, "Mathematical techniques for quantum communication theory," Open Syst. Inf. Dyn. **3**, 345–356.

Fujiwara, A., 2006, "Strong consistency and asymptotic efficiency for adaptive quantum estimation problems," J. Phys. A **39**, 12489.

Fujiwara, A., and H. Imai, 2008, "A fibre bundle over manifolds of quantum channels and its application to quantum statistics," J. Phys. A **41**, 255304.

Gabbrielli, M., L. Pezzè, and A. Smerzi, 2015, "Spin-mixing interferometry with Bose-Einstein condensates," Phys. Rev. Lett. **115**, 163002.

Gabbrielli, M., A. Smerzi, and L. Pezzè, 2018, "Multipartite entanglement at finite temperature," arXiv:1805.03139.

Gaebler, J. P., *et al.*, 2016, "High-fidelity universal gate set for $^{9}Be^{+}$ ion qubits," Phys. Rev. Lett. **117**, 060505.

García-Ripoll, J. J., P. Zoller, and J. I. Cirac, 2005, "Coherent control of trapped ions using off-resonant lasers," Phys. Rev. A **71**, 062309.

Garttner, M., J. G. Bohnet, A. Safavi-Naini, M. L. Wall, J. J. Bollinger, and A. M. Rey, 2017, "Measuring out-of-time-order correlations and multiple quantum spectra in a trapped-ion quantum magnet," Nat. Phys. **13**, 781–786.

Gati, R., B. Hemmerling, J. Fölling, M. Albiez, and M. K. Oberthaler, 2006, "Noise thermometry with two weakly coupled Bose-Einstein condensates," Phys. Rev. Lett. **96**, 130404.

Genoni, M. G., S. Olivares, and M. G. A. Paris, 2011, "Optical phase estimation in the presence of phase diffusion," Phys. Rev. Lett. **106**, 153603.

Geremia, J. M., J. K. Stockton, A. C. Doherty, and H. Mabuchi, 2003, "Quantum Kalman filtering and the Heisenberg limit in atomic magnetometry," Phys. Rev. Lett. **91**, 250801.

Gerry, C. C., R. A. Campos, and A. Benmoussa, 2004, "Comment on "interferometric detection of optical phase shifts at the Heisenberg limit"," Phys. Rev. Lett. **92**, 209301.

Gessner, M., L. Pezzè, and A. Smerzi, 2016, "Efficient entanglement criteria for discrete, continuous, and hybrid variables," Phys. Rev. A **94**, 020101.

Gessner, M., L. Pezzè, and A. Smerzi, 2017, "Resolution-enhanced entanglement detection," Phys. Rev. A **95**, 032326.

Gil, L. I. R., R. Mukherjee, E. M. Bridge, M. P. A. Jones, and T. Pohl, 2014, "Spin squeezing in a Rydberg lattice clock," Phys. Rev. Lett. **112**, 103601.

Gill, R. D., 2008, "Conciliation of Bayes and pointwise quantum state estimation," in *Quantum Stochastics and Information: Statistics, Filtering and Control*, edited by V. P. Belavkin and M. Guţă (World Scientific, Singapore), p. 239.

Gilmore, R., and D. H. Feng, 1978, "Phase transitions in nuclear matter described by pseudospin Hamiltonians," Nucl. Phys. A **301**, 189.

Giovannetti, V., S. Lloyd, and L. Maccone, 2004, "Quantum-enhanced measurements: Beating the standard quantum limit," Science **306**, 1330.

Giovannetti, V., S. Lloyd, and L. Maccone, 2006, "Quantum metrology," Phys. Rev. Lett. **96**, 010401.

Giovannetti, V., S. Lloyd, and L. Maccone, 2011, "Advances in quantum metrology," Nat. Photonics **5**, 222.

Giovannetti, V., S. Mancini, D. Vitali, and P. Tombesi, 2003, "Characterizing the entanglement of bipartite quantum systems," Phys. Rev. A **67**, 022320.

Giustina, M., *et al.*, 2015, "Significant-loophole-free test of Bell's theorem with entangled photons," Phys. Rev. Lett. **115**, 250401.

Glauber, R. J., 1963, "Coherent and incoherent states of the radiation field," Phys. Rev. **131**, 2766–2788.

Goldstein, E. V., and P. Meystre, 1999, "Quantum theory of atomic four-wave mixing in Bose-Einstein condensates," Phys. Rev. A **59**, 3896–3901.

Gordon, D., and C. M. Savage, 1999, "Creating macroscopic quantum superpositions with Bose-Einstein condensates," Phys. Rev. A **59**, 4623–4629.

Grangier, P., J. A. Levenson, and J.-P. Poizat, 1998, "Quantum non-demolition measurements in optics," Nature (London) **396**, 537.

Greenberger, D. M., M. A. Horne, A. Shimony, and A. Zeilinger, 1990, "Bell's theorem without inequalities," Am. J. Phys. **58**, 1131.

Grond, J., J. Schmiedmayer, and U. Hohenester, 2009, "Optimizing number squeezing when splitting a mesoscopic condensate," Phys. Rev. A **79**, 021603.

Gross, C., H. Strobel, E. Nicklas, T. Zibold, N. Bar-Gill, G. Kurizki, and M. K. Oberthaler, 2011, "Atomic homodyne detection of continuous-variable entangled twin-atom states," Nature (London) **480**, 219–223.

Gross, C., T. Zibold, E. Nicklas, J. Estève, and M. K. Oberthaler, 2010, "Nonlinear atom interferometer surpasses classical precision limit," Nature (London) **464**, 1165–1169.

Gühne, O., and G. Tóth, 2009, "Entanglement detection," Phys. Rep. **474**, 1.

Gühne, O., G. Tóth, and H. J. Briegel, 2005, "Multipartite entanglement in spin chains," New J. Phys. **7**, 229.

Haas, F., J. Volz, R. Gehr, J. Reichel, and J. Estève, 2014, "Entangled states of more than 40 atoms in an optical fiber cavity," Science **344**, 180.

Hadzibabic, Z., P. Krüger, M. Cheneau, B. Battelier, and J. Dalibard, 2006, "Berezinskii-Kosterlitz-Thouless crossover in a trapped atomic gas," Nature (London) **441**, 1118–1121.

Häffner, H., C. F. Roos, and R. Blatt, 2008, "Quantum computing with trapped ions," Phys. Rep. **469**, 155–203.

Häffner, H., *et al.*, 2005, "Scalable multiparticle entanglement of trapped ions," Nature (London) **438**, 643–646.

Haine, S. A., and J. J. Hope, 2005, "Outcoupling from a bose-einstein condensate with squeezed light to produce entangled-atom laser beams," Phys. Rev. A **72**, 033601.

Haine, S. A., and S. S. Szigeti, 2015, "Quantum metrology with mixed states: When recovering lost information is better than never losing it," Phys. Rev. A **92**, 032317.

Haine, S. A., S. S. Szigeti, M. D. Lang, and C. M. Caves, 2015, "Heisenberg-limited metrology with information recycling," Phys. Rev. A **91**, 041802.

Hald, J., J. L. Sørensen, C. Schori, and E. S. Polzik, 1999, "Spin squeezed atoms: A macroscopic entangled ensemble created by light," Phys. Rev. Lett. **83**, 1319–1322.

Hald, J., J. L. Sørensen, C. Schori, and E. S. Polzik, 2000, "Entanglement transfer from light to atoms," J. Mod. Opt. **47**, 2599.

Haljan, P. C., P. J. Lee, K.-A. Brickman, M. Acton, L. Deslauriers, and C. Monroe, 2005, "Entanglement of trapped-ion clock states," Phys. Rev. A **72**, 062316.

Hall, B. V., S. Whitlock, R. Anderson, P. Hannaford, and A. I. Sidorov, 2007, "Condensate splitting in an asymmetric double well for atom chip based sensors," Phys. Rev. Lett. **98**, 030402.

Hall, D. S., M. R. Matthews, J. R. Ensher, C. E. Wieman, and E. A. Cornell, 1998, "Dynamics of component separation in a binary mixture of Bose-Einstein condensates," Phys. Rev. Lett. **81**, 1539–1542.

Hall, D. S., M. R. Matthews, C. E. Wieman, and E. A. Cornell, 1998, "Measurements of relative phase in two-component Bose-Einstein condensates," Phys. Rev. Lett. **81**, 1543–1546.

Hamley, C. D., C. S. Gerving, T. M. Hoang, E. M. Bookjans, and M. S. Chapman, 2012, "Spin-nematic squeezed vacuum in a quantum gas," Nat. Phys. **8**, 305.

Hammerer, K., K. Mølmer, E. S. Polzik, and J. I. Cirac, 2004, "Light-matter quantum interface," Phys. Rev. A **70**, 044304.

Hammerer, K., A. S. Sørensen, and E. S. Polzik, 2010, "Quantum interface between light and atomic ensembles," Rev. Mod. Phys. **82**, 1041–1093.

Harty, T. P., D. T. C. Allcock, C. J. Ballance, L. Guidoni, H. A. Janacek, N. M. Linke, D. N. Stacey, and D. M. Lucas, 2014, "High-fidelity preparation, gates, memory, and readout of a trapped-ion quantum bit," Phys. Rev. Lett. **113**, 220501.

Hauke, P., M. Heyl, L. Tagliacozzo, and P. Zoller, 2016, "Measuring multipartite entanglement through dynamic susceptibilities," Nat. Phys. **12**, 778–782.

Hayashi, M., 2005, Ed., *Asymptotic Theory of Quantum Statistical Inference* (World Scientific, Singapore).

He, Q. Y., Shi-Guo Peng, P. D. Drummond, and M. D. Reid, 2011, "Planar quantum squeezing and atom interferometry," Phys. Rev. A **84**, 022107.

He, Q. Y., M. D. Reid, T. G. Vaughan, C. Gross, M. Oberthaler, and P. D. Drummond, 2011, "Einstein-Podolsky-Rosen entanglement strategies in two-well Bose-Einstein condensates," Phys. Rev. Lett. **106**, 120405.

He, Q. Y., T. G. Vaughan, P. D. Drummond, and M. D. Reid, 2012, "Entanglement, number fluctuations and optimized interferometric phase measurement," New J. Phys. **14**, 093012.
Helstrom, C. W., 1967, "Minimum mean-squared error of estimates in quantum statistics," Phys. Lett. A **25**, 101.
Helstrom, C. W., 1976, *Quantum Detection and Estimation Theory* (Academic Press, New York).
Henkel, N., R. Nath, and T. Pohl, 2010, "Three-dimensional roton excitations and supersolid formation in rydberg-excited bose-einstein condensates," Phys. Rev. Lett. **104**, 195302.
Hensen, B., *et al.*, 2015, "Loophole-free Bell inequality violation using electron spins separated by 1.3 kilometres," Nature (London) **526**, 682–686.
Herrera-Martí, D. A., T. Gefen, D. Aharonov, N. Katz, and A. Retzker, 2015, "Quantum error-correction-enhanced magnetometer overcoming the limit imposed by relaxation," Phys. Rev. Lett. **115**, 200501.
Higgins, B. L., D. W. Berry, S. D. Bartlett, H. M. Wiseman, and G. J. Pryde, 2007, "Entanglement-free heisenberg-limited phase estimation," Nature (London) **450**, 393–396.
Hill, S., and W. K. Wootters, 1997, "Entanglement of a pair of quantum bits," Phys. Rev. Lett. **78**, 5022–5025.
Hillery, M., and L. Mlodinow, 1993, "Interferometers and minimum-uncertainty states," Phys. Rev. A **48**, 1548–1558.
Hinkley, N., J. A. Sherman, N. B. Phillips, M. Schioppo, N. D. Lemke, K. Beloy, M. Pizzocaro, C. W. Oates, and A. D. Ludlow, 2013, "An atomic clock with 10^{-18} instability," Science **341**, 1215.
Ho, T. L., and C. V. Ciobanu, 2004, "The Schrödinger cat family in attractive Bose gases," J. Low Temp. Phys. **135**, 257.
Ho, T.-L., 1998, "Spinor Bose condensates in optical traps," Phys. Rev. Lett. **81**, 742–745.
Hoang, T. M., H. M. Bharath, M. J. Boguslawski, M. Anquez, B. A. Robbins, and M. S. Chapman, 2016, "Adiabatic quenches and characterization of amplitude excitations in a continuous quantum phase transition," Proc. Natl. Acad. Sci. U.S.A. **113**, 9475–9479.
Hofferberth, S., I. Lesanovsky, B. Fischer, J. Verdu, and J. Schmiedmayer, 2006, "Radiofrequency-dressed-state potentials for neutral atoms," Nat. Phys. **2**, 710.
Hofmann, J., M. Krug, N. Ortegel, L. Gérard, M. Weber, W. Rosenfeld, and H. Weinfurter, 2012, "Heralded entanglement between widely separated atoms," Science **337**, 72–75.
Holevo, A. S., 1982, *Probabilistic and statistical aspects of quantum theory* (North-Holland Publishing Company, Amsterdam).
Holland, M. J., and K. Burnett, 1993, "Interferometric detection of optical phase shifts at the Heisenberg limit," Phys. Rev. Lett. **71**, 1355–1358.
Home, J. P., M. J. McDonnell, D. L. Lucas, G. Imreh, B. C. Keitch, D. J. Szwer, N. R. Thomas, S. C. Webster, N. D. Stacey, and A. M. Steane, 2006, "Deterministic entanglement and tomography of ion-spin qubits," New J. Phys. **8**, 188.
Hong, C. K., Z. Y. Ou, and L. Mandel, 1987, "Measurement of subpicosecond time intervals between two photons by interference," Phys. Rev. Lett. **59**, 2044–2046.
Horodecki, R., P. Horodecki, M. Horodecki, and K. Horodecki, 2009, "Quantum entanglement," Rev. Mod. Phys. **81**, 865–942.
Horrom, T., R. Singh, J. P. Dowling, and E. E. Mikhailov, 2012, "Quantum-enhanced magnetometer with low-frequency squeezing," Phys. Rev. A **86**, 023803.
Hosten, O., N. J. Engelsen, R. Krishnakumar, and M. A. Kasevich, 2016, "Measurement noise 100 times lower than the quantum-projection limit using entangled atoms," Nature (London) **529**, 505–508.
Hosten, O., R. Krishnakumar, N. J. Engelsen, and M. A. Kasevich, 2016, "Quantum phase magnification," Science **352**, 1552–1555.
Hu, J., W. Chen, Z. Vendeiro, H. Zhang, and V. Vuletić, 2015, "Entangled collective-spin states of atomic ensembles under nonuniform atom-light interaction," Phys. Rev. A **92**, 063816.
Hu, J., Z. Vendeiro, W. Chen, H. Zhang, R. McConnell, A. S. Sørensen, and V. Vuletić, 2017, "Strictly nonclassical behavior of a mesoscopic system," Phys. Rev. A **95**, 030105.
Huang, Y. P., and M. G. Moore, 2006, "Creation, detection, and decoherence of macroscopic quantum superposition states in double-well Bose-Einstein condensates," Phys. Rev. A **73**, 023606.
Huang, Y. P., and M. G. Moore, 2008, "Optimized double-well quantum interferometry with Gaussian squeezed states," Phys. Rev. Lett. **100**, 250406.
Huang, Z., C. Macchiavello, and L. Maccone, 2016, "Usefulness of entanglement-assisted quantum metrology," Phys. Rev. A **94**, 012101.
Hübner, M., 1992, "Explicit computation of the Bures distance for density matrices," Phys. Lett. A **163**, 239.
Hudelist, F., J. Kong, C. Liu, J. Jing, Z. Y. Ou, and W. Zhang, 2014, "Quantum metrology with parametric amplifier-based photon correlation interferometers," Nat. Commun. **5**, 3049.
Huelga, S. F., C. Macchiavello, T. Pellizzari, A. K. Ekert, M. B. Plenio, and J. I. Cirac, 1997, "Improvement of frequency standards with quantum entanglement," Phys. Rev. Lett. **79**, 3865–3868.
Hume, D. B., I. Stroescu, M. Joos, W. Muessel, H. Strobel, and M. K. Oberthaler, 2013, "Accurate atom counting in mesoscopic ensembles," Phys. Rev. Lett. **111**, 253001.
Husimi, K., 1940, "Some formal properties of the density matrix," Proc. Phys. Math. Soc. Jpn. **22**, 264–314.
Hyllus, P., O. Gühne, and A. Smerzi, 2010, "Not all pure entangled states are useful for sub-shot-noise interferometry," Phys. Rev. A **82**, 012337.
Hyllus, P., W. Laskowski, R. Krischek, C. Schwemmer, W. Wieczorek, H. Weinfurter, L. Pezzè, and A. Smerzi, 2012, "Fisher information and multiparticle entanglement," Phys. Rev. A **85**, 022321.
Hyllus, P., L. Pezzè, A. Smerzi, and G. Tóth, 2012, "Entanglement and extreme spin squeezing for a fluctuating number of indistinguishable particles," Phys. Rev. A **86**, 012337.
Inguscio, M., and L. Fallani, 2013, *Atomic Physics: Precise Measurements and Ultracold Matter* (Oxford University Press, New York).
Inoue, R., S.-I.-R. Tanaka, R. Namiki, T. Sagawa, and Y. Takahashi, 2013, "Unconditional quantum-noise suppression via measurement-based quantum feedback," Phys. Rev. Lett. **110**, 163602.
Isella, L., and J. Ruostekoski, 2005, "Nonadiabatic dynamics of a Bose-Einstein condensate in an optical lattice," Phys. Rev. A **72**, 011601.
Islam, R., C. Senko, W. C. Campbell, S. Korenblit, J. Smith, A. Lee, E. E. Edwards, C.-C. J. Wang, J. K. Freericks, and C. Monroe, 2013, "Emergence and frustration of magnetism with variable-range interactions in a quantum simulator," Science **340**, 583–587.
Itano, W. M., J. C. Bergquist, J. J. Bollinger, J. M. Gilligan, D. J. Heinzen, F. L. Moore, M. G. Raizen, and D. J. Wineland, 1993, "Quantum projection noise: Population fluctuations in two-level systems," Phys. Rev. A **47**, 3554–3570.
Jääskeläinen, M., W. Zhang, and P. Meystre, 2004, "Limits to phase resolution in matter-wave interferometry," Phys. Rev. A **70**, 063612.
Jaskula, J.-C., M. Bonneau, G. B. Partridge, V. Krachmalnicoff, P. Deuar, K. V. Kheruntsyan, A. Aspect, D. Boiron, and C. I.

Westbrook, 2010, "Sub-Poissonian number differences in four-wave mixing of matter waves," Phys. Rev. Lett. **105**, 190402.
Javanainen, J., 1986, "Oscillatory exchange of atoms between traps containing Bose condensates," Phys. Rev. Lett. **57**, 3164–3166.
Javanainen, J., and M. Wilkens, 1997, "Phase and phase diffusion of a split Bose-Einstein condensate," Phys. Rev. Lett. **78**, 4675–4678.
Javanainen, J., and M. Yu. Ivanov, 1999, "Splitting a trap containing a Bose-Einstein condensate: Atom number fluctuations," Phys. Rev. A **60**, 2351–2359.
Jeske, J., J. H. Cole, and S. F. Huelga, 2014, "Quantum metrology subject to spatially correlated Markovian noise: restoring the Heisenberg limit," New J. Phys. **16**, 073039.
Jo, G.-B., J.-H. Choi, C. A. Christensen, T. A. Pasquini, Y.-R. Lee, W. Ketterle, and D. E. Pritchard, 2007, "Phase-sensitive recombination of two Bose-Einstein condensates on an atom chip," Phys. Rev. Lett. **98**, 180401.
Jo, G.-B., Y. Shin, S. Will, T. A. Pasquini, M. Saba, W. Ketterle, D. E. Pritchard, M. Vengalattore, and M. Prentiss, 2007, "Long phase coherence time and number squeezing of two Bose-Einstein condensates on an atom chip," Phys. Rev. Lett. **98**, 030407.
Johanning, M., A. Braun, N. Timoney, V. Elman, W. Neuhauser, and C. Wunderlich, 2009, "Individual addressing of trapped ions and coupling of motional and spin states using rf radiation," Phys. Rev. Lett. **102**, 073004.
Johanning, M., A. F. Varón, and C. Wunderlich, 2009, "Quantum simulations with cold trapped ions," J. Phys. B **42**, 154009.
Jozsa, R., 1994, "Fidelity for mixed quantum states," J. Mod. Opt. **41**, 2315–2323.
Juliá-Díaz, B., E. Torrontegui, J. Martorell, J. G. Muga, and A. Polls, 2012, "Fast generation of spin-squeezed states in bosonic Josephson junctions," Phys. Rev. A **86**, 063623.
Juliá-Díaz, B., T. Zibold, M. K. Oberthaler, M. Melé-Messeguer, J. Martorell, and A. Polls, 2012, "Dynamic generation of spin-squeezed states in bosonic Josephson junctions," Phys. Rev. A **86**, 023615.
Julsgaard, B., A. Kozhekin, and E. S. Polzik, 2001, "Experimental long-lived entanglement of two macroscopic objects," Nature (London) **413**, 400.
Jurcevic, P., B. P. Lanyon, P. Hauke, C. Hempel, P. Zoller, R. Blatt, and C. F. Roos, 2014, "Quasiparticle engineering and entanglement propagation in a quantum many-body system," Nature (London) **511**, 202–205.
Kawaguchi, Y., and M. Ueda, 2012, "Spinor Bose-Einstein condensates," Phys. Rep. **520**, 253–381.
Kay, S. M., 1993, *Fundamentals of Statistical Signal Processing, Volume I: Estimation Theory* (Prentice Hall, Upper Saddle River, NJ).
Kessler, E. M., P. Kómár, M. Bishof, L. Jiang, A. S. Sørensen, J. Ye, and M. D. Lukin, 2014, "Heisenberg-limited atom clocks based on entangled qubits," Phys. Rev. Lett. **112**, 190403.
Kessler, E. M., I. Lovchinsky, A. O. Sushkov, and M. D. Lukin, 2014, "Quantum error correction for metrology," Phys. Rev. Lett. **112**, 150802.
Kiesel, T., W. Vogel, V. Parigi, A. Zavatta, and M. Bellini, 2008, "Experimental determination of a nonclassical Glauber-Sudarshan *P* function," Phys. Rev. A **78**, 021804.
Kim, K., M. S. Chang, S. Korenblit, R. Islam, E. E. Edwards, J. K. Freericks, G. D. Lin, L. M. Duan, and C. Monroe, 2010, "Quantum simulation of frustrated Ising spins with trapped ions," Nature (London) **465**, 590–593.
Kim, K., M.-S. Chang, R. Islam, S. Korenblit, L.-M. Duan, and C. Monroe, 2009, "Entanglement and tunable spin-spin couplings between trapped ions using multiple transverse modes," Phys. Rev. Lett. **103**, 120502.
Kim, T., O. Pfister, M. J. Holland, J. Noh, and J. L. Hall, 1998, "Influence of decorrelation on Heisenberg-limited interferometry with quantum correlated photons," Phys. Rev. A **57**, 4004–4013.
Kimble, H. J., 1998, "Strong interactions of single atoms and photons in cavity QED," Phys. Scr. **T76**, 127.
Kimble, H. J., 2008, "The quantum internet," Nature (London) **453**, 1023.
Kitagawa, M., and M. Ueda, 1993, "Squeezed spin states," Phys. Rev. A **47**, 5138–5143.
Kitching, J., S. Knappe, and E. A. Donley, 2011, "Atomic sensors—a review," IEEE Sens. J. **11**, 1749–1758.
Klempt, C., O. Topic, G. Gebreyesus, M. Scherer, T. Henninger, P. Hyllus, W. Ertmer, L. Santos, and J. J. Arlt, 2010, "Parametric amplification of vacuum fluctuations in a spinor condensate," Phys. Rev. Lett. **104**, 195303.
Kohlhaas, R., A. Bertoldi, E. Cantin, A. Aspect, A. Landragin, and P. Bouyer, 2015, "Phase locking a clock oscillator to a coherent atomic ensemble," Phys. Rev. X **5**, 021011.
Kołodyński, J., and R. Demkowicz-Dobrzański, 2013, "Efficient tools for quantum metrology with uncorrelated noise," New J. Phys. **15**, 073043.
Kominis, I. K., 2008, "Sub-shot-noise magnetometry with a correlated spin-relaxation dominated alkali-metal vapor," Phys. Rev. Lett. **100**, 073002.
Kominis, I. K., T. W. Kornack, J. C. Allred, and M. V. Romalis, 2003, "A subfemtotesla multichannel atomic magnetometer," Nature (London) **422**, 596–599.
Korbicz, J. K., J. I. Cirac, and M. Lewenstein, 2005, "Spin squeezing inequalities and entanglement of *N* qubit states," Phys. Rev. Lett. **95**, 120502.
Korbicz, J. K., O. Gühne, M. Lewenstein, H. Häffner, C. F. Roos, and R. Blatt, 2006, "Generalized spin-squeezing inequalities in *N*-qubit systems: Theory and experiment," Phys. Rev. A **74**, 052319.
Koschorreck, M., M. Napolitano, B. Dubost, and M. W. Mitchell, 2010a, "Quantum nondemolition measurement of large-spin ensembles by dynamical decoupling," Phys. Rev. Lett. **105**, 093602.
Koschorreck, M., M. Napolitano, B. Dubost, and M. W. Mitchell, 2010b, "Sub-projection-noise sensitivity in broadband atomic magnetometry," Phys. Rev. Lett. **104**, 093602.
Kot, E., N. Grønbech-Jensen, B. M. Nielsen, J. S. Neergaard-Nielsen, E. S. Polzik, and A. S. Sørensen, 2012, "Breakdown of the classical description of a local system," Phys. Rev. Lett. **108**, 233601.
Krischek, R., C. Schwemmer, W. Wieczorek, H. Weinfurter, P. Hyllus, L. Pezzè, and A. Smerzi, 2011, "Useful multiparticle entanglement and sub-shot-noise sensitivity in experimental phase estimation," Phys. Rev. Lett. **107**, 080504.
Kruse, I., *et al.*, 2016, "Improvement of an atomic clock using squeezed vacuum," Phys. Rev. Lett. **117**, 143004.
Kurkjian, H., K. Pawłowski, A. Sinatra, and P. Treutlein, 2013, "Spin squeezing and Einstein-Podolsky-Rosen entanglement of two bimodal condensates in state-dependent potentials," Phys. Rev. A **88**, 043605.
Kuzmich, A., N. P. Bigelow, and L. Mandel, 1998, "Atomic quantum non-demolition measurements and squeezing," Europhys. Lett. **42**, 481.
Kuzmich, A., L. Mandel, and N. P. Bigelow, 2000, "Generation of spin squeezing via continuous quantum nondemolition measurement," Phys. Rev. Lett. **85**, 1594–1597.

Kuzmich, A., L. Mandel, J. Janis, Y. E. Young, R. Ejnisman, and N. P. Bigelow, 1999, "Quantum nondemolition measurements of collective atomic spin," Phys. Rev. A **60**, 2346–2350.

Kuzmich, A., K. Mølmer, and E. S. Polzik, 1997, "Spin squeezing in an ensemble of atoms illuminated with squeezed light," Phys. Rev. Lett. **79**, 4782–4785.

Kuzmich, A., and E. S. Polzik, 2003, "Atomic continuous variable processing and light-atoms quantum interface," in *Quantum Information with Continuous Variables*, edited by S. L. Braunstein and A. K. Pati (Kluwer Academic Publishers, Dordrecht), Chap. 18, p. 231.

Kwiat, P. G., K. Mattle, H. Weinfurter, A. Zeilinger, A. V. Sergienko, and Y. Shih, 1995, "New high-intensity source of polarization-entangled photon pairs," Phys. Rev. Lett. **75**, 4337–4341.

Laloë, F., and W. J. Mullin, 2009, "Interferometry with independent Bose-Einstein condensates: parity as an EPR/Bell quantum variable," Eur. Phys. J. B **70**, 377–396.

Lamacraft, A., 2007, "Quantum quenches in a spinor condensate," Phys. Rev. Lett. **98**, 160404.

Landini, M., M. Fattori, L. Pezzè, and A. Smerzi, 2014, "Phase-noise protection in quantum-enhanced differential interferometry," New J. Phys. **16**, 113074.

Lane, A. S., S. L. Braunstein, and C. M. Caves, 1993, "Maximum-likelihood statistics of multiple quantum phase measurements," Phys. Rev. A **47**, 1667–1696.

Lanyon, B. P., M. Zwerger, P. Jurcevic, C. Hempel, W. Dür, H. J. Briegel, R. Blatt, and C. F. Roos, 2014, "Experimental violation of multipartite Bell inequalities with trapped ions," Phys. Rev. Lett. **112**, 100403.

Lapert, M., G. Ferrini, and D. Sugny, 2012, "Optimal control of quantum superpositions in a bosonic Josephson junction," Phys. Rev. A **85**, 023611.

Law, C. K., H. T. Ng, and P. T. Leung, 2001, "Coherent control of spin squeezing," Phys. Rev. A **63**, 055601.

Law, C. K., H. Pu, and N. P. Bigelow, 1998, "Quantum spins mixing in spinor Bose-Einstein condensates," Phys. Rev. Lett. **81**, 5257–5261.

LeBlanc, L. J., A. B. Bardon, J. McKeever, M. H. T. Extavour, D. Jervis, J. H. Thywissen, F. Piazza, and A. Smerzi, 2011, "Dynamics of a tunable superfluid junction," Phys. Rev. Lett. **106**, 025302.

Lee, C., 2006, "Adiabatic Mach-Zehnder interferometry on a quantized Bose-Josephson junction," Phys. Rev. Lett. **97**, 150402.

Lee, H., P. Kok, and J. P. Dowling, 2002, "A quantum Rosetta stone for interferometry," J. Mod. Opt. **49**, 2325.

Lee, P. J., K.-A. Brickman, L. Deslauriers, P. C. Haljan, L.-M. Duan, and C. Monroe, 2005, "Phase control of trapped ion quantum gates," J. Opt. B **7**, S371.

Leggett, A. J., 2001, "Bose-Einstein condensation in the alkali gases: Some fundamental concepts," Rev. Mod. Phys. **73**, 307–356.

Leggett, A. J., and F. Sols, 1991, "On the concept of spontaneously broken gauge symmetry in condensed matter physics," Found. Phys. **21**, 353.

Leggett, A. J., and F. Sols, 1998, "Comment on 'phase and phase diffusion of a split Bose-Einstein condensate'," Phys. Rev. Lett. **81**, 1344–1344.

Lehmann, E. L., and G. Casella, 2003, *Theory of Point Estimation*, Springer Texts in Statistics (Springer, New York).

Leibfried, D., M. D. Barrett, T. Schaetz, J. Britton, J. Chiaverini, W. M. Itano, J. D. Jost, C. Langer, and D. J. Wineland, 2004, "Toward Heisenberg-limited spectroscopy with multiparticle entangled states," Science **304**, 1476.

Leibfried, D., R. Blatt, C. Monroe, and D. Wineland, 2003, "Quantum dynamics of single trapped ions," Rev. Mod. Phys. **75**, 281–324.

Leibfried, D., D. M. Meekhof, B. E. King, C. Monroe, W. M. Itano, and D. J. Wineland, 1996, "Experimental determination of the motional quantum state of a trapped atom," Phys. Rev. Lett. **77**, 4281–4285.

Leibfried, D., *et al.*, 2003, "Experimental demonstration of a robust, high-fidelity geometric two ion-qubit phase gate," Nature (London) **422**, 412.

Leibfried, D., *et al.*, 2005, "Creation of a six-atom 'Schrödinger cat' state," Nature (London) **438**, 639.

Leroux, I. D., M. H. Schleier-Smith, and V. Vuletić, 2010a, "Implementation of cavity squeezing of a collective atomic spin," Phys. Rev. Lett. **104**, 073602.

Leroux, I. D., M. H. Schleier-Smith, and V. Vuletić, 2010b, "Orientation-dependent entanglement lifetime in a squeezed atomic clock," Phys. Rev. Lett. **104**, 250801.

Leroux, I. D., M. H. Schleier-Smith, H. Zhang, and V. Vuletić, 2012, "Unitary cavity spin squeezing by quantum erasure," Phys. Rev. A **85**, 013803.

Leroux, I. D., N. Scharnhorst, S. Hannig, J. Kramer, L. Pelzer, M. Stepanova, and P. O. Schmidt, 2017, "On-line estimation of local oscillator noise and optimisation of servo parameters in atomic clocks," Metrologia **54**, 307.

Leslie, S. R., J. Guzman, M. Vengalattore, Jay D. Sau, Marvin L. Cohen, and D. M. Stamper-Kurn, 2009, "Amplification of fluctuations in a spinor Bose-Einstein condensate," Phys. Rev. A **79**, 043631.

Levy, S., E. Lahoud, I. Shomroni, and J. Steinhauer, 2007, "The a.c. and d.c. Josephson effects in a Bose-Einstein condensate," Nature (London) **449**, 579.

Lewenstein, M., and L. You, 1996, "Quantum phase diffusion of a Bose-Einstein condensate," Phys. Rev. Lett. **77**, 3489–3493.

Lewis-Swan, R. J., and K. V. Kheruntsyan, 2014, "Proposal for demonstrating the Hong–Ou–Mandel effect with matter waves," Nat. Commun. **5**, 3752.

Li, Y., Y. Castin, and A. Sinatra, 2008, "Optimum spin squeezing in Bose-Einstein condensates with particle losses," Phys. Rev. Lett. **100**, 210401.

Li, Y., L. Pezzè, M. Gessner, W. Li, and A. Smerzi, 2018, "Frequentist and Bayesian Quantum Phase Estimation," Entropy **20**, 628.

Li, Y., P. Treutlein, J. Reichel, and A. Sinatra, 2009, "Spin squeezing in a bimodal condensate: spatial dynamics and particle losses," Eur. Phys. J. B **68**, 365.

Lidar, D. A., I. L. Chuang, and K. B. Whaley, 1998, "Decoherence-free subspaces for quantum computation," Phys. Rev. Lett. **81**, 2594–2597.

Linnemann, D., H. Strobel, W. Muessel, J. Schulz, R. J. Lewis-Swan, K. V. Kheruntsyan, and M. K. Oberthaler, 2016, "Quantum-enhanced sensing based on time reversal of nonlinear dynamics," Phys. Rev. Lett. **117**, 013001.

Lipkin, H. J., N. Meshkov, and A. J. Glick, 1965, "Validity of many-body approximation methods for a solvable model: (i). exact solutions and perturbation theory," Nucl. Phys. **62**, 188.

Liu, C., Z. Dutton, C. H. Behroozi, and L. V. Hau, 2001, "Observation of coherent optical information storage in an atomic medium using halted light pulses," Nature (London) **409**, 490–493.

Liu, Y., E. Gomez, S. E. Maxwell, L. D. Turner, E. Tiesinga, and P. D. Lett, 2009, "Number fluctuations and energy dissipation in sodium spinor condensates," Phys. Rev. Lett. **102**, 225301.

Lodewyck, J., P. G. Westergaard, and P. Lemonde, 2009, "Nondestructive measurement of the transition probability in a Sr optical lattice clock," Phys. Rev. A **79**, 061401(R).

Lopes, R., A. Imanaliev, A. Aspect, M. Cheneau, D. Boiron, and C. I. Westbrook, 2015, "Atomic Hong-Ou-Mandel experiment," Nature (London) **520**, 66.

Louchet-Chauvet, A., J. Appel, J. J. Renema, D. Oblak, N. Kjaergaard, and E. S. Polzik, 2010, "Entanglement-assisted atomic clock beyond the projection noise limit," New J. Phys. **12**, 065032.

Lu, X.-M., S. Yu, and C. H. Oh, 2015, "Robust quantum metrological schemes based on protection of quantum Fisher information," Nat. Commun. **6**, 7282.

Lücke, B., J. Peise, G. Vitagliano, J. Arlt, L. Santos, G. Tóth, and C. Klempt, 2014, "Detecting multiparticle entanglement of Dicke states," Phys. Rev. Lett. **112**, 155304.

Lücke, B., *et al.*, 2011, "Twin matter waves for interferometry beyond the classical limit," Science **334**, 773.

Ludlow, A. D., *et al.*, 2008, "Sr lattice clock at 1×10^{-16} fractional uncertainty by remote optical evaluation with a Ca clock," Science **319**, 1805.

Ludlow, A. D., Martin M. Boyd, Jun Ye, E. Peik, and P. O. Schmidt, 2015, "Optical atomic clocks," Rev. Mod. Phys. **87**, 637–701.

Luis, A., 2004, "Nonlinear transformations and the Heisenberg limit," Phys. Lett. A **329**, 8.

Luis, A., 2007, "Quantum limits, nonseparable transformations, and nonlinear optics," Phys. Rev. A **76**, 035801.

Luo, X.-Y., Y.-Q. Zou, L.-N. Wu, Q. Liu, M.-F. Han, M. K. Tey, and L. You, 2017, "Deterministic entanglement generation from driving through quantum phase transitions," Science **355**, 620–623.

Lvovsky, A. I., H. Hansen, T. Aichele, O. Benson, J. Mlynek, and S. Schiller, 2001, "Quantum state reconstruction of the single-photon Fock state," Phys. Rev. Lett. **87**, 050402.

Lynch, R., 1995, "The quantum phase problem: a critical review," Phys. Rep. **256**, 367.

Ma, J., and X. Wang, 2009, "Fisher information and spin squeezing in the Lipkin-Meshkov-Glick model," Phys. Rev. A **80**, 012318.

Ma, J., X. Wang, C. P. Sun, and F. Nori, 2011, "Quantum spin squeezing," Phys. Rep. **509**, 89.

Mach, L., 1892, "Ueber einen Interferenzrefraktor," Z. Instrumentenkd. **12**, 89–93.

Macieszczak, K., 2015, "Zeno limit in frequency estimation with non-Markovian environments," Phys. Rev. A **92**, 010102.

Macrì, T., A. Smerzi, and L. Pezzè, 2016, "Loschmidt echo for quantum metrology," Phys. Rev. A **94**, 010102.

Madsen, L. B., and K. Mølmer, 2004, "Spin squeezing and precision probing with light and samples of atoms in the Gaussian description," Phys. Rev. A **70**, 052324.

Marino, A. M., N. V. Corzo Trejo, and P. D. Lett, 2012, "Effect of losses on the performance of an SU(1,1) interferometer," Phys. Rev. A **86**, 023844.

Martinez, E. A., *et al.*, 2016, "Real-time dynamics of lattice gauge theories with a few-qubit quantum computer," Nature (London) **534**, 516–519.

Matsukevich, D. N., P. Maunz, D. L. Moehring, S. Olmschenk, and C. Monroe, 2008, "Bell inequality violation with two remote atomic qubits," Phys. Rev. Lett. **100**, 150404.

Matsumoto, K., 2010, "On metric of quantum channel spaces," arXiv:1006.0300.

Matsuzaki, Y., S. C. Benjamin, and J. Fitzsimons, 2011, "Magnetic field sensing beyond the standard quantum limit under the effect of decoherence," Phys. Rev. A **84**, 012103.

Maussang, K., G. E. Marti, T. Schneider, P. Treutlein, Y. Li, A. Sinatra, R. Long, J. Estève, and J. Reichel, 2010, "Enhanced and reduced atom number fluctuations in a BEC splitter," Phys. Rev. Lett. **105**, 080403.

Mazzarella, G., L. Salasnich, A. Parola, and F. Toigo, 2011, "Coherence and entanglement in the ground state of a bosonic Josephson junction: From macroscopic Schrödinger cat states to separable Fock states," Phys. Rev. A **83**, 053607.

McConnell, R., H. Zhang, S. Ćuk, J. Hu, M. H. Schleier-Smith, and V. Vuletić, 2013, "Generating entangled spin states for quantum metrology by single-photon detection," Phys. Rev. A **88**, 063802.

McConnell, R., H. Zhang, J. Hu, S. Cuk, and V. Vuletić, 2015, "Entanglement with negative Wigner function of almost 3,000 atoms heralded by one photon," Nature (London) **519**, 439–442.

Meiser, D., J. Ye, and M. J. Holland, 2008, "Spin squeezing in optical lattice clocks via lattice-based QND measurements," New J. Phys. **10**, 073014.

Menotti, C., J. R. Anglin, J. I. Cirac, and P. Zoller, 2001, "Dynamic splitting of a Bose-Einstein condensate," Phys. Rev. A **63**, 023601.

Meyer, V., M. A. Rowe, D. Kielpinski, C. A. Sackett, W. M. Itano, C. Monroe, and D. J. Wineland, 2001, "Experimental demonstration of entanglement-enhanced rotation angle estimation using trapped ions," Phys. Rev. Lett. **86**, 5870–5873.

Mias, G. I., N. R. Cooper, and S. M. Girvin, 2008, "Quantum noise, scaling, and domain formation in a spinor Bose-Einstein condensate," Phys. Rev. A **77**, 023616.

Micheli, A., D. Jaksch, J. I. Cirac, and P. Zoller, 2003, "Many-particle entanglement in two-component Bose-Einstein condensates," Phys. Rev. A **67**, 013607.

Mielenz, M., *et al.*, 2016, "Arrays of individually controlled ions suitable for two-dimensional quantum simulations," Nat. Commun. **7**, ncomms11839.

Milburn, G. J., J. Corney, E. M. Wright, and D. F. Walls, 1997, "Quantum dynamics of an atomic Bose-Einstein condensate in a double-well potential," Phys. Rev. A **55**, 4318–4324.

Milburn, G. J., S. Schneider, and D. F. V. James, 2000, "Ion trap quantum computing with warm ions," Fortschr. Phys. **48**, 801–810.

Miller, R., T. E. Northup, K. M. Birnbaum, A. Boca, A. D. Boozer, and H. J. Kimble, 2005, "Trapped atoms in cavity QED: coupling quantized light and matter," J. Phys. B **38**, S551.

Mintert, F., and C. Wunderlich, 2001, "Ion-trap quantum logic using long-wavelength radiation," Phys. Rev. Lett. **87**, 257904.

Mitchell, M. W., 2005, "Metrology with entangled states," Proc. SPIE Int. Soc. Opt. Eng. **5893**, 589310.

Moehring, D. L., P. Maunz, S. Olmschenk, K. C. Younge, D. N. Matsukevich, L. M. Duan, and C. Monroe, 2007, "Entanglement of single-atom quantum bits at a distance," Nature (London) **449**, 68–71.

Mohammadsadegh, K., H.-W. Lau, A. Humeniuk, and C. Simon, 2016, "Large energy superpositions via rydberg dressing," Phys. Rev. A **94**, 023408.

Mølmer, K., and A. Sørensen, 1999, "Multiparticle entanglement of hot trapped ions," Phys. Rev. Lett. **82**, 1835–1838.

Monz, T., P. Schindler, J. T. Barreiro, M. Chwalla, D. Nigg, W. A. Coish, M. Harlander, W. Hänsel, M. Hennrich, and R. Blatt, 2011, "14-qubit entanglement: Creation and coherence," Phys. Rev. Lett. **106**, 130506.

Morita, H., H. Ohnishi, J. da Providência, and S. Nishiyama, 2006, "Exact solutions for the LMG model Hamiltonian based on the Bethe ansatz," Nucl. Phys. B **737**, 337.

Muessel, W., H. Strobel, D. Linnemann, D. B. Hume, and M. K. Oberthaler, 2014, "Scalable spin squeezing for quantum-enhanced

magnetometry with Bose-Einstein condensates," Phys. Rev. Lett. **113**, 103004.
Muessel, W., H. Strobel, D. Linnemann, T. Zibold, B. Juliá-Díaz, and M. K. Oberthaler, 2015, "Twist-and-turn spin squeezing in Bose-Einstein condensates," Phys. Rev. A **92**, 023603.
Muessel, W., H. Strobel, M. Joos, E. Nicklas, I. Stroescu, J. Tomkovič, D. B. Hume, and M. K. Oberthaler, 2013, "Optimized absorption imaging of mesoscopic atomic clouds," Appl. Phys. B **113**, 69–73.
Mullan, M., and E. Knill, 2014, "Optimizing passive quantum clocks," Phys. Rev. A **90**, 042310.
Mullin, W. J., and F. Laloë, 2008, "Interference of Bose-Einstein condensates: Quantum nonlocal effects," Phys. Rev. A **78**, 061605.
Murata, K., H. Saito, and M. Ueda, 2007, "Broken-axisymmetry phase of a spin-1 ferromagnetic bose-einstein condensate," Phys. Rev. A **75**, 013607.
Müstecaplıoğlu, Ö. E., M. Zhang, and L. You, 2002, "Spin squeezing and entanglement in spinor condensates," Phys. Rev. A **66**, 033611.
Myerson, A. H., D. J. Szwer, S. C. Webster, D. T. C. Allcock, M. J. Curtis, G. Imreh, J. A. Sherman, D. N. Stacey, A. M. Steane, and D. M. Lucas, 2008, "High-fidelity readout of trapped-ion qubits," Phys. Rev. Lett. **100**, 200502.
Nagata, T., R. Okamoto, J. L. O'Brien, K. Sasaki, and S. Takeuchi, 2007, "Beating the standard quantum limit with four-entangled photons," Science **316**, 726–729.
Napolitano, M., M. Koschorreck, B. Dubost, N. Behbood, R. J. Sewell, and M. W. Mitchell, 2011, "Interaction-based quantum metrology showing scaling beyond the Heisenberg limit," Nature (London) **471**, 486.
Napolitano, M., and M. W. Mitchell, 2010, "Nonlinear metrology with a quantum interface," New J. Phys. **12**, 093016.
Navon, N., N. Akerman, S. Kotler, Y. Glickman, and R. Ozeri, 2014, "Quantum process tomography of a Mølmer-Sørensen interaction," Phys. Rev. A **90**, 010103.
Negretti, A., and C. Henkel, 2004, "Enhanced phase sensitivity and soliton formation in an integrated BEC interferometer," J. Phys. B **37**, L385.
Negretti, A., C. Henkel, and K. Mølmer, 2008, "Quantum-limited position measurements of a dark matter-wave soliton," Phys. Rev. A **77**, 043606.
Nelson, K. D., X. Li, and D. S. Weiss, 2007, "Imaging single atoms in a three-dimensional array," Nat. Phys. **3**, 556–560.
Nicholson, T. L., M. J. Martin, J. R. Williams, B. J. Bloom, M. Bishof, M. D. Swallows, S. L. Campbell, and J. Ye, 2012, "Comparison of two independent Sr optical clocks with 1×10^{-17} stability at 10^3 s," Phys. Rev. Lett. **109**, 230801.
Nicholson, T. L., *et al.*, 2015, "Systematic evaluation of an atomic clock at 2×10^{-18} total uncertainty," Nat. Commun. **6**, 6896.
Nicklas, E., M. Karl, M. Höfer, A. Johnson, W. Muessel, H. Strobel, J. Tomkovič, T. Gasenzer, and M. K. Oberthaler, 2015, "Observation of scaling in the dynamics of a strongly quenched quantum gas," Phys. Rev. Lett. **115**, 245301.
Nielsen, A. E. B., and K. Mølmer, 2008, "Atomic spin squeezing in an optical cavity," Phys. Rev. A **77**, 063811.
Nielsen, M. A., and I. L. Chuang, 2000, *Quantum Computation and Quantum Information* (Cambridge University Press, Cambridge, England).
Noguchi, A., K. Toyoda, and S. Urabe, 2012, "Generation of Dicke states with phonon-mediated multilevel stimulated Raman adiabatic passage," Phys. Rev. Lett. **109**, 260502.
Nolan, S. P., S. S. Szigeti, and S. A. Haine, 2017, "Optimal and robust quantum metrology using interaction-based readouts," Phys. Rev. Lett. **119**, 193601.
Norcia, M. A., and J. K. Thompson, 2016, "Strong coupling on a forbidden transition in strontium and nondestructive atom counting," Phys. Rev. A **93**, 023804.
Oblak, D., P. G. Petrov, C. L. Garrido Alzar, W. Tittel, A. K. Vershovski, J. K. Mikkelsen, J. L. Sørensen, and E. S. Polzik, 2005, "Quantum-noise-limited interferometric measurement of atomic noise: Towards spin squeezing on the Cs clock transition," Phys. Rev. A **71**, 043807.
O'Brien, J. L., A. Furusawa, and J. Vučović, 2009, "Photonic quantum technologies," Nat. Photonics **3**, 687–695.
Ockeloen, C. F., R. Schmied, M. F. Riedel, and P. Treutlein, 2013, "Quantum metrology with a scanning probe atom interferometer," Phys. Rev. Lett. **111**, 143001.
Ockeloen, C. F., A. F. Tauschinsky, R. J. C. Spreeuw, and S. Whitlock, 2010, "Detection of small atom numbers through image processing," Phys. Rev. A **82**, 061606.
Ohmi, T., and K. Machida, 1998, "Bose-Einstein condensation with internal degrees of freedom in alkali atom gases," J. Phys. Soc. Jpn. **67**, 1822.
Opatrný, T., and K. Mølmer, 2012, "Spin squeezing and Schrödinger-cat-state generation in atomic samples with Rydberg blockade," Phys. Rev. A **86**, 023845.
Orús, R., S. Dusuel, and J. Vidal, 2008, "Equivalence of critical scaling laws for many-body entanglement in the Lipkin-Meshkov-Glick model," Phys. Rev. Lett. **101**, 025701.
Ospelkaus, C., C. E. Langer, J. M. Amini, K. R. Brown, D. Leibfried, and D. J. Wineland, 2008, "Trapped-ion quantum logic gates based on oscillating magnetic fields," Phys. Rev. Lett. **101**, 090502.
Ospelkaus, C., U. Warring, Y. Colombe, K. R. Brown, J. M. Amini, D. Leibfried, and D. J. Wineland, 2011, "Microwave quantum logic gates for trapped ions," Nature (London) **476**, 181–184.
Ou, Z. Y., 2012, "Enhancement of the phase-measurement sensitivity beyond the standard quantum limit by a nonlinear interferometer," Phys. Rev. A **85**, 023815.
Ou, Z. Y., S. F. Pereira, H. J. Kimble, and K. C. Peng, 1992, "Realization of the Einstein-Podolsky-Rosen paradox for continuous variables," Phys. Rev. Lett. **68**, 3663–3666.
Ozeri, R., 2013, "Heisenberg limited metrology using quantum error-correction codes," arXiv:1310.3432.
Pan, F., and J. P. Draayer, 1999, "Analytical solutions for the LMG model," Phys. Lett. B **451**, 1.
Paraoanu, G. S., S. Kohler, F. Sols, and A. J. Leggett, 2001, "The Josephson plasmon as a Bogoliubov quasiparticle," J. Phys. B **34**, 4689.
Paris, M., and J. Řeháček, 2004, Eds., *Quantum State Estimation*, Lecture Notes in Physics, Vol. 649 (Springer, Berlin/Heidelberg).
Paris, M. G. A., 2009, "Quantum estimation for quantum technology," Int. J. Quantum. Inform. **07**, 125–137.
Pawłowski, K., J. Estève, J. Reichel, and A. Sinatra, 2016, "Limits of atomic entanglement by cavity feedback: From weak to strong coupling," Europhys. Lett. **113**, 34005.
Peise, J., B. Lücke, L. Pezzè, F. Deuretzbacher, W. Ertmer, J. Arlt, A. Smerzi, L. Santos, and C. Klempt, 2015, "Interaction-free measurements by quantum Zeno stabilization of ultracold atoms," Nat. Commun. **6**, 6811.
Peise, J., *et al.*, 2015, "Satisfying the Einstein-Podolsky-Rosen criterion with massive particles," Nat. Commun. **6**, 8984.
Pelisson, S., L. Pezzè, and A. Smerzi, 2016, "Nonlocality with ultracold atoms in a lattice," Phys. Rev. A **93**, 022115.

Peres, A., 1995, *Quantum Theory: Concepts and Methods* (Springer, Netherlands).
Petersen, V., L. B. Madsen, and K. Mølmer, 2005, "Magnetometry with entangled atomic samples," Phys. Rev. A **71**, 012312.
Pethick, C. J., and H. Smith, 2002, *Bose-Einstein Condensation in Dilute Gases* (Cambridge University Press, Cambridge, England).
Petz, D., 1996, "Monotone Metrics on Matrix Spaces," Linear Algebra Appl. **244**, 81.
Petz, D., and C. Ghinea, 2011, "Introduction to quantum Fisher information," *Quantum probability and Related Topics*, p. 261.
Pezzè, L., 2013, "Sub-Heisenberg phase uncertainties," Phys. Rev. A **88**, 060101.
Pezzè, L., L. A. Collins, A. Smerzi, G. P. Berman, and A. R. Bishop, 2005, "Sub-shot-noise phase sensitivity with a Bose-Einstein condensate Mach-Zehnder interferometer," Phys. Rev. A **72**, 043612.
Pezzè, L., M. Gessner, P. Feldmann, C. Klempt, L. Santos, and A. Smerzi, 2017, "Heralded generation of macroscopic superposition states in a spinor Bose-Einstein condensate," arXiv:1712.03864.
Pezzè, L., Y. Li, W. Li, and A. Smerzi, 2016, "Witnessing entanglement without entanglement witness operators," Proc. Natl. Acad. Sci. U.S.A. **113**, 11459.
Pezzè, L., and A. Smerzi, 2006, "Phase sensitivity of a Mach-Zehnder interferometer," Phys. Rev. A **73**, 011801.
Pezzè, L., and A. Smerzi, 2007, "Sub shot-noise interferometric phase sensitivity with beryllium ions Schrödinger cat states," Europhys. Lett. **78**, 30004.
Pezzè, L., and A. Smerzi, 2008, "Mach-Zehnder interferometry at the Heisenberg limit with coherent and squeezed-vacuum light," Phys. Rev. Lett. **100**, 073601.
Pezzè, L., and A. Smerzi, 2009, "Entanglement, nonlinear dynamics, and the Heisenberg limit," Phys. Rev. Lett. **102**, 100401.
Pezzè, L., and A. Smerzi, 2013, "Ultrasensitive two-mode interferometry with single-mode number squeezing," Phys. Rev. Lett. **110**, 163604.
Pezzè, L., and A. Smerzi, 2014, "Quantum theory of phase estimation," in *Atom Interferometry, Proceedings of the International School of Physics "Enrico Fermi," Course 188, Varenna*, edited by G. M. Tino and M. A. Kasevich (IOS Press, Amsterdam), p. 691.
Phillips, D. F., A. Fleischhauer, A. Mair, R. L. Walsworth, and M. D. Lukin, 2001, "Storage of light in atomic vapor," Phys. Rev. Lett. **86**, 783–786.
Pichler, T., T. Caneva, S. Montangero, M. D. Lukin, and T. Calarco, 2016, "Noise-resistant optimal spin squeezing via quantum control," Phys. Rev. A **93**, 013851.
Plenio, M. B., and S. F. Huelga, 2016, "Sensing in the presence of an observed environment," Phys. Rev. A **93**, 032123.
Porras, D., and J. I. Cirac, 2006, "Quantum manipulation of trapped ions in two dimensional coulomb crystals," Phys. Rev. Lett. **96**, 250501.
Pruttivarasin, T., M. Ramm, S. G. Porsev, I. I. Tupitsyn, M. S. Safronova, M. A. Hohensee, and H. Häffner, 2015, "Michelson-Morley analogue for electrons using trapped ions to test Lorentz symmetry," Nature (London) **517**, 592–595.
Pu, H., C. K. Law, S. Raghavan, J. H. Eberly, and N. P. Bigelow, 1999, "Spin-mixing dynamics of a spinor Bose-Einstein condensate," Phys. Rev. A **60**, 1463–1470.
Pu, H., and P. Meystre, 2000, "Creating macroscopic atomic Einstein-Podolsky-Rosen states from Bose-Einstein condensates," Phys. Rev. Lett. **85**, 3987–3990.
Puentes, G., G. Colangelo, R. J. Sewell, and M. W. Mitchell, 2013, "Planar squeezing by quantum non-demolition measurement in cold atomic ensembles," New J. Phys. **15**, 103031.
Pupillo, G., A. Micheli, M. Boninsegni, I. Lesanovsky, and P. Zoller, 2010, "Strongly correlated gases of rydberg-dressed atoms: Quantum and classical dynamics," Phys. Rev. Lett. **104**, 223002.
Radcliffe, J. M., 1971, "Some properties of coherent spin states," J. Phys. A: Gen. Phys. **4**, 313.
Raghavan, S., H. Pu, P. Meystre, and N. P. Bigelow, 2001, "Generation of arbitrary Dicke states in spinor Bose-Einstein condensates," Opt. Commun. **188**, 149.
Raghavan, S., A. Smerzi, S. Fantoni, and S. R. Shenoy, 1999, "Coherent oscillations between two weakly coupled Bose-Einstein condensates: Josephson effects, π oscillations, and macroscopic quantum self-trapping," Phys. Rev. A **59**, 620–633.
Ramsey, N. F., 1963, *Molecular Beams*, International Series of Monographs on Physics (Oxford University Press, London).
Rao, C. R., 1945, "Information and the accuracy attainable in the estimation of statistical parameters," Bull. Calcutta Math. Soc. **37**, 81–91.
Rashid, M. A., 1978, "The intelligent states. i. group-theoretic study and the computation of matrix elements," J. Math. Phys. (N.Y.) **19**, 1391.
Raymer, M. G., A. C. Funk, B. C. Sanders, and H. de Guise, 2003, "Separability criterion for separate quantum systems," Phys. Rev. A **67**, 052104.
Reid, M. D., 1989, "Demonstration of the Einstein-Podolsky-Rosen paradox using nondegenerate parametric amplification," Phys. Rev. A **40**, 913–923.
Reid, M. D., P. D. Drummond, W. P. Bowen, E. G. Cavalcanti, P. K. Lam, H. A. Bachor, U. L. Andersen, and G. Leuchs, 2009, "*Colloquium*: The Einstein-Podolsky-Rosen paradox: From concepts to applications," Rev. Mod. Phys. **81**, 1727–1751.
Reinaudi, G., T. Lahaye, Z. Wang, and D. Guéry-Odelin, 2007, "Strong saturation absorption imaging of dense clouds of ultracold atoms," Opt. Lett. **32**, 3143–3145.
Rey, A. M., L. Jiang, and M. D. Lukin, 2007, "Quantum-limited measurements of atomic scattering properties," Phys. Rev. A **76**, 053617.
Ribeiro, P., J. Vidal, and R. Mosseri, 2007, "Thermodynamical limit of the Lipkin-Meshkov-Glick model," Phys. Rev. Lett. **99**, 050402.
Ribeiro, P., J. Vidal, and R. Mosseri, 2008, "Exact spectrum of the Lipkin-Meshkov-Glick model in the thermodynamic limit and finite-size corrections," Phys. Rev. E **78**, 021106.
Richerme, P., Z.-X. Gong, A. Lee, C. Senko, J. Smith, M. Foss-Feig, S. Michalakis, A. V. Gorshkov, and C. Monroe, 2014, "Non-local propagation of correlations in quantum systems with long-range interactions," Nature (London) **511**, 198–201.
Riedel, M. F., P. Böhi, Y. Li, T. W. Hänsch, A. Sinatra, and P. Treutlein, 2010, "Atom-chip-based generation of entanglement for quantum metrology," Nature (London) **464**, 1170–1173.
Rihele, F., 2004, *Frequency Standards: Basics and Applications* (Wiley-VCH, Weinhein).
Ritsch, H., P. Domokos, F. Brennecke, and T. Esslinger, 2013, "Cold atoms in cavity-generated dynamical optical potentials," Rev. Mod. Phys. **85**, 553–601.
Rivas, Á., and S. F. Huelga, 2012, *Open Quantum Systems* (Springer, New York).
Rivas, Á., and A. Luis, 2010, "Precision quantum metrology and nonclassicality in linear and nonlinear detection schemes," Phys. Rev. Lett. **105**, 010403.
Roos, C., 2014, "Quantum information processing with trapped ions," in *Fundamental Physics in Particle Traps*, Springer Tracts in

Modern Physics Vol. 256, edited by Wolfgang Quint and Manuel Vogel (Springer-Verlag, Berlin), pp. 253–292.

Roos, C. F., M. Chwalla, K. Kim, M. Riebe, and R. Blatt, 2006, "'Designer atoms' for quantum metrology," Nature (London) **443**, 316.

Roos, C. F., M. Riebe, H. Häffner, W. Hänsel, J. Benhelm, G. P. T. Lancaster, C. Becher, F. Schmidt-Kaler, and R. Blatt, 2004, "Control and measurement of three-qubit entangled states," Science **304**, 1478–1480.

Rosenband, T., 2011, Ed., "Numerical test of few-qubit clock protocols," *Proceedings of the 20th International Conference on Laser Spectroscopy* (Logos Verlag, Berlin).

Rosenfeld, W., D. Burchardt, R. Garthoff, K. Redeker, N. Ortegel, M. Rau, and H. Weinfurter, 2017, "Event-ready Bell test using entangled atoms simultaneously closing detection and locality loopholes," Phys. Rev. Lett. **119**, 010402.

Rowe, M. A., D. Kielpinski, V. Meyer, C. A. Sackett, W. M. Itano, C. Monroe, and D. J. Wineland, 2001, "Experimental violation of a Bell's inequality with efficient detection," Nature (London) **409**, 791–794.

Roy, S. M., and S. L. Braunstein, 2008, "Exponentially enhanced quantum metrology," Phys. Rev. Lett. **100**, 220501.

Sackett, C. A., *et al.*, 2000, "Experimental entanglement of four particles," Nature (London) **404**, 256.

Sadler, L. E., J. M. Higbie, S. R. Leslie, M. Vengalattore, and D. M. Stamper-Kurn, 2006, "Spontaneous symmetry breaking in a quenched ferromagnetic spinor Bose-Einstein condensate," Nature (London) **443**, 312–315.

Saffman, M., D. Oblak, J. Appel, and E. S. Polzik, 2009, "Spin squeezing of atomic ensembles by multicolor quantum nondemolition measurements," Phys. Rev. A **79**, 023831.

Saffman, M., T. G. Walker, and K. Mølmer, 2010, "Quantum information with Rydberg atoms," Rev. Mod. Phys. **82**, 2313–2363.

Salvi, L., N. Poli, V. Vuletić, and G. Tino, 2018, "Squeezing on Momentum States for Atom Interferometry," Phys. Rev. Lett. **120**, 033601.

Sanders, B. C., and G. J. Milburn, 1995, "Optimal quantum measurements for phase estimation," Phys. Rev. Lett. **75**, 2944–2947.

Sangouard, N., C. Simon, H. de Riedmatten, and N. Gisin, 2011, "Quantum repeaters based on atomic ensembles and linear optics," Rev. Mod. Phys. **83**, 33–80.

Santarelli, G., Ph. Laurent, P. Lemonde, A. Clairon, A. G. Mann, S. Chang, A. N. Luiten, and C. Salomon, 1999, "Quantum projection noise in an atomic fountain: A high stability cesium frequency standard," Phys. Rev. Lett. **82**, 4619–4622.

Sau, J. D., S. R. Leslie, M. L. Cohen, and D. M. Stamper-Kurn, 2010, "Spin squeezing of high-spin, spatially extended quantum fields," New J. Phys. **12**, 085011.

Schaff, J.-F., T. Langen, and J. Schmiedmayer, 2014, "Interferometry with atoms," in *Atom Interferometry, Proceedings of the International School of Physics "Enrico Fermi," Course 188, Varenna*, edited by G. M. Tino and M. A. Kasevich (IOS Press, Amsterdam), p. 1.

Scherer, M., B. Lücke, G. Gebreyesus, O. Topic, F. Deuretzbacher, W. Ertmer, L. Santos, J. J. Arlt, and C. Klempt, 2010, "Spontaneous breaking of spatial and spin symmetry in spinor condensates," Phys. Rev. Lett. **105**, 135302.

Schleich, W. P., 2001, *Quantum Optics in Phase Space* (Wiley-VCH, Berlin).

Schleier-Smith, M. H., I. D. Leroux, and V. Vuletić, 2010a, "Squeezing the collective spin of a dilute atomic ensemble by cavity feedback," Phys. Rev. A **81**, 021804.

Schleier-Smith, M. H., I. D. Leroux, and V. Vuletić, 2010b, "States of an ensemble of two-level atoms with reduced quantum uncertainty," Phys. Rev. Lett. **104**, 073604.

Schmaljohann, H., M. Erhard, J. Kronjäger, M. Kottke, S. van Staa, L. Cacciapuoti, J. J. Arlt, K. Bongs, and K. Sengstock, 2004, "Dynamics of $F = 2$ spinor Bose-Einstein condensates," Phys. Rev. Lett. **92**, 040402.

Schmied, R., J.-D. Bancal, B. Allard, M. Fadel, V. Scarani, P. Treutlein, and N. Sangouard, 2016, "Bell correlations in a Bose-Einstein condensate," Science **352**, 441–444.

Schmied, R., and P. Treutlein, 2011, "Tomographic reconstruction of the Wigner function on the Bloch sphere," New J. Phys. **13**, 065019.

Schmied, R., J. H. Wesenberg, and D. Leibfried, 2011, "Quantum simulation of the hexagonal Kitaev model with trapped ions," New J. Phys. **13**, 115011.

Schmied, R., 2016, "Quantum state tomography of a single qubit: comparison of methods," J. Mod. Opt. **63**, 1744–1758.

Schnabel, R., N. Mavalvala, D. E. McClelland, and P. K. Lam, 2010, "Quantum metrology for gravitational wave astronomy," Nat. Commun. **1**, 121.

Schneider, C., D. Porras, and T. Schaetz, 2012, "Experimental quantum simulations of many-body physics with trapped ions," Rep. Prog. Phys. **75**, 024401.

Schumm, T., S. Hofferberth, L. M. Andersson, S. Wildermuth, S. Groth, I. Bar-Joseph, J. Schmiedmayer, and P. Krüger, 2005, "Matter-wave interferometry in a double well on an atom chip," Nat. Phys. **1**, 57–62.

Scott, R. G., T. E. Judd, and T. M. Fromhold, 2008, "Exploiting soliton decay and phase fluctuations in atom chip interferometry of Bose-Einstein condensates," Phys. Rev. Lett. **100**, 100402.

Scully, M. O., and M. S. Zubairy, 1997, *Quantum Optics* (Cambridge University Press, Cambridge).

Sewell, R. J., M. Koschorreck, M. Napolitano, B. Dubost, N. Behbood, and M. W. Mitchell, 2012, "Magnetic sensitivity beyond the projection noise limit by spin squeezing," Phys. Rev. Lett. **109**, 253605.

Sewell, R. J., M. Napolitano, N. Behbood, G. Colangelo, F. Martin Ciurana, and M. W. Mitchell, 2014, "Ultrasensitive atomic spin measurements with a nonlinear interferometer," Phys. Rev. X **4**, 021045.

Sewell, R. J., M. Napolitano, N. Behbood, G. Colangelo, and M. W. Mitchell, 2013, "Certified quantum non-demolition measurement of a macroscopic material system," Nat. Photonics **7**, 517.

Shah, V., G. Vasilakis, and M. V. Romalis, 2010, "High bandwidth atomic magnetometery with continuous quantum nondemolition measurements," Phys. Rev. Lett. **104**, 013601.

Shaji, A., and C. M. Caves, 2007, "Qubit metrology and decoherence," Phys. Rev. A **76**, 032111.

Shalm, L. K., *et al.*, 2015, "Strong loophole-free test of local realism," Phys. Rev. Lett. **115**, 250402.

Shchesnovich, V. S., and M. Trippenbach, 2008, "Fock-space WKB method for the boson Josephson model describing a Bose-Einstein condensate trapped in a double-well potential," Phys. Rev. A **78**, 023611.

Shchukin, E., and W. Vogel, 2005, "Inseparability criteria for continuous bipartite quantum states," Phys. Rev. Lett. **95**, 230502.

Sherson, J. F., C. Weitenberg, M. Endres, M. Cheneau, I. Bloch, and S. Kuhr, 2010, "Single-atom-resolved fluorescence imaging of an atomic Mott insulator," Nature (London) **467**, 68–72.

Shiga, N., and M. Takeuchi, 2012, "Locking the local oscillator phase to the atomic phase via weak measurements," New J. Phys. **14**, 023034.

Shin, Y., M. Saba, T. A. Pasquini, W. Ketterle, D. E. Pritchard, and A. E. Leanhardt, 2004, "Atom interferometry with Bose-Einstein condensates in a double-well potential," Phys. Rev. Lett. **92**, 050405.

Shor, P. W., 1995, "Scheme for reducing decoherence in quantum computer memory," Phys. Rev. A **52**, R2493–R2496.

Simon, R., 2000, "Peres-Horodecki separability criterion for continuous variable systems," Phys. Rev. Lett. **84**, 2726–2729.

Sinatra, A., Y. Castin, and E. Witkowska, 2013, "Limit of spin squeezing in trapped Bose-Einstein condensates," Europhys. Lett. **102**, 40001.

Sinatra, A., E. Witkowska, and Y. Castin, 2012, "Spin squeezing in finite temperature Bose-Einstein condensates: Scaling with the system size," Eur. Phys. J. Spec. Top. **203**, 87.

Sinatra, A., E. Witkowska, J.-C. Dornstetter, Yun Li, and Y. Castin, 2011, "Limit of spin squeezing in finite-temperature Bose-Einstein condensates," Phys. Rev. Lett. **107**, 060404.

Slusher, R. E., L. W. Hollberg, B. Yurke, J. C. Mertz, and J. F. Valley, 1985, "Observation of squeezed states generated by four-wave mixing in an optical cavity," Phys. Rev. Lett. **55**, 2409–2412.

Smerzi, A., S. Fantoni, S. Giovanazzi, and S. R. Shenoy, 1997, "Quantum coherent atomic tunneling between two trapped Bose-Einstein condensates," Phys. Rev. Lett. **79**, 4950–4953.

Smerzi, A., and S. Raghavan, 2000, "Macroscopic quantum fluctuations in the Josephson dynamics of two weakly linked Bose-Einstein condensates," Phys. Rev. A **61**, 063601.

Smerzi, A., and A. Trombettoni, 2003, "Nonlinear tight-binding approximation for bose-einstein condensates in a lattice," Phys. Rev. A **68**, 023613.

Smirne, A., J. Kołodyński, S. F. Huelga, and R. Demkowicz-Dobrzański, 2016, "Ultimate precision limits for noisy frequency estimation," Phys. Rev. Lett. **116**, 120801.

Solano, E., R. L. de Matos Filho, and N. Zagury, 1999, "Deterministic Bell states and measurement of the motional state of two trapped ions," Phys. Rev. A **59**, R2539–R2543.

Sorelli, G., L. Pezzè, and A. Smerzi, 2015, "Fast generation of entanglement in bosonic Josephson junctions," arXiv:1511.01835.

Sørensen, A. S., 2002, "Bogoliubov theory of entanglement in a Bose-Einstein condensate," Phys. Rev. A **65**, 043610.

Sørensen, A. S., L.-M. Duan, J. I. Cirac, and P. Zoller, 2001, "Many-particle entanglement with Bose-Einstein condensates," Nature (London) **409**, 63–66.

Sørensen, A. S., and K. Mølmer, 1999, "Quantum computation with ions in thermal motion," Phys. Rev. Lett. **82**, 1971–1974.

Sørensen, A. S., and K. Mølmer, 2000, "Entanglement and quantum computation with ions in thermal motion," Phys. Rev. A **62**, 022311.

Sørensen, A. S., and K. Mølmer, 2001, "Entanglement and extreme spin squeezing," Phys. Rev. Lett. **86**, 4431–4434.

Spagnolli, G., *et al.*, 2017, "Crossing over from attractive to repulsive interactions in a tunneling bosonic josephson junction," Phys. Rev. Lett. **118**, 230403.

Spehner, D., K. Pawłowski, G. Ferrini, and A. Minguzzi, 2014, "Effect of one-, two-, and three-body atom loss processes on superpositions of phase states in Bose-Josephson junctions," Eur. Phys. J. B **87**, 157.

Spehner, D., 2014, "Quantum correlations and distinguishability of quantum states," J. Math. Phys. (N.Y.) **55**, 075211.

Spekkens, R. W., and J. E. Sipe, 1999, "Spatial fragmentation of a Bose-Einstein condensate in a double-well potential," Phys. Rev. A **59**, 3868–3877.

Stamper-Kurn, D. M., and M. Ueda, 2013, "Spinor Bose gases: Symmetries, magnetism, and quantum dynamics," Rev. Mod. Phys. **85**, 1191–1244.

Steane, A. M., 1996, "Error correcting codes in quantum theory," Phys. Rev. Lett. **77**, 793–797.

Steel, M. J., and M. J. Collett, 1998, "Quantum state of two trapped Bose-Einstein condensates with a Josephson coupling," Phys. Rev. A **57**, 2920–2930.

Sterling, R. C., H. Rattanasonti, S. Weidt, K. Lake, P. Srinivasan, S. C. Webster, M. Kraft, and W. K. Hensinger, 2014, "Fabrication and operation of a two-dimensional ion-trap lattice on a high-voltage microchip," Nat. Commun. **5**, 3637.

Streltsov, A. I., O. E. Alon, and L. S. Cederbaum, 2007, "Role of excited states in the splitting of a trapped interacting Bose-Einstein condensate by a time-dependent barrier," Phys. Rev. Lett. **99**, 030402.

Strobel, H., W. Muessel, D. Linnemann, T. Zibold, D. B. Hume, L. Pezzè, A. Smerzi, and M. K. Oberthaler, 2014, "Fisher information and entanglement of non-Gaussian spin states," Science **345**, 424.

Stroescu, I., D. B. Hume, and M. K. Oberthaler, 2015, "Double-well atom trap for fluorescence detection at the Heisenberg limit," Phys. Rev. A **91**, 013412.

Stute, A., B. Casabone, P. Schindler, T. Monz, P. O. Schmidt, B. Brandstatter, T. E. Northup, and R. Blatt, 2012, "Tunable ion-photon entanglement in an optical cavity," Nature (London) **485**, 482–485.

Sudarshan, E. C. G., 1963, "Equivalence of semiclassical and quantum mechanical descriptions of statistical light beams," Phys. Rev. Lett. **10**, 277–279.

Szańkowski, P., M. Trippenbach, and J. Chwedeńczuk, 2014, "Parameter estimation in memory-assisted noisy quantum interferometry," Phys. Rev. A **90**, 063619.

Szigeti, S. S., R. J. Lewis-Swan, and S. A. Haine, 2017, "Pumped-up su(1,1) interferometry," Phys. Rev. Lett. **118**, 150401.

Szigeti, S. S., B. Tonekaboni, W. Y. S. Lau, S. N. Hood, and S. A. Haine, 2014, "Squeezed-light-enhanced atom interferometry below the standard quantum limit," Phys. Rev. A **90**, 063630.

Takahashi, Y., K. Honda, N. Tanaka, K. Toyoda, K. Ishikawa, and T. Yabuzaki, 1999, "Quantum nondemolition measurement of spin via the paramagnetic Faraday rotation," Phys. Rev. A **60**, 4974–4979.

Takano, T., M. Fuyama, R. Namiki, and Y. Takahashi, 2009, "Spin squeezing of a cold atomic ensemble with the nuclear spin of one-half," Phys. Rev. Lett. **102**, 033601.

Takano, T., S.-I.-R. Tanaka, R. Namiki, and Y. Takahashi, 2010, "Manipulation of nonclassical atomic spin states," Phys. Rev. Lett. **104**, 013602.

Takeuchi, M., S. Ichihara, T. Takano, M. Kumakura, T. Yabuzaki, and Y. Takahashi, 2005, "Spin squeezing via one-axis twisting with coherent light," Phys. Rev. Lett. **94**, 023003.

Tanji-Suzuki, H., I. D. Leroux, M. H. Schleier-Smith, M. Cetina, A. Grier, J. Simon, and V. Vuletić, 2011, "Interaction between atomic ensembles and optical resonators: Classical description," in *Advances in Atomic, Molecular, and Optical Physics*, Vol. 60, edited by E. Arimondo, P. R. Berman, and C. C. Lin (Academic Press, New York), Chap. 4, pp. 201–237.

The LIGO Scientific Collaboration, 2011, "A gravitational wave observatory operating beyond the quantum shot-noise limit," Nat. Phys. **7**, 962–965.

Thomsen, L. K., S. Mancini, and H. M. Wiseman, 2002, "Spin squeezing via quantum feedback," Phys. Rev. A **65**, 061801.

Tóth, G., 2012, "Multipartite entanglement and high-precision metrology," Phys. Rev. A **85**, 022322.

Tóth, G., and I. Apellaniz, 2014, "Quantum metrology from a quantum information science perspective," J. Phys. A **47**, 424006.

Tóth, G., C. Knapp, O. Gühne, and H. J. Briegel, 2007, "Optimal spin squeezing inequalities detect bound entanglement in spin models," Phys. Rev. Lett. **99**, 250405.

Tóth, G., C. Knapp, O. Gühne, and H. J. Briegel, 2009, "Spin squeezing and entanglement," Phys. Rev. A **79**, 042334.

Tóth, G., and M. W. Mitchell, 2010, "Generation of macroscopic singlet states in atomic ensembles," New J. Phys. **12**, 053007.

Trail, C. M., P. S. Jessen, and I. H. Deutsch, 2010, "Strongly enhanced spin squeezing via quantum control," Phys. Rev. Lett. **105**, 193602.

Trenkwalder, A., *et al.*, 2016, "Quantum phase transitions with parity-symmetry breaking and hysteresis," Nat. Phys. **12**, 826–829.

Treutlein, P., T. W. Hänsch, J. Reichel, A. Negretti, M. A. Cirone, and T. Calarco, 2006, "Microwave potentials and optimal control for robust quantum gates on an atom chip," Phys. Rev. A **74**, 022312.

Truax, D. R., 1985, "Baker-Campbell-Hausdorff relations and unitarity of SU(2) and SU(1,1) squeeze operators," Phys. Rev. D **31**, 1988–1991.

Tura, J., R. Augusiak, A. B. Sainz, T. Vértesi, M. Lewenstein, and A. Acín, 2014, "Detecting nonlocality in many-body quantum states," Science **344**, 1256–1258.

Turchette, Q. A., C. S. Wood, B. E. King, C. J. Myatt, D. Leibfried, W. M. Itano, C. Monroe, and D. J. Wineland, 1998, "Deterministic entanglement of two trapped ions," Phys. Rev. Lett. **81**, 3631–3634.

Uhlmann, A., 1976, "The "transition probability" in the state space of a *-algebra," Rep. Math. Phys. **9**, 273.

Ulam-Orgikh, D., and M. Kitagawa, 2001, "Spin squeezing and decoherence limit in Ramsey spectroscopy," Phys. Rev. A **64**, 052106.

Ulyanov, V. V., and O. B. Zaslavskii, 1992, "New methods in the theory of quantum spin systems," Phys. Rep. **216**, 179.

Vahlbruch, H., S. Chelkowski, B. Hage, A. Franzen, K. Danzmann, and R. Schnabel, 2005, "Demonstration of a squeezed-light-enhanced power- and signal-recycled Michelson interferometer," Phys. Rev. Lett. **95**, 211102.

Vahlbruch, H., M. Mehmet, K. Danzmann, and R. Schnabel, 2016, "Detection of 15 db squeezed states of light and their application for the absolute calibration of photoelectric quantum efficiency," Phys. Rev. Lett. **117**, 110801.

Vanderbruggen, T., R. Kohlhaas, A. Bertoldi, S. Bernon, A. Aspect, A. Landragin, and P. Bouyer, 2013, "Feedback control of trapped coherent atomic ensembles," Phys. Rev. Lett. **110**, 210503.

Vanier, J., and C. Audoin, 1992, *The Quantum Physics of Atomic Frequency Standards* (Adam Higler, New York).

Van Trees, H. L., and K. L. Bell, 2007, *Bayesian Bounds for Parameter Estimation and Nonlinear Filtering/Tracking* (IEEE Press, Piscataway, NJ).

Vasilakis, G., V. Shah, and M. V. Romalis, 2011, "Stroboscopic backaction evasion in a dense alkali-metal vapor," Phys. Rev. Lett. **106**, 143601.

Vengalattore, M., J. M. Higbie, S. R. Leslie, J. Guzman, L. E. Sadler, and D. M. Stamper-Kurn, 2007, "High-resolution magnetometry with a spinor Bose-Einstein condensate," Phys. Rev. Lett. **98**, 200801.

Vernac, L., M. Pinard, and E. Giacobino, 2000, "Spin squeezing in two-level systems," Phys. Rev. A **62**, 063812.

Vidal, J., G. Palacios, and R. Mosseri, 2004, "Entanglement in a second-order quantum phase transition," Phys. Rev. A **69**, 022107.

Vitagliano, G., I. Apellaniz, I. L. Egusquiza, and G. Tóth, 2014, "Spin squeezing and entanglement for an arbitrary spin," Phys. Rev. A **89**, 032307.

Vitagliano, G., G. Colangelo, F. Martin Ciurana, M. W. Mitchell, R. J. Sewell, and G. Tóth, 2018, "Entanglement and extreme planar spin squeezing," Phys. Rev. A **97**, 020301.

Vitagliano, G., P. Hyllus, I. L. Egusquiza, and G. Tóth, 2011, "Spin squeezing inequalities for arbitrary spin," Phys. Rev. Lett. **107**, 240502.

Vitagliano, G., I. Apellaniz, M. Kleinmann, B. Lücke, C. Klempt, and G. Tóth, 2017, "Entanglement and extreme spin squeezing of unpolarized states," New J. Phys. **19**, 013027.

Volz, J., R. Gehr, G. Dubois, J. Estève, and J. Reichel, 2011, "Measurement of the internal state of a single atom without energy exchange," Nature (London) **475**, 210–213.

Wagner, S., R. Schmied, M. Fadel, P. Treutlein, N. Sangouard, and J.-D. Bancal, 2017, "Bell correlations in a many-body system with finite statistics," Phys. Rev. Lett. **119**, 170403.

Walborn, S. P., B. G. Taketani, A. Salles, F. Toscano, and R. L. de Matos Filho, 2009, "Entropic entanglement criteria for continuous variables," Phys. Rev. Lett. **103**, 160505.

Walls, D., and G. Milburn, 1994, *Quantum Optics* (Springer, New York).

Walls, D. F., 1983, "Squeezed states of light," Nature (London) **306**, 141–146.

Wang, X., and K. Mølmer, 2002, "Pairwise entanglement in symmetric multi-qubit systems," Eur. Phys. J. D **18**, 385.

Wang, X., and B. C. Sanders, 2003a, "Relations between bosonic quadrature squeezing and atomic spin squeezing," Phys. Rev. A **68**, 033821.

Wang, X., and B. C. Sanders, 2003b, "Spin squeezing and pairwise entanglement for symmetric multiqubit states," Phys. Rev. A **68**, 012101.

Wasilewski, W., K. Jensen, H. Krauter, J. J. Renema, M. V. Balabas, and E. S. Polzik, 2010, "Quantum noise limited and entanglement-assisted magnetometry," Phys. Rev. Lett. **104**, 133601.

Weinstein, J. D., K. Beloy, and A. Derevianko, 2010, "Entangling the lattice clock: Towards Heisenberg-limited timekeeping," Phys. Rev. A **81**, 030302.

Welzel, J., A. Bautista-Salvador, C. Abarbanel, V. Wineman-Fisher, C. Wunderlich, R. Folman, and F. Schmidt-Kaler, 2011, "Designing spin-spin interactions with one and two dimensional ion crystals in planar micro traps," Eur. Phys. J. D **65**, 285–297.

Werner, R. F., 1989, "Quantum states with Einstein-Podolsky-Rosen correlations admitting a hidden-variable model," Phys. Rev. A **40**, 4277–4281.

Wigner, E., 1932, "On the quantum correction for thermodynamic equilibrium," Phys. Rev. **40**, 749–759.

Wildermuth, S., S. Hofferberth, I. Lesanovsky, S. Groth, P. Krüger, J. Schmiedmayer, and I. Bar-Joseph, 2006, "Sensing electric and magnetic fields with Bose-Einstein condensates," Appl. Phys. Lett. **88**, 264103.

Windpassinger, P. J., D. Oblak, P. G. Petrov, M. Kubasik, M. Saffman, C. L. Garrido Alzar, J. Appel, J. H. Müller, N. Kjærgaard, and E. S. Polzik, 2008, "Nondestructive probing of Rabi oscillations on the cesium clock transition near the standard quantum limit," Phys. Rev. Lett. **100**, 103601.

Wineland, D. J., 2013, "Nobel Lecture: Superposition, entanglement, and raising Schrödinger's cat," Rev. Mod. Phys. **85**, 1103–1114.

Wineland, D. J., J. J. Bollinger, W. M. Itano, and D. J. Heinzen, 1994, "Squeezed atomic states and projection noise in spectroscopy," Phys. Rev. A **50**, 67–88.

Wineland, D. J., J. J. Bollinger, W. M. Itano, F. L. Moore, and D. J. Heinzen, 1992, "Spin squeezing and reduced quantum noise in spectroscopy," Phys. Rev. A **46**, R6797–R6800.

Wineland, D. J., C. Monroe, W. M. Itano, D. Leibfried, B. E. King, and D. M. Meekhof, 1998, "Experimental issues in coherent quantum-state manipulation of trapped atomic ions," J. Res. Natl. Inst. Stand. Technol. **103**, 259.

Wòdkiewicz, K., and J. Eberly, 1985, "Coherent states, squeezed fluctuations, and the SU(2) and SU(1,1) groups in quantum-optics applications," J. Opt. Soc. Am. B **2**, 458.

Wolfgramm, F., A. Cerè, F. A. Beduini, A. Predojević, M. Koschorreck, and M. W. Mitchell, 2010, "Squeezed-light optical magnetometry," Phys. Rev. Lett. **105**, 053601.

Woolley, M. J., G. J. Milburn, and C. M. Caves, 2008, "Nonlinear quantum metrology using coupled nanomechanical resonators," New J. Phys. **10**, 125018.

Wootters, W. K., 1981, "Statistical distance and Hilbert space," Phys. Rev. D **23**, 357–362.

Wootters, W. K., 1998, "Entanglement of formation of an arbitrary state of two qubits," Phys. Rev. Lett. **80**, 2245–2248.

Wu, L.-A., H. J. Kimble, J. L. Hall, and H. Wu, 1986, "Generation of squeezed states by parametric down conversion," Phys. Rev. Lett. **57**, 2520–2523.

Wu, L.-N., and L. You, 2016, "Using the ground state of an antiferromagnetic spin-1 atomic condensate for Heisenberg-limited metrology," Phys. Rev. A **93**, 033608.

Wynands, R., 2009, *Atomic Clocks*, edited by G. Muga, A. Ruschhaupt, and A. Campo, Lecture Notes in Physics, Vol. 789 (Springer, Berlin/Heidelberg).

Wynands, R., and S. Weyers, 2005, "Atomic fountain clocks," Metrologia **42**, S64.

Xiang, G. Y., B. L. Higgins, D. W. Berry, H. M. Wiseman, and G. J. Pryde, 2011, "Entanglement-enhanced measurement of a completely unknown optical phase," Nat. Photonics **5**, 43–47.

Ye, J., H. J. Kimble, and H. Katori, 2008, "Quantum state engineering and precision metrology using state-insensitive light traps," Science **320**, 1734–1738.

Yurke, B., S. L. McCall, and J. R. Klauder, 1986, "SU(2) and SU(1,1) interferometers," Phys. Rev. A **33**, 4033–4054.

Yuste, A., B. Juliá-Díaz, E. Torrontegui, J. Martorell, J. G. Muga, and A. Polls, 2013, "Shortcut to adiabaticity in internal bosonic Josephson junctions," Phys. Rev. A **88**, 043647.

Zanardi, P., and M. Rasetti, 1997, "Noiseless quantum codes," Phys. Rev. Lett. **79**, 3306–3309.

Zapata, I., F. Sols, and A. J. Leggett, 1998, "Josephson effect between trapped Bose-Einstein condensates," Phys. Rev. A **57**, R28–R31.

Zehnder, I., 1891, "Ein neuer Interferenzrefraktor," Z. Instrumentenkd. **11**, 275–285.

Zhang, H., R. McConnell, S. Ćuk, Q. Lin, M. H. Schleier-Smith, I. D. Leroux, and V. Vuletić, 2012, "Collective state measurement of mesoscopic ensembles with single-atom resolution," Phys. Rev. Lett. **109**, 133603.

Zhang, J., K. Peng, and S. L. Braunstein, 2003, "Backaction-induced spin-squeezed states in a detuned quantum-nondemolition measurement," Phys. Rev. A **68**, 035802.

Zhang, W., D. L. Zhou, M.-S. Chang, M. S. Chapman, and L. You, 2005, "Coherent spin mixing dynamics in a spin-1 atomic condensate," Phys. Rev. A **72**, 013602.

Zhang, W.-M., Da H. Feng, and R. Gilmore, 1990, "Coherent states: Theory and some applications," Rev. Mod. Phys. **62**, 867–927.

Zhang, Y.-L., C.-L. Zou, X.-B. Zou, L. Jiang, and G.-C. Guo, 2015, "Detuning-enhanced cavity spin squeezing," Phys. Rev. A **91**, 033625.

Zhang, Z., and L.-M. Duan, 2013, "Generation of massive entanglement through an adiabatic quantum phase transition in a spinor condensate," Phys. Rev. Lett. **111**, 180401.

Zhao, Z., T. Yang, Y.-A. Chen, A.-N. Zhang, M. Żukowski, and J.-W. Pan, 2003, "Experimental violation of local realism by four-photon Greenberger-Horne-Zeilinger entanglement," Phys. Rev. Lett. **91**, 180401.

Zień, P., J. Chwedeńczuk, B. Oleś, K. Sacha, and M. Trippenbach, 2008, "Critical fluctuations of an attractive Bose gas in a double-well potential," Europhys. Lett. **83**, 64007.

Zou, Y.-Q., L.-N. Wu, Q. Liu, Guo S.-F., J.-H. Cao, M. K. Tey, and L. You, 2018, "Beating the classical precision limit with spin-1 dicke state of more than 10000 atoms," arXiv:1802.10288.